DAMORHEOLOGY

CREEP-FATIGUE INTERACTION IN COMPOSITE MATERIALS

by

Ricardo Osiroff

Dissertation submitted to the Faculty of the

Virginia Polytechnic Institute and State University

in partial fulfillment of the requirements for the degree of

DOCTOR IN PHILOSOPHY

in

Materials Engineering Science

APPROVED:

W.W. Stinchcomb, Chairman

N.E. Dowling

J.W. Grant

D.P.H. Hasselman

K.L. Reifsnider

June, 1990

Blacksburg, Virginia

Damorheology:

Creep-Fatigue Interaction in Composite Materials

by

Ricardo Osiroff

Committee Chairman: Wayne W. Stinchcomb

Materials Engineering Science

(ABSTRACT)

This investigation addresses the interaction mechanisms of time dependent material behavior and cyclic damage during fatigue loading of fiber reinforced composite laminates. A new term 'damorheology' has been coined to describe such physical behavior. The lamina has been chosen as the building block and a cross ply laminate configuration was the selected test case. The chosen material system is the Radel X/T65-42 thermoplastic composite by Amoco. The fatigue performance at the lamina level is represented by the dynamic stiffness, residual strength and fatigue life of unidirectional laminates. The time dependent behavior is represented at the lamina level by a Pseudo-Analog Mechanical model. The thermo-rheological characterization procedure combines mechanical (creep) and thermal (dynamic mechanical analysis) techniques. The proposed rheological model provides a complete representation of the effects of temperature

and stress on the viscoelastic response.

The experimental investigation of unidirectional and cross ply laminates revealed that indeed there are significant changes in the time dependent response of a laminate due to fatigue loading. In turn, the viscoelastic stress redistribution is responsible for the changes in the rate of damage evolution and varying extent of damage modes. Time dependent constitutive relationships were derived for the laminate in the from of differential equations. Applying classical lamination stress analysis together with the Shear Lag model, the damage evolution of cross ply laminates was predicted.

Based on the laminae viscoelastic and fatigue characteristics, a cyclic performance simulation code - CYPERS - was developed. The code was designed to predict the long term performance of cross ply laminates subjected to cyclic loads. The analysis and/or accompanying code have produced satisfactory predictions for a variety of situations. The model and code provide a complete representation of the laminate long term performance. It includes: dynamic stiffness, global deformation, complex moduli and compliance, temperature history, frequency response of the complex moduli, damage state, time dependent stress redistribution, residual strength and fatigue life.

Acknowledgment

The author gratefully acknowledges the support of the large number of individuals and organizations that made this study possible.

Committee chairman Dr. Wayne Stinchcomb, for his guidance, efforts, and confidence, always offered in the gentlest manner. For letting the author explore new horizons and still keep the focus.

Dr. Ken Reifsnider, who in his many roles as member of the Materials Response Group, head of the Materials Engineering Science program, and director of the Virginia Institute for Materials Systems, offered his advice, enthusiasm and pointed the forest from the trees.

Dr. N.E. Dowling, Dr. J.W. Grant and Dr. D.P.H. Hasselman for serving as committee members, their advice and the opportunity to engage in exciting research topics.

Barbara Wengert and Shelia Collins, for their patience, help and outstanding disposition.

Jennifer Holmquest, who gave a new meaning to the word commitment. Her extraordinary effort has significantly improved the quality and depth of this investigation.

Chuck Chandler, the driving force behind the Center for Composite Materials and Structures Fabrication Laboratory, for the valuable work done in preparing the numerous plates required in this investigation and his willingness to overcome the difficulties imposed by a new material system.

Marshal McCord, for his enlightening work on the scanning acoustic microscope.

Dr. T.C. Ward and Paul Vail at the Chemistry department, who generously and patiently helped conduct the lengthy dynamic analysis facet of this study at their laboratory.

Mike Debusk and all fellow LBRG members, for their friendship, assistance in the laboratory and fruitful discussions which sharpened the mind.

Thomas Fleming and Amoco Performance Products, for donating a substantial portion of the thermoplastic composite used in this investigation.

The Virginia Institute for Material Systems for funding this research endeavor.

Simon and Dora Osiroff, the author's parents, for their encouragement and unrelenting support.

Last but not least, the author's wife Tali, for her inspiration, her confidence and competence, and for the myriad of ways she helps every day, while working and raising our two sons, Nir and Gal.

Table of Contents

		Page
1.	Introduction	1
2.	Literature Survey	5
	2.1 Viscoelasticity	6
	2.2 Fatigue-induced damage in composites	16
	2.3 Experimental observables and analytical methods	20
	2.4 Interaction of rate dependent and independent processes	27
3.	Analysis	43
	3.1 General concepts	43
	3.2 General lamina characterization	47
	3.3 Cross ply laminates	53
	3.4 Complex moduli and compliance	73
	3.5 Energy dissipation and temperature distribution	78
	3.6 Damorheology	82
4.	Materials and Experimental Methods	85
	4.1 Experimental program	85
	4.2 Radel x/T650-42 thermoplastic system	87
	4.3 Specimen preparation and mechanical tests	90
	4.4 Nondestructive tests	93
	4.4 Thermorheological characterization	95
5.	Results	102
	5.1 Quasi static tensile testing	102
	5.2 Preliminary shear lag analysis	106

	5.3 Thermal properties	112
	5.4 Fatigue response	125
	5.5 Nondestructive damage evaluation	147
	5.6 Time dependent behavior	161
6.	CYPERS, Cyclic Performance Simulation	188
	6.1 Introduction	188
	6.2 Data input	190
	6.3 Main procedures	193
	6.4 Predictive output	203
7.	Discussion	211
	7.1 Viscoelastic characterization	211
	7.2 Fatigue characterization	219
	7.3 Fatigue, analytical-experimental comparison	226
	7.4 Damorheology	242
8.	Summary and Conclusions	253
9.	References	257

1 Introduction

ΠΑΝΤΑ PEI - "Everything flows, everything changes". This statement by the old Greek philosopher Heraclitus expresses the fundamental idea of rheological research [1]. The name "rheology" introduced by E.C. Bingham in 1926 is a branch of physics, closely related to mechanics. Its fundamental theory, developed by M. Reiner [2], has found wide applications in numerous fields of research.

Rheology - time dependent deformation - plays an important role in the behavior of all solid and liquid material: soil, concrete, metals, ceramics and especially high polymers. Elasticity, plasticity, viscosity and strength are all rheological properties that every real material possesses in some degree [2]. Many branches of rheology have emerged in the last three decades. The branches range from georheolgy, the rheological properties of the earth crust; to biorheology, the rheological behavior of living matter. In this study the term 'damorheology' is introduced in order to describe the coupling of cyclic damage processes in fiber reinforced composite materials and thermorheological behavior.

Composite materials systems are, and will be, used in components and structures subjected to dynamic loads. Applications include civilian and military aircraft, space structures, boat hulls, sports equipment, telecommunications, weapons systems and more. Many composite material systems, such as polymeric fiber reinforced composites, or metal matrix composites at elevated temperatures, sustain considerable cyclic creep deformation in addition to damage when subjected to dynamic loads. It is conceivable that localized damage and global inelastic deformation attributable to viscoelastic effects interact in a synergistic manner to change the internal state of stress, accelerating or perhaps retarding failure. Many efforts have been made to understand the time dependent behavior and fatigue response of isotropic and composite materials, and their possible interaction. A survey of these efforts is presented in Chapter 2.

In many instances, composite components and structures are designed to sustain cyclic loads and perform their function over extended periods of time. Several damage modes may appear during the life of a composite structure. Each damage mode will affect in different ways the state of the material. To design such structures, the designer requires analytical and experimental tools to predict the effects of cyclic damage on the long term performance. Most importantly, the designer should be able to predict the remaining strength in the structure in order to prevent catastrophic failure.

Models with capabilities to predict remaining strength of damaged composite materials and structures should be based on a thorough understanding of time and/or cycle dependent damage - property - performance relationships during long term loading. The main objectives of this effort are to evaluate the magnitude of the interaction of rate dependent and independent processes in composite laminates and consider the effect on remaining stiffness and strength.

Specifically; based on laminae static, fatigue and viscoelastic characterizations, develop a rationale to predict the anelastic deformation, stiffness change and residual strength of the laminate, at any point in the loading history.

In the approach taken, the nonlinear time-dependent behavior of each different material and/or lamina orientation is represented by a five parameter, pseudo-analog rheological model using a modified Wilshire-Evans procedure. Classical lamination theory (including thermal stresses) and the usual plane stress assumptions are used to compute the stresses at the lamina level and evaluate a suitable effective stress. The fundamentals of the proposed model are presented in Chapter 3.

A new fiber reinforced amorphous thermoplastic composite system was chosen to be the subject of this study. Unidirectional laminates were subjected to quasi-static, fatigue, thermal and viscoelastic characterization using methods described in Chapter 4. Cross-ply laminates were chosen as a test case because of the relatively simple stress state and the wealth of knowledge about the cyclic damage modes. They were loaded in static and fatigue modes and the results are shown in Chapter 5.

Laboratory data and analytical stress analysis codes are combined to evaluate the initiation, growth and interaction of rate dependent and independent damage mechanisms. Representing these events as changes in the response of the different plies, the rheological model coefficients are determined in terms of stress, temperature and other suitable internal variables. A governing equation that describes the constitutive behavior of the laminate is obtained; and a numerical procedure, described in Chapter 6, is developed to emulate the performance evolution of the laminate. The measured performance is compared to the analytical predictions in Chapter 7. Possible interaction mechanisms are discussed.

2 Literature Survey

The following survey is intended to review the essential aspects of time and cyclic dependent processes, and their interaction, from an analytical and experimental perspective. The discussion of time dependent effects (section 2.1) includes basic viscoelastic phenomena in isotropic media, the treatment of fiber reinforced materials and several examples of the use of mechanical analogs as a tool to describe constitutive time dependent behavior. This is followed by a review of fatigue induced damage mechanisms (section 2.2) in composites and the available experimental methods (section 2.3) to evaluate their effect on the laminate's performance. Some of the analytical work in this field is succinctly summarized. Lastly, the interaction of time dependent and fatigue damage is discussed in detail (section 2.4). This includes analytical and experimental studies on creep- fatigue interaction in engineering metals at elevated temperatures, the Continuum Damage Mechanics (CDM) approach and its extension to composite materials. In this context, the surprising and sometimes contradictory findings of the limited experimental investigations of such interactions in composite materials are highlighted.

2.1 Viscoelasticity

Viscoelasticity is the study of materials whose mechanical response is a function of time and previous history, often referred to as a memory effect. The material is said to "remember" its original geometry and recovers with time towards this original configuration. The creep - creep recovery response is widely used to determine the viscoelastic nature and properties of both isotropic and composite materials [3].

Viscoelastic materials subjected to static or cyclic loads not only exhibit time and history dependent deformation but also exhibit delayed failures, commonly referred to as creep rupture. Creep damage may accumulate in many ways, as ductile transgranular or brittle intergranular damage for metals, as chain scission for thermoplastic polymers, debonding or cavitation for particulate composites, etc. The prediction of delayed failures is very complex and involves knowledge of the complete load, temperature and environmental history.

Viscoelastic materials can be further characterized as linear or nonlinear. Isochronous stress-strain curves are usually examined to distinguish between the linear and nonlinear behavior. In most cases, linear viscoelastic behavior is observed up to a certain stress level and at a certain time [4]. Ultimately, at high stress levels or long times, nonlinear behavior is expected.

For isotropic materials, linear viscoelastic behavior is most commonly represented with the aid of mechanical analogs, linear springs and dashpots connected in series or in parallel. Two of the most basic models are the Kelvin solid and the Maxwell fluid. Often, the linear time dependent response of a given material cannot be realistically modeled with a single Kelvin or a single Maxwell element. However, by combining a sufficient number of the basic elements, an accurate representation of the material properties can usually be achieved.

A series of Kelvin elements with a free dashpot, a free spring (Prony series), or both is commonly used to describe the creep compliance function of a given solid over an extended period of time. Each of the multiple Kelvin elements accounts for different periods of time. For a series of Kelvin elements, the time dependent creep compliance is,

$$D(t) = \sum_{i=1}^{n} \frac{1}{E_i}\left[1 - e^{-E_i t/\mu_i} \right] \qquad (2.1.1)$$

where E_i is the stiffness of the i^{th} spring and μ_i is the viscosity of the i^{th} dashpot. If a free spring is added, the model would describe a viscoelastic solid with instantaneous elastic response and no permanent flow. If, on the other hand, a single dashpot is added allowing for a permanent deformation, the model describes a viscoelastic fluid.

Mechanical analogs are widely used in order to represent the response of viscoelastic media under different loading conditions and geometries. Huang et al. [5] described tensile, creep and cyclic behavior of stainless steels using a three parameter model with elastic (spring), viscoelastic (dashpot), and plastic (slider) elements. Hayman [6] used Maxwell and 3 parameter models to treat the problem of creep buckling of columns. Amijima el al. [7] used a 16 element Prony series to model the polyester resin behavior in compression of a glass/ polyester composite. Szyszkowsky and Glockner [8] used combinations of nonlinear Kelvin elements to model nonlinear constitutive behavior accounting for the stress history. Lately, Inoue and Imatani [9] compared the capabilities of different elastic-viscoplastic analogs, and used them to propose a unified constitutive behavior. The most comprehensive study of the use of mechanical analogs in the area of material characterization has been done by Sobotka [1], who developed complete three-dimensional models able to represent the elastic, viscoelastic and plastic behavior of multiphase anisotropic materials. Using ingenious combination of diverse elements and rigorous mechanics, Sobotka presents exact solutions to very intricate problems.

The Boltzmann Superposition Principle is employed to find the response of a linear viscoelastic material to any arbitrary stress history. This is done by representing the stress history as series of small steps in stress.

$$\varepsilon(t) = \int_{0^-}^{t} D\,(t-\tau)\,\frac{d\sigma}{d\tau}\,d\tau \qquad (2.1.2)$$

where D (t) is the compliance function of the material, t is the time at the end of each step, τ is a dummy time variable, and σ is the stress level at each step.

Another central issue in the characterization of viscoelastic materials is the time- temperature superposition principle and the computation of master curves. First reported by Leaderman [10], temperature is widely used as an accelerating factor of the viscoelastic behavior. Creep compliance curves at different temperatures are superimposed by using a horizontal (time) shift factor. Several investigators have found expressions correlating the shift factor to a suitable reference temperature and other material properties, such as activation energies. Although an empirical technique, the long term behavior of thermorheological simple materials can be predicted using short term data.

Regrettably, the use of the Boltzmann and time- temperature superposition principles in a cyclic load situation is limited by the assumptions of linear viscoelasticity, isothermal conditions and consistent material behavior. Very early on Barenblatt [11] showed that even small vibrational loads accelerate creep due to heating. Ponter [12] used creep energy dissipation concepts to evaluate the upper limits of deformation of a body subjected to cyclic loads and temperature. Parkus [13] showed that the rupture time is greatly reduced by small amplitudes of thermal cycling. Ohno, Murakami and Kawabata [14] considered secondary effects and demonstrated the significant hardening that occurs due to aging in steels.

Also, most composite materials are thermorheological complex materials, requiring vertical (magnitude) in addition to horizontal shifting. Apart from temperature and density corrections, no explanation has been found for the need of vertical shifting.

In conclusion, there are many sources of material nonlinearities and linear viscoelastic behavior may be assumed only with great caution. Many investigators have addressed the problem of characterizing the thermo- viscoelastic rheological behavior of engineering materials, the approaches vary greatly in mathematical complexity and the relationship between the representation and the physical phenomena.

Following the Boltzmann approach, Green and Rivlin [15] introduced the multiple integral to account for nonlinearity. In order to use this model, there is a need to determine experimentally a large number of kernel functions, which makes the use of this model impractical.

The Schapery [16] integral model is another nonlinear viscoelastic model which is widely used and has been expanded for use in composite materials including damage. The model is derived from the fundamental principles of irreversible thermodynamics. In its one dimensional version, the strain for an applied uniaxial stress is given by,

$$\varepsilon(t) = g_0 D_0 \sigma + g_1 \int_{\infty}^{t} \Delta D(\psi - \psi') \frac{d(g_2 \sigma)}{d\tau} d\tau \tag{2.1.3}$$

where D_0 and $\Delta D(\psi)$ are the initial and transient compliance for the linear viscoelastic response. The reduced time ψ and ψ' are defined by

$$\psi = \psi(t) = \int_0^t \frac{dt'}{a_\sigma} \quad \text{and} \quad \psi' = \psi'(\tau) = \int_0^\tau \frac{dt'}{a_\sigma} \tag{2.1.4}$$

The nonlinear stress effects are introduced through the Schapery functions: g_0, g_1, g_2, and the "stress shift factor" a_σ. A detailed description of the experimental procedure to obtain these functions and parameters is found in Tuttle [17].

Although it is not common practice, nonlinear viscoelastic materials can be modeled by modifying the generalized Kelvin and Maxwell models. This is done by using nonlinear springs and dashpots. Thus, the relaxation times, are not constant for each element and are a function of the stress level. A most interesting and efficient variation on this approach was the introduction of fractional calculus mechanical analog elements as proposed by Bagley and Torvik [18] and Koeller [19]. "Spring-pots", pseudo analog elements having fractional derivative stress- strain constitutive relationships are introduced. Instead of the usual large Prony series required to describe long term behavior (one Kelvin element per decade of time); 3, 4 and 5 parameter models have been found to match the creep compliance of real materials over several decades of time.

An empirical approach was used by Daugste [20], who considered the combined effects of temperature and stress and proposed a combined time- temperature- stress superposition principle (TTSSP), where temperature and stress are considered creep accelerating factors. The approach has been extended to other variables such as moisture, radiation, etc. Griffith [21] combined the data from creep tests at varying stress levels/ constant temperature and varying temperature/ constant stress level creating a series of master curves. Two shift factors were evaluated, one representing the effect of stress and the other accounting for temperature. A single master curve can be obtained on condition of sufficiently simple thermorheological behavior.

Wilshire and Evans [22] introduced lately a new approach to, termed the "θ projection", to predict complex creep behavior. The fundamental differences from all other mathematical creep models are:

- The effects of stress and temperature are not separated.
- Primary and tertiary creep is accounted for.
- The extent and duration of the primary and tertiary creep stages change with temperature and stress.

The θ projection predicts the complete creep curve as the sum of a decaying primary and and accelerating tertiary component. Thus, the so called constant secondary creep rate occurs when the decay of the primary component is offset by the accelerating third component. The complete creep strain curve is given by,

$$\varepsilon_c = \theta_1(1 - e^{-\theta_2 t}) + \theta_3(e^{\theta_4 t} - 1) \qquad (2.1.5)$$

where t is time, θ_1 and θ_3 act as scaling terms defining the extent of the primary and tertiary stages, while θ_2 and θ_4 are rate parameters governing the curvatures of the primary and tertiary components. They proposed that the dependence of the θ terms on stress and temperature is represented by,

$$\log \theta_i = a_i + b_i\sigma + c_iT + d_i\sigma T \tag{2.1.6}$$

where a_i, b_i, c_i, d_i are material constants, σ is stress and T is temperature. An experimental procedure to obtain this constants is described in [22]. Good experimental results are shown for polycrystalline copper at a wide range of temperatures and stress levels.

Examining the behavior of general anisotropic materials, Betten [23] has proposed constitutive equations to represent inelastic behavior in terms of creep potentials. Onat [24] used tensorial state variables to account for the orientation and internal symmetries of the material.

In the last decade a large number of investigators have concentrated their efforts on developing analytical and experimental tools to characterize the viscoelastic behavior of orthotropic materials and fiber reinforced laminates.

On the analytical side, it is worthwhile noting the efforts of Schapery [25] and Tonda and Schapery [26] which use pseudo strains and work potentials to reduce viscoelastic to elastic behavior, and propose accounting for damage using modified stresses. Brouwer [27] used this approach to predict the transverse, shear and longitudinal compliance changes in cross ply thin cylinders. Cardon et al. [28] expand on the Schapery model introducing nonlinearities in the stress shift factor. Oytana et al. [29] critique the Schapery approach stating that there is no steady state creep for a composite lamina, regardless of orientation. They propose a different nonlinear model and experimental technique. Sun and Chen [30] presented a much simpler one- parameter model to predict the nonlinear response of unidirectional laminates for all orientations using effective inelastic strains and effective stresses. Amijima and Adachi [31] use a micromechanics approach, viscoelastic matrix and fiber, to compute an apparent time dependent compliance tensor. With the aid of classical lamination theory they computed and compared successfully the time dependent response of a cross ply laminate.

Beckwith [32] evaluated the combined effects of temperature (reversible deformation) and stress (irreversible deformation due to damage). He observed the need for mechanical conditioning to isolate both effects. Yancey and Pindera [33] investigated the effects of elevated temperature and radiation on the creep response of unidirectional graphite/ epoxy. They based their analysis on the micromechanics approaches of Hashin [34] and Aboudi [35]. Pyrz [36] addressed the issue of strength reduction due to creep. He predicts strength changes for all lamina directions using a modified Norris Distortional Energy criterion.

The gathering of experimental data is difficult, time consuming and thus, scattered. Of special relevance to this investigation is the complete viscoelastic characterization of PEEK (polyether- ether-ketone) and AS4/PEEK recently performed by Xiao [37]. Isothermal stress dependence was measured with the stress increment technique, while temperature accelerated short term data was used to generate a master curve. He also reports the fact that the glass transition temperature of the virgin resin is greater than the composite by 20°C, leading to the conclusion that the constraint imposed by the fibers alters the molecular motion within the matrix, accelerating creep.

The characterization and analytical modeling of viscoelastic composite materials are at the heart of an extensive research program at VPI&SU which has contributed to the understanding and modeling of the time dependent effects taking place in fiber reinforced laminates [38,39,40,41]. Most recently, Gramoll [42] has reviewed these efforts. He summarized the basic formulation and assumptions of a viscoelastic lamination theory where all four elastic coefficients of the orthotropic ply compliance matrix are assumed to be time dependent. The stress-strain relationship is given by,

$$\begin{Bmatrix} \varepsilon_1(t) \\ \varepsilon_2(t) \\ \gamma_{12}(t) \end{Bmatrix} = \begin{bmatrix} S_{11}(t,T,\sigma_1) & S_{12}(t,T,\sigma_1) & 0 \\ S_{12}(t,T,\sigma_1) & S_{22}(t,T,\sigma_2) & 0 \\ 0 & 0 & S_{66}(t,T,\tau_{12}) \end{bmatrix} \begin{Bmatrix} \sigma_1 \\ \sigma_2 \\ \tau_{12} \end{Bmatrix} \qquad (2.1.7)$$

where S_{ij} is the compliance lamina tensor, ε_{ij} are the strains, and

σ_{ij} are the applied stresses.

Gramoll also proposed a much simpler "quadratic power law", which he used to characterize and model the creep behavior of fiber reinforced composite laminates. The nonlinearity is expressed by quadratic functions of the form,

$$S_{ij}(t,T,\sigma) = S^0_{ij}(1 + g_{ij}\sigma^2) + m_{ij}(1 + f_{ij}\sigma^2)t^{n_{ij}} \tag{2.1.8}$$

where S^0_{ij} and m_{ij} are the linear constants, while g_{ij} and f_{ij} are nonlinear stress constants. This modification eliminates the numerical difficulties caused by other schemes and also allows one to regain the linear form by setting the values of g_{ij} and f_{ij} equal to zero. A three dimensional treatment and several numerical procedures to solve the creep deformation of a laminate are presented in [42].

2.2 Fatigue induced damage in composites

Fatigue damage in composites consists of combinations of matrix cracks, broken fibers, interfacial cracks, and debonds that form a very complex damage state [43]. The material system, stacking sequence, geometry, stress state and environmental factors, interact and affect the engineering properties in many intricate ways. While present technology can be used to detect almost every type of damage, there is currently no general approach to damage assessment. Damage interpretation and response prediction remain a frontier.

Different loading conditions result in distinctive fatigue processes that cause changes in the local geometry and changes of local stress. A review of the mechanics of fatigue in composite materials is given by Stinchcomb and Reifsnider [44]. Investigators such as Schapery [45] and Christensen [46] have addressed the nature of damage in a viscoelastic isotropic media and composites.

The critical event that governs final failure of composites has not yet been identified. Accumulation of fiber fractures often dominates the tensile failure of composite laminates. Most investigators share the assumptions that a critical number or arrangement of broken fibers is the triggering mechanism for cascading fiber fracture and composite failure, and, that given the microstructural scale involved, linear elastic fracture methodologies are inadequate.

Limited knowledge and experimental data are available on the details of these microscopic events (see Jamison and Reifsnider [47]) which define how this mode of damage influences and is influenced by matrix-related damage modes and other global physical/ chemical processes which take place simultaneously. The damage process involves sequential changes in local geometry causing a local stress redistribution which adversely affects the damaged region. Additional processes and loading parameters, such as anelastic deformation, temperature transients and frequency, may accelerate or diminish the rate of damage localization and growth. Such interactions are poorly understood.

In recent years, the long term characterization of new fiber reinforced thermoplastic composites has attracted the attention of many investigators. Along with the potential for great improvement in mechanical performance, when compared to conventional thermoset resins, there is concern over their less stable nature. The conventional wisdom and cumulative experience collected over years of study of thermoset composites are being continually updated. Such issues as viscoelastic effects, temperature, frequency, environmental durability and sensitivity of (especially of semi- crystalline) thermoplastic polymers to manufacturing parameters, have been readdressed in this context.

New commercial material systems are emerging daily, Quinn and O'Brien [48] present a comprehensive list of thermal, physical and mechanical properties of short and continuous glass and carbon fiber reinforced thermoplastics, at room and elevated temperature. Amorphous versus semi- crystalline polyaryl sulfides have been compared by O'Connor et al. [49], they conclude that the amorphous material has better property retention at high temperature and higher T_g. Kim et al. [50] point out that cooling rate has little effect on the high residual thermal stresses of amorphous resins and that there is minimal stress relaxation during cooling. Jeronimidis and Parkyn [51] also found high residual tensile stresses in the 90° plies of a cross ply (semi- crystalline matrix) composite, greatly reducing the transverse tensile strength.

Much work has been done to identify and characterize the damage modes peculiar to thermoplastic composites. Davies et al. [52] show that unstable crack growth in DCB specimens of Gr/ PEEK at room temperature turns stable at elevated temperature. Newaz and Mall [53] measure mode I delamination growth of Gr/PEEK. While growth follows a Paris law at 70°F, it slows at 200°F and a large damage zone in front of the crack tip is observed. They suggest that at high temperature time dependent relaxation and creep damage form ahead of the crack tip, controlling damage rate.

Other investigators have compared the fatigue response of thermoplastic and thermoset composites. Curtis [54] compares unidirectional and cross ply tensile fatigue behavior of several carbon fibers with epoxy, toughened epoxy, BMI and semi- crystalline thermoplastic. Little change is caused by the different fibers, but great changes are caused by the resin. The thermoplastic had less delamination but has the shortest lives in both, unidirectional and cross ply configurations. Croman [55] found that the flexural fatigue response of Gr/Epoxy is better than Gr/J-polymer. They both fail in compression but have radically different damage, the thermoset delaminated extensively but the thermoplastic did not. Simmonds et al. [56] examined the fatigue response (R=-1) of notched AS4/PEEK and T300/Epoxy. Baron and Schulte [57] do similar comparative work for tensile unnotched fatigue. Both investigations conclude that the higher toughness of PEEK as measured in quasi- static tests does not translate into better long term behavior. For the notched configuration, at low stress levels PEEK lives are much higher and all failures are in compression. At high stress levels, the delaminations in PEEK are confined to the notch area and result in large stress concentrations leading to a transition to tensile failure and much shorter lives than epoxy. In the unnotched configuration, PEEK exhibits less longitudinal and transverse cracks but has lower life at all stress levels.

2.3 Experimental observables and analytical methods

Ideally, the three dimensional state of strain in a material should be known through direct measurement or analysis. Together with knowledge of the stiffness and suitable analytical tools, the state of stress and state of the material could be determined, thus allowing predictions of residual strength and life.

Available techniques of nondestructive testing interrogate the material and assess the damage state by measuring variations in material uniformity and/or material properties caused by imperfections. A variety of non destructive methods have been developed or modified specifically for implementation in composite materials. These include surface replication, X-ray radiography, vibrothermography, ultrasonic C-scans, acoustic emission, etc. A review of NDE techniques and the associated physical phenomena is found in [58].

Special attention has been given to the measurement of stiffness since its reduction has been found to correlate well with damage in many cases and depends only on the material's condition. O'Brien [59], Daniel et al. [60], and others have presented applications of stiffness measurements for indirect assessment of damage growth for different configurations and loading conditions. Reifsnider and Stinchcomb [61] reviewed, described, and investigated the concept of stiffness change as a nondestructive fatigue damage parameter. In general, they found that stiffness change can be quantitatively related to the fatigue life and residual strength of composite laminates through various models of observed micro-damage events and the damage patterns formed by those events. During cyclic loading several damage modes may occur, resulting in a corresponding degradation of stiffness. Many investigators have found that every damage mode is associated with a specific and distinct stage in a typical damage vs life fraction curve.

Laws et al. [62] have developed constitutive equations for unidirectional laminates with an array of parallel cracks, where all terms of the compliance matrix are given as functions of crack density. The same problem was addressed by Gottesman et al. [63], who used complimentary and minimum potential energy principles to evaluate upper and lower bounds on the effective moduli. Both investigations report that fiber dominated properties change very little, but transverse and shear properties change significantly. Supporting this analytical effort are the studies of Camponeschi and Stinchcomb [64], Rotem [65], Daniel et al. [66] and Talreja [67], who have measured changes in all or some moduli during cyclic loading. In general, transverse cracks affect E_{11}, while delaminations and longitudinal cracks affect G_{12}.

Other investigators have focused on correlating stiffness changes to other parameters, such as temperature and frequency. For example, Tsai [68] discusses the effects of cyclic loading frequency on stiffness degradation on terms of viscoelastic behavior. Davidson and Saddler [69] match temperature transients to stiffness changes, as do Neubert et al. [70]. Wevers et al. [71] correlated stiffness and hysteresis loops to acoustic emissions for different damage types.

As damage develops the strength is changed. Fracture occurs when strength is reduced to the applied stress level. Withworth [72] presents a semi- empirical model that correlates residual strength to remaining stiffness as a function of the initial stiffness and strength, stress level and life fraction.

One additional experimental technique that is receiving increasing attention in the composites community in the last few years is the Dynamic Mechanical Analysis, DMA. DMA is a member in a family of experimental techniques initially developed for the characterization of polymers. Other members include Differential Scanning Calorimetry (DSC), Thermo Gravimetric Analysis (TGA), and more. In all these techniques, a relatively small sample is introduced into a temperature controlled chamber. In the instance of DMA, the sample is mechanically vibrated at controlled frequencies and stress levels. Several configurations are available: torsional pendulum, free-edge three point bending and fixed-ends double cantilever beam. The measured parameters include deformation, complex longitudinal, flexural and shear moduli, phase angle, etc. Depending on the sophistication of the equipment and data processing software, different test procedures may be designed (stress, frequency and temperature load histories are determined), ranging from simple stress relaxation to multiplexing and the use of superposition to evaluate time and frequency dependent master curves.

Ting [73] has recently reviewed the theories on dynamic response of composites, including viscoelastic effects. Because of its versatility, a wide range of DMA procedures (by themselves or in combination with mechanical tests) are used in the characterization of many chemical and physical processes taking place in composite materials. Some of the early work was done by Schultz and Tsai [74] and Heller et al. [75], who measured the complex moduli and evaluated master curves using data from different frequencies. The same approach is still widely used, as shown in the work of Sichina and Gill [76] who studied AS4/PEEK. They showed that the master curves change with different crystallinity content. Zhang et al [77] studied the differences between static and dynamic moduli and concluded that these are larger for matrix dominated properties. Camponeschi et al. [78] found that moisture intake affects tanδ for matrix dominated laminates, but E' remains unchanged. Curtis et al. [79] investigated the effect of cooling rate on tanδ of semi- crystalline composites and how that is reflected on toughness by measuring G_{Ic} and G_{IIc}. Ha and Springer [80] predict the behavior of unidirectional laminates at high temperatures based on the DMA characterization of the matrix. Travis et al. [81] investigated the effects of aging on the complex moduli and reported that aging leads to reduced imaginary moduli, lower damping and increased brittleness.

DMA techniques play a very important role in the characterization of interfaces and interphases in composite materials, a subject of great interest that has focused a lot of attention lately. Suzuki and Saitoh [82] have proposed to correlate tanδ to fiber/ matrix interphase strength. Comparing surface treated to untreated glass fibers, they have measured for treated fibers lower tanδ values and higher flexural strength. Banerjee et al. [83] examine the effects of surface treatment of carbon fibers. They found good correlation between treatment and lower tanδ values, but the short beam shear test data is inconclusive. Chua [84] failed to predict the tanδ of unidirectional glass/ polyester with various fiber treatments based on fiber and resin data using the rule of mixtures. He attributes the difference to the interaction and found an inverse relationship between tanδ at the glass transition temperature and short beam shear strength. Silverman and Jones [85] compared the damping and transverse tensile strength of unidirectional laminates of AS4 fibers and 5208 epoxy, polyphenylene sulfide (PPS) and PEEK. They conclude that the thermoplastics laminates have higher damping than thermosets. AS4/PPS has a higher tanδ than the PEEK laminate, but a lower transverse tensile strength.

Of special interest to the present investigation is the magnitude and interaction of rate dependent (frequency) and independent (damage) processes, such as reported by Reifsnider and Williams [86] and Reifsnider et al. [87]. They investigated the changes in compliance, energy dissipation and surface temperature during cyclic loading of notched B/Al and B/Ep specimens at different frequencies. They conclude that strong interactions are present and these affect significantly the cyclic performance as evidenced by the extent and location of damage. Stinchcomb et al. [88] also examined acoustic emission from similar tests and conclude that while E" is frequency dependent, E' changed very little in the range of experimental frequencies but is a function of damage (rate independent). They found that compliance changes correlated well with temperature changes and acoustic emission counts, indicating cyclic dependent damage. Reifsnider et al. [89] discuss all possible heat generating mechanisms and their relative importance. Earlier, Dally and Broutman [90] had assumed that the heat being generated is a linear function of the frequency. They attributed the shorter fatigue life at high frequency to higher specimen temperature. Broutman and Gaggar [91] measured longer fatigue life for neat epoxy and polyester specimens that were cooled during cyclic loading or when loading is regularly stopped to allow the specimen to cool down. They conclude that cumulative damage laws cannot be applied to the evaluation of fatigue life.

DMA techniques have been used by several investigators, such as

Davies et al. [92] and Putter et al [93], to study the frequency response of fiber reinforced composites. Others have used it as a complimentary fatigue characterization tool, such as Adams et al. [94], who measured the changes in frequency response due to cyclic and static damage. Drew and White [95] monitored the natural frequency and damping as a function of flexure cycles, and report good correlation between damping, delaminated area and stiffness degradation. Sims and Bascombe [96] used high speed data acquisition to monitor E', E" and hysteresis loops during fatigue. They found that E' is reduced and $\tan\delta$ increases. They succeeded in correlating the number of cracks to the cyclic and original values of E' and E".

As damage develops strength changes. Hahn and Kim [97] suggested that for a constant amplitude fatigue test, the strain to failure is the same as in a quasi static test. At failure the elastic modulus decreases until is equal to the applied stress divided by the failure strain. This reduction may be achieved in the last few cycles and should be carefully measured. Fracture occurs when strength is reduced to the applied stress level.

Many ongoing investigations have the purpose of understanding the exact relationship between damage state, stiffness, residual strength and fatigue life, and the development of appropriate models. Rotem [98] described a lamina based analysis. The fracture mechanics approach was chosen by Wilkins et. al [99], Chou [100], and Wang and Slomiana [101]. Hashin and Rotem [102] and Poursartip [103] proposed phenomenological theories. Chariewicz and Daniel [104] presented a cumulative damage model based on residual strength and the concept of equal damage curves.

Reifsnider and co-workers [105,106,107] take a hybrid approach; a stiffness based cumulative damage model is used to predict residual strength and life. Subcritical and critical elements within a representative volume are identified. The former are involved in fatigue damage development, while the latter are responsible for the eventual failure. Stiffness changes and models of the damage events are used to estimate stress redistribution, as well as time dependent effects. Residual strength is evaluated at every point in time, and, with the aid of an appropriate failure theory, life is predicted.

2.4 Interaction of rate dependent and independent processes

2.4.1 Isotropic media

The interaction of rate dependent and independent processes in isotropic media has been frequently addressed in the context of low cycle fatigue in a high temperature environment. Wareing and Tomkins [108] discuss all possible interaction mechanisms, but emphasis of analytical and experimental work has been on the interaction of cyclic damage and creep. Manson et al. [109] discussed the role of creep in high temperature low cycle fatigue and Manson [110] reviewed life predictions methods, including the double linear damage rule to account for loading sequence, strain range conversion and the principle of minimum commitment for multi-heat analysis. Batte [111] and Del Puglia and Manfredi [112] commented on the Manson- Coffin theories and proposed approaches to linear and nonlinear damage accumulation. Plumtree [113] suggested adding an interaction term to the double linear damage rule. This term is a function of hold times, the number of cycles between hold times and the stress intensity range.

Many investigators have collected large amounts of experimental data showing interaction effects in isotropic media. For example, Piechnik and Pachla [114] studied the effects of damage on the creep process for concrete. They developed the idea of a limit (failure) strain dependent on load history. Lloyd [115] studied how temperature, frequency, waveform and hold time affect creep- fatigue interaction. Pinau [116] found that creep prior to cyclic loading greatly diminishes life. Evans [117] and Harrison et al. [118] measured order of magnitudes decrease in fatigue life when the specimens are subjected to dwell periods at peak stress, which lead to the accumulation of large plastic strains and change the character of the fracture surface. Wang et al. [119] measured the cyclic creep behavior of Cr-Mo-V steel at ambient and elevated (550°C) temperatures for varying stress ratios ($0 \leq R \leq 1$) and stress levels. They found that at room temperature, cyclic loading with increasing maximum load accelerates creep; increasing R retards creep. At elevated temperature these effects are reversed. They conclude that at low temperature the cyclic part of the load leads to acceleration but at high temperature cyclic creep is dominated by the amount of time spent at the maximum load. In effect, cyclic creep may accelerate or retard creep for the same material at different temperatures. Regrettably, because of the broad range of material properties and behavior, it is hard to draw general conclusions.

Other investigators have approached the interaction at stress concentration points and its effects on damage propagation. Freed and Sandor [120] present evidence that in the vicinity of notches there is great cyclic creep enhancement of damage due to localized plastic deformation. Wareing [121] shows interaction of crack growth and cavitation; and, that cavitation may lead to failure before crack initiation. Sadananda and Shahinian [122] reviewed extensively the experimental data and theoretical models of fatigue and creep crack growth, and the possible interaction mechanisms. They conclude that combined creep- fatigue conditions can either accelerate or retard the growth. Ohji and Kubo [123] reached a somewhat different conclusion. They stated that time dependent and cycle dependent mechanisms compete, crack growth is governed by one dominant mechanism and a transition exists.

Continuum damage mechanics (CDM) offers a completely different approach to the mathematical treatment of damage and its interaction with other processes. Kachanov [124] has reviewed extensively the formulation of its basic principles, the basic assumption being that isotropic materials decrease in strength due to the accumulation of microstructural changes. For example, damage in metals may consist of creep damage, ductile plastic damage, embrittlement, chemomechanical damage and fatigue damage. Polymeric materials may sustain additional types of damage, such as chain scission due to radiation, heat, hydrolysis or reactive compounds, plastification or dissolution by solvents, etc [125,126].

By introducing a new internal variable to account for damage, Kachanov and Rabotonov [127] were able to develop models for creep - fatigue interaction in structures. The one dimensional analysis is extended to multiaxial loading by means of an effective stress. Using appropriate failure criteria, the time to ductile, viscous and brittle failure are predicted. The predictions include time necessary to initiate and propagate damage by means of an idealized moving damage front. Following Lemaitre and Chaboche [128], Kachanov assumes that the total damage sustained by the material can be separated into creep damage and fatigue damage components, and presents a scheme for the nonlinear summation of those. No data is presented in this compendium [124] and only partial success is claimed for the metals studied.

Since the original work by Kachanov more than 30 years ago, many scientists have adopted this approach. Investigators differ in their chosen internal variables(s) or the complexity of damage representation. Chaboche [129] summarizes uniaxial and multiaxial creep- fatigue theories. Krajcinovic [130,131] offers a complete review of CDM philosophies as they have evolved and a critique of the approach.

One of the fundamental problems of the continuum damage approach to creep is the description of creep damage. Belloni et al. [132] propose using density changes, Leckie [133] suggested using creep ductility - the ratio of failure strain and steady state creep strain, and a reference stress method to account for three dimensional stresses. Hult [134] surveys the effects of different void shapes on residual modulus and damage rate. Betten [135] adopted a generalized tensorial power law to model multiaxial stresses, and introduced damage in the creep equations using effective stresses. Murakami and Ohno [136,137] also propose a tensorial description of damage based on changing areas. In other words, creep damage results in the material becoming anisotropic, and a scalar quantity is no longer adequate. They propose a second order symmetric damage tensor and develop anisotropic damage evolution equations that account for creep- fatigue interaction. They also discuss the limitations of fracture mechanics and life prediction based on CDM.

2.4.2 *Fiber reinforced composites, Analytical Efforts*

In recent years Kachanov's approach to damage mechanics has been extended to composite materials by several investigators. Fiber reinforced composite materials, because of their complex micro structure, are susceptible to additional types of damage stemming from the process by which they are put together. Damage representation varies in scale and mathematical complexity, from a single scalar function to high order nonsymmetric tensors for each damage mode.

The simplest approach was suggested by Sidoroff [138], who used a scalar damage function derived from loss of rigidity (distributed though the thickness) to describe damage and damage evolution equations during bending fatigue. Beaumont [139] examined damage growth during tensile cyclic loading and also suggested a scalar representation. Each damage mode, matrix cracking and delamination, is represented by an analytically and experimentally derived scalar function based on stiffness reduction and stress range. Damage growth equations were integrated to obtain the damage state and remaining life predictions for different loading levels, sequences, R ratios and layups. Withworth [72,140] defined a damage function in terms of the original and current axial stiffness. Assuming equal damage rule for different stress levels and the available S/N data, he predicts residual life for dual stress level fatigue. Wnuk and Kriz [141] also use a single scalar damage function, but assume that damage has two stages: localization and propagation. Following the creation of the characteristic damage state [172], a damage band of fiber breaks is formed ahead of a dominant crack. Crack growth was computed using a finite element solution of the stress field ahead of the crack. Failure is assumed to occur when the total damage reaches a critical value.

Although Beaumont and Withworth show good agreement with experimental data using scalar damage representation based on global stiffness reduction, most investigators agree that all the terms in the lamina and/or laminate compliance tensor are potentially affected by damage. Accordingly, only second (or higher) order damage tensors are appropriate to fully describe these effects.

The variety of approaches to the definition of the damage tensor reflects the difficulties in applying CDM concepts to composite materials. Shen et al. [142] represent damage caused by a crack and the damaged surroundings by an area of reduced stiffness. Then, a second order damage tensor is defined in terms of the damaged compliances. Peng et al. [143] stress the anisotropic nature of damage. They define three principal damage parameters in terms of degraded stiffnesses using Lekhnitskii's stress analysis and show results for notched plates. Talreja [144,145] goes one step further, defining second order damage tensors for each damage mode which is represented by a vector field averaging the size and area of the damage. The "damaged" constitutive equation is obtained by adding the elastic and damage tensors. For simple cases the damage tensor components are derived from measured changes in the four elastic constants of the orthotropic material. In a series of papers, Allen and co-workers [146,147,148,149] propose internal damage variables associated with crack opening and direction, derived from free energy thermodynamic considerations. Based on this approach, they propose second order symmetric damage tensors for each damage mode. Constitutive equations including damage were developed for the cases of matrix cracking and interply delamination. The stress redistribution among plies and the corresponding changes in the laminate's moduli were evaluated. An even more complex representation is proposed by Zhen Shen et al. [150], who suggest a fourth order damage tensor together with a damage strain energy release rate concept, a function of the original elastic properties and reduced/ damaged moduli. Englblom [151] changed the scale of the approach by looking at the effects of damage at the lamina level. The laminate's response is computed using damaged lamina compliance tensors and classical lamination theory.

Whether a single scalar or a fourth order tensor, all of the above studies approach damage as an internal variable that accounts for the change in the elastic response of the laminate. In fact, some of the more complex theories offer only marginal advantages over the simpler ones. It is important to note that none of the above address the interaction of cyclic damage modes with other processes, are unable to discern between rate dependent and independent processes, and cannot deal with phenomena not directly represented by stiffness changes.

In this respect, the analytical treatment by Weitsman is unique, and closest to the spirit of the present study. Weitsman [152] first approached the coupling between damage and moisture transport. Damage is represented by a skew symmetric second order tensor where each term is a function of the ratio of the fiber/matrix debond area within a representative cell and the cell's surface area. The analysis shows that stress and moisture have a synergistic effect. In a later paper, Weitsman [153] discusses the coupling of damage and heat conduction in unidirectional composites. Here damage is represented by two second order symmetric tensors, who represent the open and closed crack surfaces. These are used to compute heat conduction coefficients for the damaged laminate. Weitsman [154] also formulated a continuum damage model for viscoelastic materials (linear viscoelastic bodies and particulate reinforced). Using the same two damage tensors described above and assuming that all the compliance terms have the same time dependency, he evaluates the overall compliance tensor changes and the changes of symmetry in the material. Weitsman also shows how this model can be reduced to Schapery's integral equation for time dependent strain with an added damage term. Weitsman reaches interesting conclusions. Contrary to the findings of Tobolsky [125] and Murakami and Ono [126] who studied the effect of chemical damage on the rheological behavior, Weitsman suggests that the retardation times are unaffected by cyclic damage, although damage growth is influenced by the inherent viscoelasticity of the material. In his work, Weitsman addresses only briefly the issue of damage evolution equations, and deplores the lack of adequate data necessary to validate and calibrate such equations.

2.4.3 Fiber reinforced composites, Experimental Efforts

Some of the experimental studies that consider the mechanisms and extent of the interaction between cyclic damage and viscoelastic behavior in composite materials will be discussed in the following paragraphs. In many instances, it is the findings in the laboratory that have lead the investigators to consider viscoelastic effects. Only a few have dedicated their efforts to this specific task.

Rotem [155] and later Rotem and Nelson [156] characterized the fatigue response of [0/±θ/0] graphite/epoxy laminates at 22, 74 and 114°C. They found that the stress relaxation in the ±θ° plies changes the stresses in the 0° plies, reducing the fatigue life of the laminate. The magnitude of this effect increased at higher temperatures. They postulate that on the basis of the strength and S/N curves of unidirectional and ±θ° laminates at various temperatures, the fatigue response of [0/±θ/0] laminates can be predicted by appropriate shift factors.

The temperature of the specimen may also rise due to viscoelastic heat dissipation. In their study, Menges and Thebing [157] predicted the equilibrium temperature rise under sinusoidal loading and the additional cyclic deformation when compared to creep at constant mean load. In fact, Jinen [158] showed that the creep deformation could be as little as half of the cyclic creep deformation in short fiber reinforced thermoplastics. He also found evidence of different damage modes for fatigue and creep failures.

Lifshitz [159] investigated the compressive creep and fatigue response of 0°, 90° and ±45° graphite/epoxy laminates. He found that 0° plies are elastic but 90° and ±45° laminates creep significantly with large hysteresis (for ±45°). Lifshitz comments on possible mechanisms by which viscoelastic behavior affects the stress redistribution during fatigue loading.

Sturgeon [160] conducted tensile creep, intermittent creep and tensile fatigue (R=0) loading experiments on $[\pm 45_2]_s$ carbon/epoxy laminates, to study the possible interaction of cyclic and time dependent behavior, also looking at the effects of temperature and frequency. Although intended to be a preliminary study, it is interesting to note that Sturgeon addressed all major issues and described an experimental procedure to capture such interactions. Sturgeon found that all the tested loadings result in creep strains that have recoverable and permanent components, but the absolute and relative magnitudes of these components vary for different conditions. For creep loading a constant creep rate was achieved but cyclic loading exhibited a tertiary accelerating stage accompanied by extensive inter and intra ply cracking, temperature rise and large stiffness degradation. Higher temperature, intermittent creep and cyclic loading also resulted in larger permanent deformation, increasing with the number of cycles, and larger than expected from the measured stiffness reduction. Significant temperature rise was measured in fatigue specimens cycled at 10 Hz, but it was negligible at 1 Hz. For fatigue specimens, the stages in the temperature rise match the deformation stages at maximum cyclic load. Sturgeon concluded that cyclic damage in the form of cracks occurs mainly during the tertiary stage and managed to correlate remaining life at this stage with the deformation at maximum load, clearly indicating that cyclic and time dependent effects interact in a synergistic fashion.

Sun and Chan [161] examined the frequency effect on the tensile fatigue life of $[\pm 45]_{2s}$ Gr/Ep laminates with a central hole, by testing at four frequencies and three stress levels. They measured the temperature rise next to the hole and found that its magnitude grew larger with increasing frequency and/or stress level. They found that fatigue life at constant stress level peaks at a certain frequency and lower the stress level had higher frequency peaks. The authors explain their findings in terms of competing damage modes (see Ohji and Kubo [123] for isotropic materials). They suggest that at constant stress level a transition from creep to cyclic dominated fatigue damage occurs by increasing the frequency. At low frequencies creep damage is dominant (see Newaz and Mall [53]), and life is proportional to frequency, at high frequencies there are large temperature rises, cyclic damage dominates and life is inversely proportional to frequency. Following this argument, higher stress levels lead to lower a peak fatigue life frequency. Again, time dependent behavior has been shown to influence fatigue life in unexpected ways.

Saff [162] repeated the work of Sun and Chan [161] for three laminate configurations with a center hole, but he cooled the specimens so that these tests were conducted at constant temperature. He confirmed the findings of Sun and Chan. Contrary to the findings of Broutman and Gaggar [91] for unreinforced resins, Saff concluded that higher frequency usually leads to longer fatigue lives and that cooling does not affect fatigue life significantly. This effect is saturated for fiber dominated lay ups for frequencies above 1 Hz. In fact, the arguments presented by Sun and Chan can be easily applied to explain the perplexing results reported by Reifsnider et al. [87] and

Stinchcomb et al. [88], who measured a transition in the fatigue stiffness degradation and specific damping of B/Al and B/Ep laminates with a central hole when the frequency was varied from 0.5 to 45 Hz.

Sun and Chim [163] investigated the possible consequences of intermittent tensile fatigue with hold times at the maximum cyclic load or periods of unloading for $[\pm 45]_{2s}$ Gr/Ep laminates with a central hole. The effects of dual frequency loading were also examined, as well as the heating of the specimen near the hole. They found that hold periods result in increasing fatigue life, in complete contradiction to Evans [117] and Freed and Sandor [120] findings for isotropic plates with a hole. Also, low frequency loading accompanied by significant creep followed by high frequency has a much larger fatigue life than vice versa, in contradiction to Pineau [116] who found that creep prior to high cyclic loading greatly diminished fatigue life for isotropic media. These findings, which defy any damage summation rule and are in complete contradiction to the results presented in the previous section on isotropic media, were qualitatively explained by allowing for cyclic and time dependent interaction in a fashion unique to composite materials. Sun and Chim suggest that in general hold periods allow for cooling of the specimen (see also Broutman and Gaggar [91]), thus retarding fatigue damage. Hold periods at maximum load also accelerate creep deformation at the notch relaxing the stress concentration and resulting in even greater fatigue retardation. As Sun and Chan [161] before them, they explain the dual frequency behavior by suggesting that at low frequencies creep deformation is dominant, slowing down cyclic damage and increasing life.

Mandell and Meier [164] conducted a similar study where they varied the stress ratio, frequency and wave shape in cross ply glass/epoxy laminates. They measured fatigue lives for trapezoidal, loading spikes and unloading spikes wave forms. They also measured creep rupture times. The found that S/N curves change position and slope for different frequencies and wave forms but never intersect. Higher frequency leads to a higher number of cycles to failure. The order of the S/N curves is reversed when plotted versus the cumulative time to failure. At the same maximum load, trapezoidal loading has the shortest life, then unloading spikes and loading spikes. Like Saff [162], Mandell and Meier suggest that cumulative time under load dominates life time at room temperature. Varying the stress ratio had a nonlinear effect on the cumulative time to failure. They also measured the effect of 100 pre-cycles on creep rupture time. They found that low frequency pre-cycling leads to significant reductions in creep rupture times.

The work of Sun and Chan [161] and Sun and Chim [163] has been extended recently by Dan-Jumbo, Zhou and Sun [165] to include thermoplastic laminates. They investigated the frequency response of three layups of IMP6/APC-2 graphite/thermoplastic and a $[\pm45]_{2s}$ graphite/BMI (IM7/5250-2) laminate with center holes. The temperature next to the hole, specimen stiffness and hysteresis loops were monitored. The found that the tension-tension fatigue life of the

$[\pm45]_{2s}$ thermoplastic laminate decreases as frequency increases, contradicting measured behavior of similar thermoset laminates [161, 162, 164]. Generally, the fatigue response of the thermoplastic $[\pm45]_{2s}$ laminate is better than that of the thermoset $[\pm45]_{2s}$ laminate at low frequencies. At high frequencies the thermoplastic composite generates much more heat reducing the fatigue life significantly. This effect could explain the findings of Croman [55], Simmonds et al. [56], and Baron and Schulte [57] who reported poorer fatigue response for thermoplastic composites when compared to thermoset counterparts. For other layups, the magnitude of the viscoelastic interaction depended on stress level and stress ratio. Like in the previous studies, the fatigue life of matrix dominated laminate exhibit a maximum at some intermediate frequency.

Lang et al. [166] investigated the crack propagation in short glass fiber reinforced nylon at different frequencies. They postulate that heat generation occurs at the bulk level - hysteretic, and at the local level due to the stress concentration and plastic deformation at the crack tips. The temperature increase at the crack tip results in a higher plastic deformation zone and lower yield stress, retarding crack propagation. Bulk hysteretic heating reduces the storage modulus and increases crack opening displacement, thus accelerating crack propagation. The magnitude of these two competing mechanisms is frequency dependent and could explain the maxima in the maxima in the fatigue life versus frequency response.

While damage growth has been shown to be affected by viscoelastic effects, very little has been done to find if the reverse applies. It is interesting to note the work by Ke et al. [167], who used the DMA technique to study how the viscoelastic response of Gr/Ep unidirectional laminates changes during fatigue loading. By examining the complex moduli, they found that very little changes occur in the real component of the axial stiffness, but the shape and values of the imaginary component change significantly (compare to Sims and Bascombe [96]). The authors attribute these changes to damage of the fiber/matrix interphase (see also Suzuki and Saitoh [82] and Banerjee et al. [83]). This study confirms that damage affects the viscoelastic response in more ways than assumed by Weitsman [154], and opens additional avenues for study and research.

Some of these experimental findings seem to be at odds with the observed behavior of isotropic media. The inconsistency and intricacy are attributed to the unique microstructure and thermorheological complex nature of fiber reinforced composites. While the continuum damage mechanics approach has been partially successful dealing with such interactions for engineering metals, it has been extremely difficult to extend it to composite materials. At this time there are no alternative analytical models, able to predict the surprising behavior of composite materials.

3 Analysis

3.1 General Concepts

Modeling coupling effects of rheological behavior during fatigue loading could be attempted at different scale levels and with different degrees of rigor and sophistication, starting from the atomic/ molecular domain and progressing up to the global/ structural regime. There is no unique "right" way to proceed; but, in order to capture the details of the physical phenomena being modeled, the scale should be similar to that of the process. Even then, the appropriate scale is arbitrary in the sense that only global changes can be experimentally measured and used to calibrate or corroborate the analytical assumptions. The lamina level has been chosen as the adequate building block, averaging all events and processes occurring within its volume. In turn, the lamina performance is measured in terms of deformation, temperature, stiffness and strength.

In the present approach, each lamina of different material and/or orientation is represented by a rheological pseudo-analog mechanical - **PAM** - model. In the most general case, as shown in Figure 3.1 for the one dimensional case, the lamina model consists of a free spring, a series of Kelvin elements and a series of pseudo-Kelvin elements with "negative" spring coefficients. Adopting a modified Wilshire-Evans approach [22], five parameter pseudo-analog models are used to

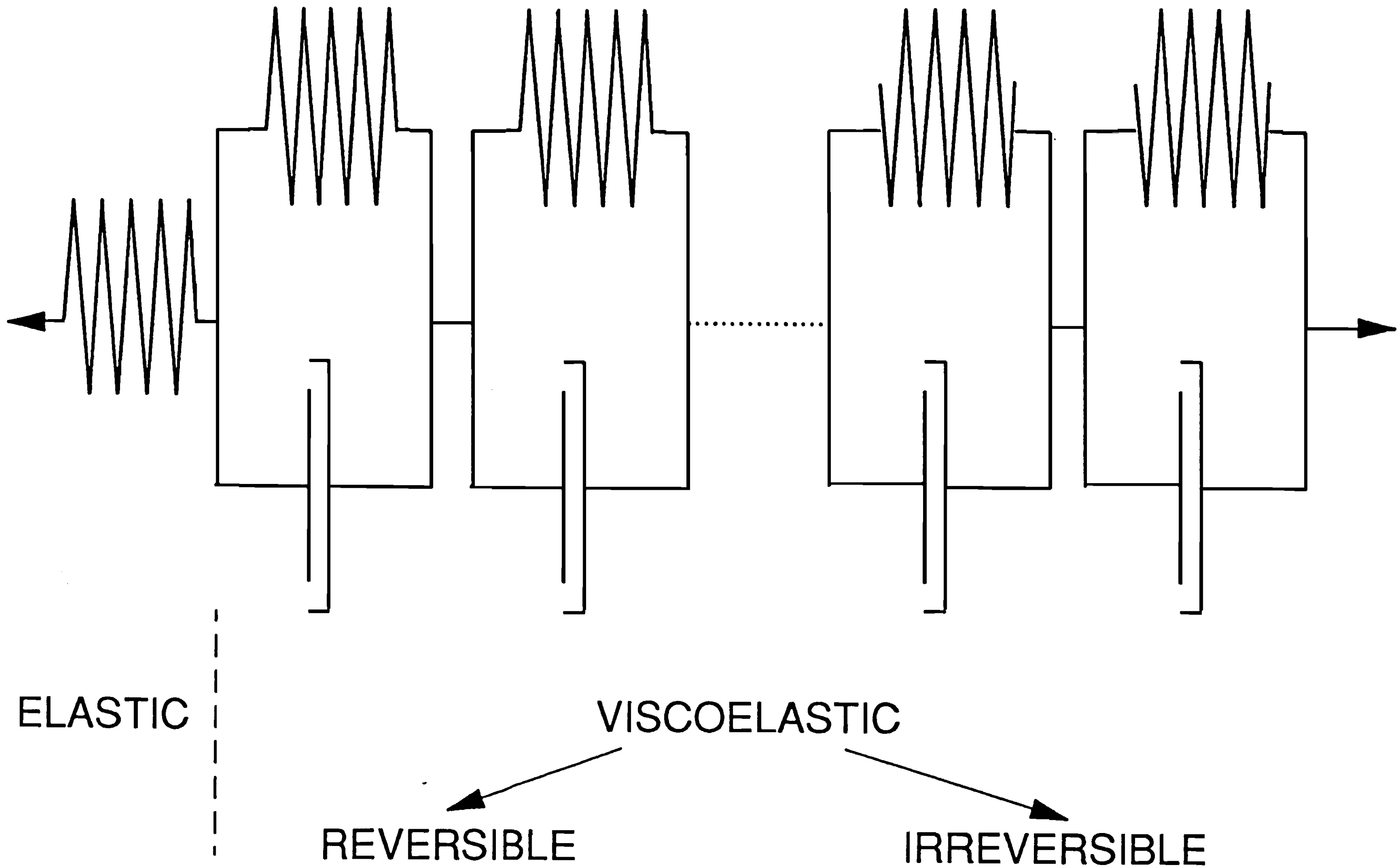

Figure 3.1 **Generalized PAM lamina model**

describe the time-dependent behavior and nonlinear viscoelastic effects (see details of the Wilshire-Evans approach in chapter 2). This is the most simple representation of the general lamina model that still retains all of its major features. The laminate general model, consisting of 5-parameter lamina sub-models, is shown in Figure 3.2.

The analytical tools used to compute local stresses within the representative volume may be as simple as classical lamination theory or as complex as three dimensional solutions derived from anisotropic elasticity theory and the appropriate boundary value problems. Multiaxial loading may be simplified by evaluating a uniaxial effective stress and using a one dimensional model. Obviously, tradeoffs between accuracy and complexity of analysis are warranted. At this stage, classical lamination theory (with thermal stresses) and the usual plane stress assumptions will be used to compute the stresses at the lamina level and a suitable effective stress.

Laboratory data and analytical stress analysis codes are used to evaluate the initiation, growth and interaction of rate dependent and independent damage mechanisms. These events are represented as suitable changes in the response of the different plies. The rheological model coefficients are evaluated as functions of stress, temperature and other suitable internal variables. A governing differential equation that describes the constitutive behavior of the laminate is obtained. Depending on the complexity of the analog representation and loading conditions, a closed form or a numerical

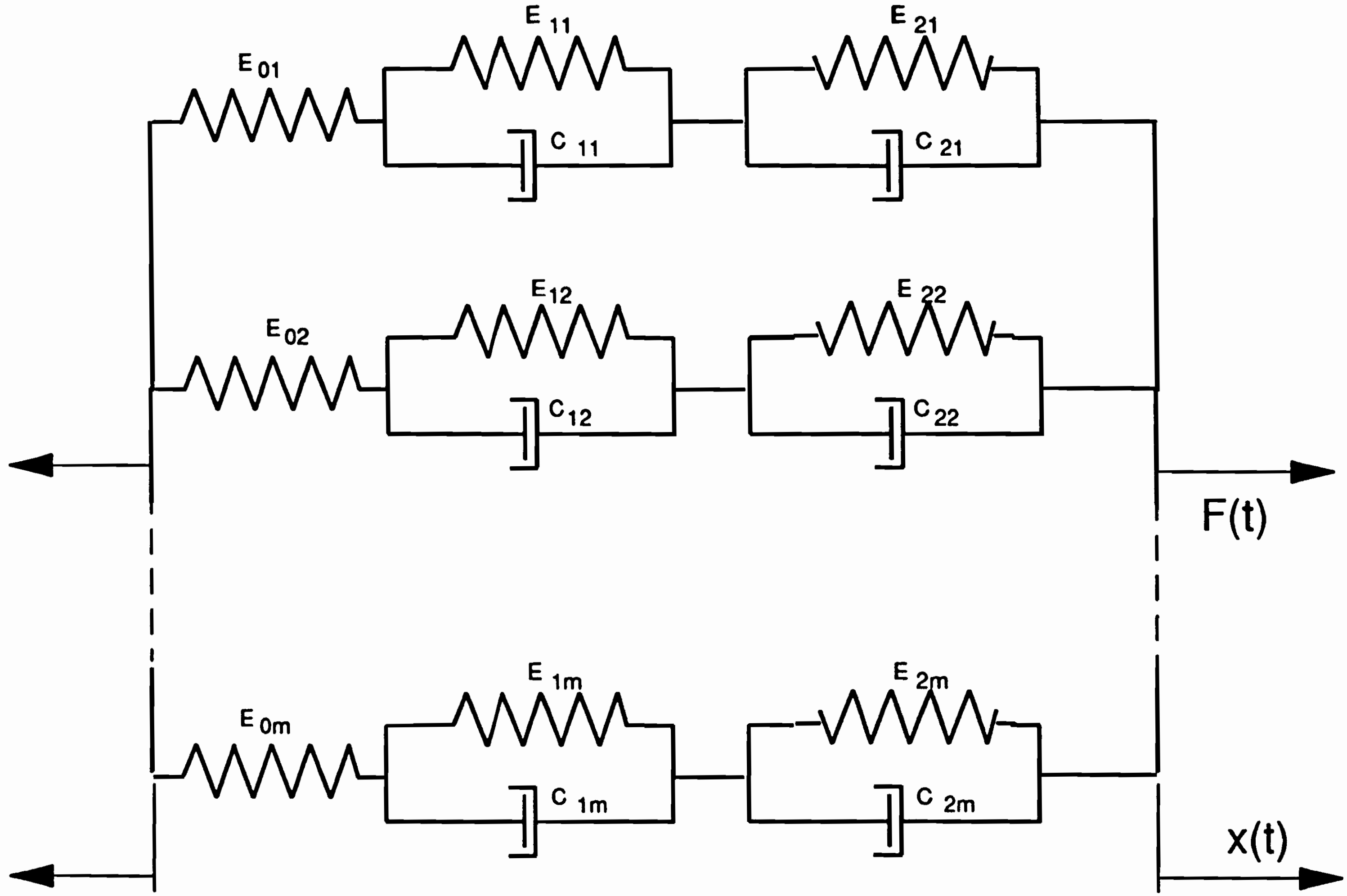

Figure 3.2 **Generalized laminate model with 5-parameter branches**

solution can be found. This relationship is assumed to hold constant for a certain time interval where the coefficients are relatively constant. The rate of change and other convergence criteria are used to determine the time span for which this assumption is valid. The end result is a numerical procedure able to predict the interaction of time and cyclic processes and to emulate the performance evolution of a laminate subjected to any arbitrary cyclic loading. With the aid of an appropriate failure criterion, it could be used in the future to evaluate the remaining life of the structure.

3.2 General Lamina Characterization

3.2.1 Thermorheological Viscoelastic Model

The procedure employed in the thermorheological characterization of the selected composite material system is based on the arguments of Wilshire and Evans [22] and the similarity of the θ projection to a five parameter mechanical analog model. Adding the elastic response term to Eqn. 2.1.5 makes it equivalent to a mechanical analog model with two Kelvin elements and a free spring,

$$\varepsilon(t) = \frac{\sigma}{E_0} + \frac{\sigma}{E_1}\left[1-\exp(-E_1 t/\mu_1)\right] + \frac{\sigma}{E_2}\left[1-\exp(-E_2 t/\mu_2)\right] \qquad (3.2.1)$$

or expressed as time dependent compliance,

$$D(t) = D_0 + D_1\ [1-\exp(-t/\tau_1)] + D_2\ [1-\exp(-t/\tau_2)] \tag{3.2.2}$$

where the first term reflects the elastic response, and the usual W-E parameters can be expressed in terms of the pseudo-analog mechanical (PAM) model parameters

$$\theta_0 = \frac{\sigma}{E_0} \qquad \theta_1 = \frac{\sigma}{E_1} \qquad \theta_3 = \frac{-\sigma}{E_2} \qquad \theta_2 = \frac{E_1}{\mu_1} \qquad \theta_4 = \frac{-E_2}{\mu_2}$$

A new set of ϕ_i parameters is defined as,

$$\phi_0 = D_0 = \frac{1}{E_0} \qquad \phi_1 = D_1 = \frac{1}{E_1} \qquad \phi_2 = -D_2 = \frac{-1}{E_2}$$

$$\phi_3 = \tau_1 = \frac{\mu_1}{E_1} \qquad \phi_4 = \tau_2 = \frac{-\mu_2}{E_2} \tag{3.2.3}$$

To express the stress and temperature dependence of the new ϕ_i parameters, Eqn. 2.6 proposed by Wilshire and Evans is modified to account for the polymeric nature of the matrix. Eqn. 3.2.4 shows the proposed relationship which includes the matrix glass transition temperature T_g,

$$\log \phi_i = a_i + b_i\sigma + c_i \ln \frac{T_g - T}{T_g} + d_i\sigma \ln \frac{T_g - T}{T_g} \qquad (3.2.4)$$

where i=0 through 4, T is the absolute temperature, and the relationships hold only for temperatures below T_g.

A complete stress and temperature sensitive 5-parameter pseudo-mechanical analog model of the lamina is obtained consisting of up to 20 material constants. The constants can be determined independently from a series of tests at constant temperature - variable stress and at constant stress - variable temperature.

It should be noticed that linear elastic and viscoelastic behavior reduces this number to 10 constants. A small temperature dependence within the test range may reduce further this number to the original 5 parameter model. The stress and temperature dependence of the 5-parameter model is given by,

$$E_0(\sigma,T) = \frac{1}{\exp\left[a_0 + b_0\sigma + c_0 \ln \frac{T_g - T}{T_g} + d_0\sigma \ln \frac{T_g - T}{T_g}\right]} \qquad (3.2.5)$$

$$E_1(\sigma,T) = \frac{1}{\exp\left[a_1 + b_1\sigma + c_1 \ln \frac{T_g - T}{T_g} + d_1\sigma \ln \frac{T_g - T}{T_g}\right]} \qquad (3.2.6)$$

$$E_2(\sigma,T) = \frac{-1}{\exp\left[a_2 + b_2\sigma + c_2 \ln \dfrac{T_g - T}{T_g} + d_2\sigma \ln \dfrac{T_g - T}{T_g}\right]} \tag{3.2.7}$$

$$\mu_1(\sigma,T) = \exp\left[(a_3-a_1)+(b_3-b_1)\sigma + (c_3-c_1)\ln \frac{T_g - T}{T_g} + (d_3-d_1)\sigma \ln \frac{T_g - T}{T_g}\right] \tag{3.2.8}$$

$$\mu_2(\sigma,T) = \exp\left[(a_4-a_2)+(b_4-b_2)\sigma + (c_4-c_2)\ln \frac{T_g - T}{T_g} + (d_4-d_2)\sigma \ln \frac{T_g - T}{T_g}\right] \tag{3.2.9}$$

By checking the dimensions of all parameters, it can be shown that E_0, E_1 and E_2 have units of stiffness (stress) and μ_1 and μ_2 have units of viscous coefficients (stress-time). The only peculiarity is the negative value of E_2, which reflects the damage accelerating nature of this term.

3.2.2 Constitutive Behavior

The conditions of a 5-parameter PAM require that,

$$\varepsilon = \varepsilon_0 + \varepsilon_1 + \varepsilon_2 \tag{3.2.10}$$

and $\sigma = \sigma_0 = \sigma_1 = \sigma_2$ (3.2.11)

where

ε is the total strain,

0,1,2 subscripts denote the elastic, first and second Kelvin elements of the 5-parameter PAM model, and

σ is the applied stress

Using the Laplace Transform, the transformed strain is given by,

$$\bar{\varepsilon} = \frac{\bar{\sigma}}{E_0} + \frac{\bar{\sigma}}{E_1 + \mu_1 s} + \frac{\bar{\sigma}}{E_2 + \mu_2 s} \tag{3.2.12}$$

where bars denote the values in the transform domain and s is the Laplace transform variable.

The constitutive equation is derived by applying the Inverse Laplace Transform,

$$(E_0E_1E_2)\ \varepsilon + (E_0E_1\mu_2 + E_0E_2\mu_1)\ \dot{\varepsilon} + (E_0\mu_1\mu_2)\ \ddot{\varepsilon} =$$

$$(E_1E_2 + E_0E_2 + E_0E_1)\ \sigma + (E_1\mu_2 + E_2\mu_1 + E_0\mu_2 + E_0\mu_1)\ \dot{\sigma} + \ddot{\sigma} \tag{3.2.13}$$

or in short notation and dividing by the coefficient of σ, the constitutive behavior of the 5-parameter PAM is given by,

$$qa0\ \varepsilon + qa1\ \dot{\varepsilon} + qa2\ \ddot{\varepsilon} = \sigma + pa1\ \dot{\sigma} + pa2\ \ddot{\sigma} \tag{3.2.14}$$

where,

$$qa0 = \frac{E_0 E_1 E_2}{E_1 E_2 + E_0 E_2 + E_0 E_1} \tag{3.2.15}$$

$$qa1 = \frac{E_0 E_1 \mu_2 + E_0 E_2 \mu_1}{E_1 E_2 + E_0 E_2 + E_0 E_1} \tag{3.2.16}$$

$$qa2 = \frac{E_0 \mu_1 \mu_2}{E_1 E_2 + E_0 E_2 + E_0 E_1} \tag{3.2.17}$$

$$pa1 = \frac{E_1 \mu_2 + E_2 \mu_1 + E_0 \mu_2 + E_0 \mu_1}{E_1 E_2 + E_0 E_2 + E_0 E_1} \tag{3.2.18}$$

$$pa2 = \frac{\mu_1 \mu_2}{E_1 E_2 + E_0 E_2 + E_0 E_1} \tag{3.2.19}$$

The complete solution to Eqn. 3.2.14 requires that the two roots (r) of the characteristic equation 3.2.20 be real and distinct,

$$qa0 + qa1 * r + qa2 * r^2 = 0 \tag{3.2.20}$$

This condition can be expressed as

$$qa1^2 - 4 * qa0 * qa2 > 0 \tag{3.2.21}$$

Substituting Equations 3.2.15 through 3.2.19 into Equation 3.2.21, it can be shown that

$$qa1^2 - 4 * qa0 * qa2 = \frac{[E_0 E_1 \mu_2 - E_0 E_2 \mu_1]^2}{(E_1 E_2 + E_0 E_2 + E_0 E_1)^2} > 0 \tag{3.2.22}$$

Condition 3.2.21 is always met since the numerator is always positive.

3.3 Cross-Ply Laminates

Cross-ply laminates were selected as a testing case because of the relative simplicity of the stresses, known damage mechanisms, and limited thermorheological characterization needed to predict the behavior of such laminates under a variety of loading conditions.

3.3.1 Cyclic Stress Analysis and Life Prediction

Global stress analysis is performed using Classical Lamination Theory (CLT). Details of CLT and the multiaxial stress evaluation at the ply level are found in [170]. In the undamaged state the plies are assumed to be linear elastic and perfectly bonded. CLT is used to compute the initial mechanical and thermal stresses and the global cyclic stress and strain ranges.

Damage mechanisms in cross-ply laminates occurring during cyclic loading consist of:

1. transverse matrix cracking in the 90° plies,
2. dispersed longitudinal matrix cracking in the 0° plies,
3. localized (major) longitudinal cracking,
4. delamination of the 0°/90° interface along transverse cracks,
5. small local delaminations at the intersection of longitudinal and transverse cracks.
6. fiber-matrix debonding and fiber fracture at preferential locations are also observed.

The first stage in the evolution of cyclic damage is the development and multiplication of transverse cracks in the 90° plies. The state of damage depends on the current state of stress and the fatigue characteristics of the 90° lamina [60,66]. The crack density increases with number of cycles. Eventually a saturation pattern, named the Characteristic Damage State (CDS), is reached. It is dependent on geometry, material properties and stacking sequence. It is independent of load history, initial stresses and global geometry. As cracking progresses, the load is redistributed to the 0° plies which carry an increasingly larger share of the global load. Additionally, at the tips of the cracked plies there is a local stress concentration and a complex three dimensional tensile state of stress [171].

Global and local considerations combine to determine the remaining life of the laminate after the CDS has been achieved. Reifsnider [172] and later Highsmith and Reifsnider [173] have postulated a shear-lag mathematical model to predict the CDS. Based on these analytical capabilities, available software developed by the Materials Response Group at VPI&SU [174] was used to predict the saturation crack spacing in the 90° and 0° plies, the stress concentration in the 0° plies at the crack tip, and the average stiffness of the cracked plies for any crack spacing up to the CDS.

Following Lee et al. [175], the first step in the evaluation of lamina stresses once damage has initiated in the 90° plies is to find the average stress in the 90° plies as a function of crack density λ,

$$\sigma_2(\lambda) = \frac{E_2(\lambda)}{E_x(\lambda)} * \sigma_{max} \tag{3.3.1}$$

where

σ_{max} maximum applied global cyclic stress,

$\sigma_2(\lambda)$ stress in the load direction, 90° plies with crack density λ,

$E_2(\lambda)$ average transverse modulus, 90° plies with crack density λ,

$E_x(\lambda)$ axial laminate modulus with crack density λ given by the rule of mixtures as,

$$E_x(\lambda) = \frac{1}{1+k90} [E_1 + k90 * E_2(\lambda)] \tag{3.3.2}$$

where

k90 is the ratio of 90° to 0° plies and,

E_1 is the longitudinal lamina modulus.

Ryder and Crossman [176] have shown that the variation of the in-situ transverse modulus of the 90° plies can be represented by an approximately linear normalized master curve for all cross ply laminates. The general form of this master curve is,

$$E_2(\lambda) = E_2(0)[1 + \beta*\lambda*h90] \tag{3.3.3}$$

where

$E_2(0)$ is the undamaged transverse modulus,

h90 is the total thickness of the 90° plies, and

β is the slope of the master curve $E_2(\lambda)/E_2(0)$ vs. λ*h90.

From the work of Ryder and Crossman, it follows that the average stress in the cracked 90° plies is,

$$\sigma_2(\lambda) = (1+k90)\,\frac{1 + \beta*\lambda*h90}{E_1/E_2(\lambda) + k90\ (1+\beta*\lambda*h90)} \tag{3.3.4}$$

For global cyclic stress levels below the static load at which the CDS is achieved, the second step is to evaluate the number of cycles necessary to reach the CDS. For higher stress levels this number is 1. The fatigue life of the 90° plies could be approximated by a simple logarithmic expression for the stress-life relationship,

$$\log \sigma_2 = b90 * \log N_f(90°) + \log YT \tag{3.3.5}$$

where

YT is transverse static tensile strength,

$N_f(90°)$ number of cycles to failure at a maximum cyclic stress σ_2, and

b90 is a curve fitting parameter

Using the in-house CDS software, the saturation crack spacing λ_{cds} and the parameter β can be evaluated. Using Eqn. 3.3.4, the stress in the 90° plies is determined at λ_{cds}. Using Eqn. 3.3.5 and the computed stress $\sigma_2(\lambda_{cds})$, the number of cycles to the saturation cracking is predicted.

The third step is to determine the average stiffness of the 90° plies as a function of cycles. Using Equations 3.3.1 - 3.3.4,

$$1 + \beta*\lambda*h90 = \frac{\sigma_2(\lambda)*E_1}{\sigma_{max}*E_2(0)*\left(1 + k90 - \frac{\sigma_2(\lambda)}{\sigma_{max}} * k90\right)} \tag{3.3.6}$$

Using the fatigue life relationship 3.3.5,

$$1 + \beta*\lambda*h90 = \frac{E_1*YT*n^{b90}}{E_2(0)*\left(\sigma_{max} + \sigma_{max}k90 - k90*YT*n^{b90}\right)} \qquad (3.3.7)$$

Finally, introducing 3.3.7 in 3.3.3, the average transverse modulus is obtained as a function of cycles n,

$$E_2(n) = \frac{E_1*YT*n^{b90}}{\sigma_{max}(1+k90) - k90*YT*n^{b90}} \qquad (3.3.8)$$

It is obvious that the average transverse modulus of the 90° cracked plies is a complex function of the lamina undamaged properties, 90° fatigue characteristics, laminate stacking sequence and the global cyclic loads. Equation 3.3.8 is similar to that obtained by Lee et al. [175].

In addition to the changes in average modulus, the progressive cracking of the 90° plies changes the strain concentration at the tip of the cracked plies. Examining the shear-lag model, as it was presented in [174], the present author observed that the local strain concentration at tip of the cracked 90° plies obeys a linear relationship with the normalized crack spacing. This relationship can be expressed as,

$$\frac{K(\lambda)}{K(0)} = 1 + \delta * \lambda * h90 \tag{3.3.9}$$

where

K(λ) is the strain concentration for λ crack spacing,

K(0) is the strain concentration for the first crack, and

δ is the slope of the master curve K(λ)/K(0) vs. λ*h90

Using the relationships developed above, the stress concentration as a function of cycles, K(n), can be expressed as,

$$\frac{K(n)}{K(0)} = 1 + \frac{\delta}{\beta}\left[\frac{E_1/E_2(0)*YT*n^{b90}}{\sigma_{max}(1+k90) - k90*YT*n^{b90}} - 1\right] \tag{3.3.10}$$

or in terms of the transverse modulus after n cycles,

$$\frac{K(n)}{K(0)} = 1 + \frac{\delta}{\beta}\left[\frac{E_2(n)}{E_2(0)} - 1\right] \tag{3.3.11}$$

After the CDS is achieved, the transverse modulus and local stress concentration are assumed to remain approximately constant until delaminations or damage in the 0° plies develops. The above equations are used in the cyclic CLT stress analysis to evaluate the local stresses and strain ranges to which the 0° plies are subjected.

The last step is to compute the stiffness, strength and remaining life of the 0° plies, the critical element whose failure causes the laminate to fail. The residual stiffness and strength of a 0° unidirectional laminate subjected to cyclic loading are evaluated using a modified Withworth approach [72,140]. The dynamic stiffness is fitted with a power law,

$$E_1(n) = E_1(0) - mb * \left(\frac{n}{N_f(0°)} \right)^{pb} \tag{3.3.12}$$

where

$E_1(0)$ is the undamaged longitudinal modulus,

$E_1(n)$ is the longitudinal modulus after n cycles,

$N_f(0°)$ is the number of cycles to failure at the current stress level, 0° unidirectional laminate,

pb is curve fitting parameter, and

mb = $E_1(0)$ - E_1(fracture), the total axial stiffness change.

The residual strength during cyclic loading of a unidirectional laminate is also fitted with a power law,

$$RS(n) = RS(0) - [RS(0) - \sigma_{max}]* \left(\frac{n}{N_f(0°)} \right)^{qb} \tag{3.3.13}$$

where

RS(0) is the quasi static strength in the fiber direction,

RS(n) is the residual strength after n cycles,

σ_{max} is the maximum cyclic stress, and

qb is a curve fitting parameter.

Combining 3.3.12 and 3.3.13, the normalized residual strength is given by,

$$\frac{RS(n)}{RS(0)} = 1 - \left(1 - \frac{\sigma_{max}}{RS(0)}\right)\left[\frac{E_1(0) - E_1(n)}{mb}\right]^{qb/pb} \qquad (3.3.14)$$

3.3.2 Time-Dependent Constitutive Behavior

The general pseudo-analog viscoelastic model for a cross ply laminate and denominations of the PAM elements are shown in Figure 3.3. It consists of two parallel branches, a single spring element depicting the elastic behavior of the 0° plies, and a full 5-parameter analog branch representing the 90° plies. The conditions of this 2-branch, 6-parameter PAM require that,

$$\varepsilon_s = \varepsilon_c \qquad (3.3.15)$$

and $$\sigma = v_s * \sigma_s + v_c * \sigma_c \qquad (3.3.16)$$

where

s,c subscripts, denote the s-subcritical (90°) and c-critical (0°) components of the laminate,

v is the component volume fraction,

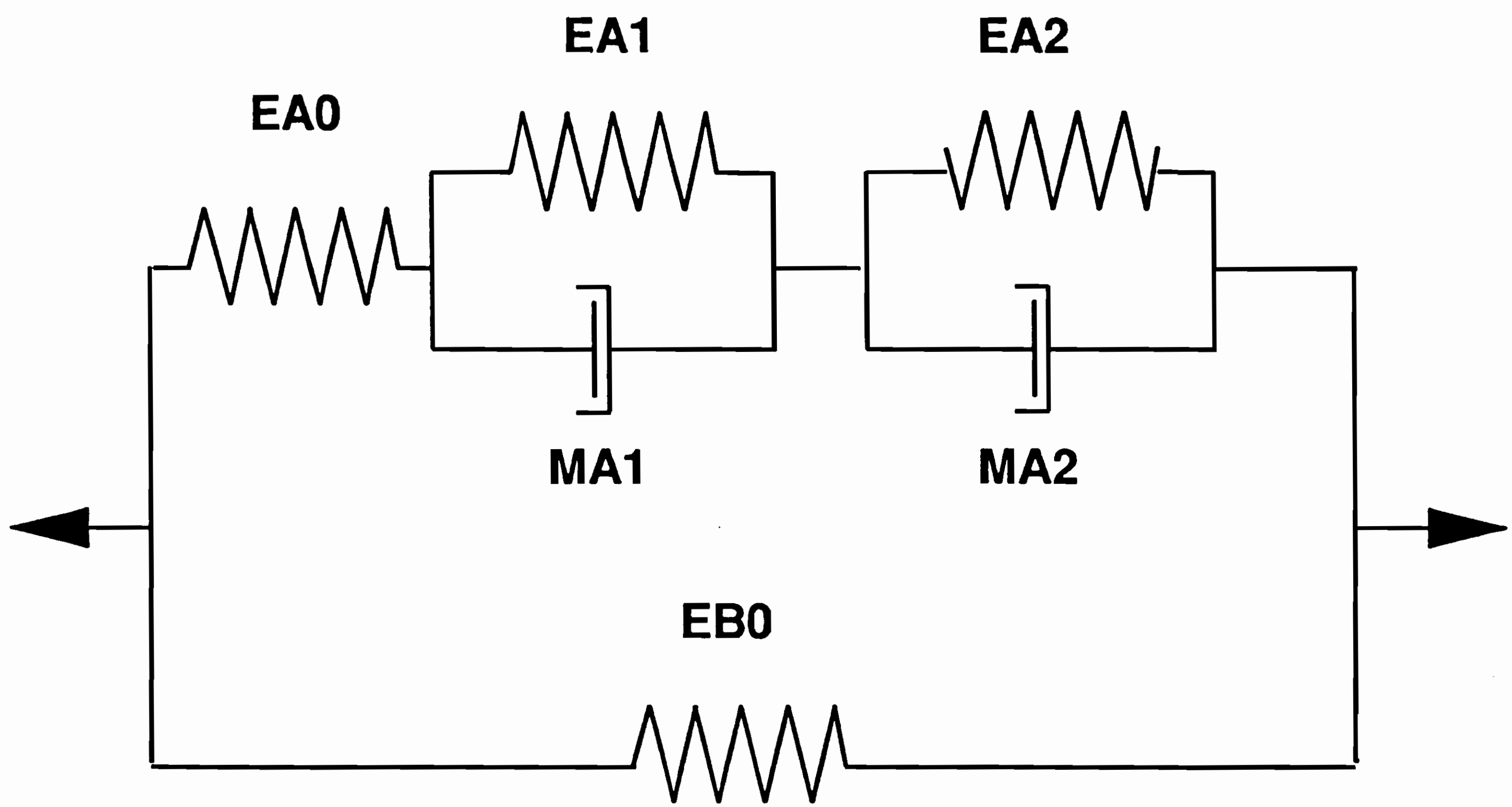

Figure 3.3 Cross-ply laminate 6-parameter PAM model

σ is the applied stress,

$\varepsilon_s, \varepsilon_c$ are the component strains, and

σ_s, σ_c are the component stresses.

Following the same procedure as in section 3.2, the governing equation is given by,

$$ql0\ \varepsilon + ql1\ \dot{\varepsilon} + ql2\ \ddot{\varepsilon} = \sigma + pl1\ \dot{\sigma} + pl2\ \ddot{\sigma} \qquad (3.3.17)$$

where

$$ql0 = v_s * qa0 + v_c * eb0 \qquad (3.3.18)$$

$$ql1 = v_s * qa1 + v_c * pa1 * eb0 \qquad (3.3.19)$$

$$ql2 = v_s * qa2 + v_c * pa2 * eb0 \qquad (3.3.20)$$

$$pl1 = pa1 \qquad (3.3.21)$$

$$pl2 = pa2 \qquad (3.3.22)$$

where qa0, qa1, qa2, pa1 and pa2 have been defined in Eqn's 3.2.15 through 3.2.19, and eb0 is the free spring representing the 0° plies.

3.3.3 *Static and Sinusoidal Loading*

The governing equation 3.3.17 can be solved for any arbitrary loading function. In this section, the analytical solutions for static (creep) and dynamic (sinusoidal) loading are presented.

For the case a of constant global stress σ_0 applied to the laminate,

$$\dot{\sigma} = \ddot{\sigma} = 0 \tag{3.3.23}$$

and Eqn. 3.3.17 is reduced to,

$$ql0\ \varepsilon + ql1\ \dot{\varepsilon} + ql2\ \ddot{\varepsilon} = \sigma_0 \tag{3.3.24}$$

The complete strain response to a constant load is of the form,

$$\varepsilon(t) = C1\ \exp(r1*t) + C2\ \exp(r2*st) + \sigma_0/ql0 \tag{3.3.25}$$

where C1 and C2 are constants, t is time, and r1, r2 are the roots of the characteristic equation

$$ql0 + ql1 * r + ql2 * r^2 = 0 \tag{3.3.26}$$

with the condition that,

$$ql1^2 - 4 * ql0 * ql2 > 0 \tag{3.3.27}$$

Following the same procedure as for the 5-parameter PAM, it can be shown that the condition 3.3.27 is always met.

The initial conditions are,

$$\varepsilon(0) = \frac{\sigma_0}{HST} \tag{3.3.28}$$

and $$\overset{\circ}{\varepsilon}(0) = \sigma_s^* \left(\frac{1}{\mu_1} + \frac{1}{\mu_2} \right) \equiv \Gamma \tag{3.3.29}$$

where

$\varepsilon(0)$ is the instantaneous elastic deformation,

HST is the laminate's axial stiffness as determined from CLT,

Γ is the initial strain rate, and

σ_s is the initial stress in the 90° plies as determined from the CLT analysis.

Applying the boundary conditions, the coefficients are given by

$$C1 = \left[\sigma_0 \left(\frac{1}{HST} - \frac{1}{q10} \right) - \frac{\Gamma}{r2} \right] \frac{r2}{r2 - r1} \tag{3.3.30}$$

$$C2 = \left[\sigma_0 \left(\frac{1}{HST} - \frac{1}{q10} \right) - \frac{\Gamma}{r1} \right] \frac{r1}{r1 - r2} \tag{3.3.31}$$

Eqn's 3.3.25, 3.3.30 and 3.3.31 represent the complete the solution for creep loading of a cross ply laminate.

The applied global sinusoidal stress can be expressed as,

$$\sigma(t) = \sigma_m + \sigma_a \sin(\omega t) \tag{3.3.32}$$

where

σ_m is the mean global stress,

σ_a is the stress amplitude,

ω $= 2\pi f$, is the cyclic frequency (radians/sec), and

f is the frequency in Hertz.

Substituting 3.3.32 and its time derivatives in Equation 3.3.17,

$$ql0\ \varepsilon + ql1\ \dot{\varepsilon} + ql2\ \ddot{\varepsilon} =$$

$$\sigma_m + \sigma_a \sin(\omega t) + pl1\ \sigma_a \omega \cos(\omega t) - pl2\ \sigma_a \omega^2 \sin(\omega t) \tag{3.3.33}$$

The strain response to sinusoidal cyclic loading is given by the solution to the governing equation 3.3.33,

$$\varepsilon(t) = D1 \exp(r1*t) + D2 \exp(r2*t) + \sigma_m/ql0 + A \sin(\omega t) + B \cos(\omega t) \tag{3.3.34}$$

where

D1,D2 are coefficients to be determined from the boundary conditions

r1,r2 are the same roots as for creep loading,

$$B = \frac{sb*q12*\omega^2 + sa*q11*\omega - sb*q10}{-q12*\omega^4 + (2*q10*q12 - q11^2)\omega^2 - q10^2} \tag{3.3.35}$$

$$A = \frac{sb + B(q12*\omega^2 - q10)}{q11*\omega} \tag{3.3.36}$$

and sa, sb are defined as

$$sa = \sigma_a \omega \, (1 - pl2\ \omega^2) \tag{3.3.37}$$

$$sb = \sigma_a \omega \ pl1 \tag{3.3.38}$$

The initial strain and strain rate for sinusoidal loading are,

$$\varepsilon(0) = \frac{\sigma_m}{HST} \tag{3.3.39}$$

and $$\mathring{\varepsilon}(0) = A\omega + \sigma_s * \left(\frac{1}{\mu_1} + \frac{1}{\mu_2} \right) = A\omega + \Gamma \tag{3.3.40}$$

Solving for the coefficients,

$$D1 = \left[\sigma_m \left(\frac{1}{HST} - \frac{1}{q10} \right) - \frac{\Gamma}{r2} - B \right] \frac{r2}{r2 - r1} \tag{3.3.41}$$

$$D2 = \left[\sigma_m \left(\frac{1}{HST} - \frac{1}{q10} \right) - \frac{\Gamma}{r1} - B \right] \frac{r1}{r1-r2} \tag{3.3.42}$$

For the special case $\sigma_m = \sigma_0$, it is easy to recognize that

$$D1 = C1 - \frac{B*r2}{r2-r1} \tag{3.3.43}$$

and
$$D2 = C2 - \frac{B*r1}{r1-r2} \tag{3.3.44}$$

While C1, C2, r1 and r2 depend on the PAM parameters only, the appearance of the coefficient B causes D1 and D2 to be also dependent on stress amplitude and loading frequency.

In fact, Eqn. 3.3.34 can be rewritten in terms of the creep problem coefficients, C1 and C2. The cyclic strain response is

$$\varepsilon(t) = C1 \exp(r1*t) + C2 \exp(r2*t) + \sigma_m/q10 + A \sin(\omega t) + B \cos(\omega t) +$$

$$+ \frac{B}{r1-r2} \left(r2 \exp(r1*t) - r1 \exp(r2*st) \right) \tag{3.3.45}$$

Examining the definitions of A and B, it is obvious that for $\sigma_a=0$ then A = B = 0, and the static creep solution (Eqn. 3.3.34) is recovered. Further examination of Eqn. 3.3.45 reveals that,

$C1\ \exp(r1*t)+C2\ \exp(r2*t)+\sigma_m/ql0$	is the static creep response at σ_m
$A\ \sin(\omega t)$	is the in-phase strain response
$B\ \cos(\omega t)$	is the out-of-phase strain response

and $\frac{B}{r1-r2}\left(r2\ \exp(r1*t)-r1\ \exp(r2*st)\right)$ is an additional transient due to cyclic loading.

The static load response can be compared to the cyclic load solution when $\omega t = 2\pi n$ $(n = 0, 1, 2, ..)$ and $\sigma_m = \sigma_0$. Eqn. 3.3.45 reduces to

$$\varepsilon(t)\Big|_{t=\frac{2\pi n}{\omega}} = C1\ \exp(r1*t) + C2\ \exp(r2*t) + \sigma_m/ql0 +$$

$$+ B\left[\frac{r1\ [1 - \exp(r2*t)] - r2\ [1 - \exp(r1*t)]}{r1-r2}\right] \tag{3.3.46}$$

Eqn. 3.3.46 shows that the static creep solution is disturbed by a cyclic creep transient term that may accelerate or slow the progress of time dependent deformation. As stated above, the creep solution is recovered when stress amplitude is zero because then B=0. Also, it is reassuring to notice that the disturbance term disappears at t=0. The term in square brackets is solely dependent on the PAM parameters, which also determine the magnitude and sign of the disturbance.

But B is a complex function and it reveals some of the problems and potential advantages of this approach. The coefficient B, defined in Eqn. 3.3.35, can be more conveniently rewritten as

$$B = -\sigma_a \omega \left[\frac{(ql1 - pl1*ql0) + \omega^2 (pl1*ql2 - ql1*pl2)}{(ql0 - ql2 * \omega^2)^2 + ql1^2 * \omega^2} \right] \qquad (3.3.47)$$

In general terms, B is linearly proportional to the stress amplitude σ_a ; i.e., a larger stress amplitude leads to a greater disturbance of the static creep solution; which is expected.

B has a complex dependence on the frequency ω. It is easy to verify that B is equal to zero for no cyclic loading (ω=0). At very large frequencies, B becomes roughly proportional to $1/\omega$ and should approximate zero asymptotically.

The coefficient B could also be equal zero for a certain frequency where the numerator of Eqn. 3.3.47 equals zero. This frequency would be,

$$\omega_0 = \left(\frac{ql1 - pl1*ql0}{ql1*pl2 - ql2*pl1} \right)^{1/2} \qquad (3.3.48)$$

The condition for ω_0 to be real is that the term in brackets is bigger than zero, uniquely a function of the PAM parameters. If such frequency ω_0 exists, it would represent a transition frequency from cyclic creep enhancement to cyclic creep inhibition !

Substituting Equations 3.2.15 through 3.2.19 into Equations 3.3.18 through 3.3.22, and these into 3.3.48 it can be shown that,

$$\omega_0^2 = - \frac{E_1^2\mu_2 + E_2^2\mu_1}{\mu_1\mu_2\ (\mu_1 + \mu_2)} < 0 \qquad (3.3.49)$$

Thus, ω_0^2 depends exclusively on the PAM parameters of the 90° plies, and it is always negative since the values of μ_1 and μ_2 are always positive. A real frequency ω_0 does not exist and no transition frequency in the cyclic creep mechanism is possible. Whatever the sign of B is, for a certain combination of PAM parameters and loading conditions, it will remain the same for the whole frequency range.

The coefficient B may exhibit several local maxima and minima and four potential singular frequencies when the denominator of Eqn. 3.3.47 is zero,

$$(ql0 - ql2 * \omega^2)^2 + ql1^2 * \omega^2 = 0 \qquad (3.3.50)$$

Since there is no apparent physical reason behind a singularity in the out-of-phase strain component, Eqn. 3.3.50 warrants some attention.

Substituting $\varphi \equiv \omega^2$, Eqn. 3.3.50 can be rewritten as

$$ql2^2\varphi^2 + (ql1^2 - 2*ql0*ql2)\ \varphi + ql0^2 = 0 \qquad (3.3.51)$$

Solving 3.3.51,

$$\varphi_{1,2} = \frac{ql0}{ql2} + \frac{ql1}{ql2}\left(\frac{-ql1 \pm (ql1^2 - 4*ql0*ql2)^{1/2}}{2*ql2}\right) \qquad (3.3.52)$$

The term in brackets is the roots of the homogeneous equation 3.3.26, and Eqn. 3.3.52 can be rewritten in terms of the roots r1, r2

$$\varphi_{1,2} = \frac{ql0}{ql2} + \frac{ql1}{ql2}(r1,r2) \qquad (3.3.53)$$

For the general case, the explicit form of $\varphi_{1,2}$ is very complex and a simpler case will be examined. Letting $v_s = 1$ (a 90° laminate), Eqn. 3.3.53 is reduced to the simpler expression

$$\varphi_{1,2} = \frac{qa0}{qa2} + \frac{qa1}{qa2}(r1,r2) \qquad (3.3.54)$$

After some algebra, the roots of this simpler case are

$$r1 = -\frac{E_2}{\mu_2} \quad \text{and} \quad r2 = -\frac{E_1}{\mu_1} \qquad (3.3.55)$$

Substituting 3.3.55 in 3.3.54

$$\varphi_1 = -\frac{E_2^2}{\mu_2} < 0 \quad \text{and} \quad \varphi_2 = -\frac{E_1^2}{\mu_1} < 0 \qquad (3.3.56)$$

In conclusion, there are no real singular frequencies in this simple case. Due to the complexity of the function B, and the intricate dependence of the PAM parameters on stress level and temperature (Eqn's 3.2.5 through 3.2.9), it is very hard to draw general conclusions. Some additional implications of the above results are presented in the next section.

3.4 Complex Modulus and Compliance

An additional feature of the PAM representation is the ability to express the complex moduli and compliance of the laminate in terms of the material and loading parameters. This capability offers an opportunity to predict the frequency response of the in-phase and out-of-phase components and the amount of viscoelastically generated energy being dissipated and transformed into heat.

3.4.1 Complex Modulus

To evaluate the complex moduli, input the strain

$$\varepsilon(t) = \varepsilon_a \, e^{i\omega t} \qquad (3.4.1)$$

to the governing equation 3.3.17. The output stress is

$$\sigma(t) = \varepsilon_a \, E^*(i\omega) \, e^{i\omega t} \qquad (3.4.2)$$

where

ε_a is the input strain amplitude,

i is the square root of -1, and

$E^*(i\omega)$ is the complex modulus.

Rewriting Eqn. 3.3.17 as

$$\sum_{k=0}^{2} pl_k \frac{d^k\sigma}{dt^k} = \sum_{k=0}^{2} ql_k \frac{d^k\varepsilon}{dt^k} \tag{3.4.3}$$

then the complex modulus is the ratio of

$$E^*(i\omega) = \frac{\sum_{k=0}^{2} ql_k (i\omega)^k}{\sum_{k=0}^{2} pl_k (i\omega)^k} \tag{3.4.4}$$

Introducing the definitions of governing equation coefficients,

$$E^*(i\omega) = \frac{(ql0 - ql2*\omega^2) + i\,(ql1*\omega)}{(1 - pl2*\omega^2) + i\,(pl1*\omega)} \tag{3.4.5}$$

From Eqn. 3.4.5, the storage modulus $E'(\omega)$ and the loss modulus $E''(\omega)$ are given by,

$$E'(\omega) = \frac{(ql0 - ql2*\omega^2)(1 - pl2*\omega^2) + ql1*pl1*\omega^2}{(1 - pl2*\omega^2)^2 + pl1^2*\omega^2} \tag{3.4.6}$$

$$E''(\omega) = \frac{ql1*\omega\ (1 - pl2*\omega^2) - pl1*\omega\ (ql0 - ql2*\omega^2)}{(1 - pl2*\omega^2)^2 + pl1^2*\omega^2} \tag{3.4.7}$$

The phase lag angle $\delta(\omega)$ is defined as the ratio of the loss and storage moduli,

$$\tan\ \delta(\omega) = \frac{ql1*\omega\ (1 - pl2*\omega^2) - pl1*\omega\ (ql0 - ql2*\omega^2)}{(ql0 - ql2*\omega^2)(1 - pl2*\omega^2) + ql1*pl1*\omega^2} \tag{3.4.8}$$

Note that while E' and E" are very complex functions of the frequency ω, it is easy to verify that for $\omega=0$ (no cyclic loading), E" reduces to zero as expected.

3.4.2 Complex Compliance

To evaluate the complex compliance, input the stress

$$\sigma(t) = \sigma_a\ e^{i\omega t} \tag{3.4.9}$$

into the governing equation 3.3.17. The output strain is

$$\varepsilon(t) = \sigma_a D^*(i\omega)\, e^{i\omega t} \tag{3.4.10}$$

where

σ_a is the input stress amplitude, and

$D^*(i\omega)$ is the complex compliance.

Using the same method as in paragraph 3.4.1 then the complex compliance can be expressed as the ratio

$$D^*(i\omega) = \frac{\sum_{k=0}^{2} pl_k (i\omega)^k}{\sum_{k=0}^{2} ql_k (i\omega)^k} \tag{3.4.11}$$

Introducing the definitions of governing equation coefficients,

$$D^*(i\omega) = \frac{(1 - pl2*\omega^2) + i\,(pl1*\omega)}{(ql0 - ql2*\omega^2) + i\,(ql1*\omega)} \tag{3.4.12}$$

From Eqn. 3.4.12, the storage compliance $D'(\omega)$ and the loss compliance $D''(\omega)$ are given by,

$$D'(\omega) = \frac{(ql0 - ql2*\omega^2)(1 - pl2*\omega^2) + ql1*pl1*\omega^2}{(ql0 - ql2*\omega^2)^2 + ql1^2*\omega^2} \tag{3.4.13}$$

$$D''(\omega) = \frac{-\omega*ql1\ (1 - pl2*\omega^2) + \omega*pl1\ (ql0 - ql2*\omega^2)}{(ql0 - ql2*\omega^2)^2 + ql1^2*\omega^2} \tag{3.4.14}$$

Not surprisingly, the storage and loss compliance, as well as the phase lag angle, are simple functions of the in-phase and out-of-phase terms. Using the definitions of A and B in Equations 3.3.36 and 3.3.47, the compliance can be readily simplified to

$$D'(\omega) = \frac{A}{\sigma_a} \tag{3.4.15}$$

$$D''(\omega) = \frac{B}{\sigma_a} \tag{3.4.16}$$

$$\tan\delta(\omega) = \frac{-B}{A\ \omega} \tag{3.4.17}$$

3.5 Energy Dissipation and Temperature Distribution

The total amount of energy being generated (W) is

$$W = \int \sigma \, d\varepsilon \tag{3.5.1}$$

If the real part of the input stress in Eqn. 3.4.9 is given by,

$$\mathrm{Re}\,[\sigma(t)] = \sigma_a \cos(\omega t) \tag{3.5.2}$$

and the real part of the output strain in Eqn. 3.4.10 is

$$\mathrm{Re}[\varepsilon(t)] = \sigma_a [D'(\omega) \cos(\omega t) + D''(\omega) \sin(\omega t)] \tag{3.5.3}$$

then

$$d\,\varepsilon(t) = -\omega\, \sigma_a [D'(\omega) \sin(\omega t) - D''(\omega) \cos(\omega t)]\, dt \tag{3.5.4}$$

Introducing 3.5.2 and 3.54 in 3.5.1, the amount of energy per cycle is

$$W = \int_0^{2\pi/\omega} -\omega\, \sigma_a^2\, [D' \sin(\omega t) + D'' \cos(\omega t)]\, dt \tag{3.5.5}$$

Integrating 3.5.5 and using the relationship 3.4.16,

$$W = -\pi\, \sigma_a^2\, D''(\omega) = -\pi\, \sigma_a\, B \qquad \text{(energy/cycle/volume)} \qquad (3.5.6)$$

or $$\check{W} = -\frac{\omega}{2}\, \sigma_a^2\, D''(\omega) = -\frac{\omega}{2}\, \sigma_a\, B \quad \text{(energy/time/volume)} \qquad (3.5.7)$$

The energy dissipated per unit time - $\check{W}$ - is linearly proportional to the square of the global stress amplitude and a complex function of the loading frequency: $\omega * D''(\omega)$.

To approximate the steady state temperature, it will be assumed that the temperature is uniform across any cross-section of the laminate perpendicular to the loading axis and heat is being transferred from the specimen through convection (to the surrounding air) and conduction (at the grips) mechanisms.

For this one-dimensional steady state case, the heat transfer is governed by differential equation

$$\frac{d^2 T_{ds}}{d\, x^2} - \frac{h\, R}{k''}\, T_{ds} + \frac{\check{W}}{k''} = 0 \qquad (3.5.8)$$

and the boundary conditions are,

$$@\ x = 0,\ \frac{d\, T_{ds}}{d\, x} = 0 \quad \text{and } @\ x = \pm b,\ T_{ds} = 0 \qquad (3.5.9)$$

where

$T_{ds}(x)$ is the temperature differential between the specimen surface T_s and the ambient temperature, T_a.

x is the load axis, x = 0 at the middle of the gripped length,

b is half the gripped length of the coupon,

h is the overall conduction and convection heat transfer coefficient of the outer surface plies,

k" is the effective thermal conductivity of the specimen in the loading axis direction,

R is the surface to volume ratio of the gripped length, and

$\check{W}$ is the energy source per unit volume per unit time as defined in Eqn. 3.5.7

The initial conditions reflect the requirements that the temperature gradient be zero at the middle of the specimen and that at the grips the specimen reaches ambient temperature.

The solution to Eqn. 3.5.8 and the boundary conditions 3.5.9 is,

$$T_{ds}(x) = \frac{\check{W}}{h\,R}\left[1 - \frac{\exp(x\sqrt{hR/k''}) + \exp(-x\sqrt{hR/k''})}{\exp(b\sqrt{hR/k''}) + \exp(-b\sqrt{hR/k''})}\right]$$

$$= \frac{\check{W}}{h\,R}\left[1 - \frac{\cosh(x\sqrt{hR/k''})}{\cosh(b\sqrt{hR/k''})}\right] \qquad (3.5.10)$$

with the condition that $hR/k'' \geq 0$, which is always met.

Once the steady state solution to the heat transfer problem is known, the transient temperature field is assumed to be of the form,

$$T_d(x,t) = T_{ds}(x)\ [\ 1 - \exp(\eta t)] \tag{3.5.11}$$

where η is a constant to be determined.

Checking the boundary conditions; at $t = 0$ the specimen's temperature is equal to the ambient temperature:

$$T_d\ (x,0) = T_{ds}(x)\ [\ 1 - 1] = 0, \qquad \text{O.K.} \tag{3.5.12}$$

at $t \to \infty$ the specimen reaches the steady state temperature distribution:

$$T_d\ (x,\infty) = T_{ds}(x)\ [\ 1 - 0] = T_{ds}(x) \qquad \text{O.K.} \tag{3.5.13}$$

at the grips the temperature of the specimen and the grip are always the same:

$$T_d\ (b,t) = T_{ds}(b)\ [\ 1 - \exp(\eta t)] = 0 \qquad \text{O.K.} \tag{3.5.14}$$

the temperature gradient at the center of the specimen is always 0:

$$T_{d,x}(0,t) = T_{ds,x}(0)\ [\ 1 - \exp(\eta t)] = 0 \qquad \text{O.K.} \tag{3.5.15}$$

Then, Eqn. 3.5.11 satisfies all boundary conditions and can be rearranged to read as the sum of a steady state term and a transient term,

$$T_d(x,t) = T_{ds}(x) + T_{dt}(x,t) = T_{ds}(x) - T_{ds}(x)\exp(\eta t) \tag{3.5.16}$$

The transient heat transfer is governed by the partial differential equation

$$\frac{\partial^2 T_d}{\partial x^2} - \frac{h\,R}{k''} T_d + \frac{\check{W}}{k''} = \frac{\partial T_d}{\partial t} \tag{3.5.17}$$

Finally, the solution to the transient temperature distribution is,

$$T_d(x,t) = T_{ds}(x)\left[1 - \exp\left(-\frac{\check{W}\;t}{k'' * T_{ds}(x)}\right)\right] = \tag{3.5.18}$$

$$= \frac{\check{W}}{h\;R}\left[1 - \frac{\cosh\left(x\sqrt{hR/k''}\right)}{\cosh\left(b\sqrt{hR/k''}\right)}\right]\left[1 - \exp\left(\frac{-(hR/k'')\,t}{1 - \dfrac{\cosh\left(x\sqrt{hR/k''}\right)}{\cosh\left(b\sqrt{hR/k''}\right)}}\right)\right]$$

3.6 Damorheology

The term damorheology has been coined in an effort to characterize the interaction between damage accumulated due to cyclic loading and time dependent behavior. This new phrase follows a similar term - chemorheology - proposed by Tobolsky [125] to describe the interaction between the damage of polymeric chains (chain scission, network degradation, etc.) and the changes in the rheological behavior of the bulk polymer. Murakami and Ono [126] review the fundamentals of polymer degradation and define chemorheology as encompassing the physical and chemical aspects involved in the mechanisms, at the molecular level, of the structural degradation of polymers leading to changes in the viscoelastic behavior. Murakami and Ono specifically address the problem of polymers subjected to oscillating strains at different temperatures and conclude that transitions in the cyclic stress relaxation behavior are attributable to interaction mechanisms.

Similarly, the existence of a damorheological effect in fiber reinforced composites implies that a degradation of the residual elastic response of the laminate due to cyclic damage is accompanied by changes in the viscoelastic behavior of the material (supported by Ke et al. [167]). Local damage events not only affect the global elastic response, but the redistribution of the stresses among the plies changes the global viscoelastic behavior and vice versa. Stress relaxation in the vicinity of damage loci may affect the rate of damage growth (as suggested by Sturgeon [160], Sun and Chan [161], Saff [162], Sun and Chim [163], Mandell and Meier [164] and others). In a more general sense we may state that both phenomena, fatigue damage development and viscoelastic effects, are coupled.

In the extensive mathematical treatment of creep-fatigue interaction in isotropic media (see discussion in section 2.4.1), rate dependent and independent damage initiation and growth are separated into different components for convenience. Usually, the summation is nonlinear and generally unknown. Unfortunately, rigorous treatment of such coupling effects in composite materials using the continuum damage mechanics or other semi- empirical approaches is philosophically and mathematically complex. Often, fiber reinforced composites exhibit surprising damorheological behavior.

The pseudo-analog mechanical model discussed above is only an aid, capable of representing damorheological effects. It is a tool to account for time dependent stress redistribution among plies and the effect of different fatigue damage modes on the model coefficients for each lamina, material, direction, etc. Thus, the changes in the global damping characteristics are captured in the form of time dependent storage and loss moduli. From these, the temperature history and distribution in the material could be computed by assuming appropriate boundary conditions and heat transfer mechanisms.

Complete histories of the performance of the laminate may be evaluated only with the aid of a numerical procedure. The rapid changes in the test conditions due to temperature changes, load redistribution and damage development preclude a convenient close form solution. Based on the analysis presented in this chapter, a computer program has been developed to predict the performance of cross ply laminates subjected to cyclic loading on the basis of elastic, fatigue and thermorheological lamina characterization. An overview of the code is presented in Chapter 6.

4 Materials and Experimental Methods

4.1 Experimental Program

The objectives of the experimental program are to generate the necessary data to characterize the material system being used in this study and probe some of the capabilities of the proposed model to predict the damorheological effect; i.e., deformation, stiffness and strength changes during different load histories involving cyclic and/or static loads.

The experimental program, shown in Table 4.1, has two phases. The first phase is to characterize the compliance of 0° and 90° unidirectional laminates as a function of time, temperature, and stress. The data from isothermal creep tests at different stress levels and DMA results at different frequencies and temperatures (multiplexing) are combined using the procedure described in Chapter 3. The appropriate five parameter pseudo-analog mechanical model is determined for each lamina orientation. In the second phase, the response of a $[0/90_3]_s$ cross ply laminate subjected to static and cyclic loads is measured and compared to the predictions of the proposed model.

Table 4.1 Experimental Program

Stacking Sequence	Test	Stress levels	Life Fraction	Specimens
$[0]_8$	Q-static tension			5
	Fatigue	4		12
	Res. Strength	2	3	18
	Creep (*)	6		2
	DMA (**)			2
$[90]_8$	Q-static tension			5
	Fatigue	2		8
	Res. Strength	1	2	6
	Creep (*)	6		4
	DMA (**)	1	3	6
$[0/90_3]_s$	Q-static tension			5
	Fatigue	4		12
	Res. Strength	2	3	18
	Creep (*)	3		2
	DMA (**)	1	5	5

(*) Room temperature mechanical creep tests

(**) Includes fixed frequency, multiplexing and creep tests

4.2 Radel X/T650-42 Thermoplastic System

Radel X/T650-42 by Amoco, a new amorphous polyarylsulphone thermoplastic - graphite fiber composite, has been chosen as the subject of this study. This system has advantages over both thermosets and semi-crystalline thermoplastic matrices, and is especially suited to the purpose of this investigation. Unlike thermosets, this thermoplastic polymer is able to sustain large deformations. Its amorphous nature eliminates the large dependency of the properties of the consolidated laminate on the manufacturing process and crystallinity content. On the other hand, as a new product on the market, the amount of available data is restricted. Thermal properties, not available from the supplier, had to be measured using Differential Scanning Calorimeter (DSC) and Thermo-Mechanical Analysis (TMA) techniques. Tables 4.2 and 4.3 show a summary of the available data on the matrix, fiber and composite system.

Panels of Radel X were consolidated using autoclave and hot press procedures in the Center for Composite Materials and Structures Fabrication Laboratory. Due to the significant mismatch of coefficients of thermal expansion between the fibers and the aluminum tool plate in the autoclave, ripples developed in the surface of the laminate and this procedure had to be abandoned. A new steel mold, Richmond E-5555 high temperature glass fiber release fabric and Kapton film were used in the hot press to ensure good quality panels without out-of-plane or in-plane fiber waviness. Figure 4.1 shows a cross

Table 4.2 T650-42 graphite fiber and

Radel X (amorphous polyarylsulphone thermoplastic)

Commercially Available Data

Property	T650-42 Thornel[a]	Radel X Amoco[b]
Tensile Strength (Ksi)	730	12
Tensile Modulus (Msi)	42	0.4
Tensile Impact (ft-lb/in2)		160
Density (lb/in3)	0.064	
Strain to failure (%)	1.7	40
Longitudinal CTE (PPM/°F)	-0.3	
Longitudinal K (BTU/hr/ft2/°F)	9	
Glass transition temperature (°F)		419
Equilibrium water sorption (wt %)		1.5 - 1.8
Notched Izod (ft-lb/in)		1.6

a Thornel, Advance Composite Systems

b Amoco Performance Products

Table 4.3 T650-42/Radel X Thermoplastic Composite
Commercially Available Data (62% fiber by volume)[a]

0° Tension	Strength (Ksi)	330
	Strain (%)	1.35
	Modulus (Msi)	23.7
0° Compression	Strength (Ksi)	155
	Strain (%)	0.35
	Modulus (Msi)	23.4
90° Tension	Strength (Ksi)	6.91
	Strain (%)	0.61
	Modulus (Msi)	1.17
+/- 45° Tension	Strength (Ksi)	33.8

a Amoco Performance Products

section of the laminate inside the mold. The hot press consolidating cycle recommended by the supplier, is shown in Figure 4.2.

4.3 Specimen Preparation and Mechanical Tests

The panels were C-scanned to determine their quality and consistency. The surface was inspected visually for fiber waviness and depression marks. Imperfect panels or sections were discarded. Specimens were cut from 12"x12" panels using a water cooled diamond saw.

All mechanical tests: static and cyclic creep, quasi static and fatigue loading were conducted on 20 kip MTS servo-hydraulic, closed loop testing machines, equipped with hydraulic, wedge action grips.

Strains were measured with MTS extensometers having one or two inch gage lengths. The extensometers were mounted on V-notched aluminum tabs bonded to the specimen with a compliant silicone adhesive. The extensometer is held in place by four rubber bands. A layer of emory cloth was placed between the grip surface and the specimen and the lowest possible grip pressure was applied (depending on stacking sequence) to avoid grip-induced damage and premature failure.

All fatigue and cyclic creep tests were conducted in load control using sinusoidal loading. Fatigue tests were run either to failure or to a pre-selected number of cycles, followed by the determination of

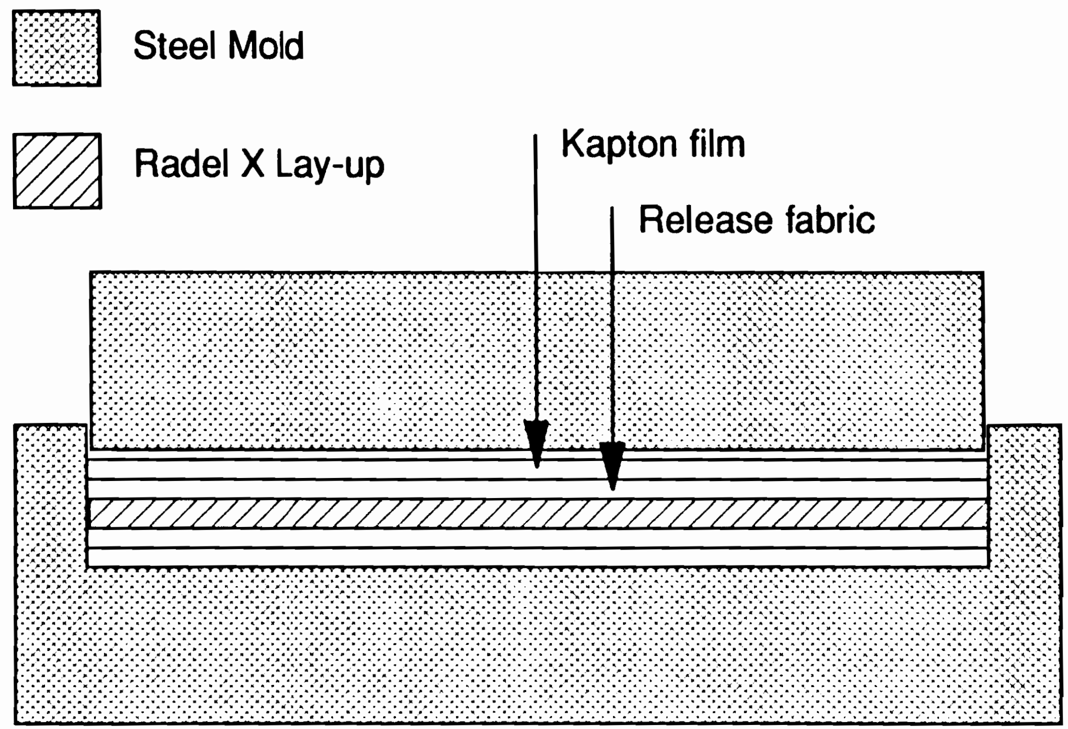

Figure 4.1 **Cross section of laminate and hot press mold**

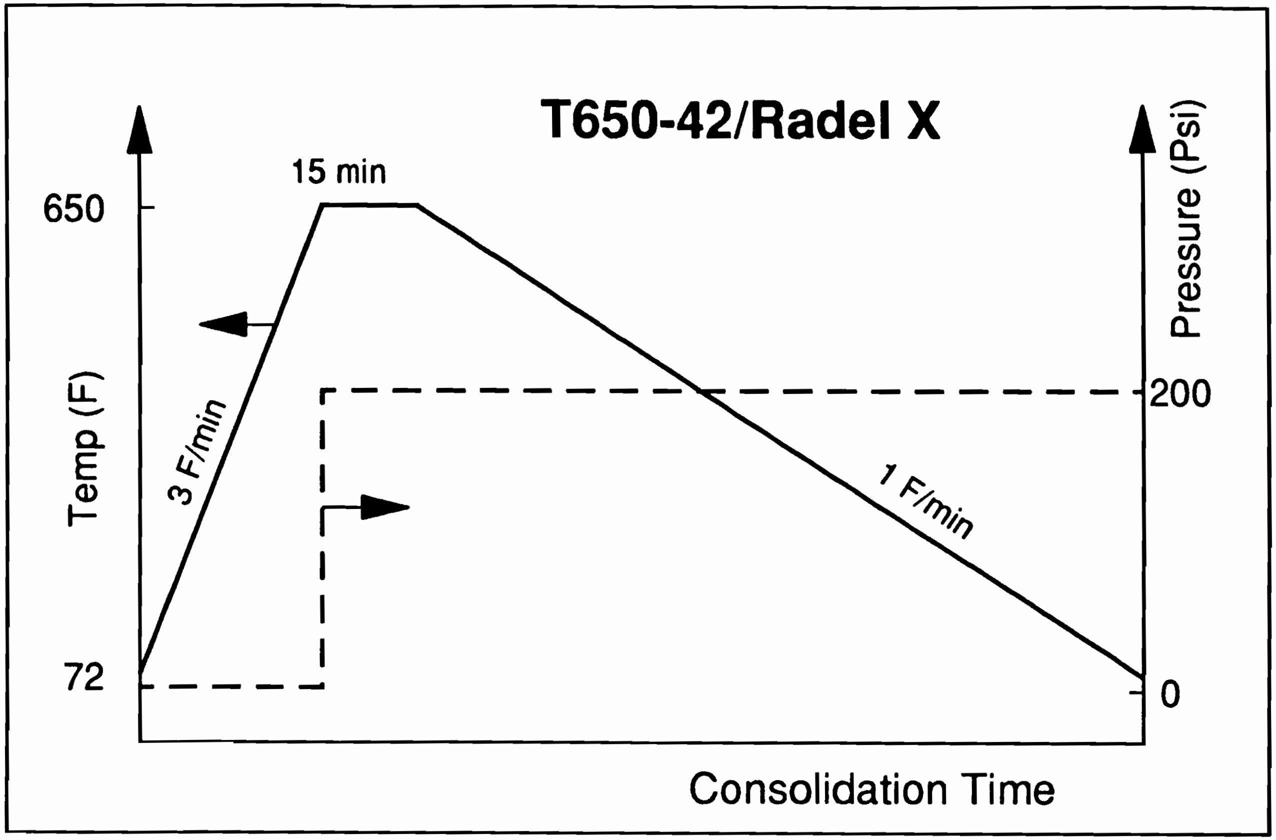

Figure 4.2 Hot press curing cycle

the damage state and residual tensile strength tests.

Changes in secant modulus were monitored to follow the development of damage during cyclic loading. The secant modulus is defined as,

$$E_{sec} = \frac{\sigma_{max} - \sigma_{min}}{\varepsilon_{max} - \varepsilon_{min}} \qquad (4.2.1)$$

where

σ_{min}, σ_{max}	minimum and maximum cyclic stress,
ε_{min}, ε_{max}	minimum and maximum cyclic strain, and
E_{sec}	secant modulus.

4.4 Nondestructive Tests

Additional information on the possible damage modes and damage sequence was obtained by several nondestructive techniques. The acoustic emission data from selected quasi static and cyclic tests were recorded. The energy released by damage events such as matrix cracking or fiber failure creates a sound wave. These events are detected by a transducer mounted on the specimen and transformed into an electrical signal. The signal is amplified and can be analyzed to study the many characteristic of the wave, each carrying specific information about the damage modes and extent. In this investigation, the RMS voltage of the signal (related to the total energy released by the event) was recorded as a function of time. This record revealed the amount and energy of events as a function of load in a quasi static test, or as a function of time/cycles in a fatigue test.

Ultrasonic C-scans of all residual strength specimens were performed, as well as more detailed ultrasonic imaging with the aid of Scanning Acoustic Microscopy. Both techniques use high frequency sound waves emitted and received by an ultrasonic transmitter. The C-scan receives the signal after passing through the specimen immersed in a tank of water that acts a coupling agent. All of the wave characteristics carry information. Usually the variations in the amplitude of the signal are used to measure the local attenuation related to defects in the plane of the layered composite such as delaminations, voids, etc. The nature of the C-scan is such that it integrates the damage thorough the thickness of the specimen, losing some of the information. The Scanning Acoustic Microscope is able to focus the ultrasonic energy at a selected depth and purge the signal of other information. Scanning the plane of the composite produces an image of the state of the material at a constant depth. It complements the C-scan technique by extracting the information at planes of particular interest. Details on acoustic emission, ultrasonic scans and many other techniques are found in [58].

Combining the nondestructive techniques with in situ temperature and secant stiffness measurements it was possible to evaluate the time of appearance, type and extent of the several damage modes that occurred in unidirectional and cross ply laminates. Cross referencing the information obtained by different techniques provided a more detailed account of the events.

4.5 Thermorheological Characterization

To provide for the numerous data required by the pseudo-analog model described in Chapter 3, two independent sets of tests were conducted for each lamina orientation.

The incremental stress creep (ISC) test consists of a series of increasingly higher load isothermal creep tests with stress relaxation intervals between loading periods (details are found in [42]). ISC tests were conducted on 1.2"x10" 8-ply unidirectional coupons in the 0° and 90° orientations. The stress levels increased from 10 to 90% of the ultimate tensile strength as determined from quasi static loading tests. Each stress level is repeated three times. The loading period is 30 minutes and the unloading interval is at least 90 minutes. After the three repetitions the specimen is unloaded for 16 hours, or 10 times the total loading time. The specimen's temperature and deformation were recorded on a strip chart recorder.

Creep tests at constant load and varying temperature were conducted on a Dupont 983 Dynamic Mechanical Analyzer (DMA). A 0.5"x2" coupon is held between two arms as shown in Figure 4.3 and deforms as shown in Figure 4.4 [179]. The load is held constant for the duration of the test while the temperature is increased in steps. The load,

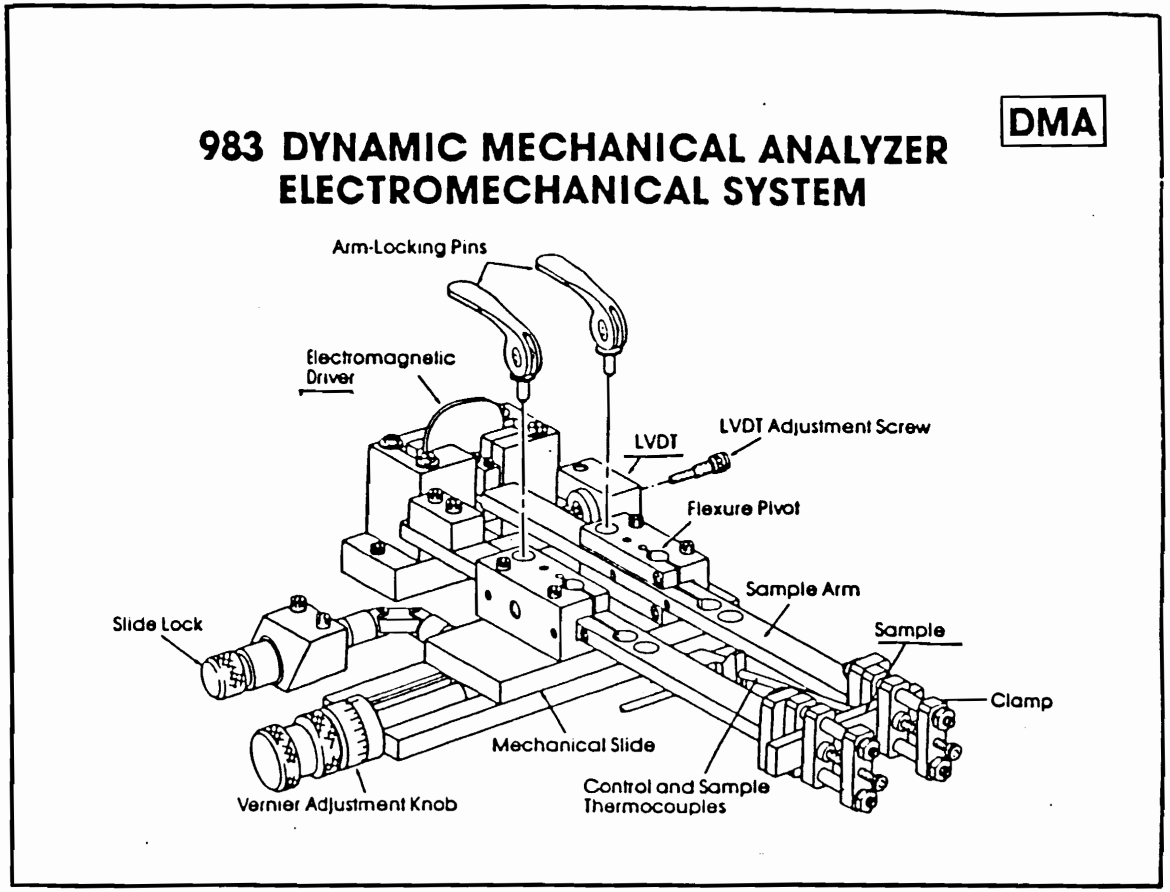

Figure 4.3 DMA electromechanical system [179]

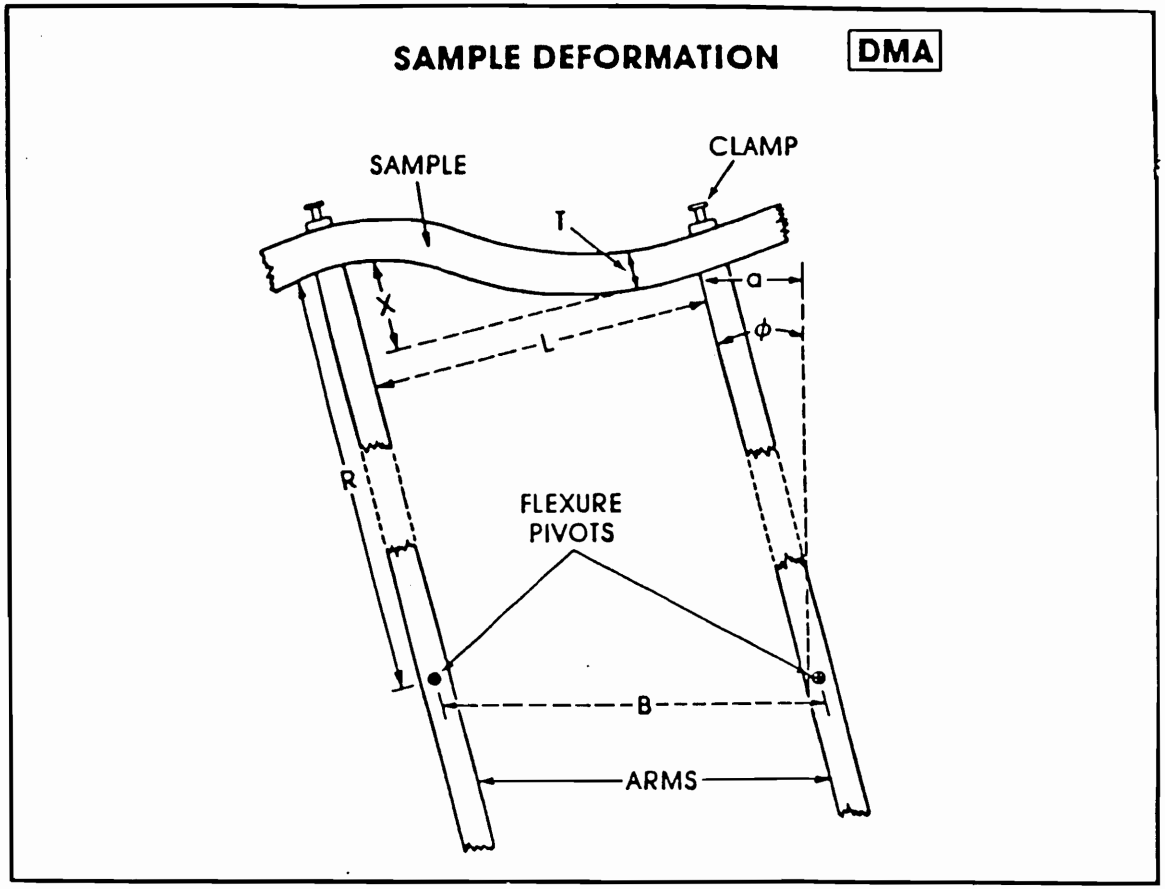

Figure 4.4 DMA sample deformation [179]

deformation and temperature are controlled and recorded by the computerized data acquisition system [179].

The thermorheological characterization also included the lamina frequency response. Dynamic loading experiments at constant strain amplitude and varying frequency - multiplexing - were conducted on the same Dupont 983 Dynamic Mechanical Analyzer. The data analysis software package available with the Dupont DMA system was used to perform on-screen time-temperature and frequency-temperature superposition based on the data from creep and multiplexing tests. Compliance and complex moduli master curves were evaluated with this option and the corresponding shift factors were recorded.

The data collected from the isothermal ISC and fixed load DMA creep tests were first fitted with a five parameter PAM (using linear regression) and then were combined with a modified Time - Temperature - Stress Superposition technique. The DMA creep data, obtained at a nominal stress σ_0, were plotted as

$$\ln \phi_i \Big|_{\sigma^0} = \left(a_i + b_i \, \sigma^0 \right) + \left(c_i + d_i \, \sigma^0 \right) \ln \frac{T_g - T}{T_g}$$

$$\ln \phi_i \Big|_{\sigma^0} = h_i + j_i \ln \frac{T_g - T}{T_g} \qquad (4.4.1)$$

where

T is the absolute temperature, and

T_g is the absolute glass transition temperature.

The ISC data (obtained at room temperature T^0 were plotted as,

$$\ln \phi_i \Big|_{T^0} = \left(a_i + c_i \ln \frac{T_g - T^0}{T_g} \right) + \left(b_i + d_i \ln \frac{T_g - T^0}{T_g} \right) \sigma$$

$$\ln \phi_i \Big|_{T^0} = k_i + l_i \sigma \tag{4.4.2}$$

Figure 4.5 shows a schematic of both relationships, as obtained from DMA and ISC tests.

From the experimentally measured h_i, j_i, k_i, l_i, and the relationships between the Φ and PAM parameters, the explicit dependence of the ply PAM parameters on temperature and stress is found by solving

$$\begin{Bmatrix} a_i \\ b_i \\ c_i \\ d_i \end{Bmatrix} = \begin{bmatrix} 1 & \sigma^0 & 0 & 0 \\ 0 & 0 & 1 & \sigma^0 \\ 1 & 0 & \ln \frac{T_g - T^0}{T_g} & 0 \\ 0 & 1 & 0 & \ln \frac{T_g - T^0}{T_g} \end{bmatrix}^{-1} \begin{Bmatrix} h_i \\ j_i \\ k_i \\ l_i \end{Bmatrix} \qquad i = 0,..,4 \tag{4.4.3}$$

Making use of these coefficients, and defining the normalized temperature

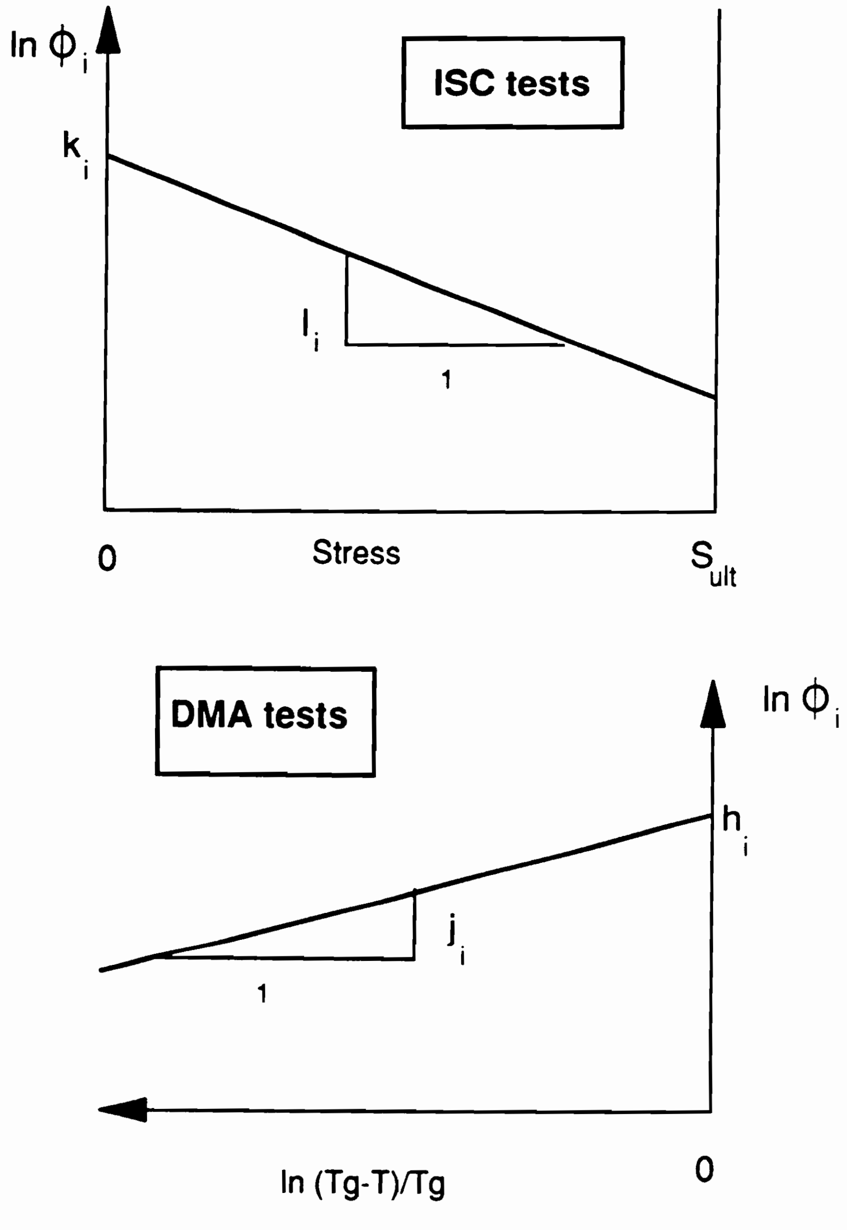

Figure 4.5 ISC and DMA data integration to obtain the PAM parameters

$$T^* = \frac{T_g - T}{T_g} \qquad (4.4.4)$$

Equations 3.2.5 through 3.2.9 can be rewritten as,

$$E_0(\sigma,T) = \exp\left[-\left(a_0 + b_0\sigma + c_0 \ln T^* + d_0\sigma \ln T^*\right)\right] \qquad (4.4.5)$$

$$E_1(\sigma,T) = \exp\left[-\left(a_1 + b_1\sigma + c_1 \ln T^* + d_1\sigma \ln T^*\right)\right] \qquad (4.4.6)$$

$$E_2(\sigma,T) = -\exp\left[-\left(a_2 + b_2\sigma + c_2 \ln T^* + d_2\sigma \ln T^*\right)\right] \qquad (4.4.7)$$

$$\mu_1(\sigma,T) = \exp\left[(a_3-a_1)+(b_3-b_1)\sigma + (c_3-c_1)\ln T^* + (d_3-d_1)\sigma \ln T^*\right] \qquad (4.4.8)$$

$$\mu_2(\sigma,T) = \exp\left[(a_4-a_2)+(b_4-b_2)\sigma + (c_4-c_2)\ln T^* + (d_4-d_2)\sigma \ln T^*\right] \qquad (4.4.9)$$

5 Results

Two major sets of results are presented in this chapter. The first set consists of the mechanical and thermorheological characterizations of Radel X/T650-42 unidirectional laminates. This portion of the experimental program was designed to provide the input data necessary to run the performance simulation code. The second set consists of quasi-static, creep, and fatigue tests performed on $[0/90_3]_s$ cross ply laminates of the same material system. In Chapter 7 the data are examined and compared to the values predicted by the analytical model. To avoid duplications, all the results for each test procedure are presented together.

5.1 Quasi Static Tensile Testing

The results of quasi static tensile testing of $[0]_8$, and $[90]_8$ laminates (5 specimens each) are summarized in Table 5.1. The 90° laminates show linear elastic behavior up to failure. The 0° laminates exhibit marked stiffening as the strain increases. The increase in stiffness is approximately 15%. Specimens with higher values of initial stiffness generally have higher values of tensile strength and strain to failure, as shown in Figures 5.1.a and 5.1.b.

The $[0/90_3]_s$ cross ply laminates were loaded along the direction of the outer 0° plies. The summary of quasi static tensile testing

Table 5.1 Quasi static tensile properties, 0° and 90° Specimens (mean ± standard deviation)

Property	0° laminates	90° laminates
Tensile Strength (Ksi)	332 ± 12.1	10.56 ± 0.51
Initial Tensile Modulus (Msi)	22.9 ± 0.52	1.085 ± 0.045
Failure Strain (%)	1.397 ± 0.023	0.978 ± 0.053

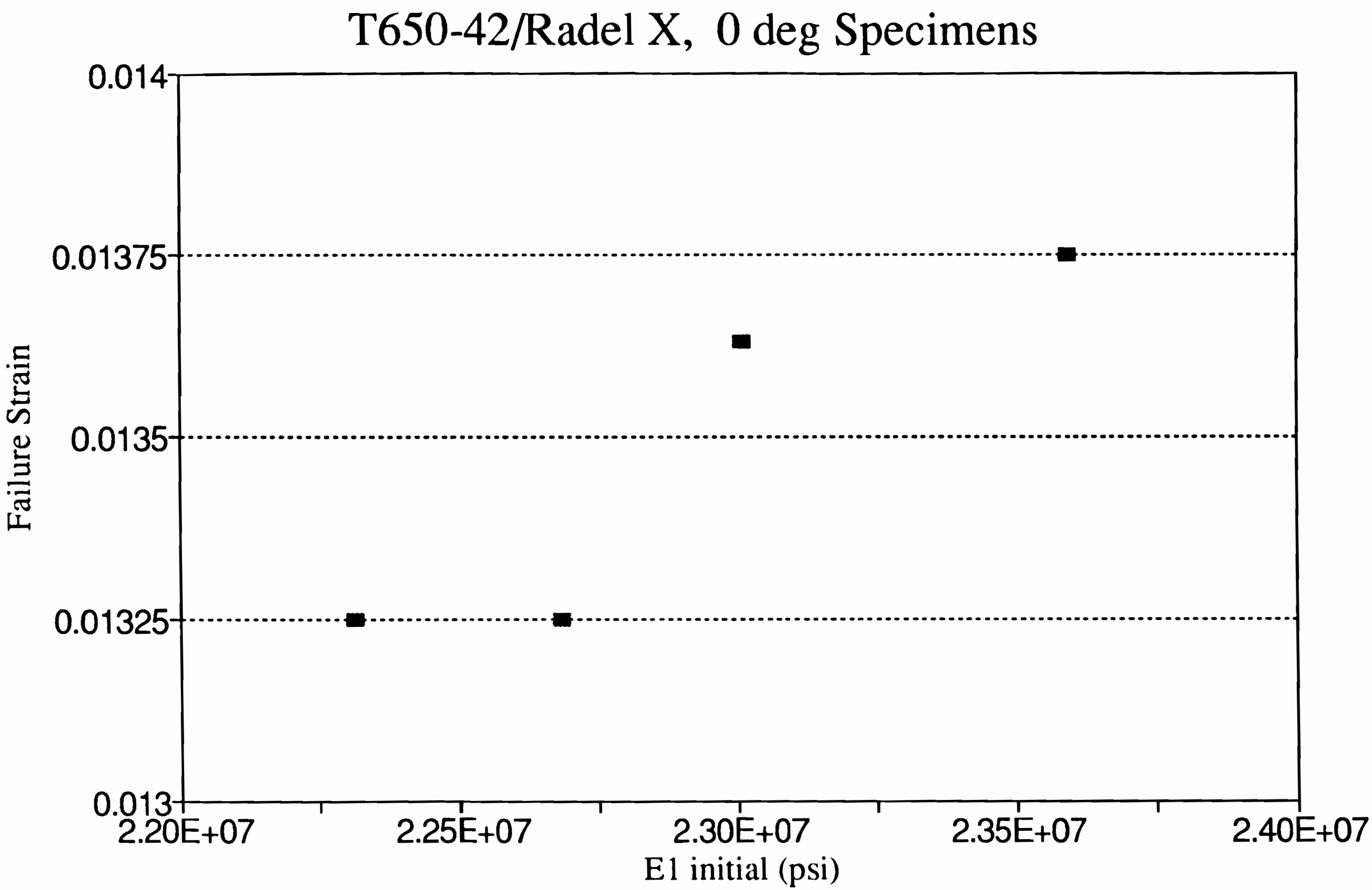

Figure 5.1.a **Strain to failure vs. Axial stiffness, 0° laminates**

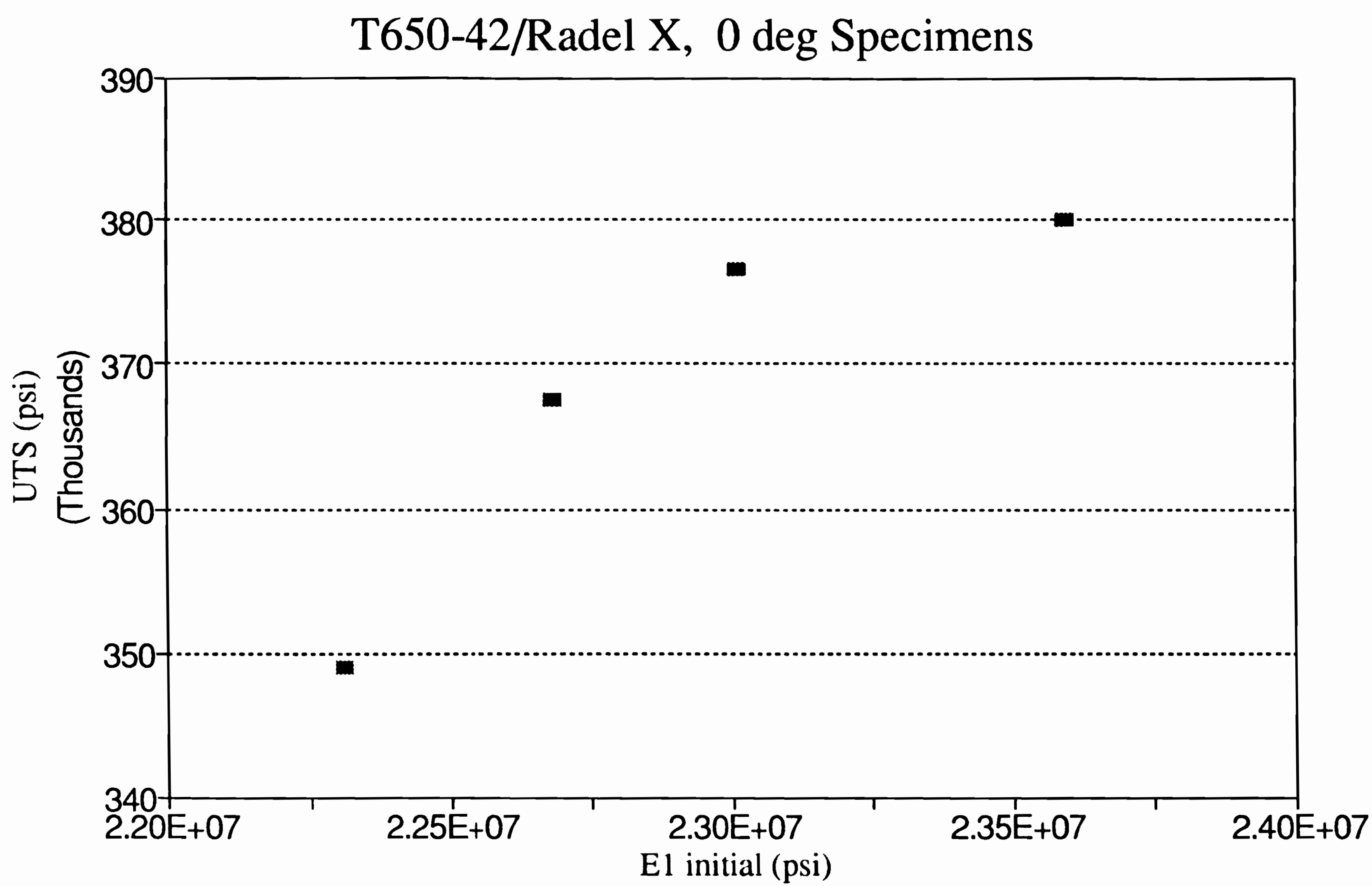

Figure 5.1.b Ultimate tensile strength vs. Axial stiffness, 0° laminates

results is shown in Table 5.2. These laminates have bilinear stress-strain behavior with a ragged knee point centered at 0.69% strain and 46200 psi, as shown in Figure 5.2. The stiffness above the knee decreases by up to 19%. The initial stiffness is predicted with good accuracy by Classical Lamination Theory and the knee corresponds to the first failure of the 90° plies according to the Tsai-Hill failure criterion.

The global failure strain of the cross ply laminate is lower than the failure strain of the 0° laminate. If the local stress concentration in the 0° plies at the tip of the cracked adjacent 90° plies is accounted for (using the shear lag model described in the next section), the local strain does match the 0° unidirectional laminate ultimate strain.

5.2 Preliminary Shear Lag Analysis

Taking advantage of the in-house shear lag analytical software [174], the saturation crack spacing, apparent stiffness, and stress concentration as functions of crack spacing were evaluated for a $[0/90_3]_s$ laminate (see section 3.3.1). The predicted minimum saturation transverse crack spacing in the 90° plies is 0.06 inch. For this spacing, the apparent transverse stiffness of the 90° plies is 6.59e5 psi, or 61% of its original undamaged value. The relationship between the ratio of apparent to initial transverse stiffness of the

Table 5.2 Quasi static tensile properties, cross ply laminates

(mean ± standard deviation)

Property	Radel X, $[0/90_3]_s$
Tensile Strength (Ksi)	72.4 ± 3.05
Knee Stress (Ksi)	46.2 ± 2.38
Initial Tensile Modulus (Msi)	6.47 ± 0.24
Secondary Tensile Modulus (Msi)	5.22 ± 0.14
Knee Strain (%)	0.693 ± 0.02
Failure Strain (%)	1.202 ± 0.04

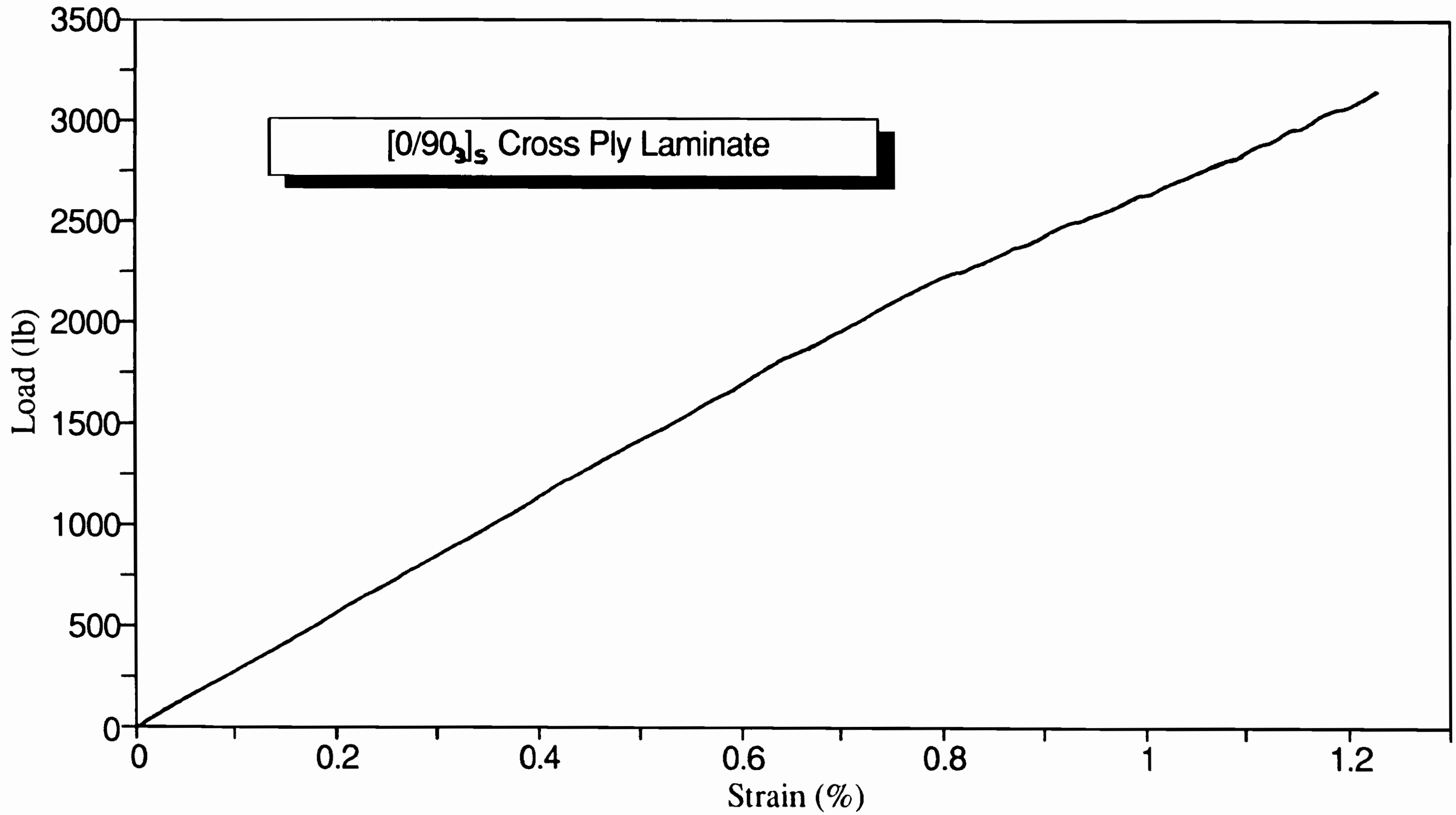

Figure 5.2 Quasi static Load-Strain response, $[0/90_3]_s$ laminate

90° plies and the normalized crack density λ*h90 is given by the master curve shown in Figure 5.3 and predicted by Eqn. 3.3.3,

$$\frac{E_2^{90}(\lambda)}{E_2^{90}(0)} = 1 + \beta(90) * [\lambda*h90] \tag{5.2.1}$$

where the constant $\beta(90)$ = -0.754, as determined with the aid of the CDS code.

Applying the same analysis in the transverse direction of the 0° plies yields the minimum saturation longitudinal crack spacing in the 0° plies, which is 0.055 inch. For this spacing, the apparent transverse stiffness of the 0° plies is 8.203e5 psi, or 76% of its original undamaged value. The relationship between the ratio of apparent to initial transverse stiffness of the 0° plies and the normalized longitudinal crack density λ*h0 is given by the master curve shown in Figure 5.4 and predicted by,

$$\frac{E_2^{0}(\lambda)}{E_2^{0}(0)} = 1 + \beta(0) * [\lambda*h0] \tag{5.2.2}$$

where the constant $\beta(0)$ = -1.278, as determined with the aid of the CDS code.

The CDS code also provided a prediction of the stress concentration in the 0° plies for a given crack spacing. When the first crack appears across the thickness of all the 90° plies the initial stress concentration is 1.142. The magnitude of the stress

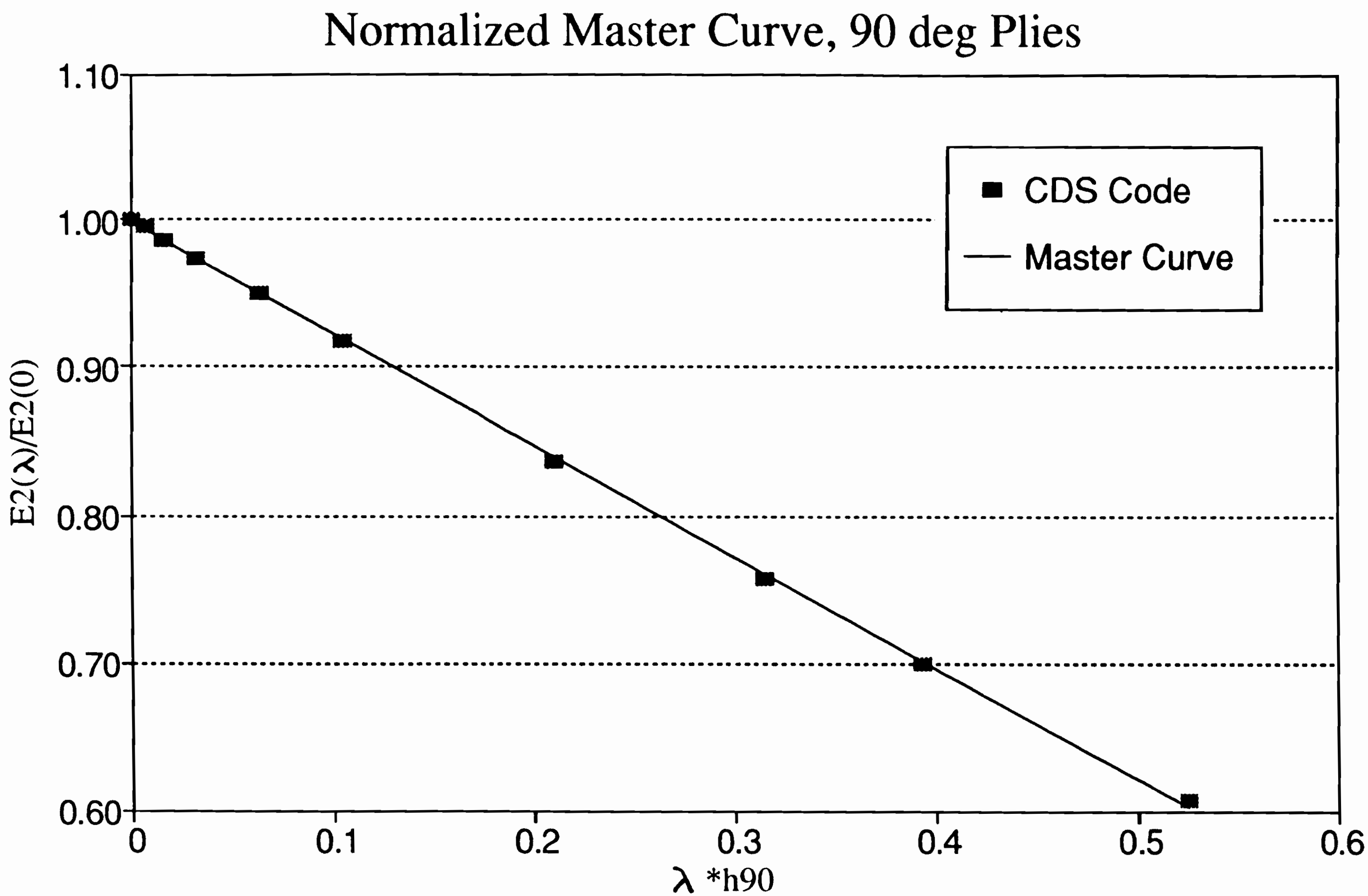

Figure 5.3 Transverse stiffness vs. normalized crack density, 90° plies

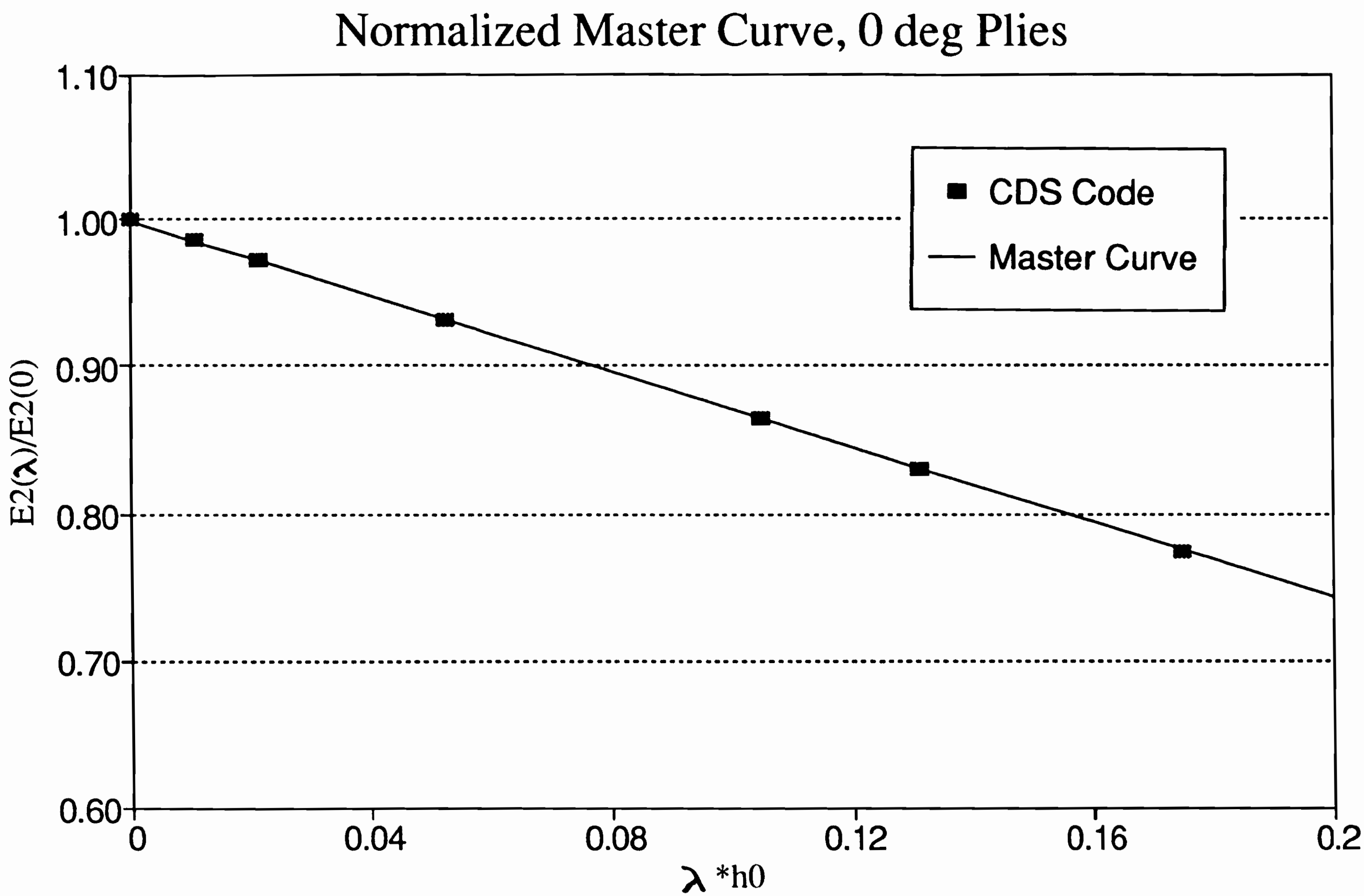

Figure 5.4 Transverse stiffness vs. normalized crack density, 0° plies

concentration as a function of normalized crack density can be represented by the master curve presented in Eqn. 3.3.9 and shown in Figure 5.5.

$$\frac{K(\lambda)}{K(0)} = 1 + \delta * [\lambda * h90] \qquad (5.2.3)$$

where the constant δ = -0.0941, as determined with the aid of the CDS code. The magnitude of the stress concentration decreases to 1.088 after the cracked laminate reaches the characteristic damage state.

5.3 Thermal Properties

Thermal properties are required to complete a proper laminate analysis. Some of the thermal properties of the the T650-42/Radel X thermoplastic composite system were not available and had to be measured. Using the Dupont TMA7 Thermo Mechanical Analyzer, the lamina coefficients of thermal expansion in the fiber and transverse direction were measured. With this technique, the thermal expansion was measured as a function of temperature up to and beyond the glass transition temperature. Figures 5.6 and 5.7 show the thermal expansion of a $[0]_8$ laminate in the fiber and transverse direction. Due to the configuration of the test, only the values obtained below the T_g (419°F) are valid.

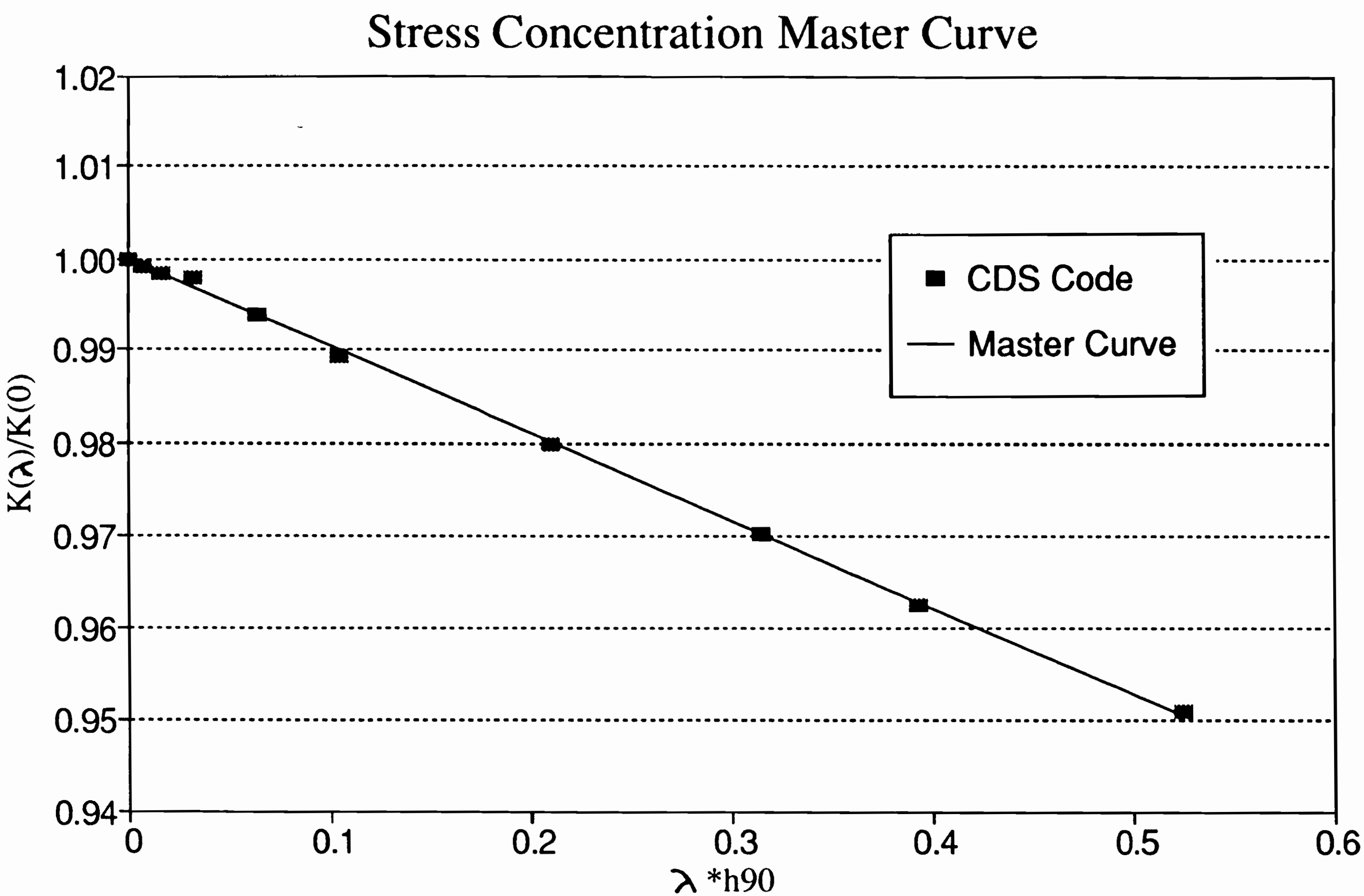

Figure 5.5 **Stress concentration vs normalized crack density**

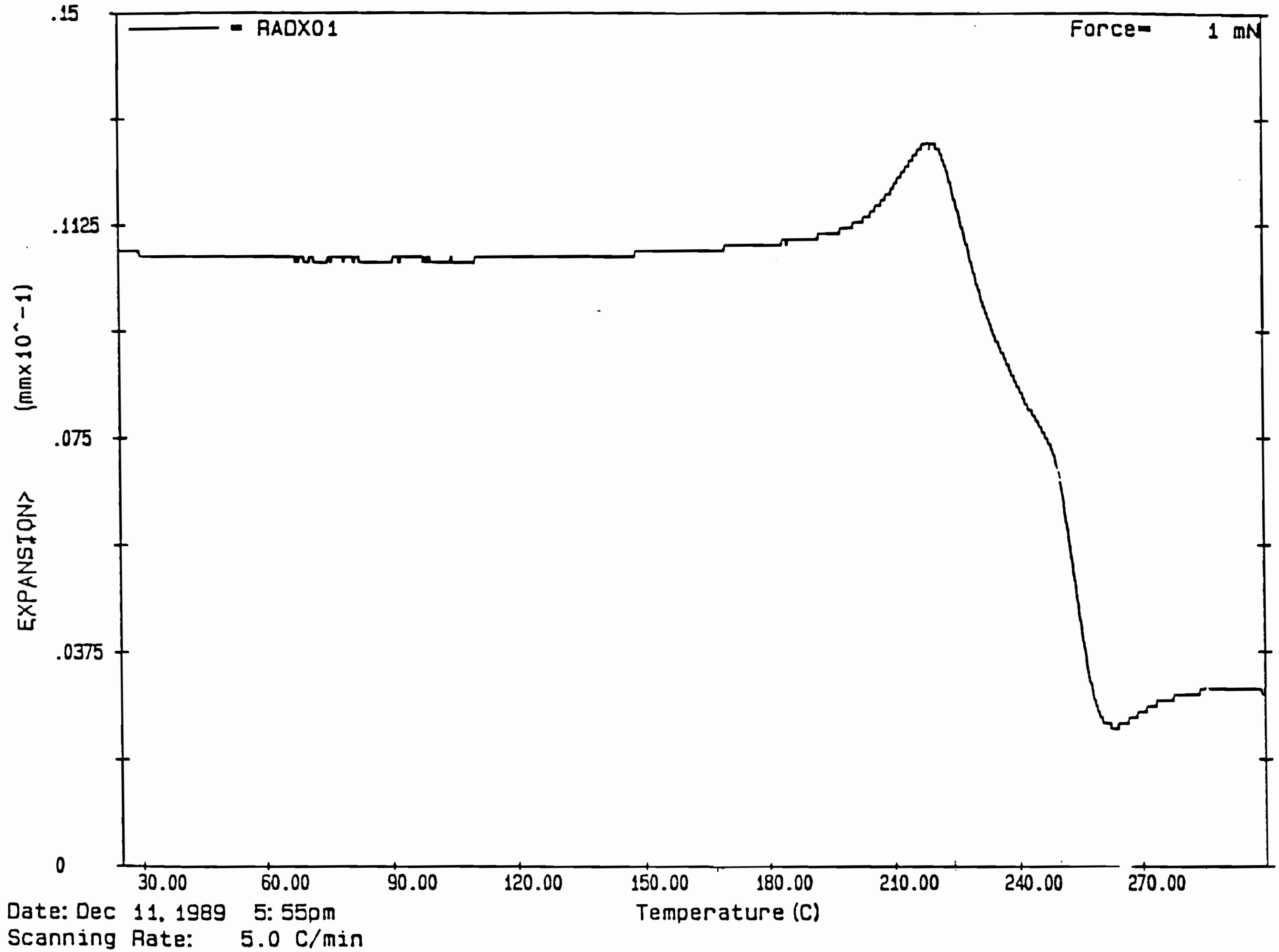

Figure 5.6 Thermal expansion vs. temperature, 0° orientation

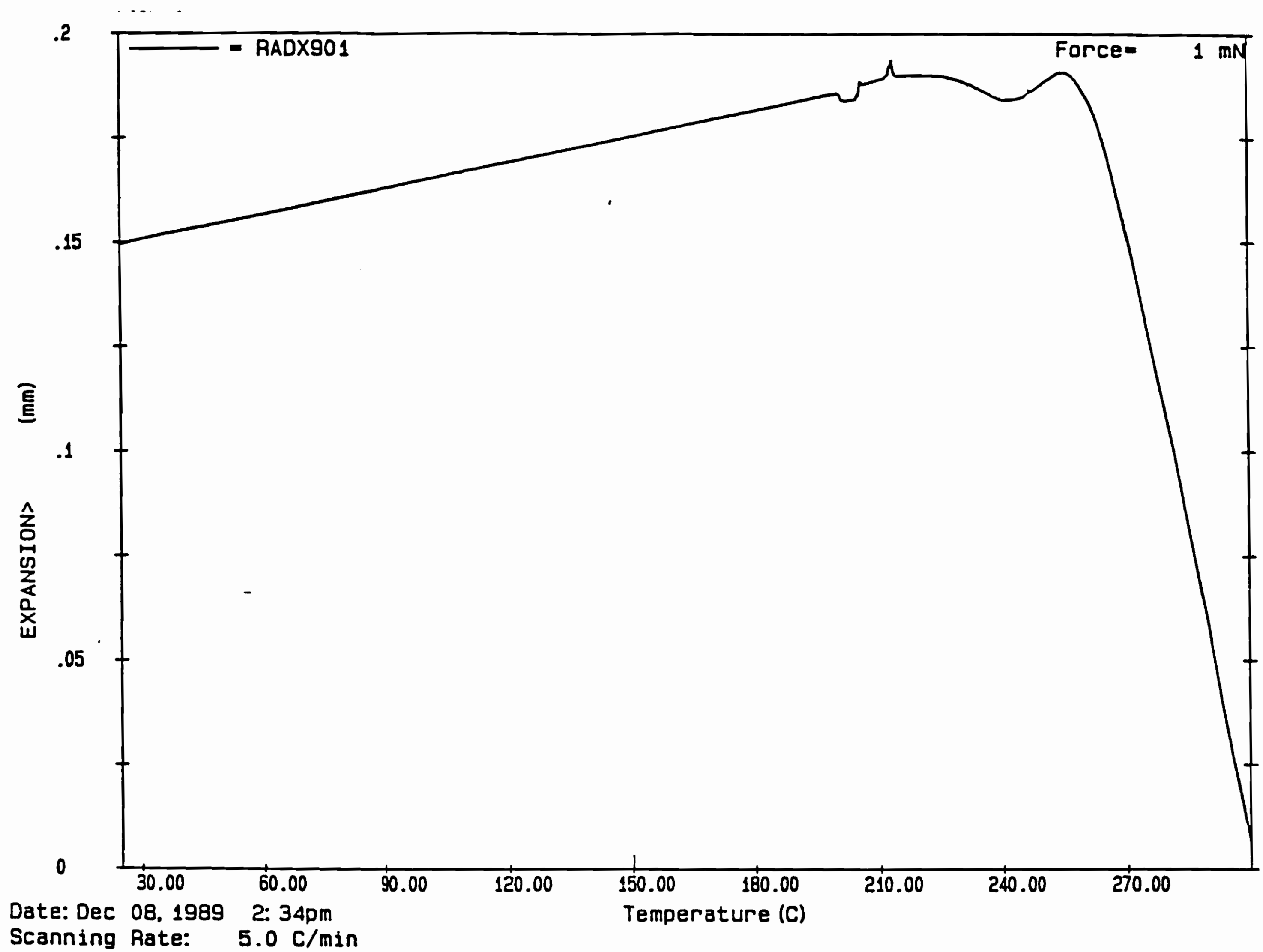

Figure 5.7 **Thermal expansion vs. temperature, 90° orientation**

The analysis of the data is performed by linear regression over a user-specified range of temperatures. The change in length (ΔL) due to a change in temperature (ΔT) is given by the relationship: $\Delta L = \alpha * L * \Delta T$ where L is the original length and α is coefficient of thermal expansion. In the temperature range of this experimental program, the coefficients of thermal expansion in the fiber (0°) and transverse (90°) directions are,

$\alpha(0°) = 0 \quad 1/°F$ $\qquad\qquad$ $\alpha(90°) = 1.83 \text{ e-5} \quad 1/°F$

The longitudinal (along the direction of the outer 0° plies) and transverse coefficients of thermal expansion for the $[0/90_3]_s$ cross ply laminate were measured as well and are shown in Figures 5.8 and 5.9. The measured laminate values are lower than those predicted by classical lamination theory by as much as 30% ,

$\alpha(L) = 1.004 \text{ e-5} \quad 1/°F$ $\qquad\qquad$ $\alpha(T) = 3.47 \text{ e-6} \quad 1/°F$

To measure the exact glass transition temperature, a small sample of T650-42/Radel X was tested in a Dupont 2100 DSC, Differential Scanning Calorimeter. The actual measured value of T_g is 419°F (215°C), and it matches exactly the manufacturer's data for the Radel X thermoplastic resin. The DSC trace is shown in Figure 5.10.

The storage and loss moduli thermal response were measured using the Dupont 983 Dynamic Mechanical Analyzer (DMA). The traces for

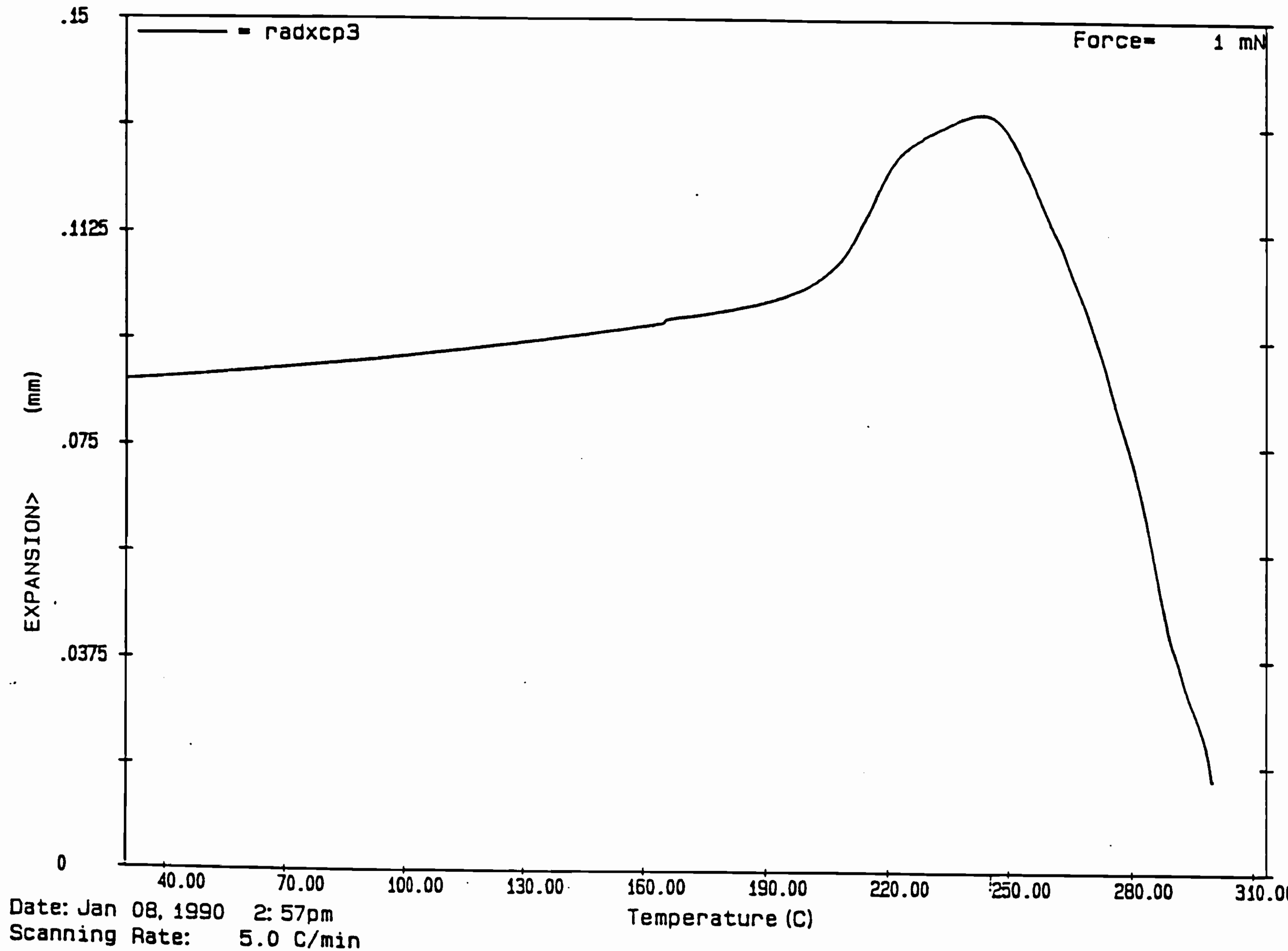

Figure 5.8 **Thermal expansion vs. temperature Cross ply, longitudinal**

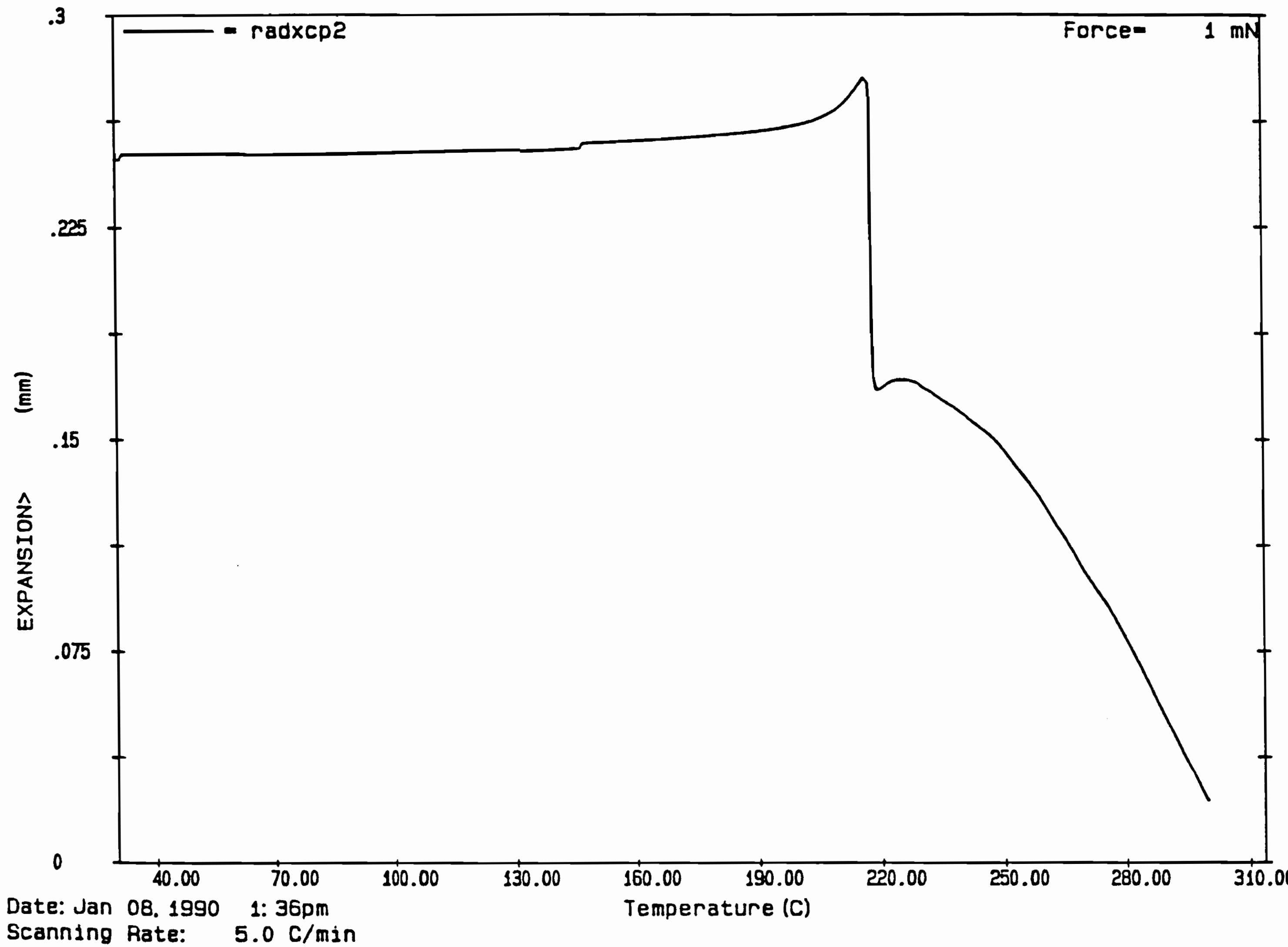

Figure 5.9 **Thermal expansion vs. temperature, Cross ply, transverse**

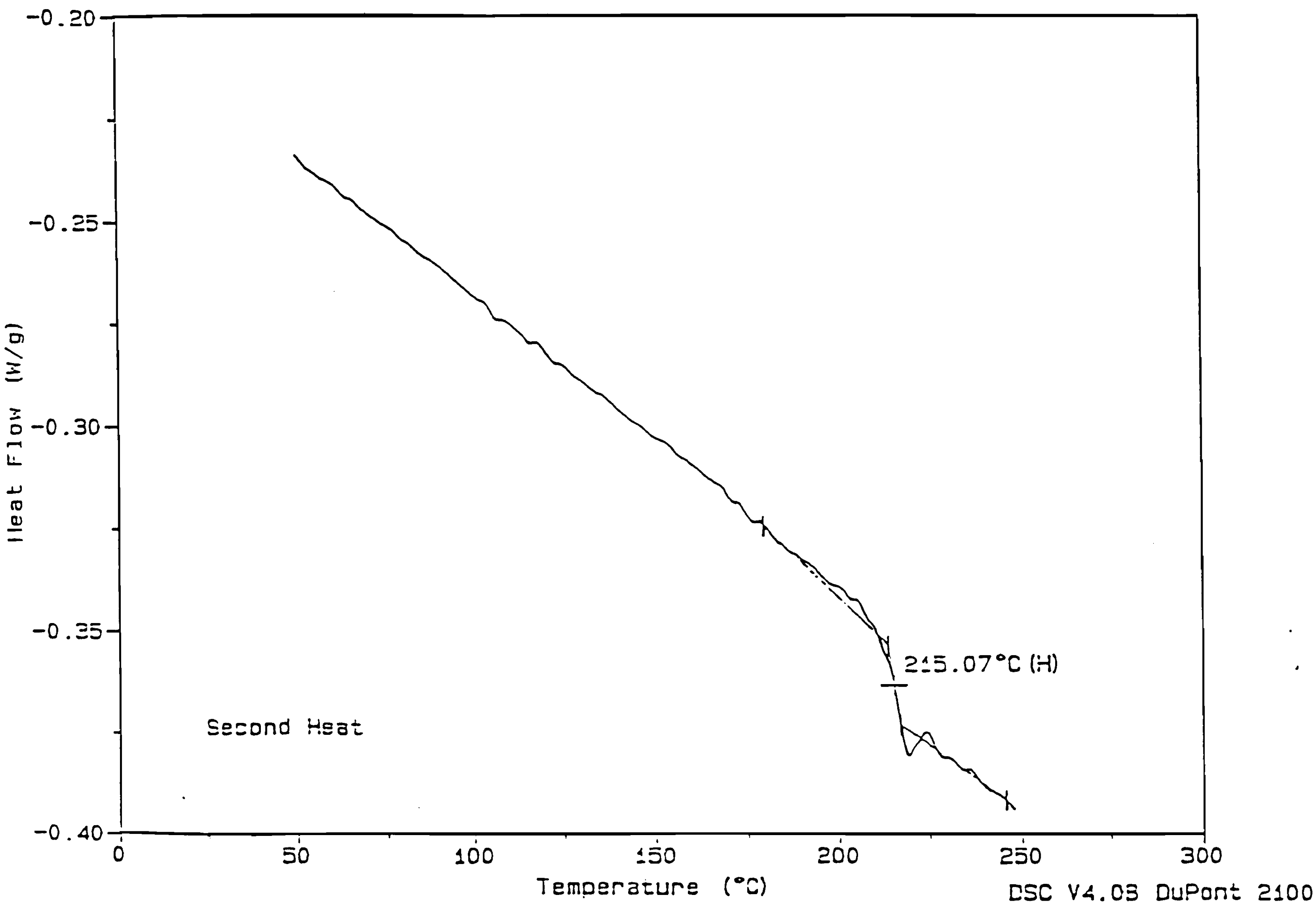

Figure 5.10 **Differential Scanning Calorimetry trace**

undamaged 0°, 90° and $[0/90_3]_s$ laminates are shown in Figures 5.11, 5.12 and 5.13. The storage modulus of the 0° laminate shows little dependence on temperature up to 177°C and an order of magnitude drop over a narrow temperature range centered at 225°C. The loss modulus is very small with a sharp peak at 235°C. The storage modulus of the 90° laminates decreases continuously up to 200°C and then drops to zero over a narrow temperature range centered at 215°C, which is the T_g of the matrix. The loss modulus is very small with a sharp peak centered at 220°C. This difference of 15°C in the location of the E" peak between longitudinal and transverse reinforcement is found in many fiber composites, as shown by Theocaris [177], and it is the result of the different constraint on the matrix material.

The storage modulus of the cross ply laminates shows traits of both the 0° and 90° laminates. Its value is constant up to 100°C, it slowly decreases up to 220°C and then drops by an order of magnitude over a narrow temperature range centered at 225°C. The loss modulus is small with a relatively broader peak centered at 235°C, exactly the same peak temperature as the 0° unidirectional laminates.

To ensure that no structural damage occurs to the matrix when coupons are subjected to long creep tests in the DMA at temperatures up to 482°F (250°C), a specimen was tested in a Dupont 2100 TGA, Thermal Gravimetric Analyzer. As shown in Figure 5.14, no significant weight loss occurs up to 788°F (420°C), well beyond the range of DMA tests.

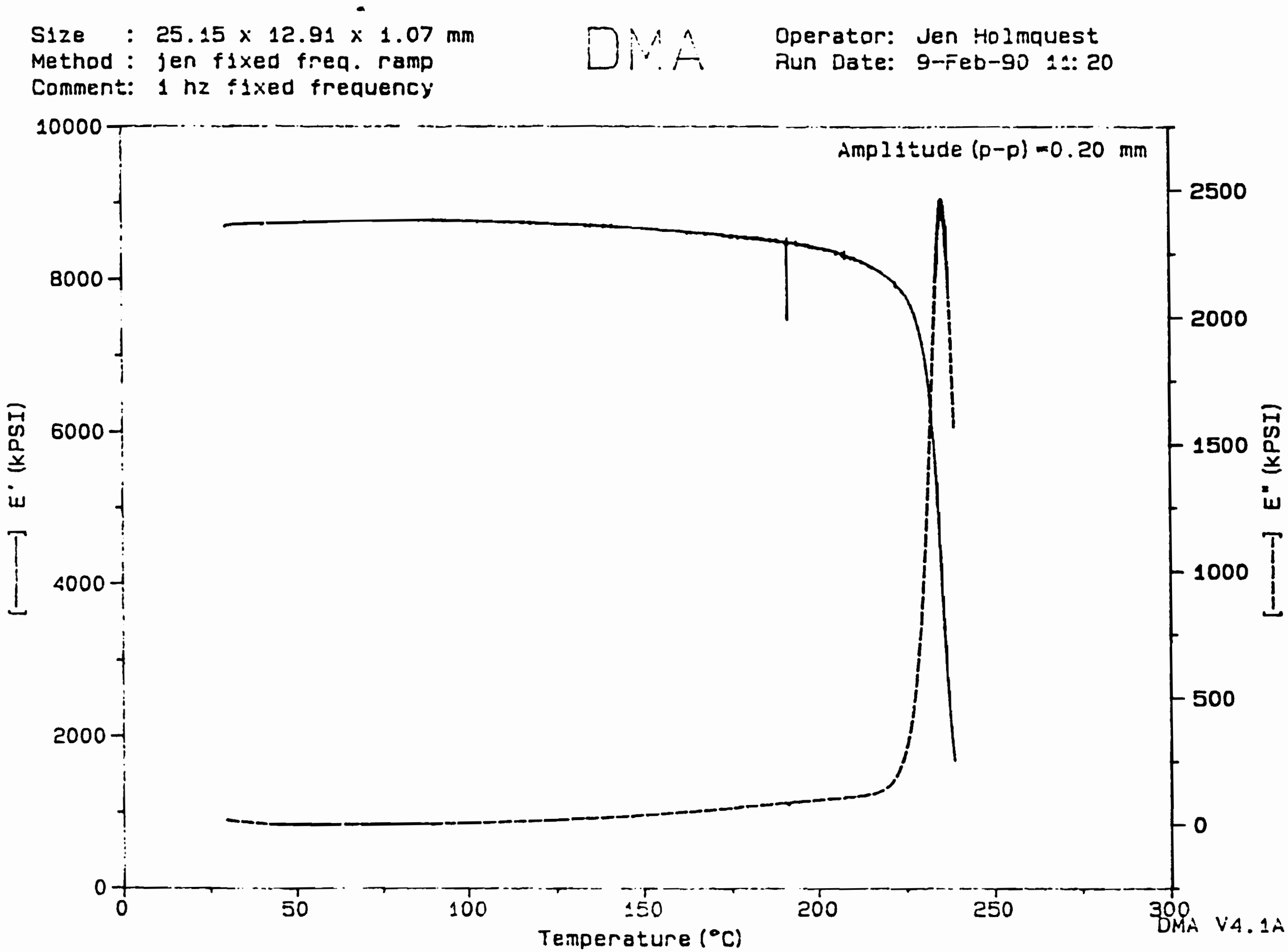

Figure 5.11 **Storage and Loss Moduli vs. Temperature, 0°**

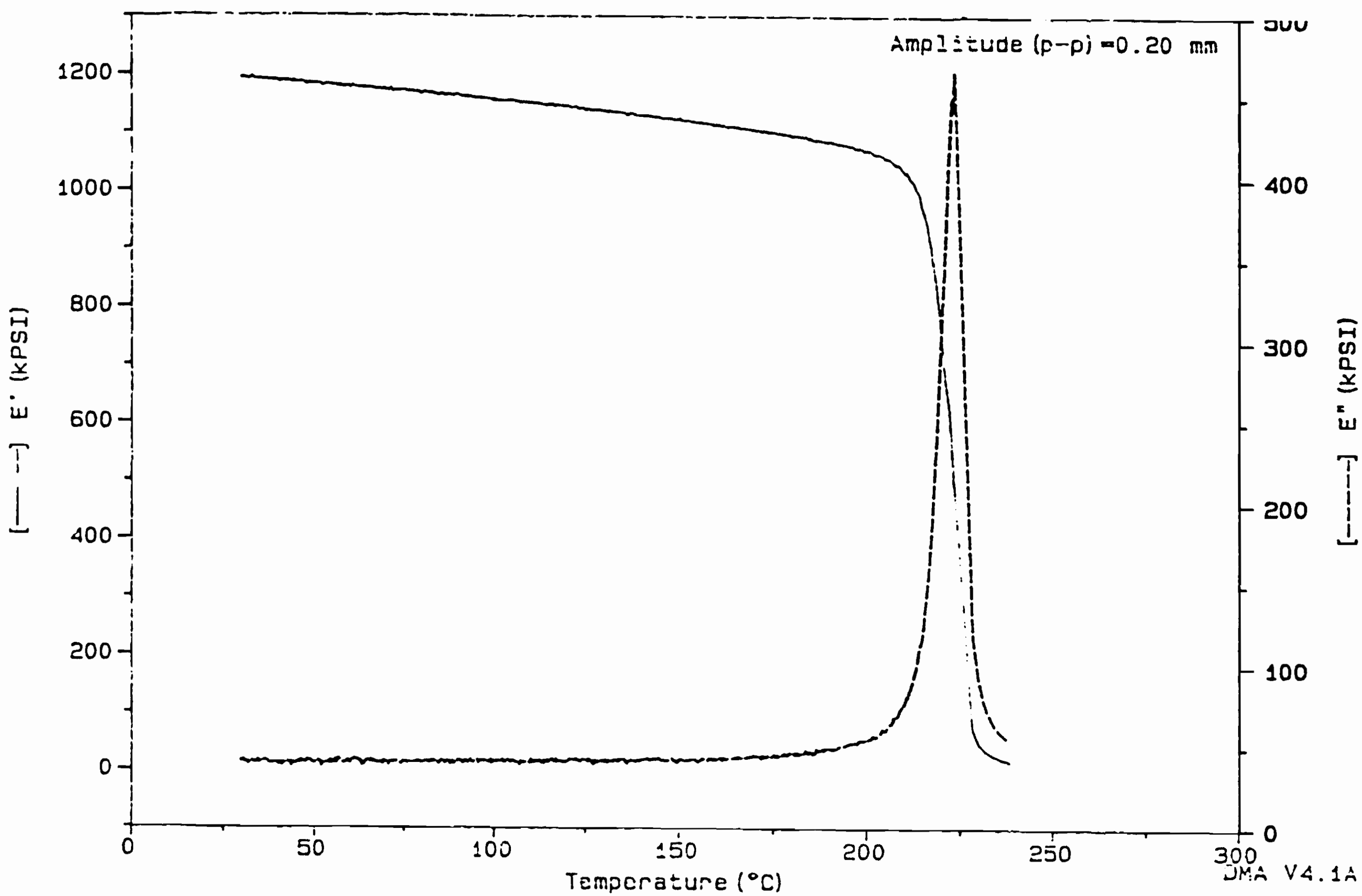

Figure 5.12 Storage and Loss Moduli vs. Temperature, 90°

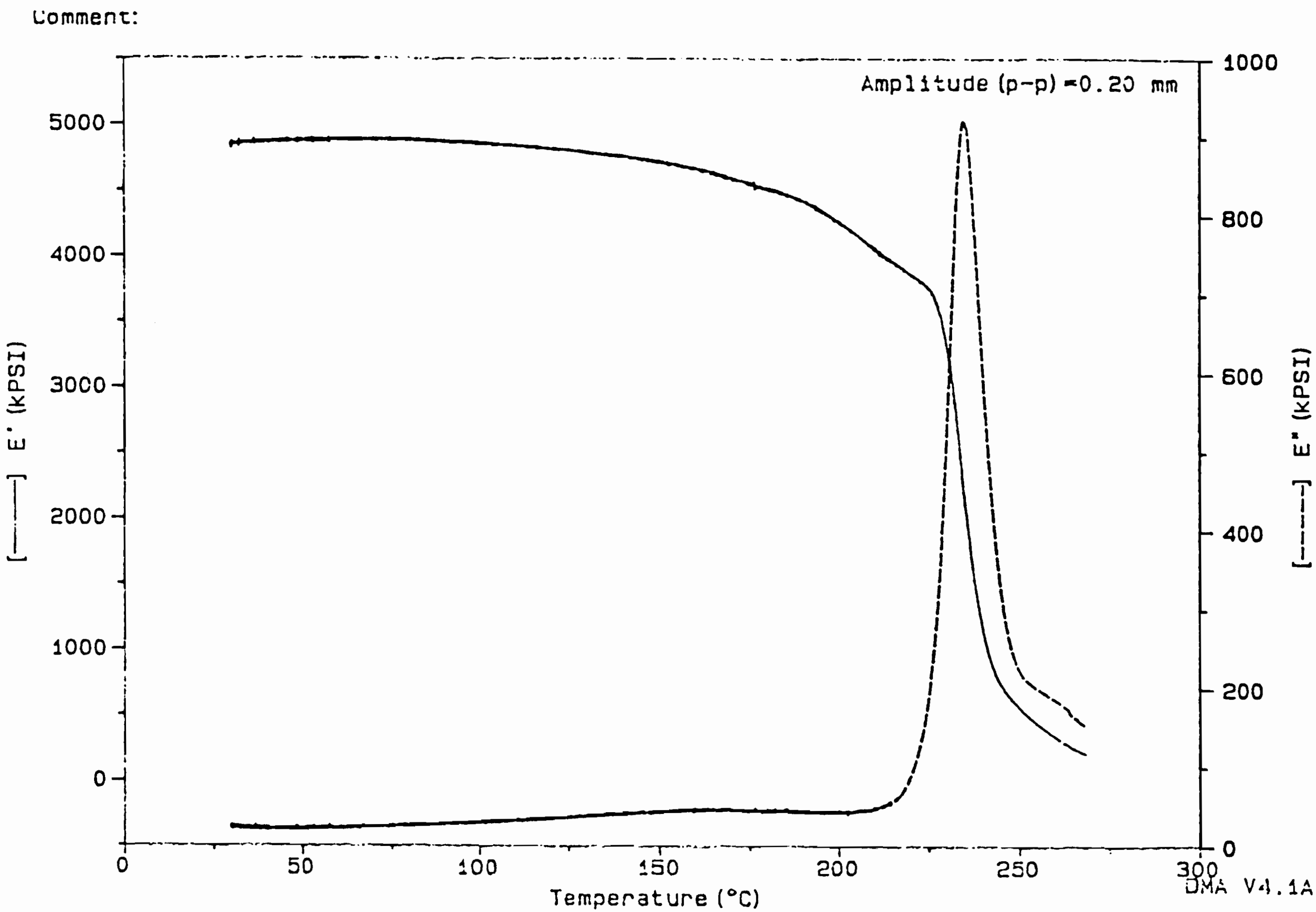

Figure 5.13 Storage and Loss Moduli vs. Temperature, Cross ply

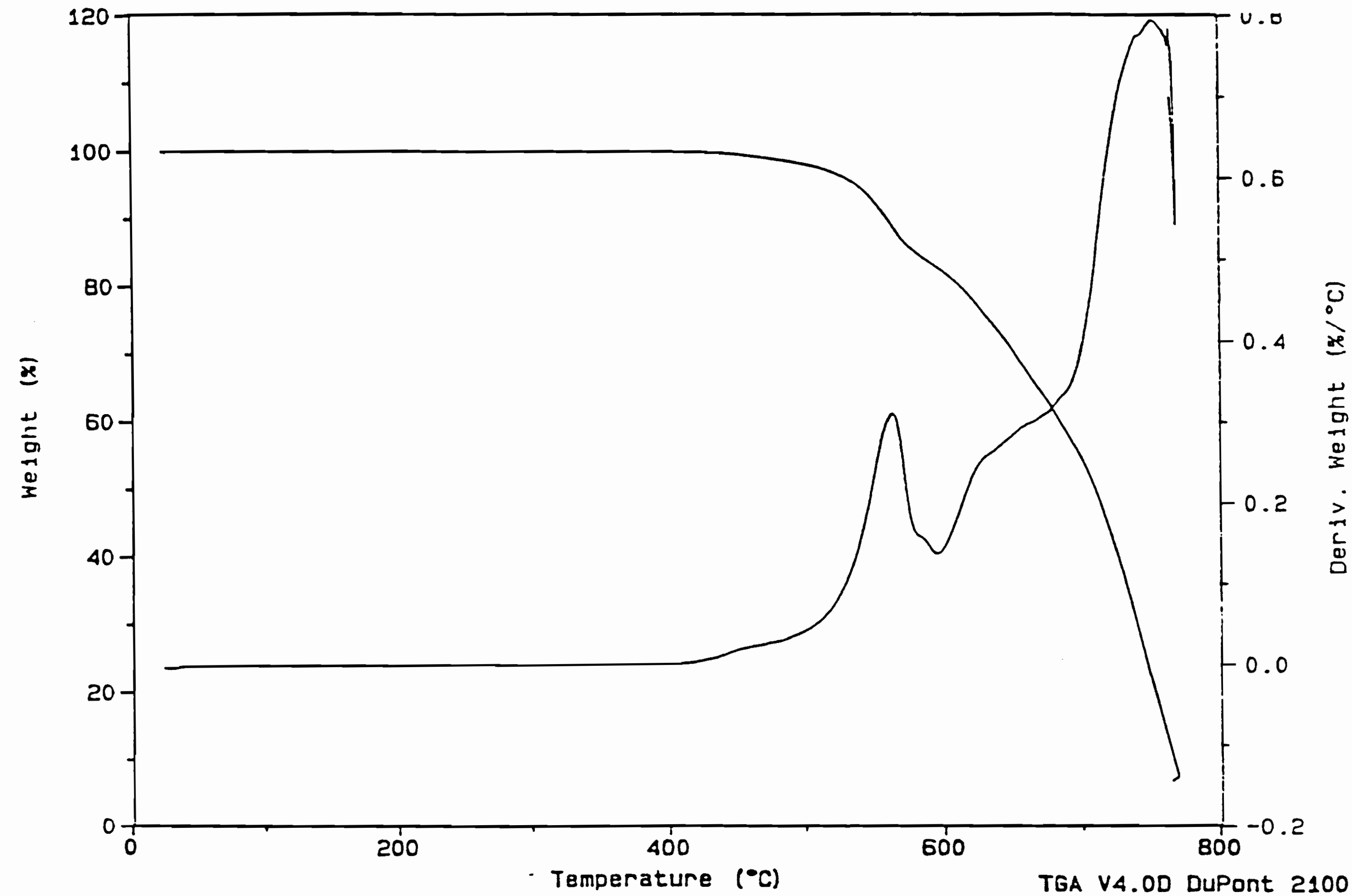

Figure 5.14 Thermo Gravimetric Analysis of Radel X/T650-42 specimen

5.4 Fatigue Response

The fatigue characterization of the T650-42/Radel X system included S/N curves for 0° and 90° unidirectional laminates at 10 Hz and a stress ratio R=0.1, secant stiffness monitoring, temperature profiles, and residual strength measurements.

The S/N data for the 0° and 90° laminates are plotted in logarithmic form in Figures 5.15.a and b. The unidirectional fatigue response has been fitted with the linear logarithmic relationships,

$$\text{Log}\,\frac{\sigma_{max}}{XT} \equiv \text{Log}\,S = b0 * \text{Log}\,N_f \qquad (0^\circ \text{ plies}) \qquad (5.4.1)$$

$$\text{Log}\,\frac{\sigma_{max}}{YT} \equiv \text{Log}\,S = b90 * \text{Log}\,N_f \qquad (90^\circ \text{ plies}) \qquad (5.4.2)$$

where:

σ_{max}	is the maximum cyclic stress,
XT	is the ultimate longitudinal tensile strength,
YT	is the ultimate transverse tensile strength,
S	is the stress level,
N_f	is the number of cycles to failure, and
b0, b90	are coefficients obtained from linear regression,

b0 = -0.0263, R^2 = 0.963

b90 = -0.10106, R^2 = 0.979

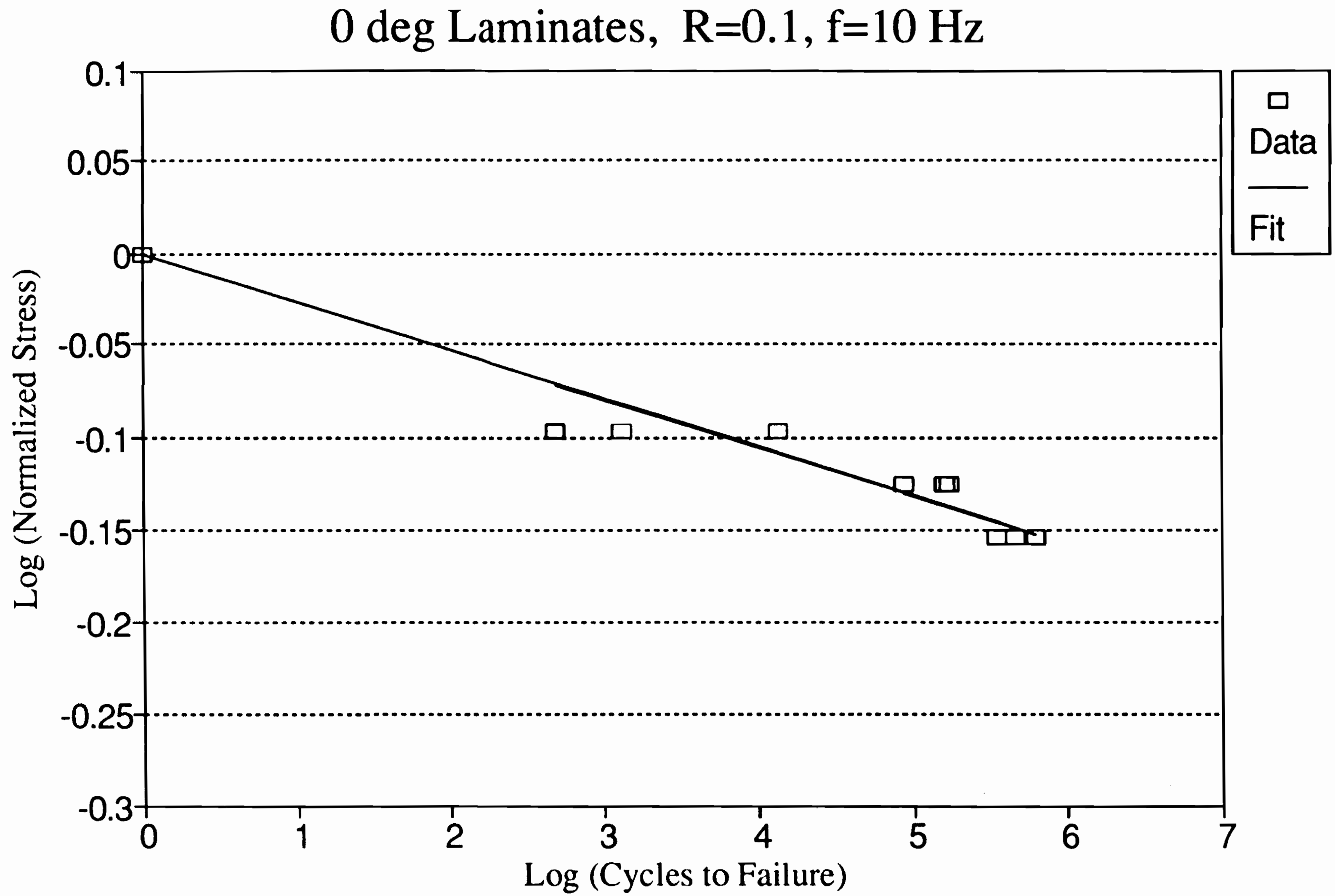

Figure 5.15.a **S/N data, 0° orientation**

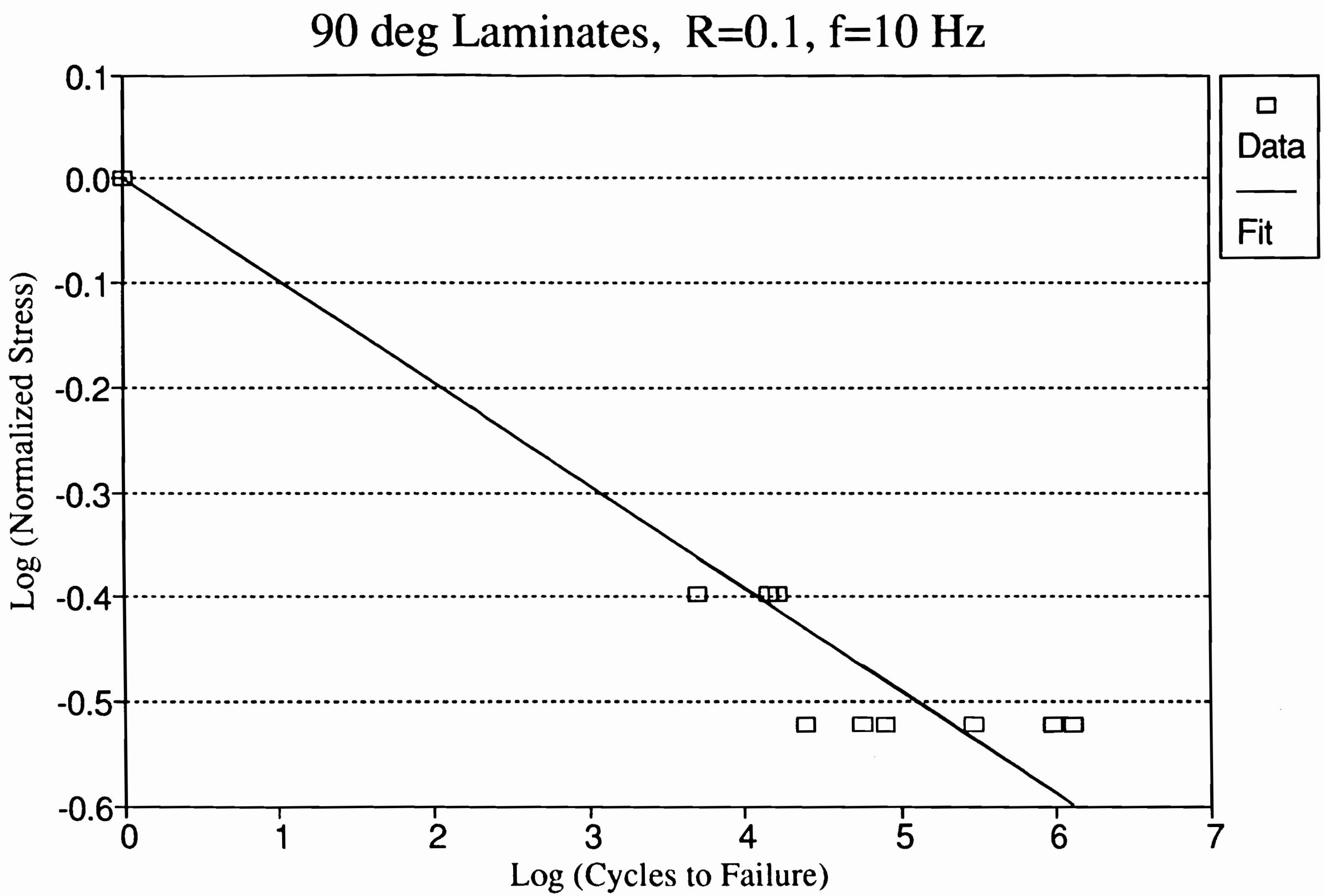

Figure 5.15.b S/N data, 90° orientation

Stiffness and temperature monitoring of the 90° coupons during cyclic loading reveal that there are no measurable temperature or stiffness changes preceding failure. Failure occurs as a crack rapidly propagates across the width of the specimen. The crack surfaces are relatively smooth.

The 0° unidirectional coupons exhibit only a minor degradation of stiffness throughout most of their life. As shown in Figure 5.16, there is less than 1.5% degradation in the axial stiffness after more than 90% of the fatigue life. In some instances there is a small increase ($\leq$0.1%) in the early stages that could be attributed to cyclic stiffening but it is probably due to the inaccuracy of the dynamic measurements.

Figure 5.17 is a characteristic temperature and acoustic emission (AE) profile. The AE profile (inverted scale in Figure 5.17) shows that events occur throughout the fatigue life, generally with an increasing amplitude (RMS voltage) trend. High energy events occur upon loading. Extremely energetic events that exceed the scale precede failure. The temperature profile shows a small initial rise in temperature (its magnitude depending on the stress level), constant temperature throughout most of the test (with a small increase due to the increasing temperature of the grips), and a sharp rise towards the end of life. Both profiles complement one another. The temperature peak and high energy events are accompanied by a rapid decrease in residual strength and even faster degradation of longitudinal stiffness. Failure is of the broom type and the test section of the

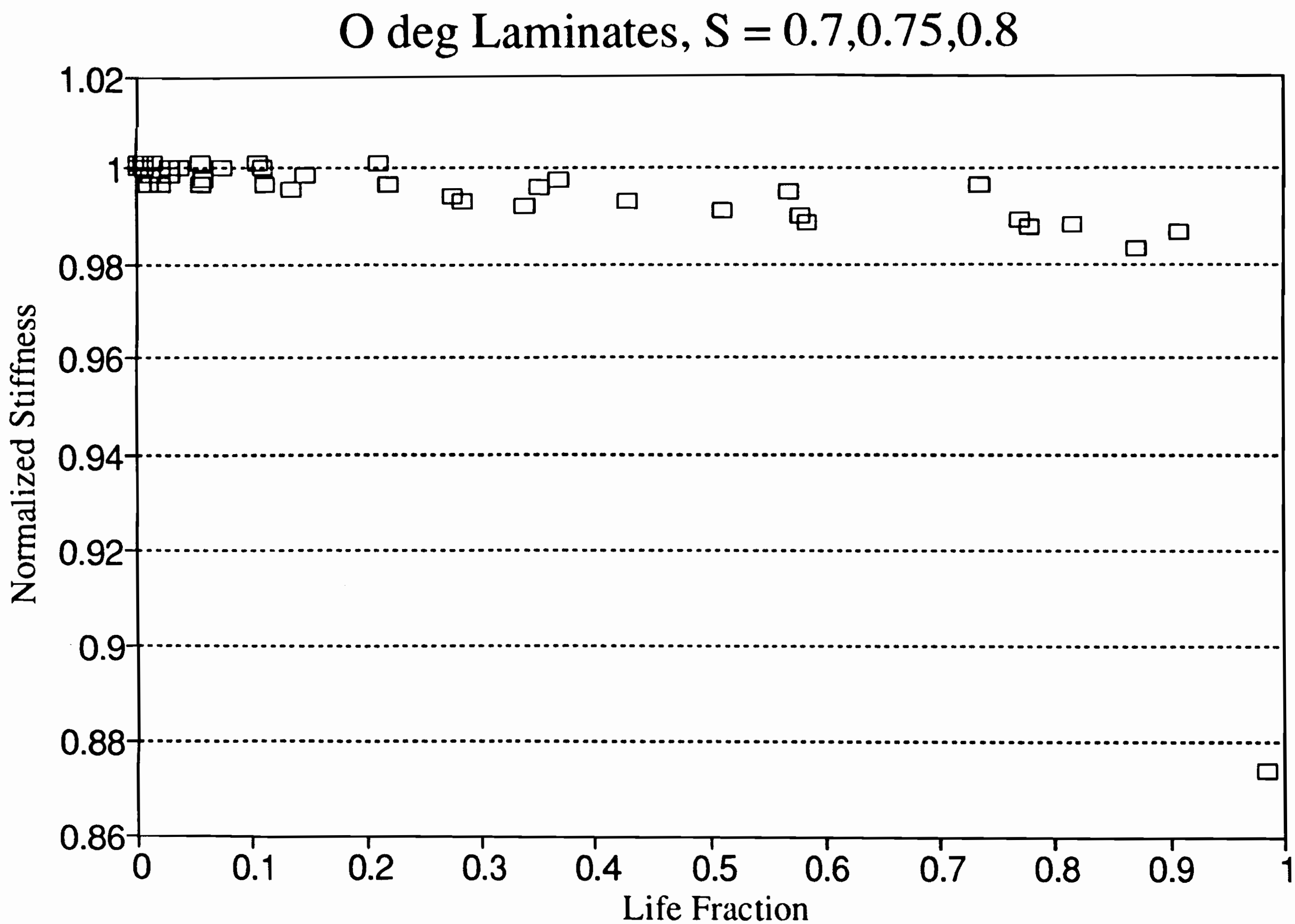

Figure 5.16 Normalized stiffness vs. Life fraction, 0° laminates

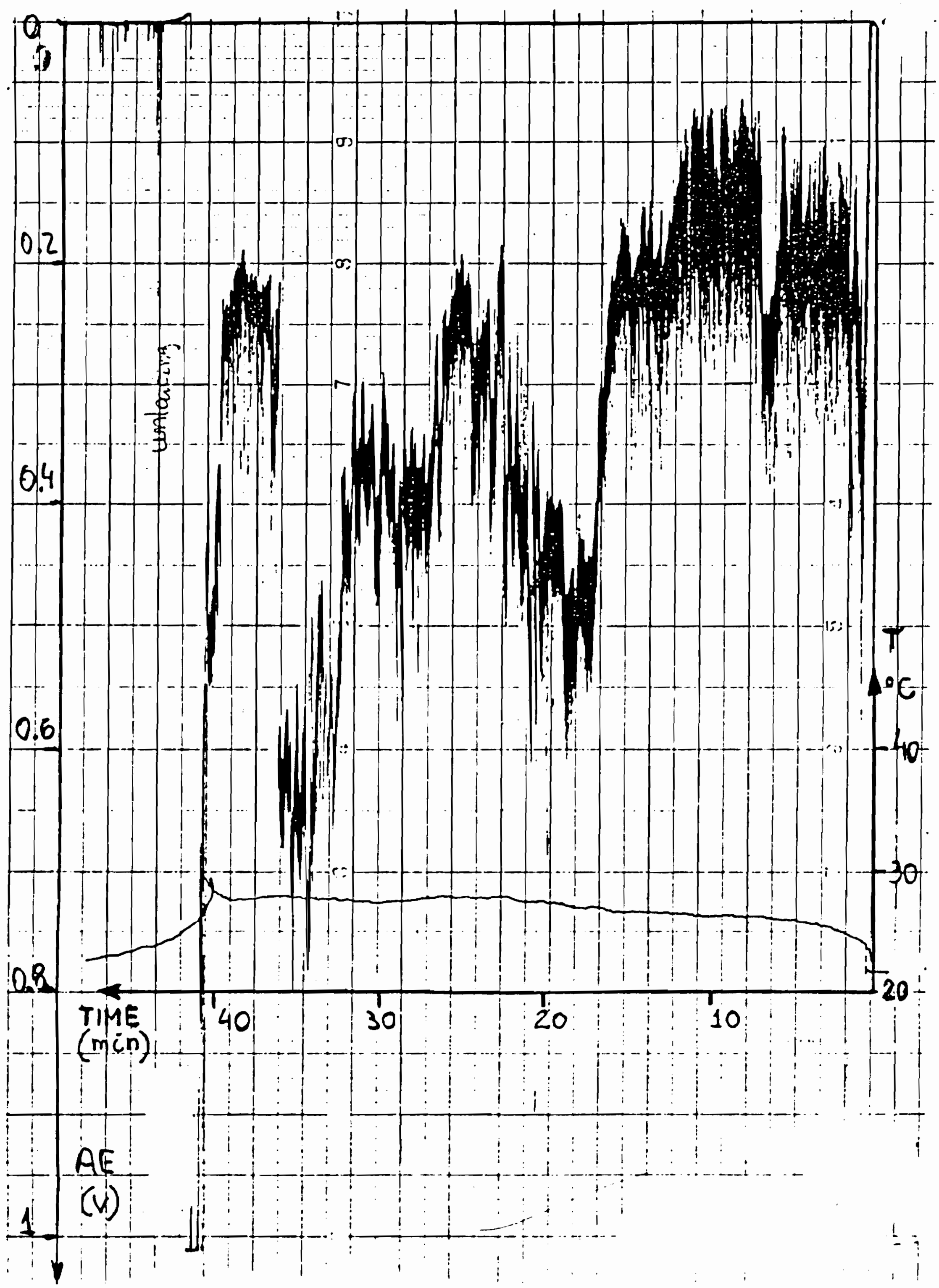

Figure 5.17 Temperature and Acoustic Emission profile of fatigue test, 0°

fatigue specimen practically disintegrates with fibers and pieces coming apart.

Residual strength results are plotted vs. approximated life fraction (n/N_f, where N_f is the average number of cycles to failure) in Figure 5.18 and vs. normalized remaining stiffness in Figure 5.19. Strength and remaining stiffness seem to be correlated in a nonlinear fashion creating a concave curve; i.e. strength reduction precedes stiffness degradation. The remaining stiffness - $E_1(n)$, and residual strength - RS(n) of the 0° coupons were correlated with life fraction with corresponding power law relationships, as described in Chapter 3. Simplifying Equations 3.3.12 and 3.3.13,

$$E_1(n) = E_1(0) \left[1 - (1-S) \left(\frac{n}{N_f} \right)^{pb} \right] \tag{5.4.3}$$

$$RS(n) = RS(0) \left[1 - (1-S) \left(\frac{n}{N_f} \right)^{qb} \right] \tag{5.4.4}$$

where:

where:	$E_1(0)$	is the initial stiffness,
	RS(0)	is the initial tensile strength,
	S	is the constant cyclic stress level,
	N_f	is the number of cycles to failure at constant S,
	n	is the number of cycles, and
	pb,qb	are coefficients obtained from linear regression,

pb = 105, qb = 35

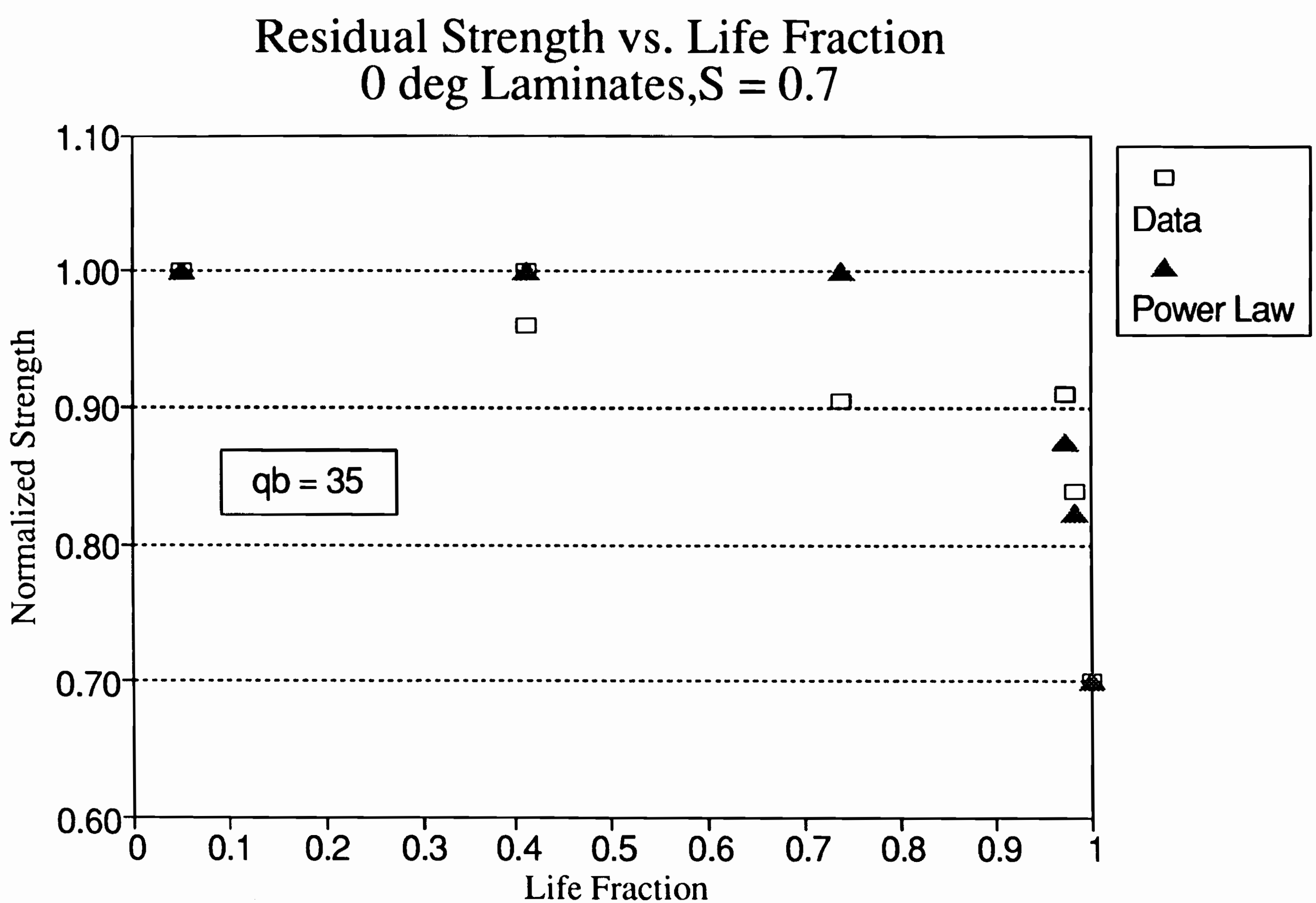

Figure 5.18 **Residual strength vs. Life fraction, 0° laminates**

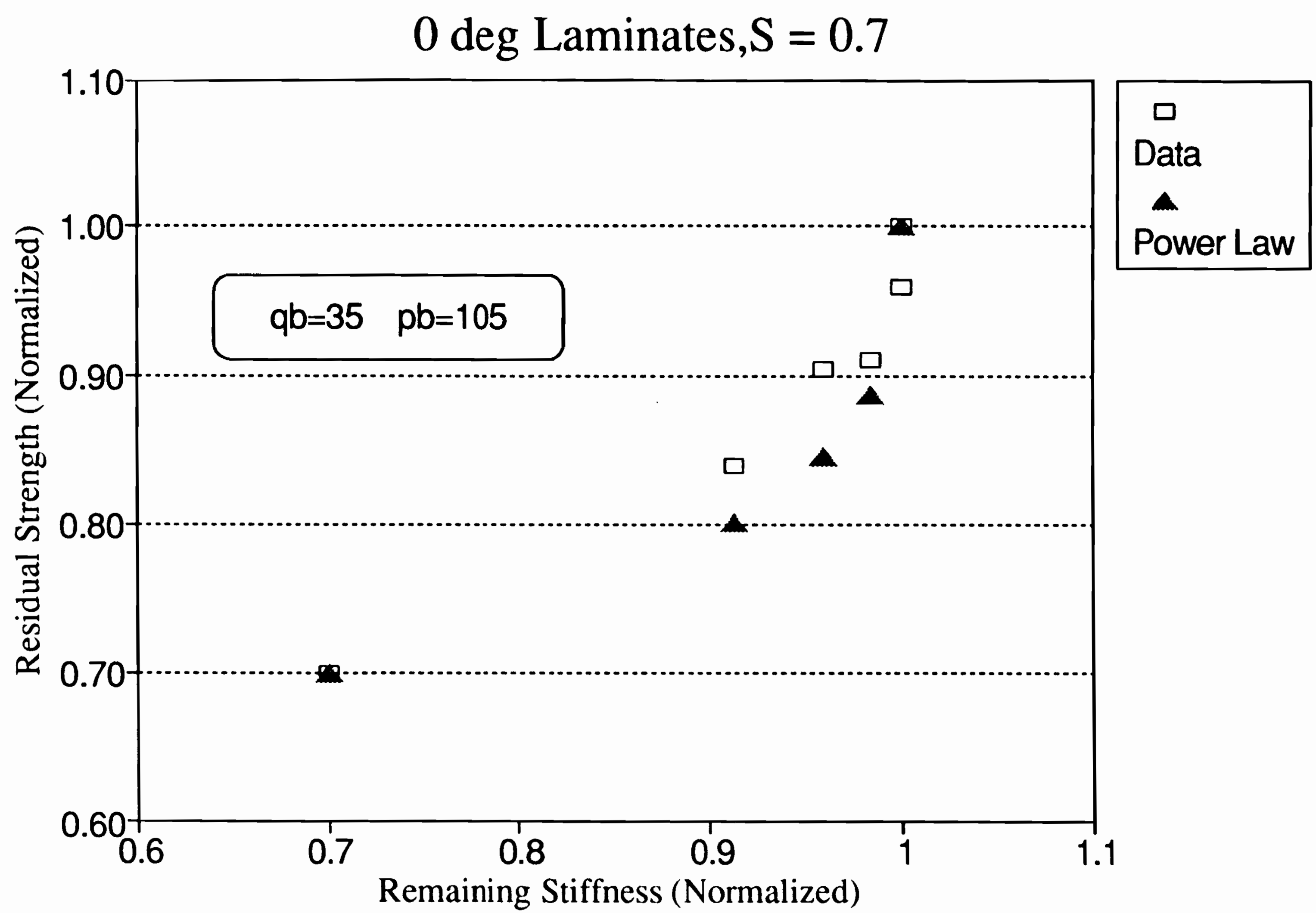

Figure 5.19 Residual strength vs. Remaining stiffness, 0° laminates

Cross ply laminates were tested at stress levels of 0.70, 0.65, 0.60 and 0.55. The resulting fatigue lives range from a few hundred cycles to over one million cycles, as shown in Figure 5.20. The normalized stiffness traces for S=0.65, 0.60 and 0.55 are shown in Figures 5.21.a, b and c. For the highest stress level, S=0.7, the stiffness changes constantly throughout its very short life. For S=0.65 the stiffness reduced to approximately 93% of the initial stiffness during the first 30% of life. Between 30 and 90% of life stiffness decreases to 90% of the initial value. During the final 10% of life, the stiffness decreases rapidly. For S=0.6 a secondary stable stiffness of approximately 88 to 90% of the undamaged laminate stiffness is reached during the initial 5 to 10% of life. After the initial degradation, the stiffness remains fairly constant for most of the life. Near the end of life, stiffness reduces rapidly, forewarning of impending failure. For S=0.55, the behavior of the stiffness is very similar to that recorded for S=0.6; but life exceeded one million cycles.

The fracture surfaces of the $[0/90_3]_s$ specimens demonstrate the effects of loading history on the damage and fracture processes. For low stress levels ($S \leq 0.60$), the outer 0° plies exhibit a broom type failure with extensive delamination at the 0/90 interfaces, as shown in Figure 5.22 next to a quasi static failure, which has a well defined fracture surface and only minor delaminations. The inner core of 90° plies fracture at several locations into multiple pieces.

The transient cyclic deformation exhibits behavior corresponding

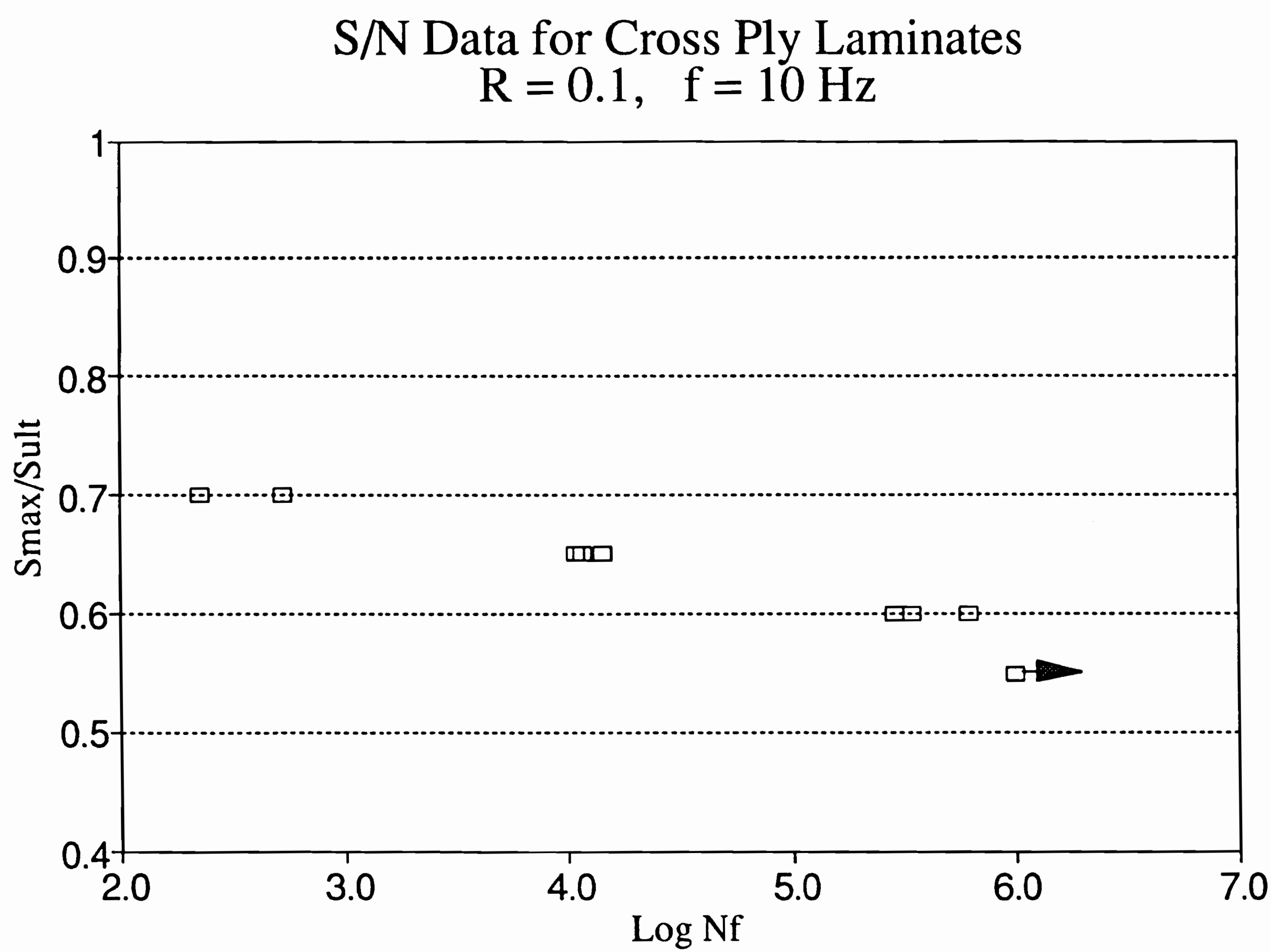

Figure 5.20 S/N data, Cross ply laminates

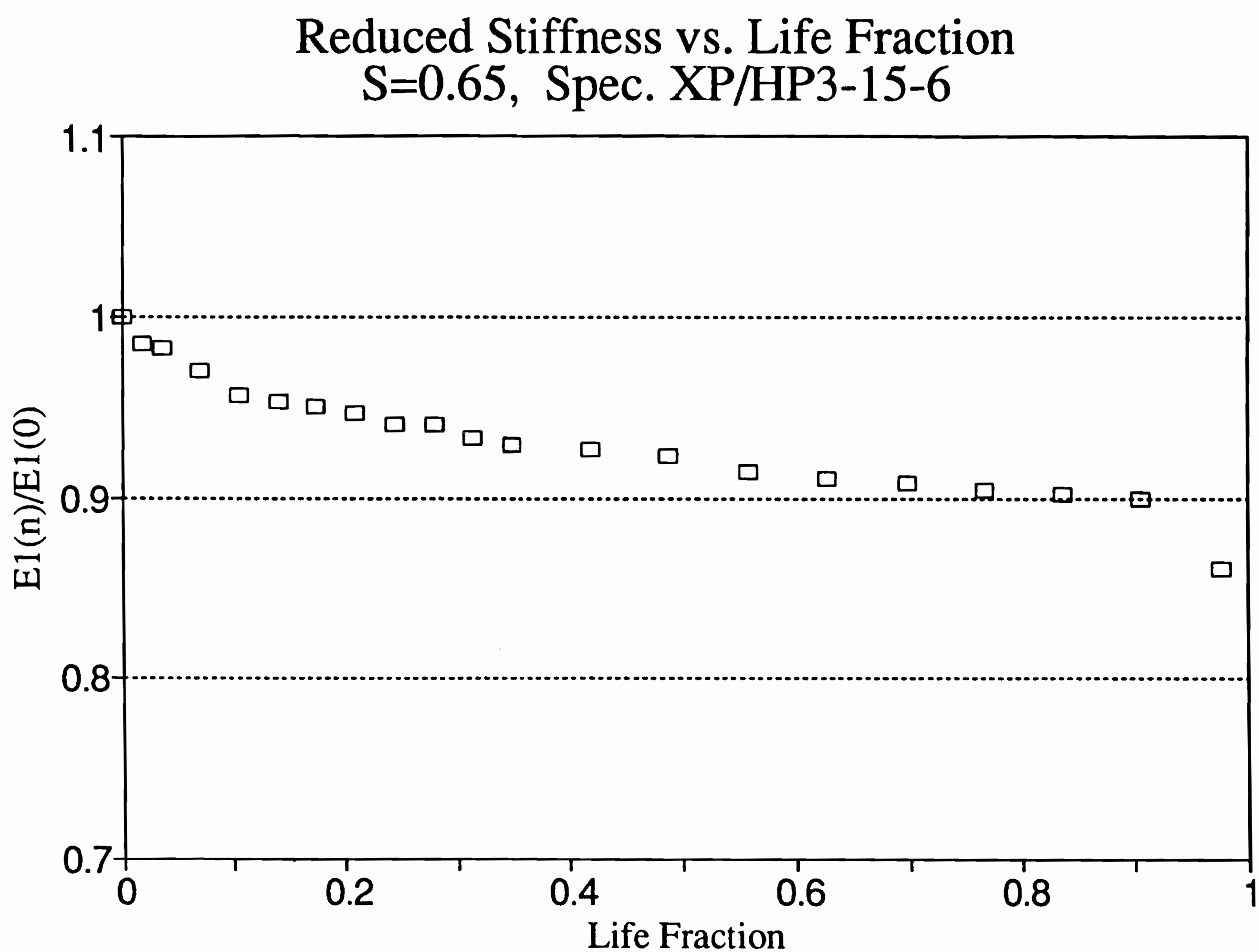

Figure 5.21.a Global axial stiffness vs. Life fraction, Cross ply @ S=0.65

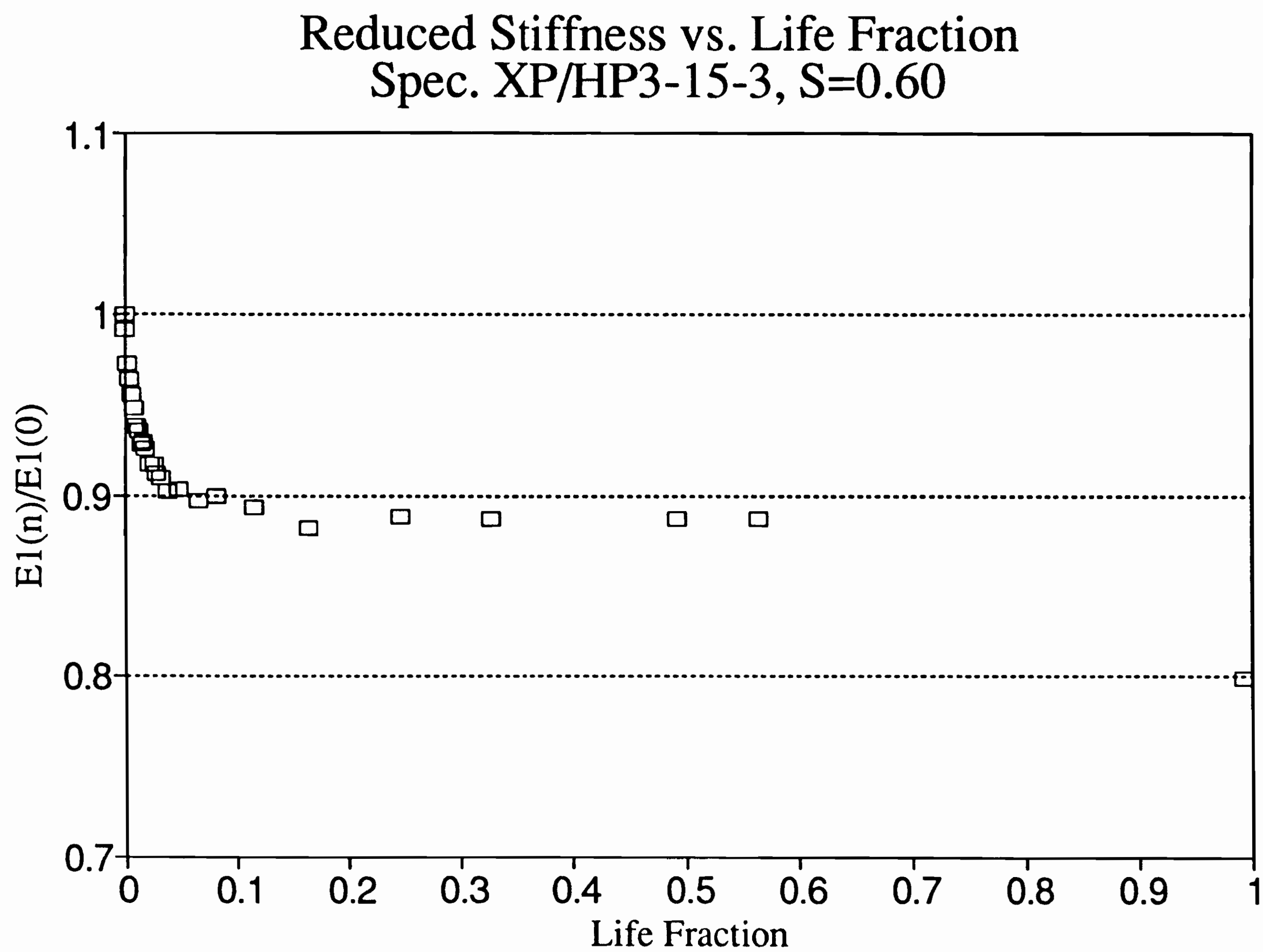

Figure 5.21.b Global axial stiffness vs. Life fraction, Cross ply @ S=0.60

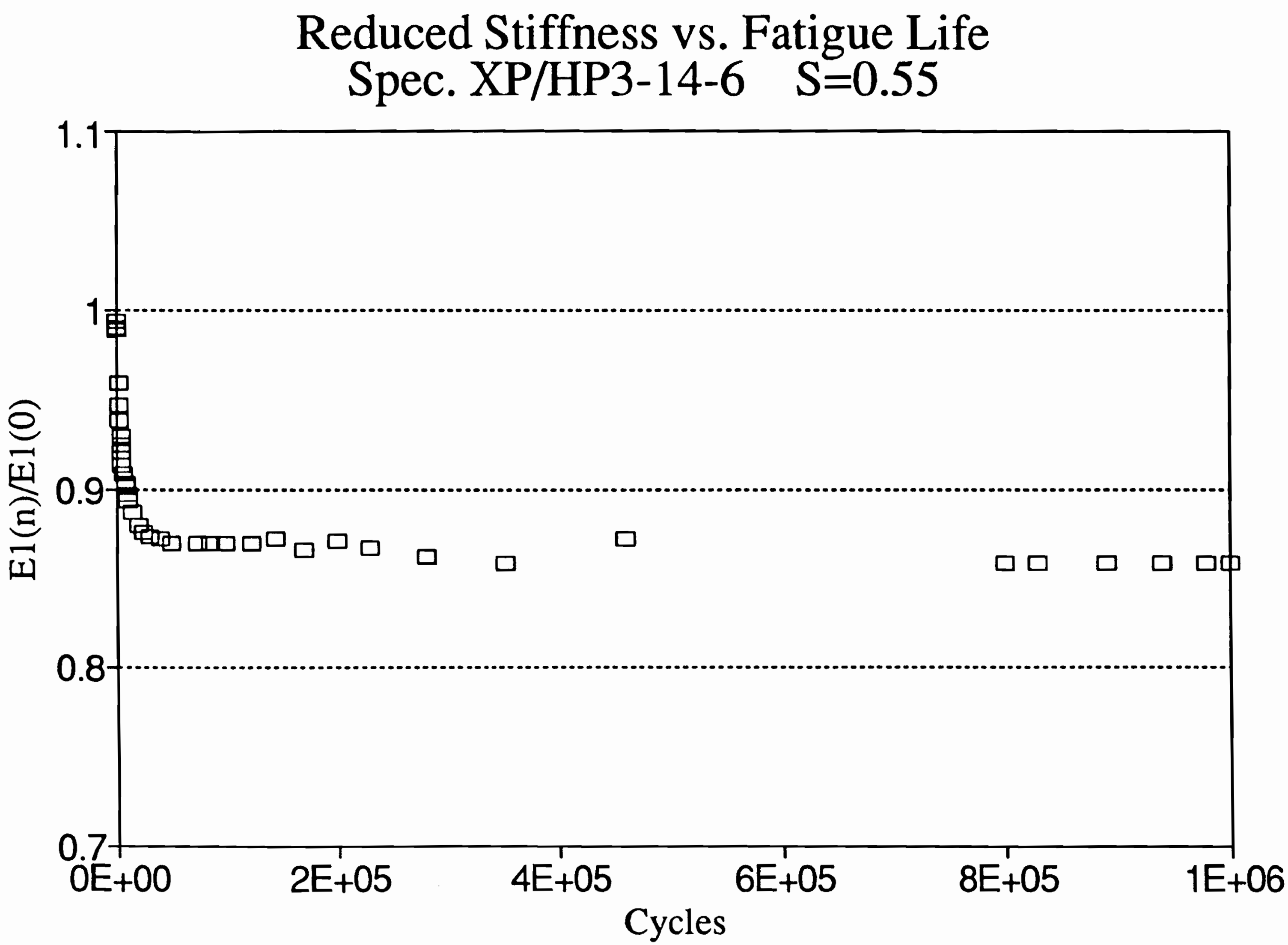

Figure 5.21.c Global axial stiffness vs. Life fraction, Cross ply @ S=0.55

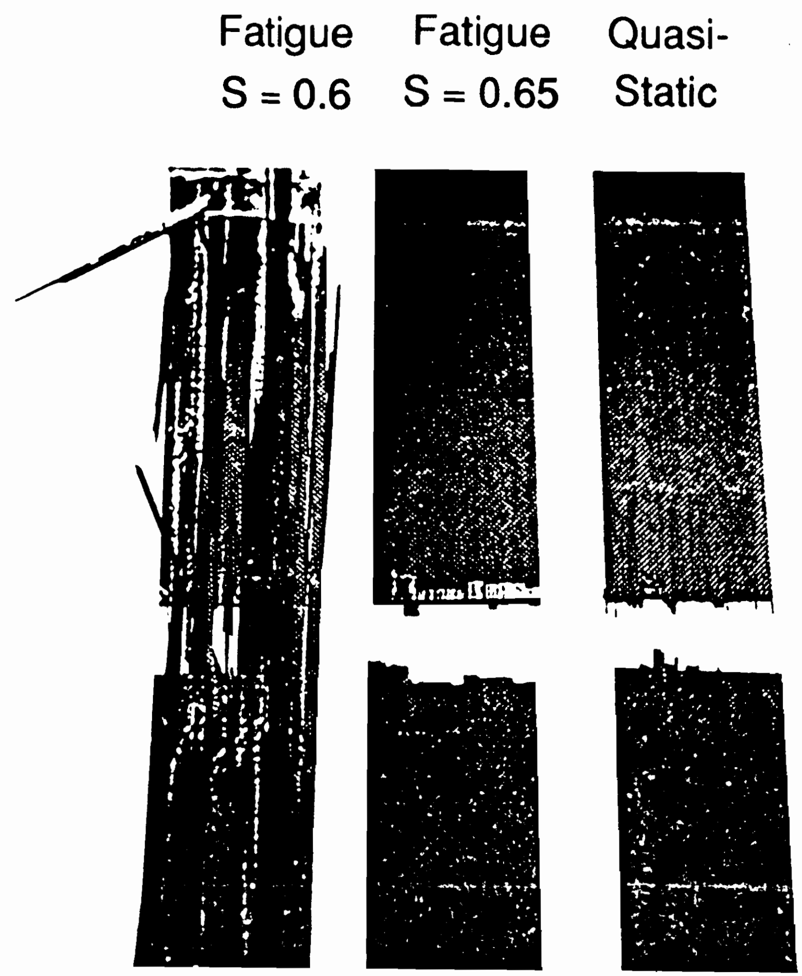

Figure 5.22 Cross ply coupons, fatigue and quasi static failures

to the stiffness degradation, as shown in Figures 5.23.a, b and c for the same stress levels. In these figures, transient deformation (open squares) is plotted as the difference between the dynamic and first cycle strain at maximum load vs. number of cycles. Due to cyclic anelastic deformation, the magnitude of the transient cyclic deformation is much larger than that anticipated by stiffness changes (filled triangles) alone. The ratio is approximately 40% for all stress levels.

The residual strength of cross ply laminates was determined for S=0.60 and 0.55 at three different life fractions. Three replicates were run at each life fraction. The selected points are,

1. midway through the initial stiffness degradation stage,
2. immediately after the initial stiffness degradation stage is completed and a stable stiffness is achieved,
3. 200000 cycles for S=0.6 ($n/N_f \geq 0.50$) and 1 million cycles for S=0.55.

The results of the residual strength tests are presented in Tables 5.3 and 5.4, and plotted vs. normalized stiffness in Figure 5.24. It is apparent that the strength and stiffness reduction do not correspond directly. Unlike the case of the 0° laminates, a significant stiffness reduction due to cracking in the 90° plies occurs with no significant reduction in strength. Strength reduction is also linked to a reduction in failure strain and is dependent on the fatigue stress level.

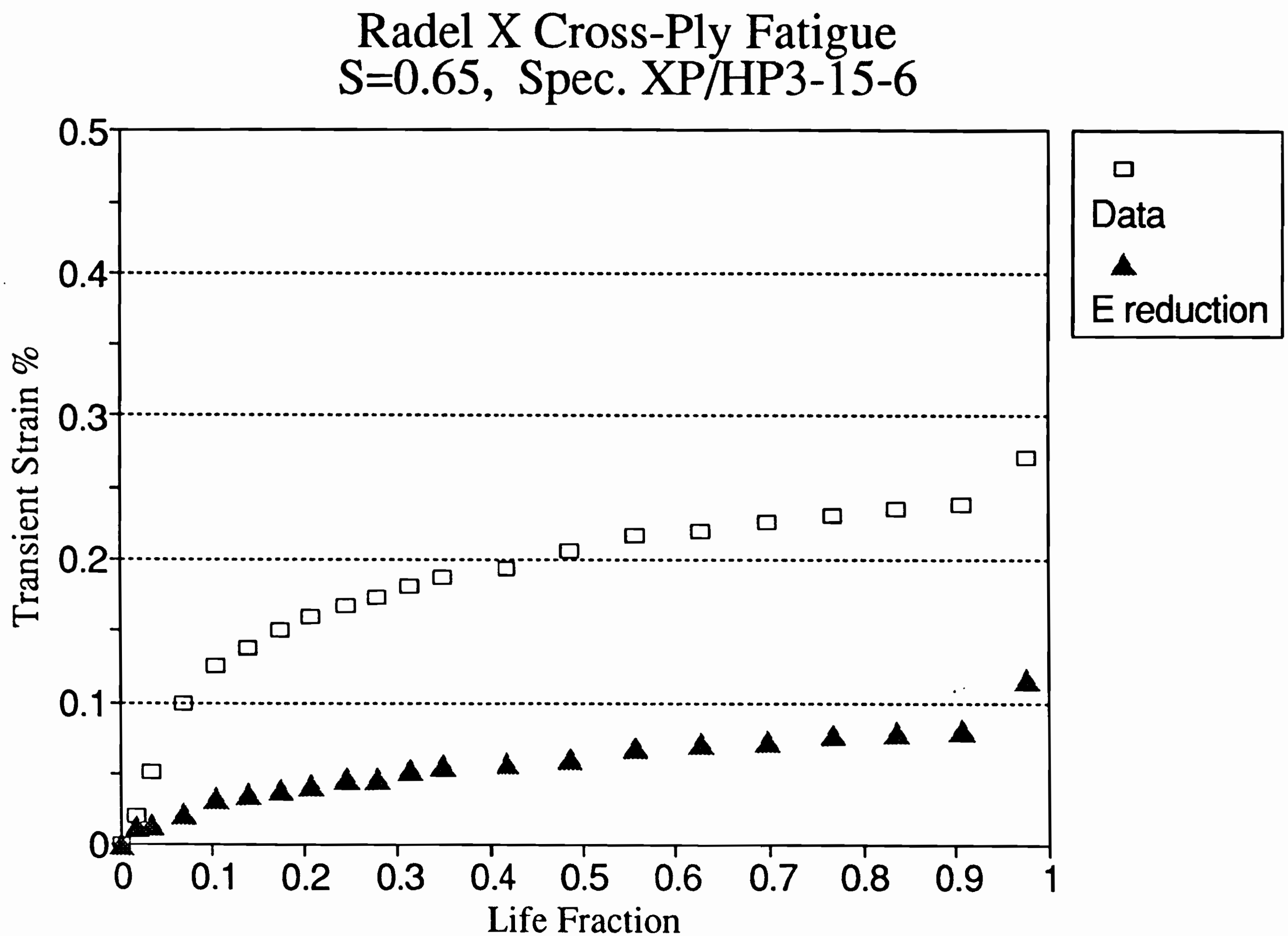

Figure 5.23.a Transient strain curves, Cross ply laminates, S=0.65

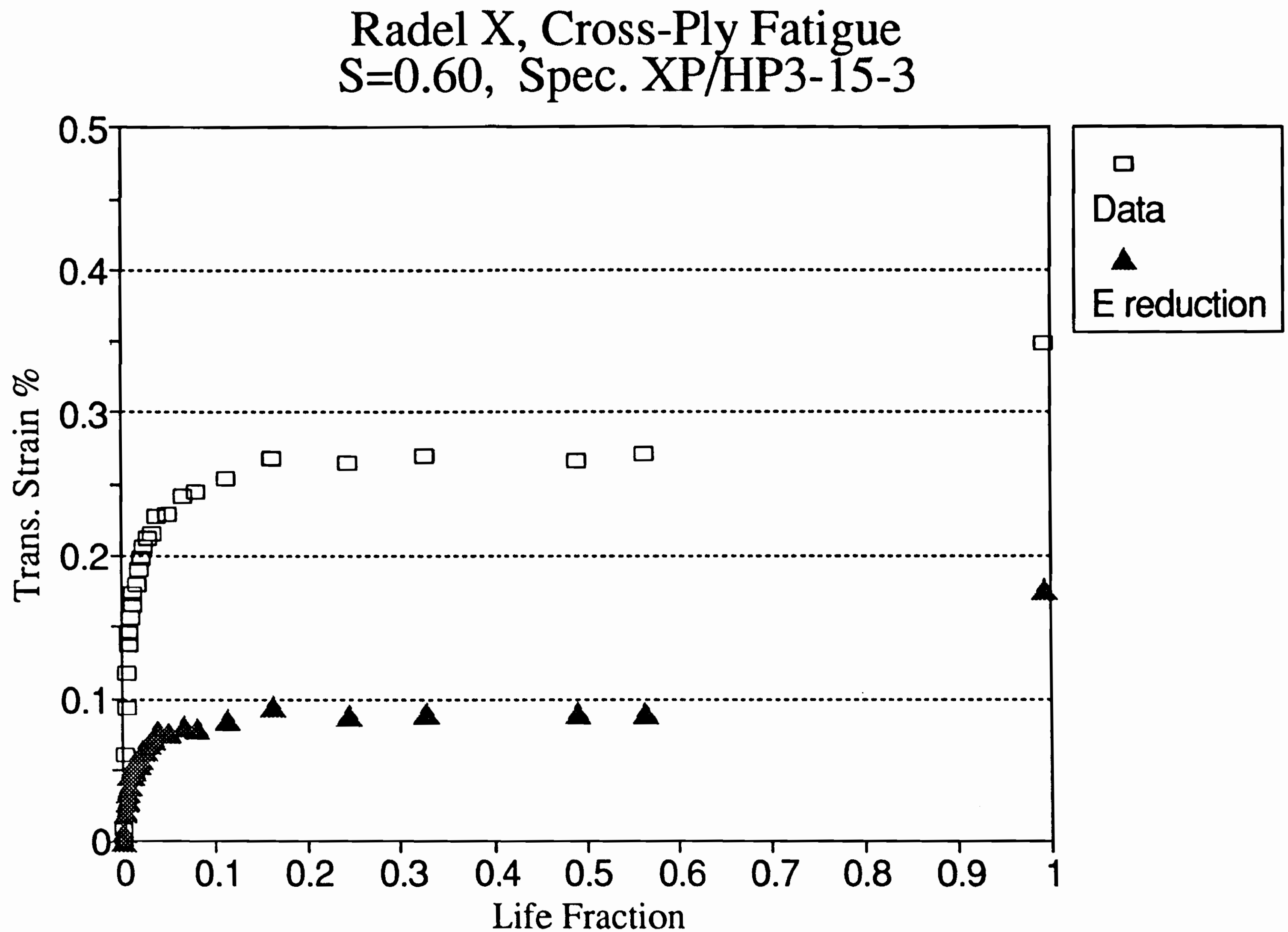

Figure 5.23.b **Transient strain curves, Cross ply laminates, S=0.60**

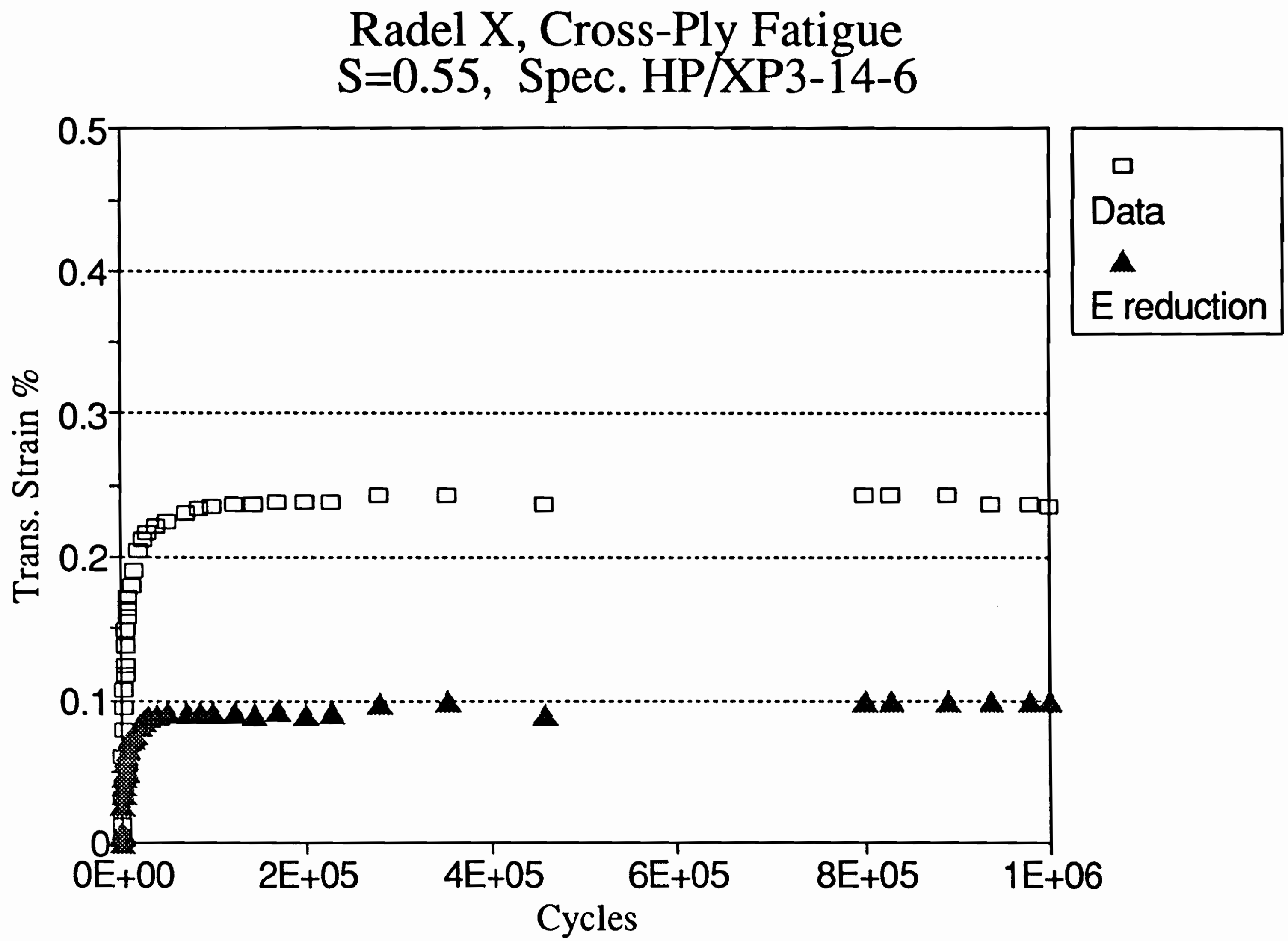

Figure 5.23.c Transient strain curves, Cross ply laminates, S=0.55

Table 5.3 Tensile Residual Properties, Cross Ply Laminates, S=0.55

Cycles	Residual Strength psi	$\frac{R.S.}{UTS}$	Initial Modulus Msi	$\frac{E1\ init.}{E1\ R.S.}$	Failure Strain %
4000	70417	0.97	5.88	0.92	1.19
50000	66349	0.92	5.57	0.86	1.17
1e6	58492	0.81	5.43	0.87	1.09

Table 5.4 Tensile Residual Properties, Cross Ply Laminates, S=0.60

Cycles	Residual Strength psi	R.S. / UTS	Initial Modulus Msi	E1 init. / E1 R.S.	Failure Strain %
1500	73214	1.01	6.17	0.94	1.20
20000	61429	0.85	5.72	0.90	1.06
200000	62143	0.86	5.57	0.87	1.12

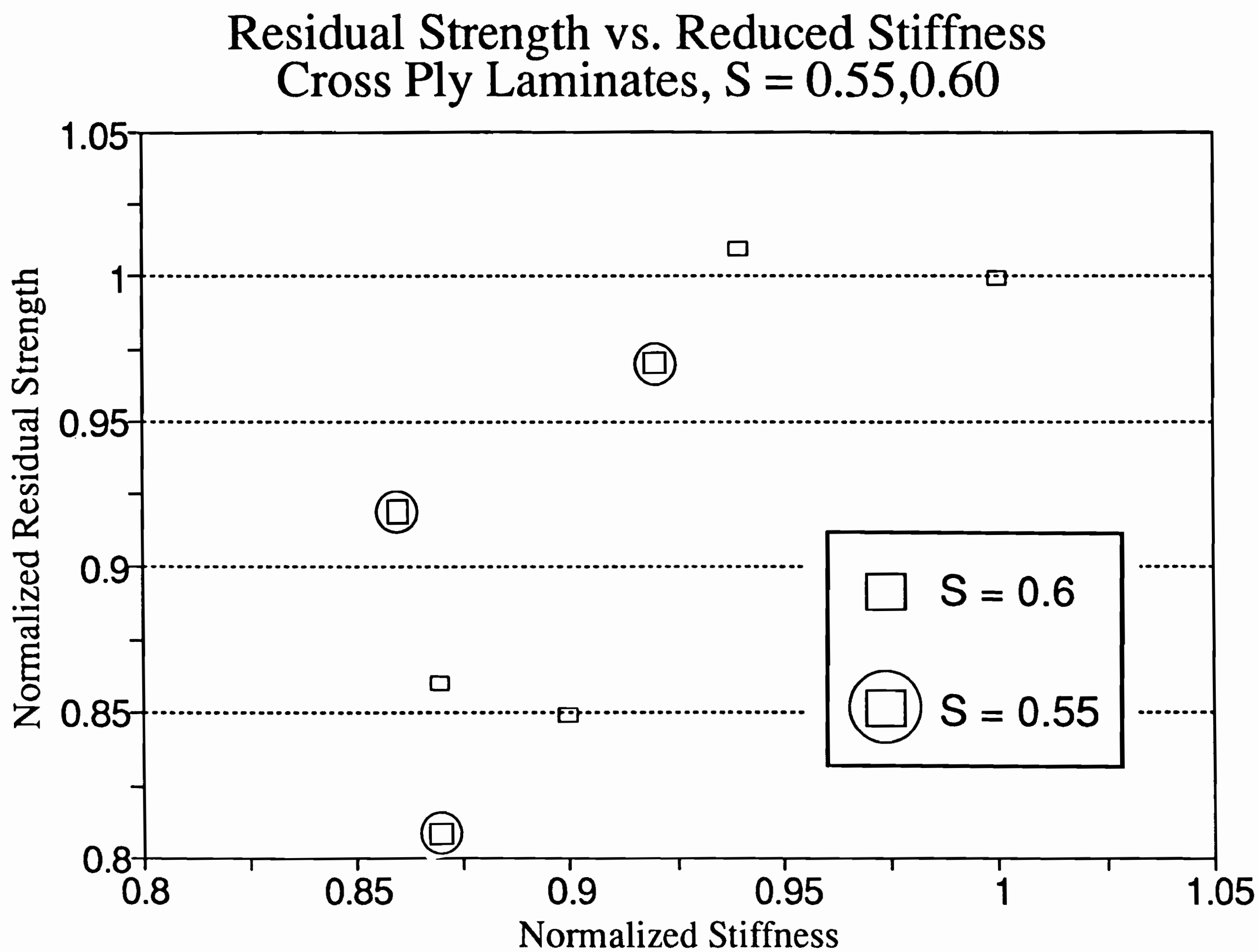

Figure 5.24 Residual strength vs. remaining stiffness, Cross ply laminates, S=0.55 and 0.6

5.5 Nondestructive Damage Evaluation

In order to aid in the investigation of the damage sequence occurring during the fatigue loading of cross ply laminates, all residual strength specimens were C-scanned at 15 MHz before and after being cycled. Such C-scans are presented in Figures 5.25 through 5.31. In these figures it is evident that damage has evolved in the form of matrix cracking and progressive delamination. It seems that the amount of delamination is greater in specimens cycled at lower stress levels.

In order to further investigate the amount and types of damage present in the cross ply laminates, Acoustic Scanning Microscopy was used to produce images of the surface, 0/90 interface, and interior 90° plies. A series of images is shown in Figures 5.32 through 5.34, for specimens tested at S=0.55 up to 4000, 50000 and 1 million cycles, as well as the image from a quasi-static failed specimen, Figure 5.35. The length of the photograph is always along the fiber direction in the 0° outer plies.

By examination of the cycled specimens, it is easy to recognize that two sets of cracks develop in cross-ply laminates, as predicted by the Shear Lag Analysis presented in 5.2. First, a transverse crack array develops across the width of the specimen in the 90° plies. It is partially developed at 4000 cycles where the spacing is irregular and some cracks do not span across the width of the specimen. At 50000 cycles, the array is regular and fully developed. The spacing has an

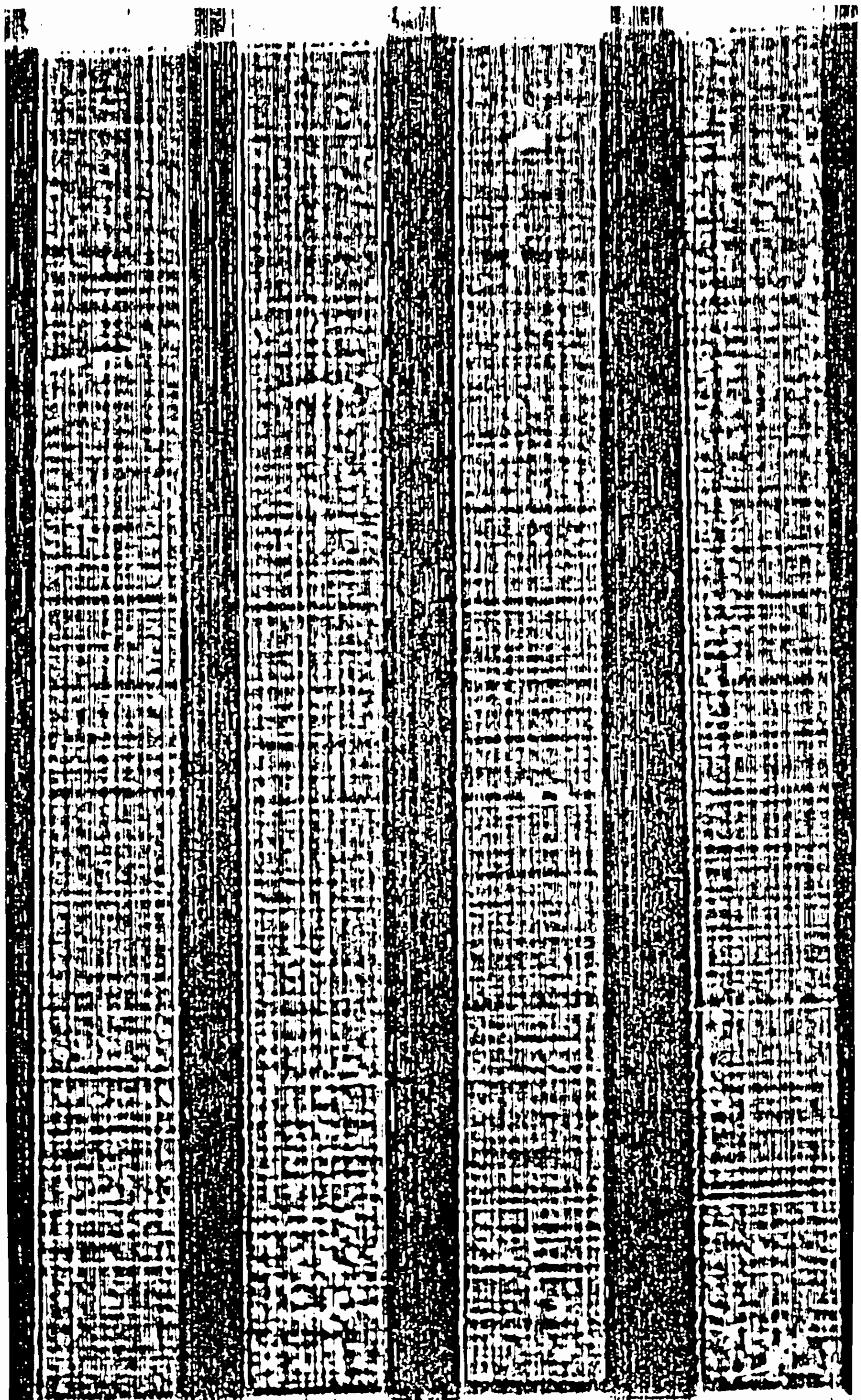

Figure 5.25 C-scans, virgin cross ply specimens

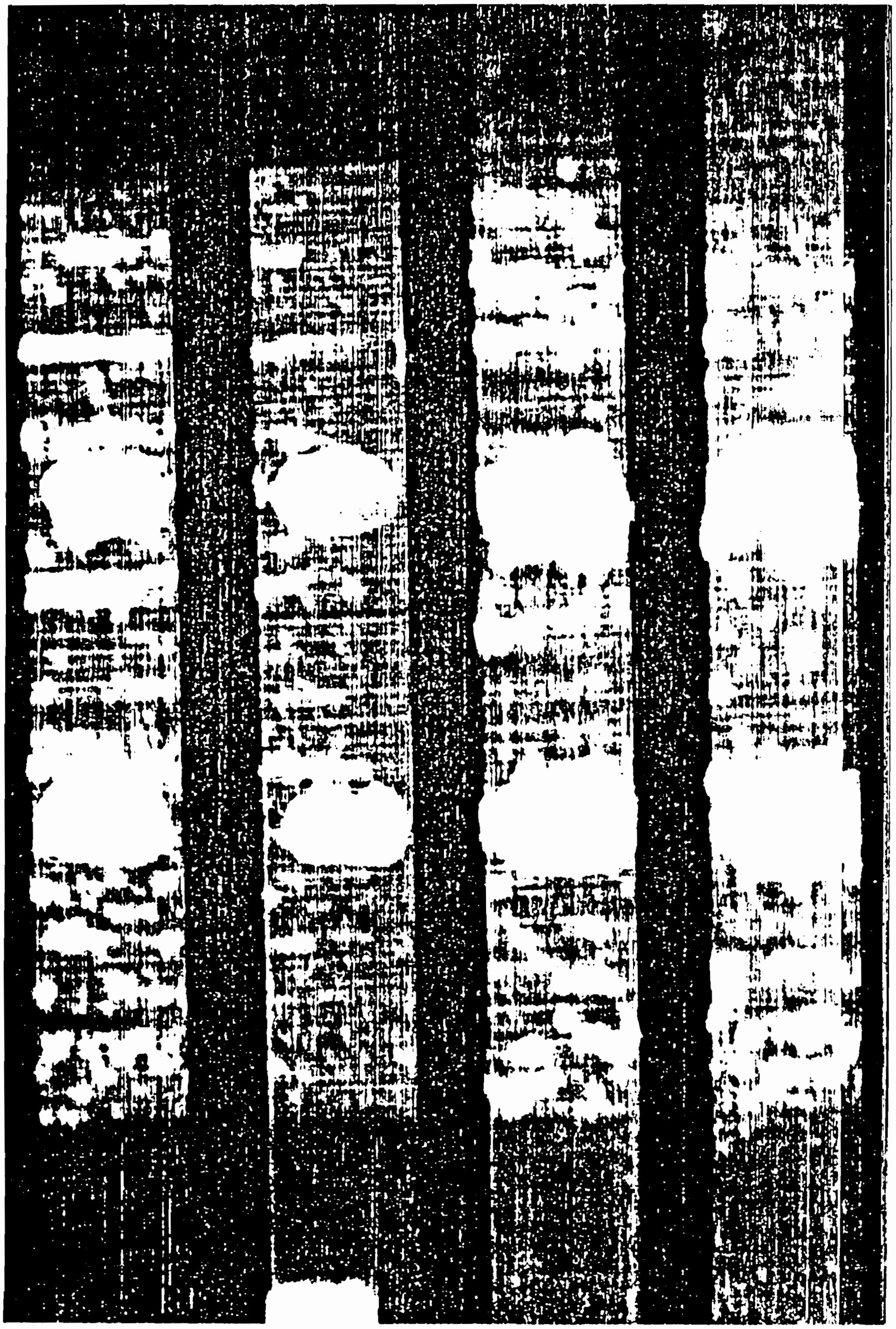

Figure 5.26 C-scans, S=0.55, 4000 cycles

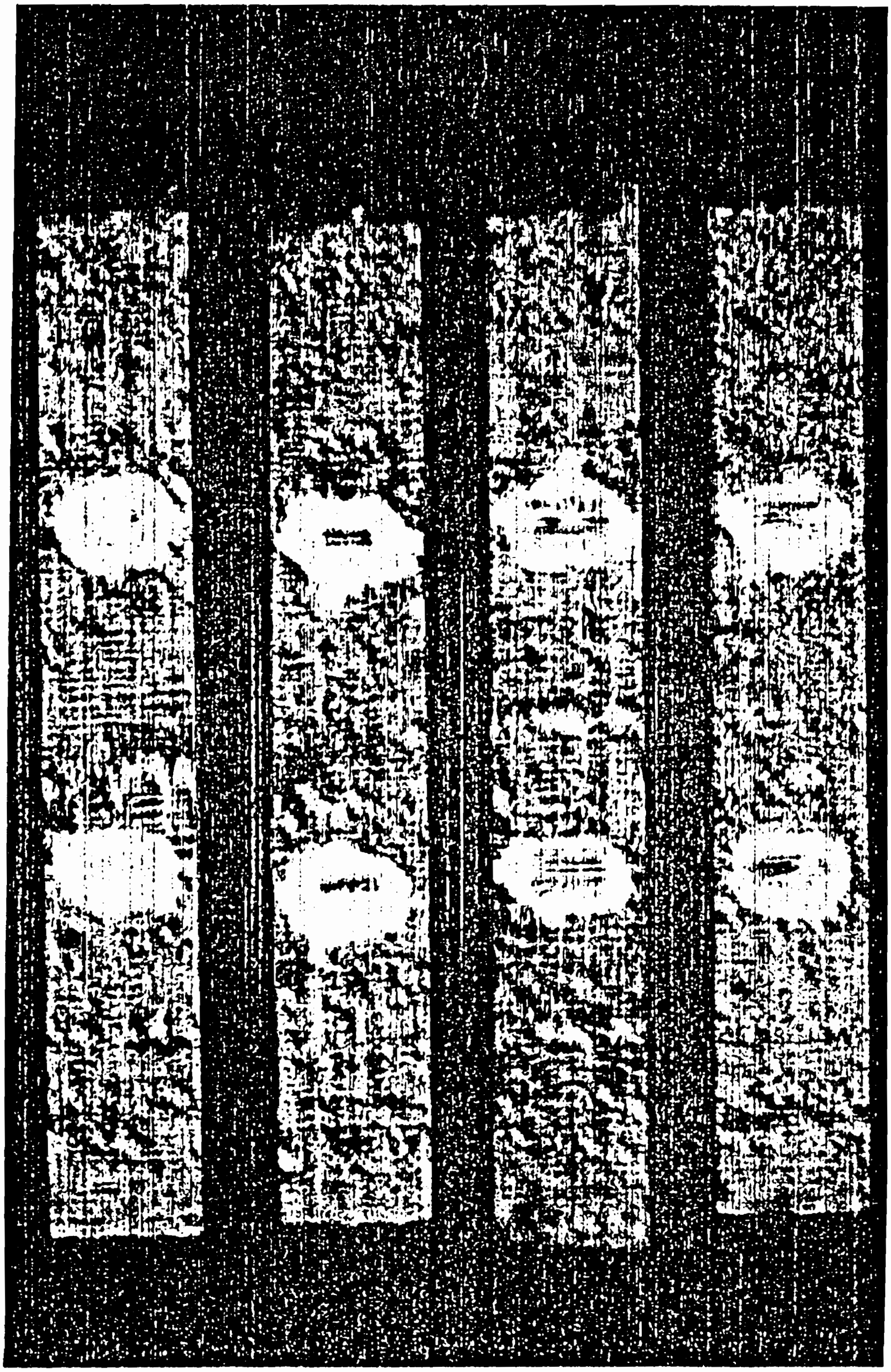

Figure 5.27 C-scans, S=0.55, 5e4 cycles

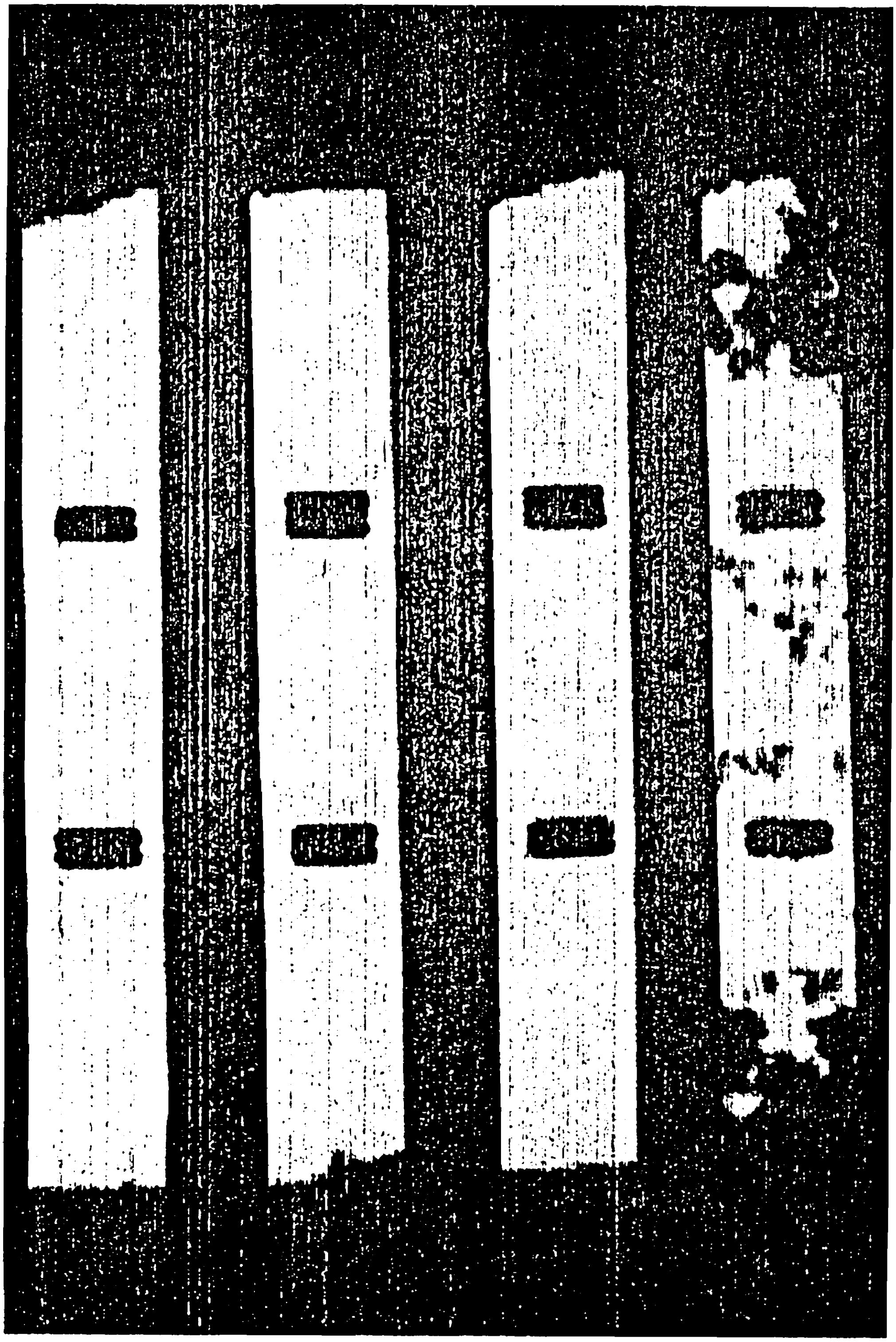

Figure 5.28 C-scans, S=0.55, 1e6 cycles

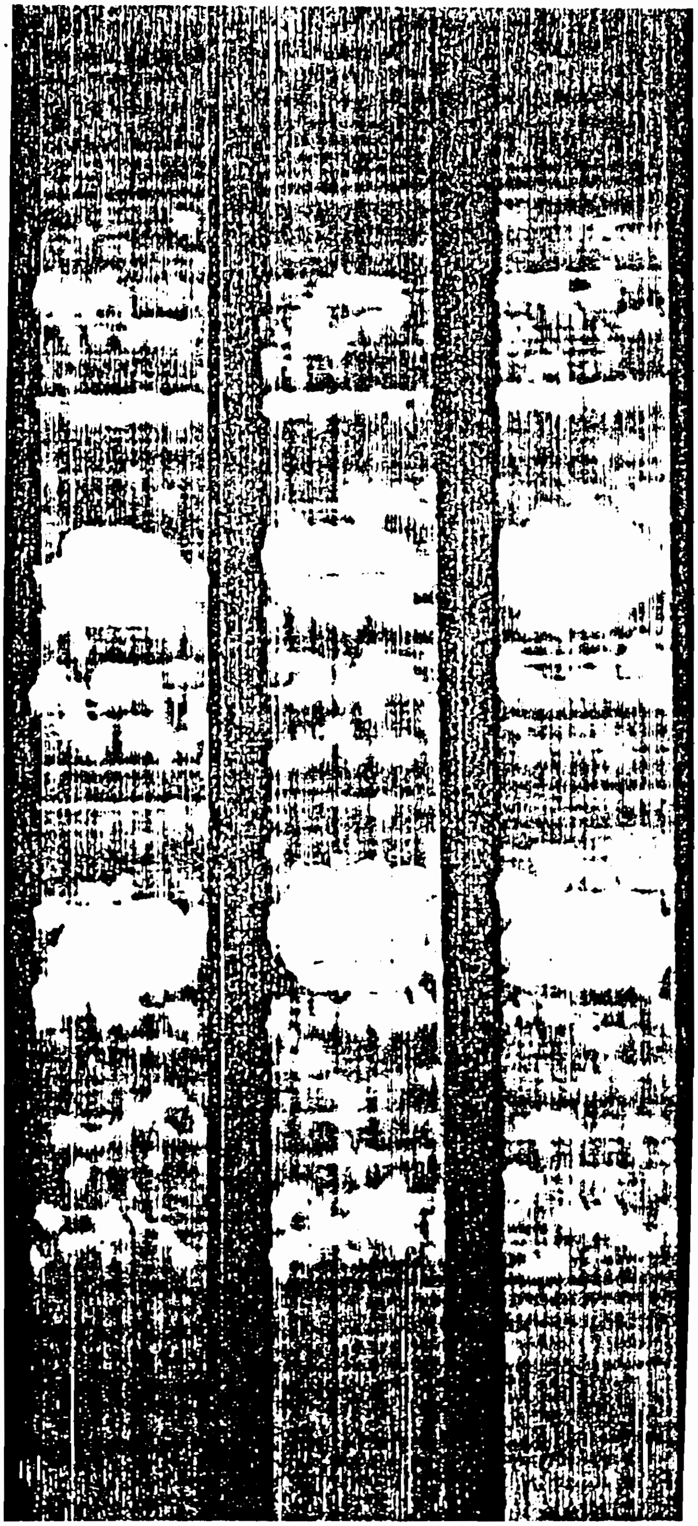

Figure 5.29 C-scans, S=0.60, 1500 cycles

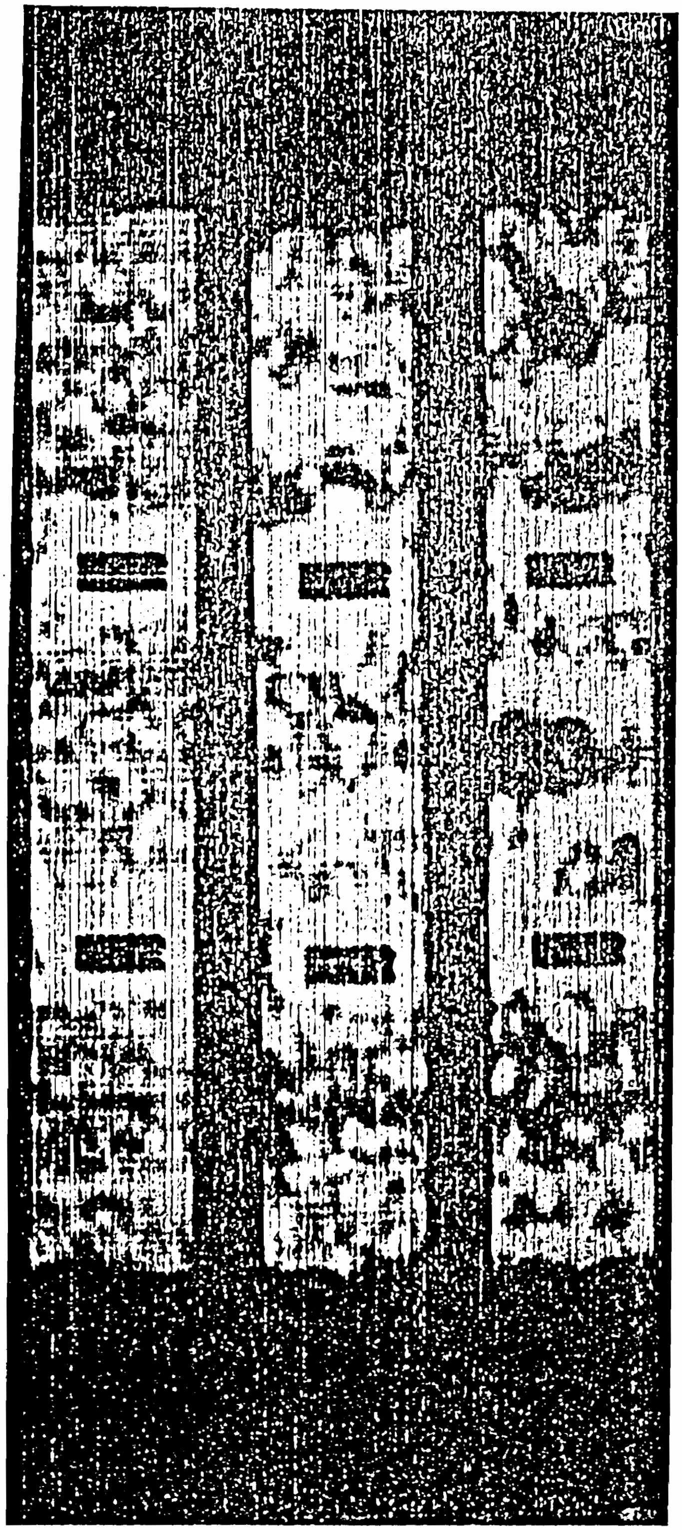

Figure 5.30 C-scans, S=0.60, 2e4 cycles

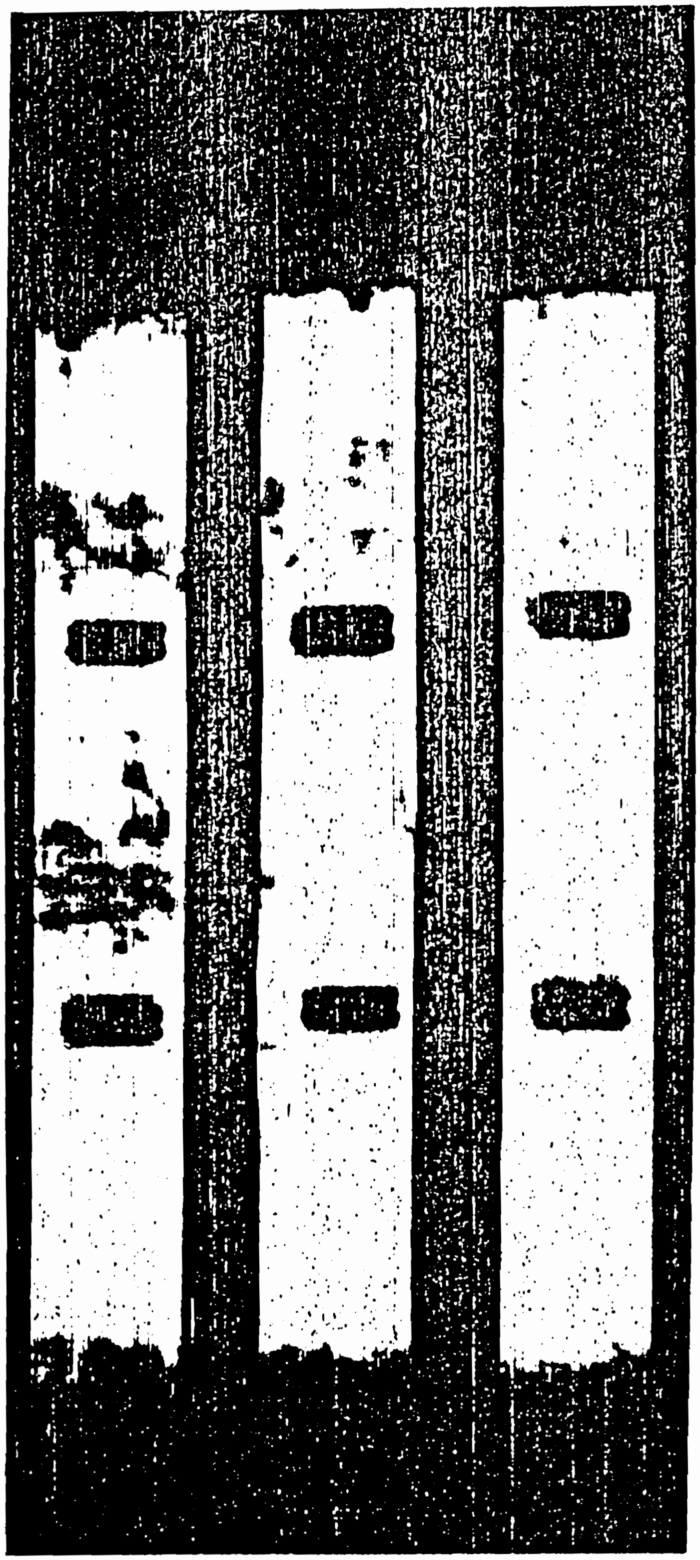

Figure 5.31 C-scans, S=0.60, 2e5 cycles

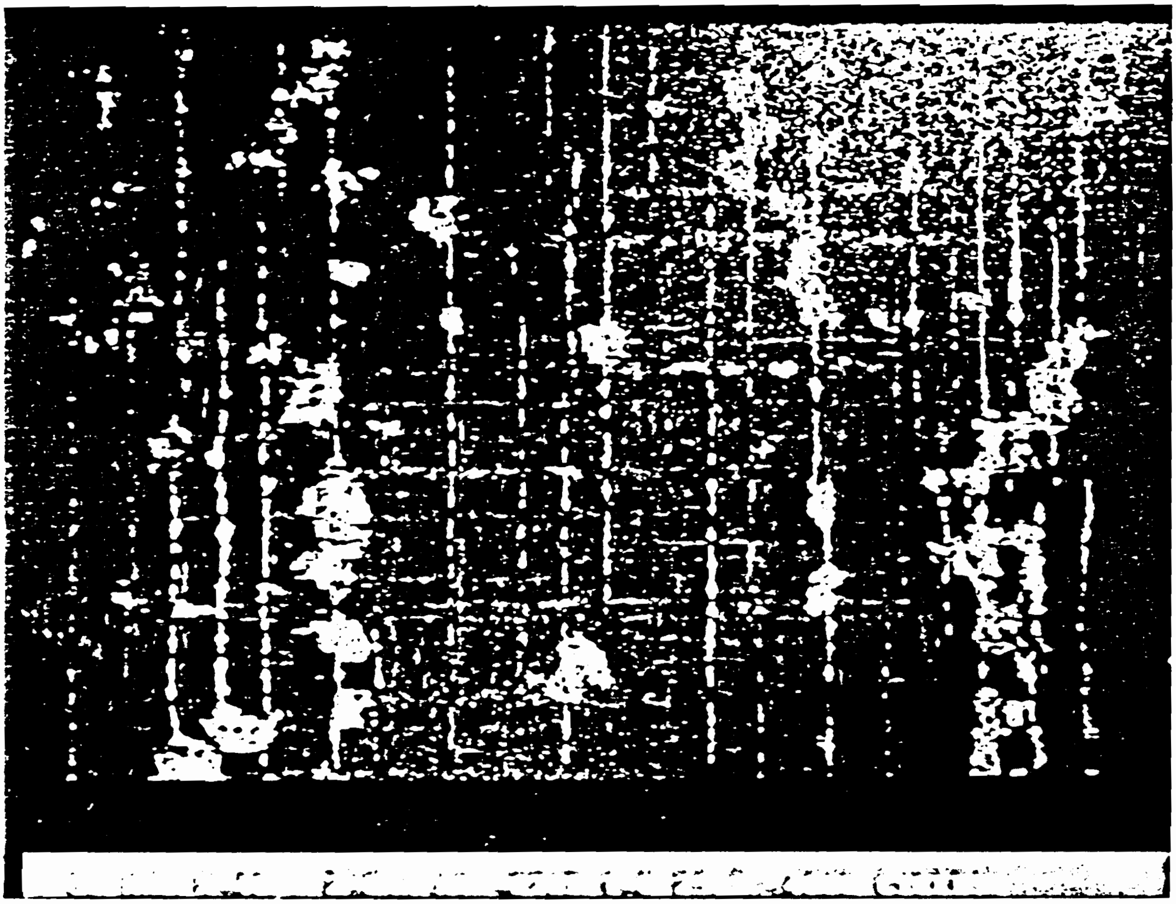

Figure 5.32 Scanning Acoustic Microscope image, S=0.55, 4000 cycles, 0/90 interface

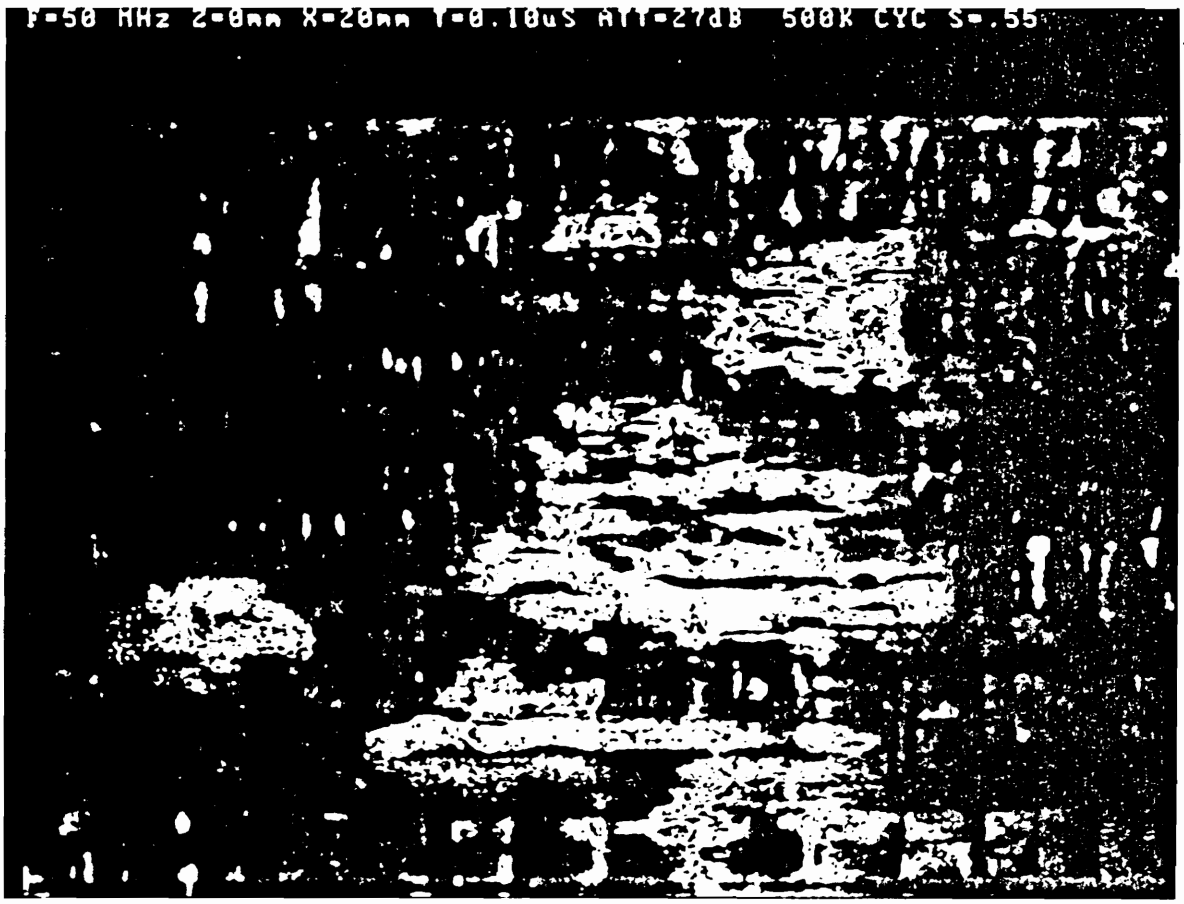

Figure 5.33 Scanning Acoustic Microscope image, S=0.55, 50000 cycles, 0/90 interface

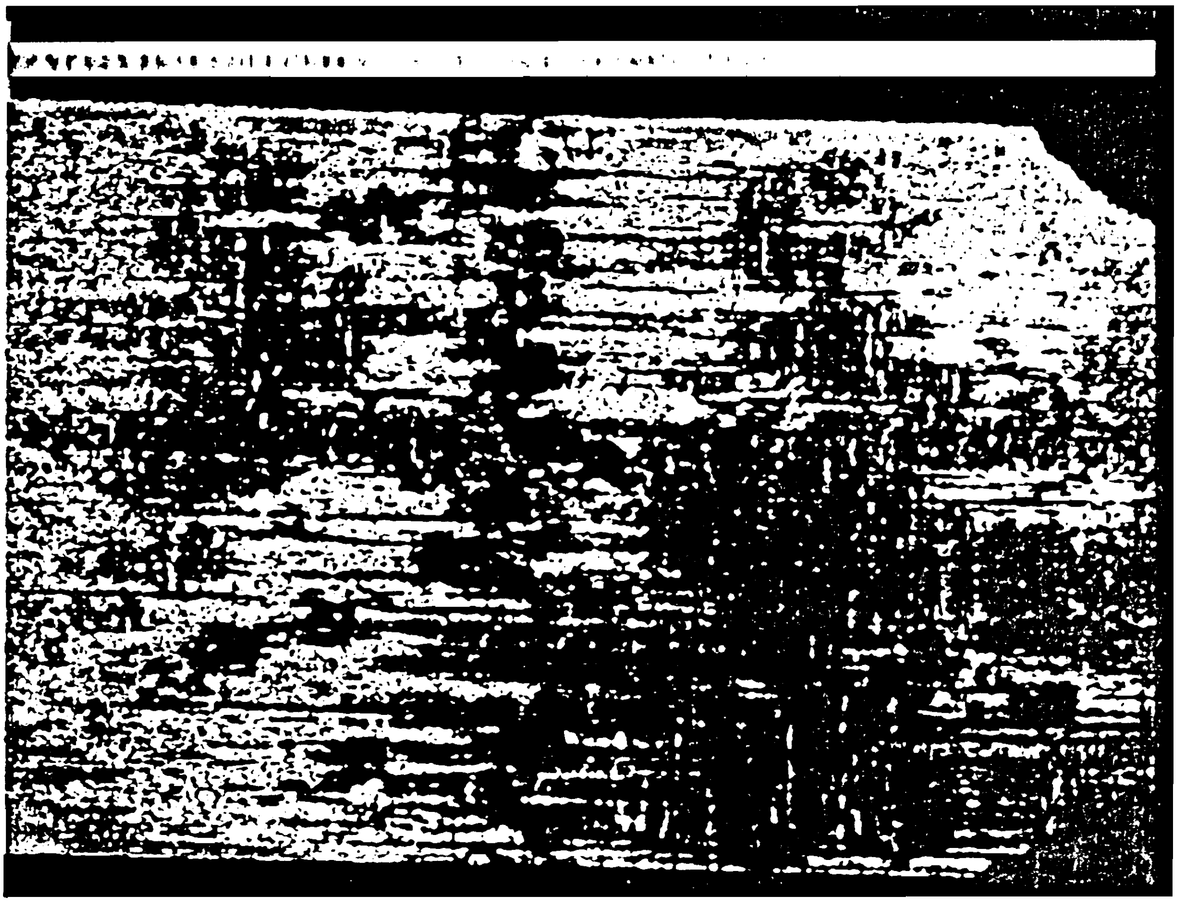

Figure 5.34.a Scanning Acoustic Microscope image, S=0.55, 1e6 cycles, top 0° ply

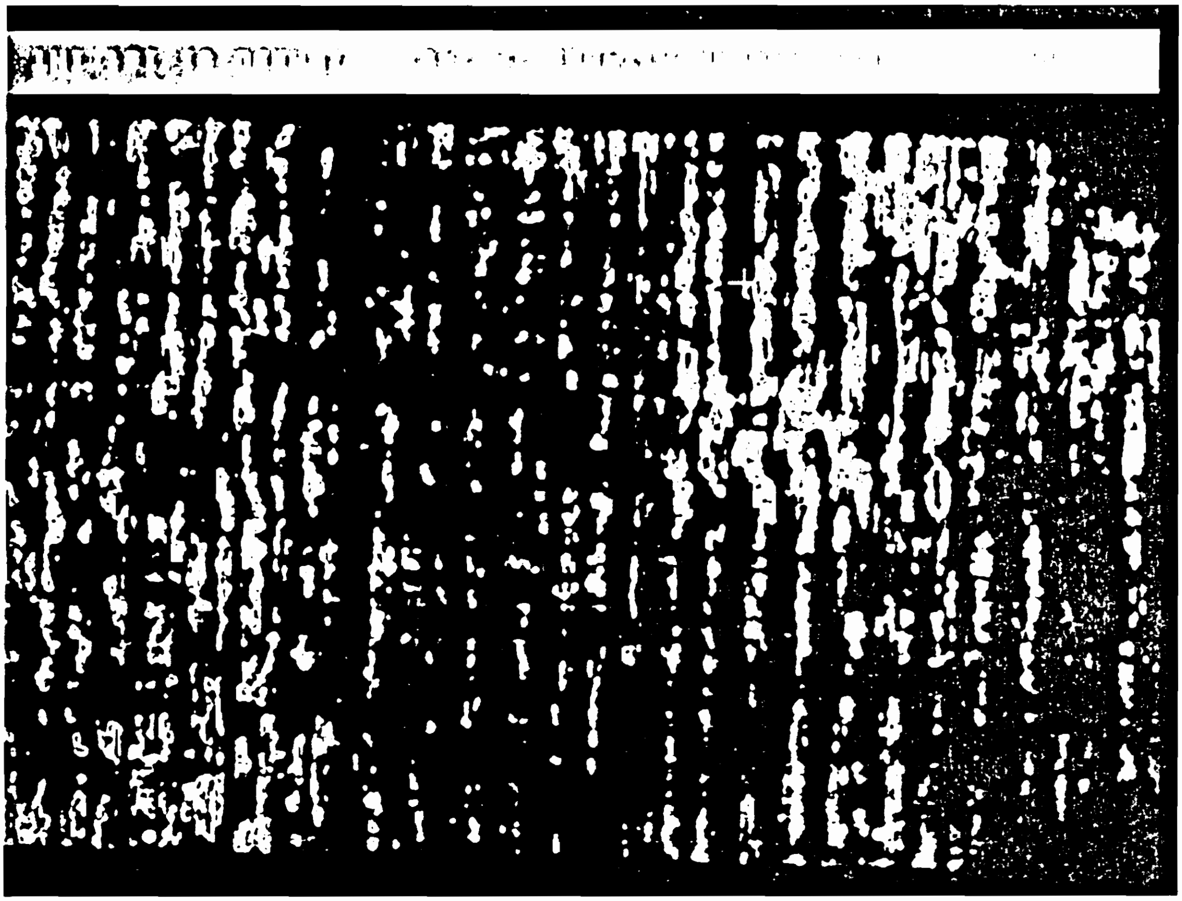

Figure 5.34.b Scanning Acoustic Microscope image, S=0.55,

1e6 cycles, 0/90 interface

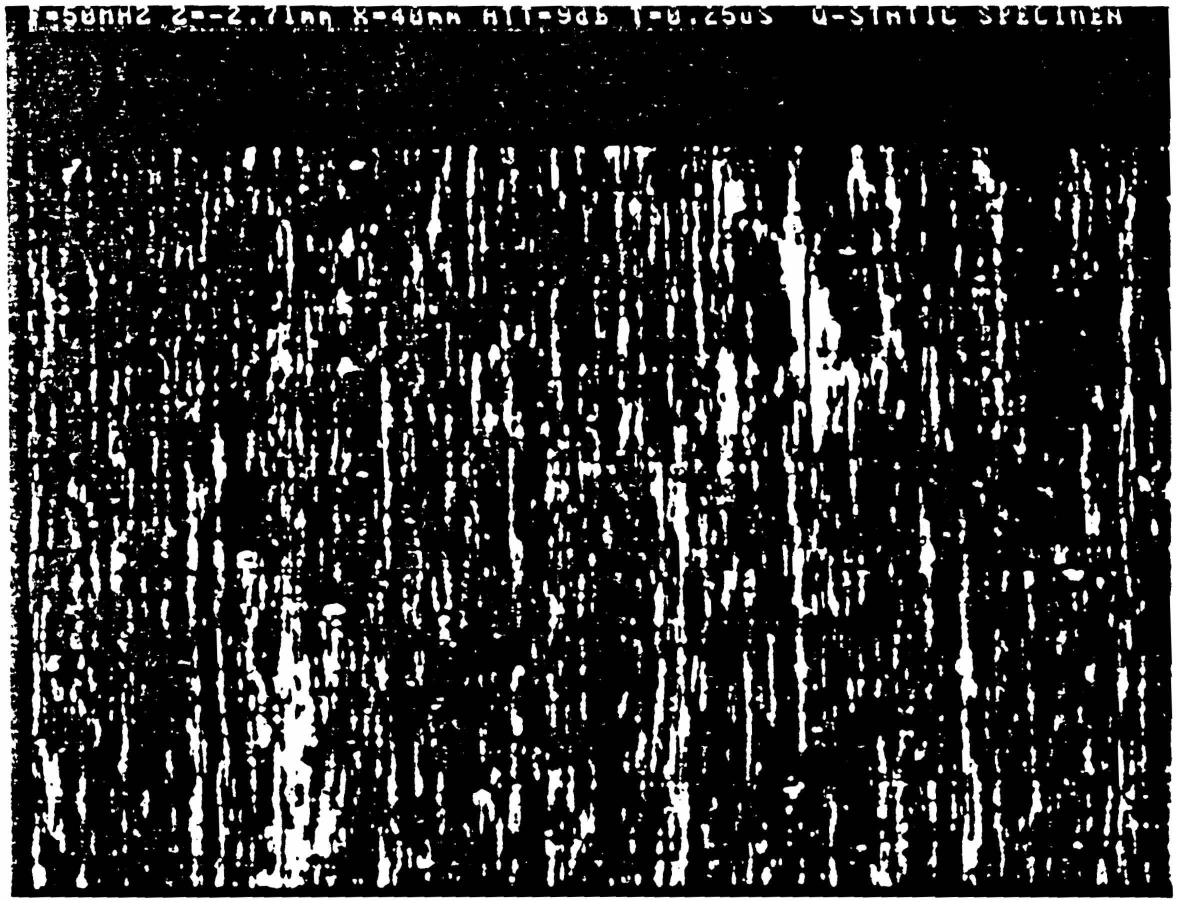

Figure 5.35 Scanning Acoustic Microscope image, quasi static failure, 0/90 interface

average value of 0.063", which compares very well with the Shear Lag value of 0.06". At 1 million cycles, large delaminations emanating from the crack and extending in the direction of the load are present.

Secondly, a longitudinal crack array develops in the 0° plies. It appears at the same time as the first array but the spacing remains irregular. The average spacing varies between 0.035" and 0.06". Again, it is consistent with the predicted value of 0.055". Even at 1 million cycles no delaminations seem to initiate at these cracks. But, it is evident that many internal delaminations initiate at the intersection of longitudinal and transverse cracks.

Examination of the failed quasi-static specimen reveals that the crack arrays are only partially developed. The crack spacing is irregular, some cracks do not span the width of the specimen and delaminations at the interface are very limited. This observation indicates that damage which accumulates during cyclic loading is much more extensive and diverse than that for quasi static loading.

From the body of nondestructive evaluation results, it is evident that delaminations do not initiate preferentially at the edges, and that damage is evenly distributed along both axis of the specimen. It is expected that damage sustained by a volume spanning transverse and longitudinal cracks and the thickness of the coupon represents the total damage present in the specimen.

5.6 Time Dependent Behavior

The investigation of the viscoelastic response of the T650-42/Radel X was conducted using two independent techniques;

a. mechanical and cyclic creep tests of 0° and 90° laminates at stress levels ranging from 20 to 90% of their ultimate tensile strength.

b. creep and multiplexing tests on the Dynamic Mechanical Analyzer at temperatures ranging from room temperature to 475°F.

Combining the compliance and temperature data obtained from these two techniques, the pseudo-analog model parameters are computed.

5.6.1 Mechanical Creep Tests

Incremental stress creep (ISC) tests were conducted on 0° and 90° coupons. The 0° specimens showed no measurable compliance changes, even when loaded at 90% of their ultimate tensile strength for prolonged periods of time. Consequently, the 0° plies will be considered elastic at room temperature.

The transient compliance of 90° specimens at stress levels ranging from 50 to 90% of UTS is shown in Figure 5.36. The data suggest that the compliance is independent of stress level. Isochronous stress-strain curves at 400 and 24000 seconds are shown in Figure 5.37. Both results indicate that the 90° plies exhibit linear viscoelastic behavior. The apparent modulus drops from an initial value of 1.085 Msi at t=0 to 1.082 Msi at 600 seconds, and 1.07 Msi at

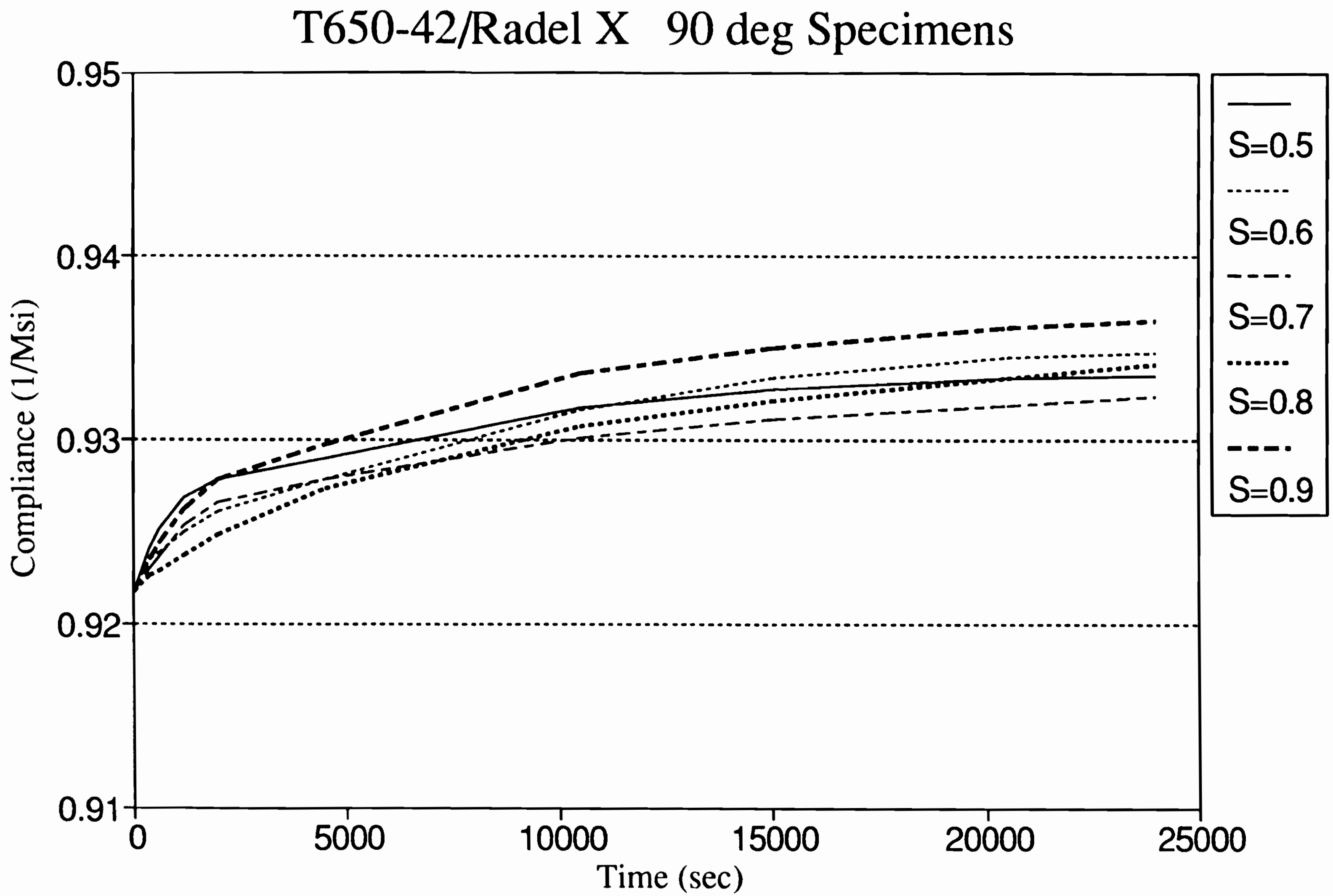

Figure 5.36 **Time dependent compliance for S = 0.5-0.9, 90°**

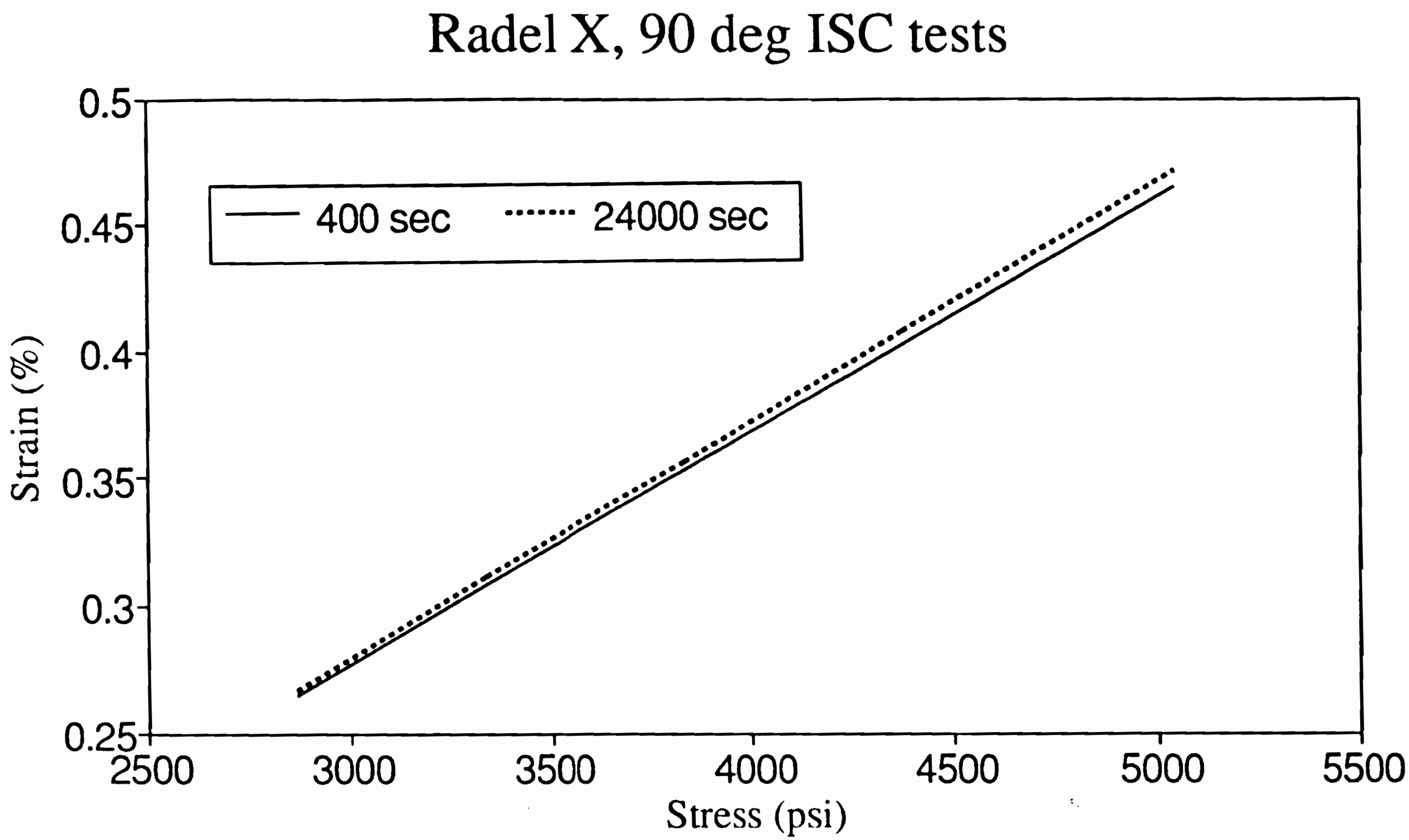

Figure 5.37 **Isochronous stress-strain curves, 90°**

24000 seconds.

The room temperature average compliance of the 90° laminates was fitted with a 5-parameter PAM. The values are,

E_0= 1.085e6 psi from the quasi static measurements.

E_1= 1.280e8 psi μ_1= 1.325e11 psi-sec

E_2= -4.946e7 psi μ_2= 6.42e12 psi-sec

The average measured compliance for S=0.5 to 0.9 and fitted 5-parameter PAM are shown in Figure 5.38. The long term compliance of a different coupon tested in creep at 90% UTS is shown in Figure 5.39, together with the prediction based on the above parameters.

Additional experiments were performed to explore the capabilities of the analytical model to predict the transient deformation where no fatigue damage is involved. These experiments include cyclic creep loading of 90° coupons at mean loads corresponding to 60, 70 and 80% of UTS, with a cyclic amplitude of 10% UTS at 0.1 Hz, and static creep loading of cross ply laminates. The comparison of these results and the model predictions is discussed in Chapter 7.

5.6.2 Dynamic Mechanical Analysis

Creep and multiplexing tests were performed on 90° unidirectional laminates as part of the thermoviscoelastic characterization effort. Specimens were cut from virgin, undamaged coupons and tested at very low stresses at temperatures ranging from 30°C to 240°C, well above

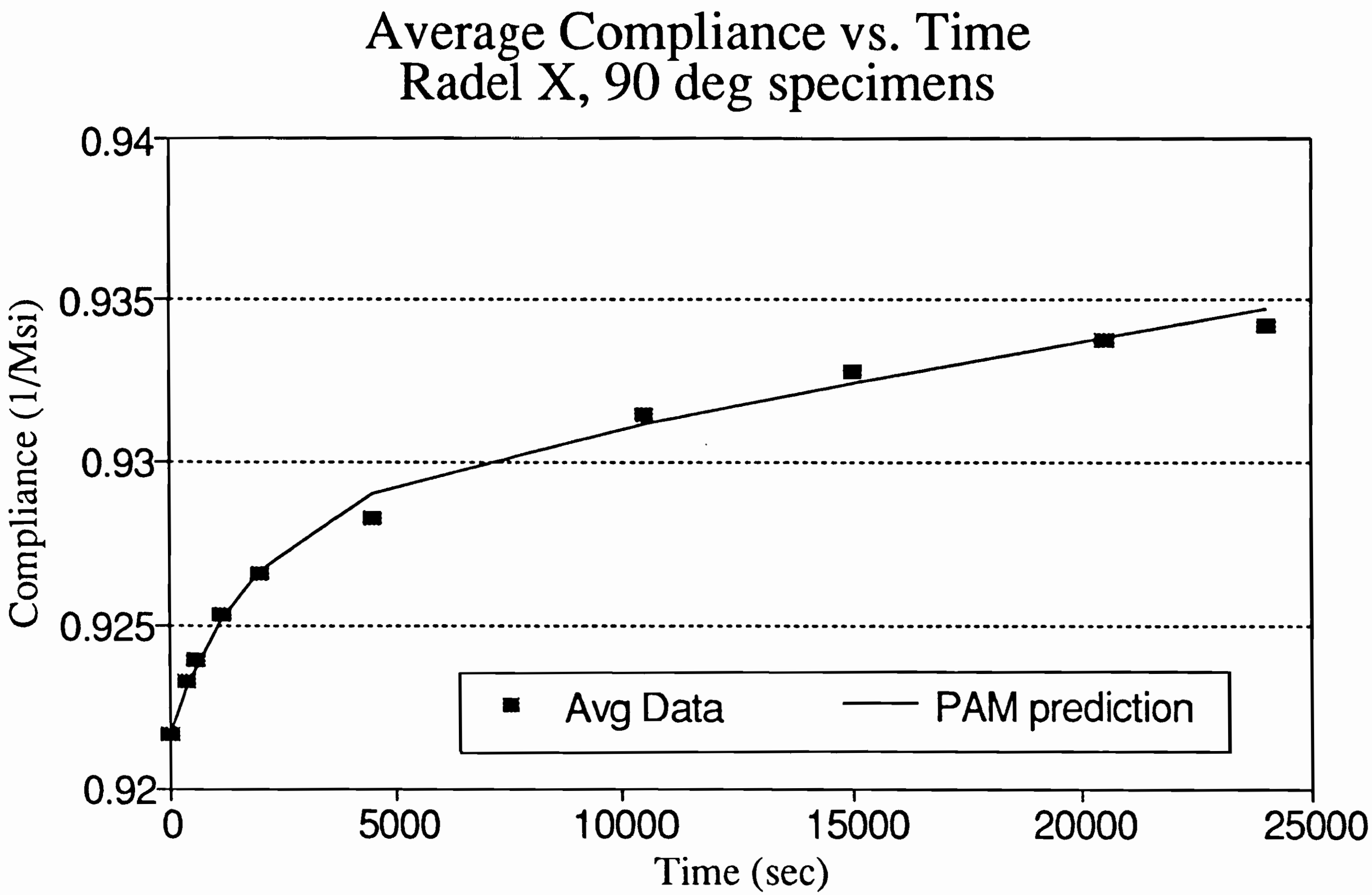

Figure 5.38 Average measured compliance and PAM prediction at R.T.

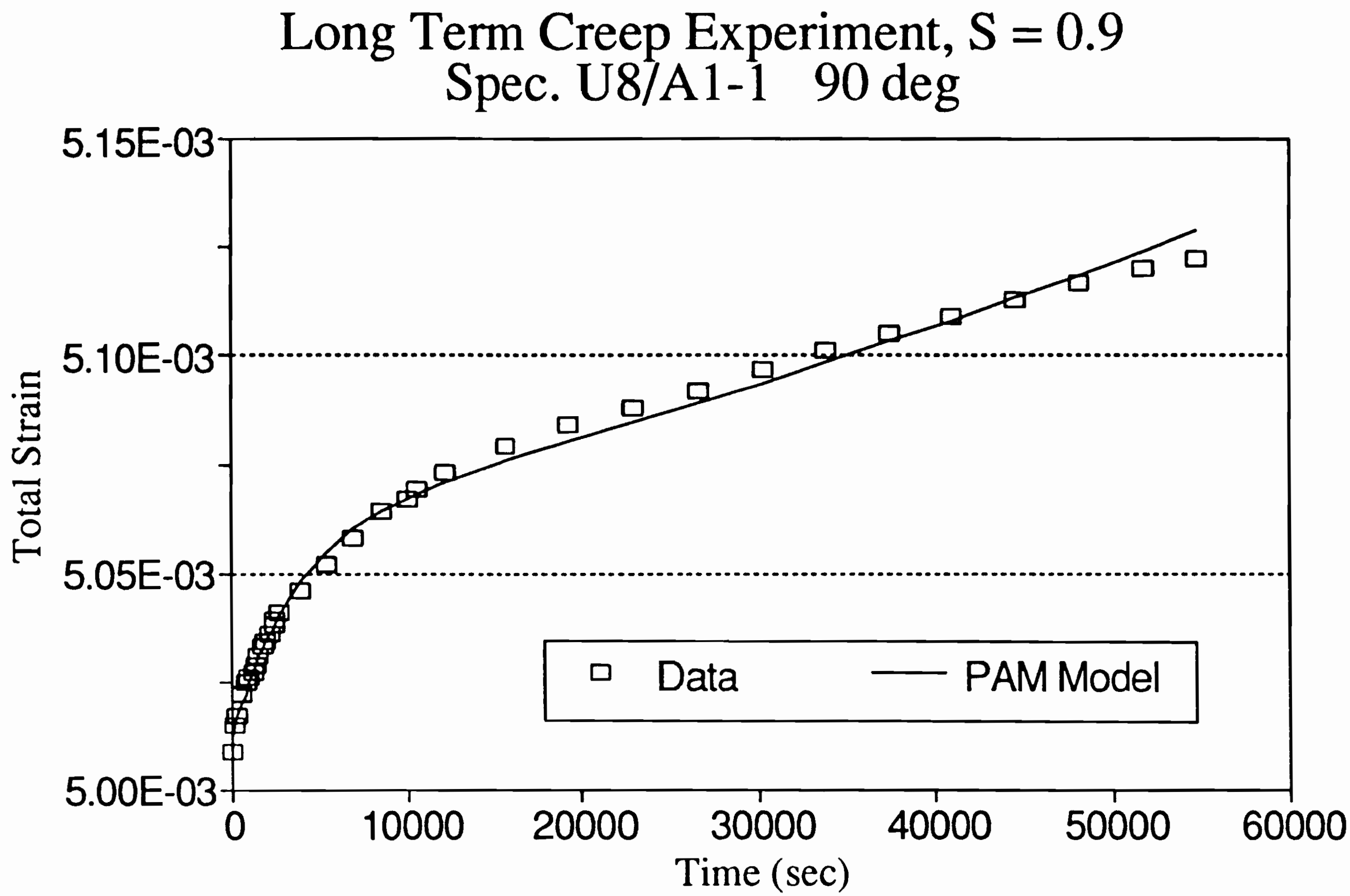

Figure 5.39 Long term deformation, 90° at 90% UTS, data and prediction

the glass transition temperature. It is important to note that the absolute moduli values computed by the commercial DMA software are erroneous. The moduli are evaluated from displacement and force measurements using formulae applicable to isotropic materials only. The error is proportional for all computed values. The results represent the true time dependent behavior and should be regarded in this context.

Unidirectional Laminates

The results are best presented in the form of master curves by employing the superposition method, described in [3,10] and section 2.3. The frequency response of the storage and loss moduli of undamaged 90° laminates are shown in Figures 5.40 and 5.41 for all seven test frequencies, between 0.1 and 10 Hz. Using frequency - temperature superposition the data collected at different frequencies is shifted horizontally to produce a frequency master curve. The master curves, as shown in Figures 5.42 and 5.43, are double logarithmic plots where the shifted storage (E') or loss (E") moduli are plotted versus the loading frequency - f.

At 210°C the storage modulus decreases with decreasing frequencies with a particularly sharp decrease between log[f(Hz)]=0 and -4. The loss modulus exhibits a broad peak, approximately at log[f(Hz)]=-5. The same response could be plotted at any temperature by employing the corresponding horizontal shift factors. The shift factors do not obey the Arrhenius or WLF relationships. There are two

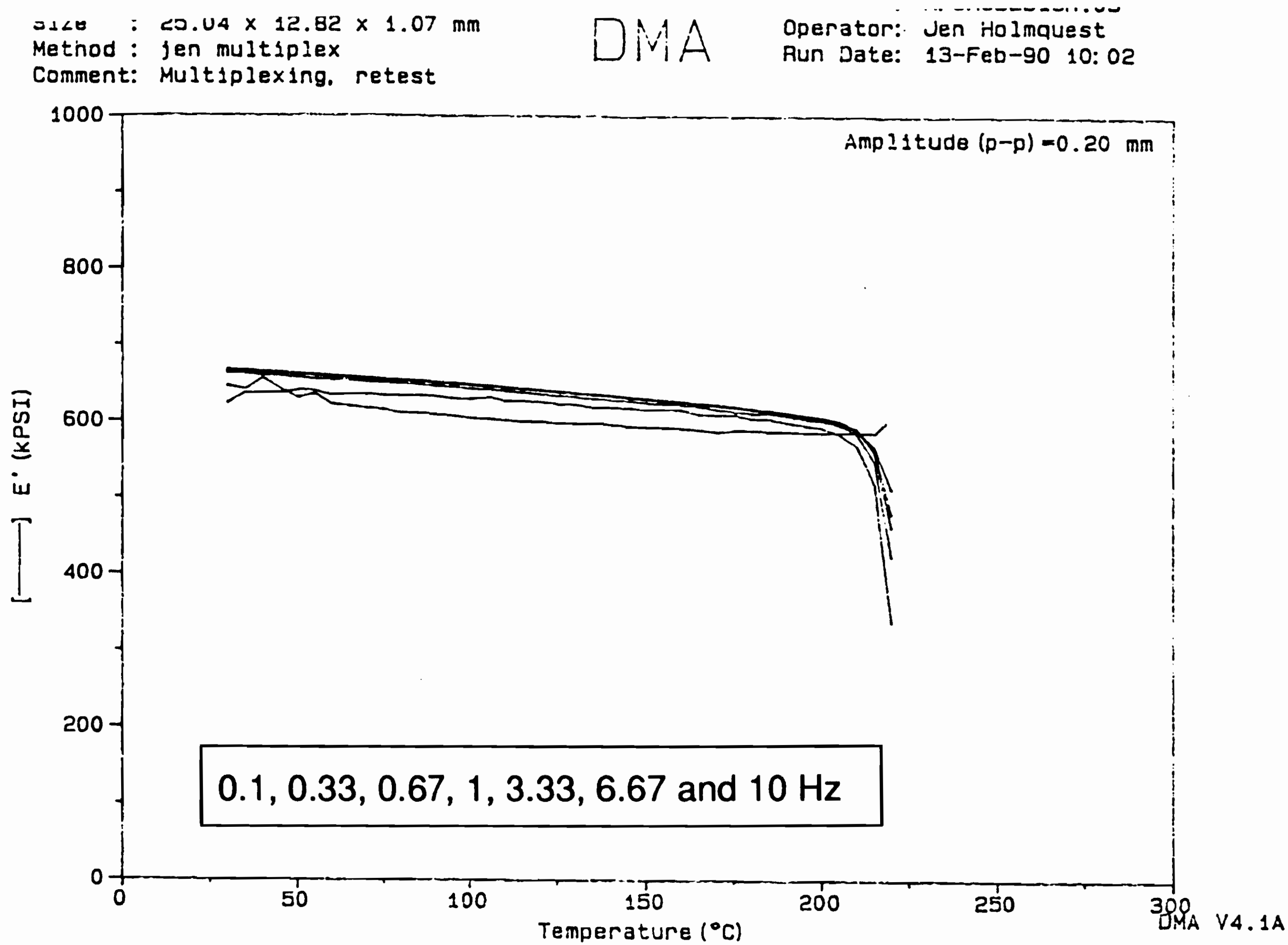

Figure 5.40 Storage modulus vs. Temperature, 90° undamaged

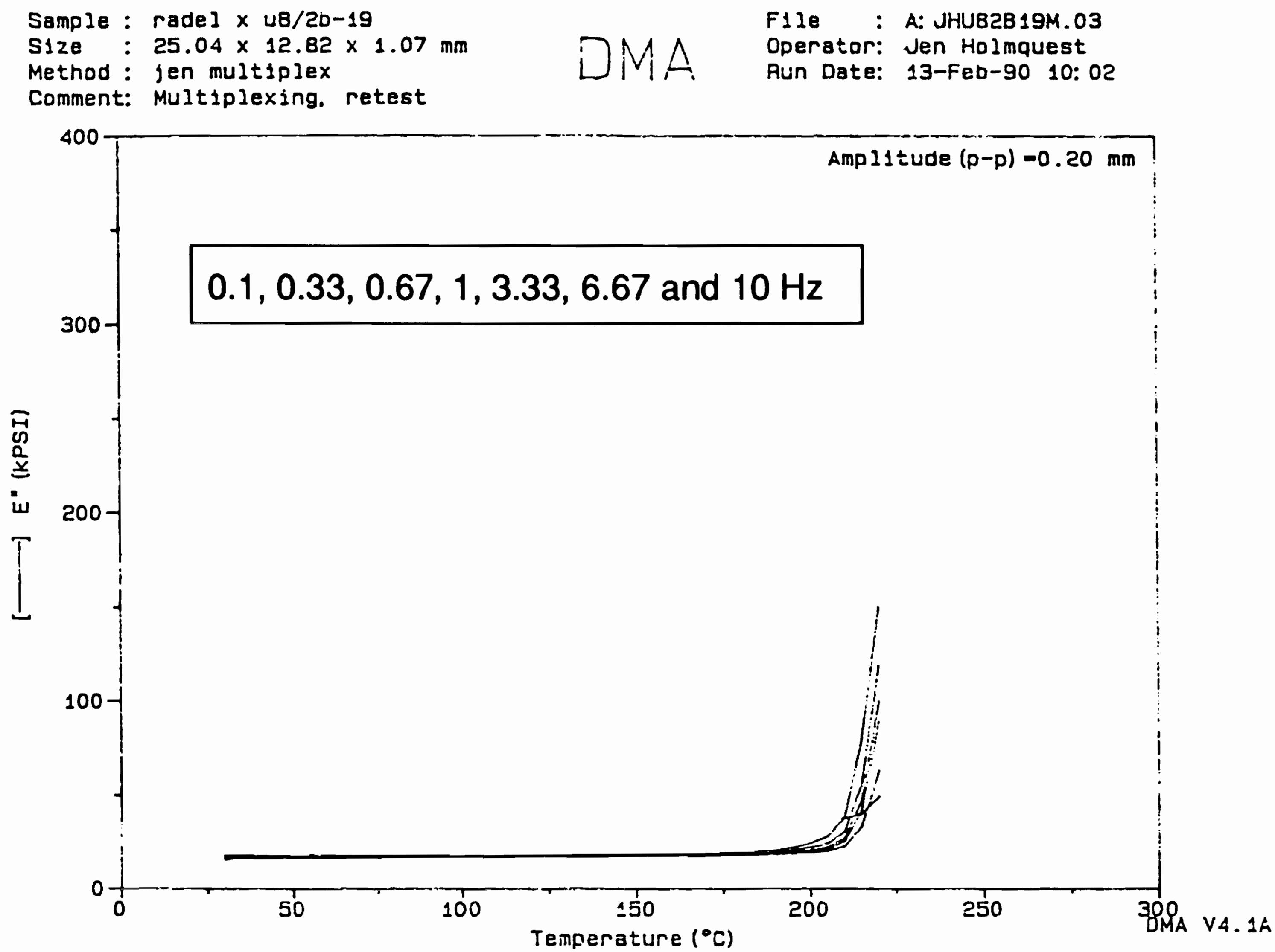

Figure 5.41 Loss modulus vs Temperature, 90° undamaged

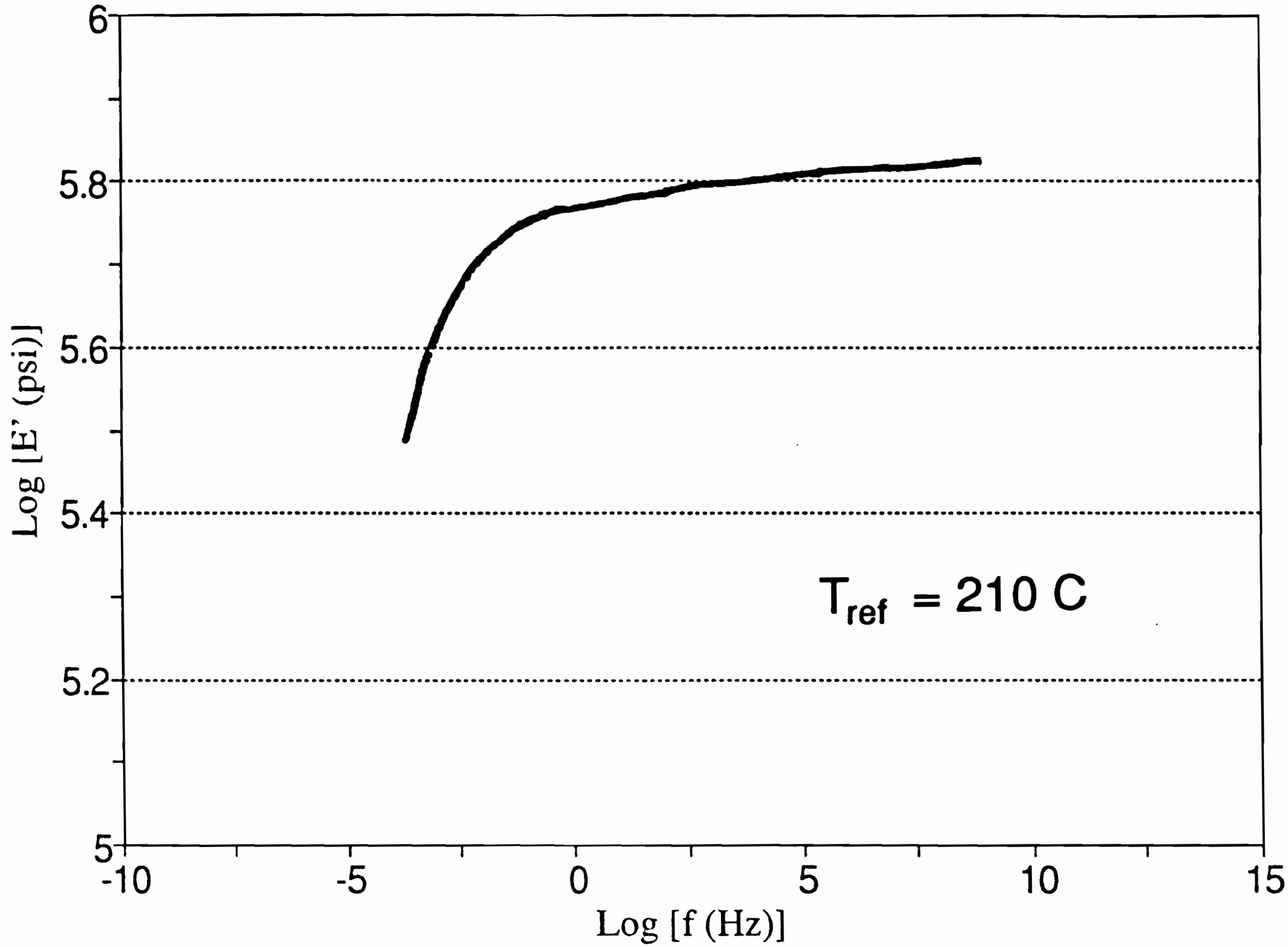

Figure 5.42 **Storage modulus frequency master curve, 90° undamaged**

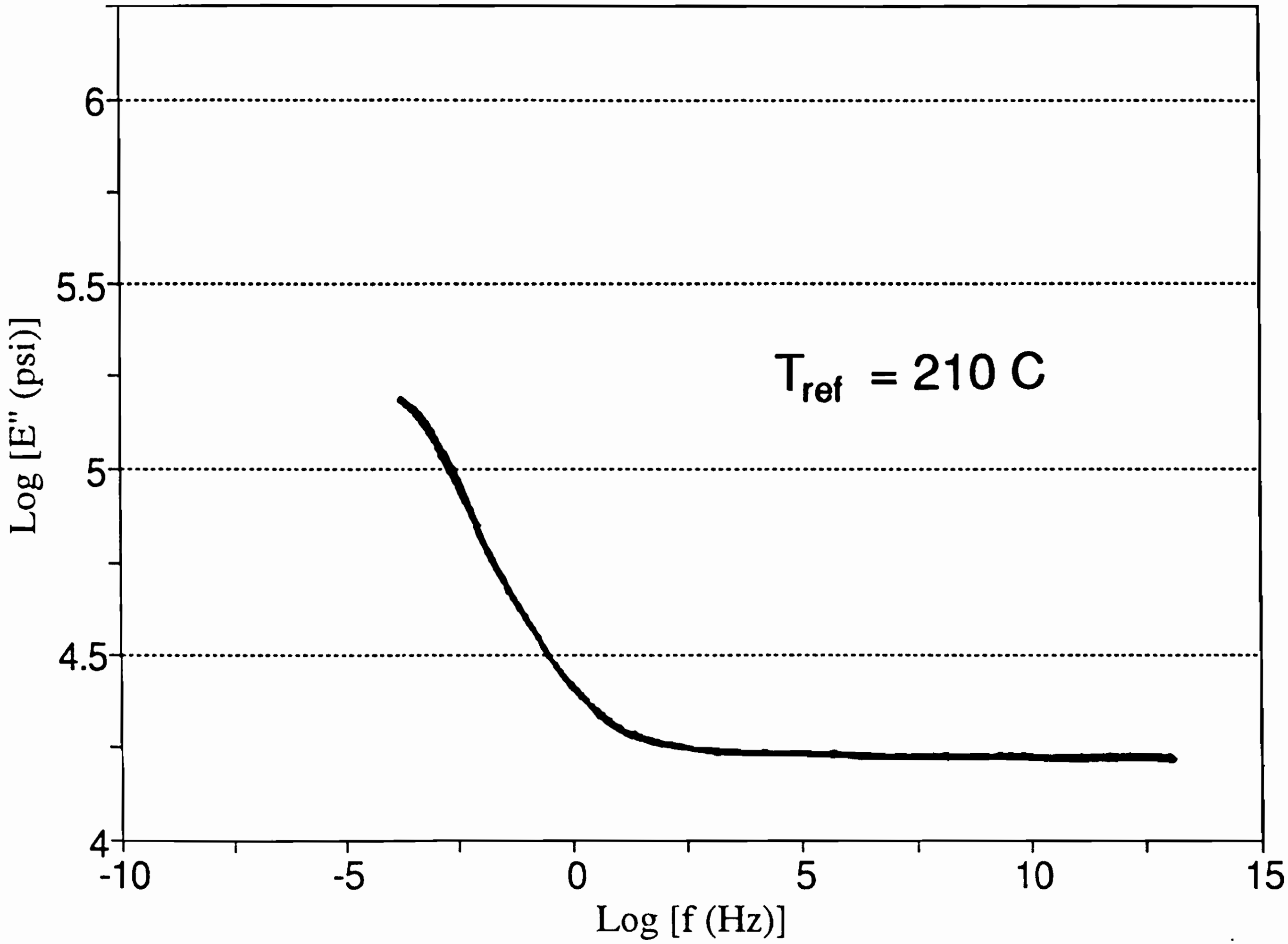

Figure 5.43 Loss modulus frequency master curve, 90° undamaged

distinct regions. Above T_g the shift factors decrease rapidly, but they change very little for temperatures below the glass transition temperature.

The response of cycled 90° unidirectional specimens was also measured to asses the effects of damage on the viscoelastic response. Fixed frequency, creep and multiplexing tests were conducted. It is assumed that the DMA testing procedure, which employs very small loads, does not increase the amount of cyclic damage already present in the specimen.

A comparison of the storage and loss moduli vs. temperature response is shown in Figure 5.44. The damaged specimen was cut from a 90° coupon, cycled at S=0.3, which failed after 959000 cycles. Extensive matrix cracking is evident from visual inspection of the failed coupon. The magnitude of the storage modulus and the peak of the loss modulus are reduced significantly. The position of the peak shifts from 220°C to 235°C, which is the peak temperature of undamaged 0° laminates.

Storage and loss moduli frequency master curves (at a reference temperature of 210°C) are shown in Figures 5.45.a and b. The magnitude of the storage modulus diminishes and the curve slightly shifts to the right. The magnitude of the loss modulus also decreases but there is not enough information to determine whether there is a shift. The creep compliance master curves, shown in Figure 5.46 at a reference temperature of 210°C, show that the response of the damaged specimen has a definite shift to the right and towards higher compliance. But,

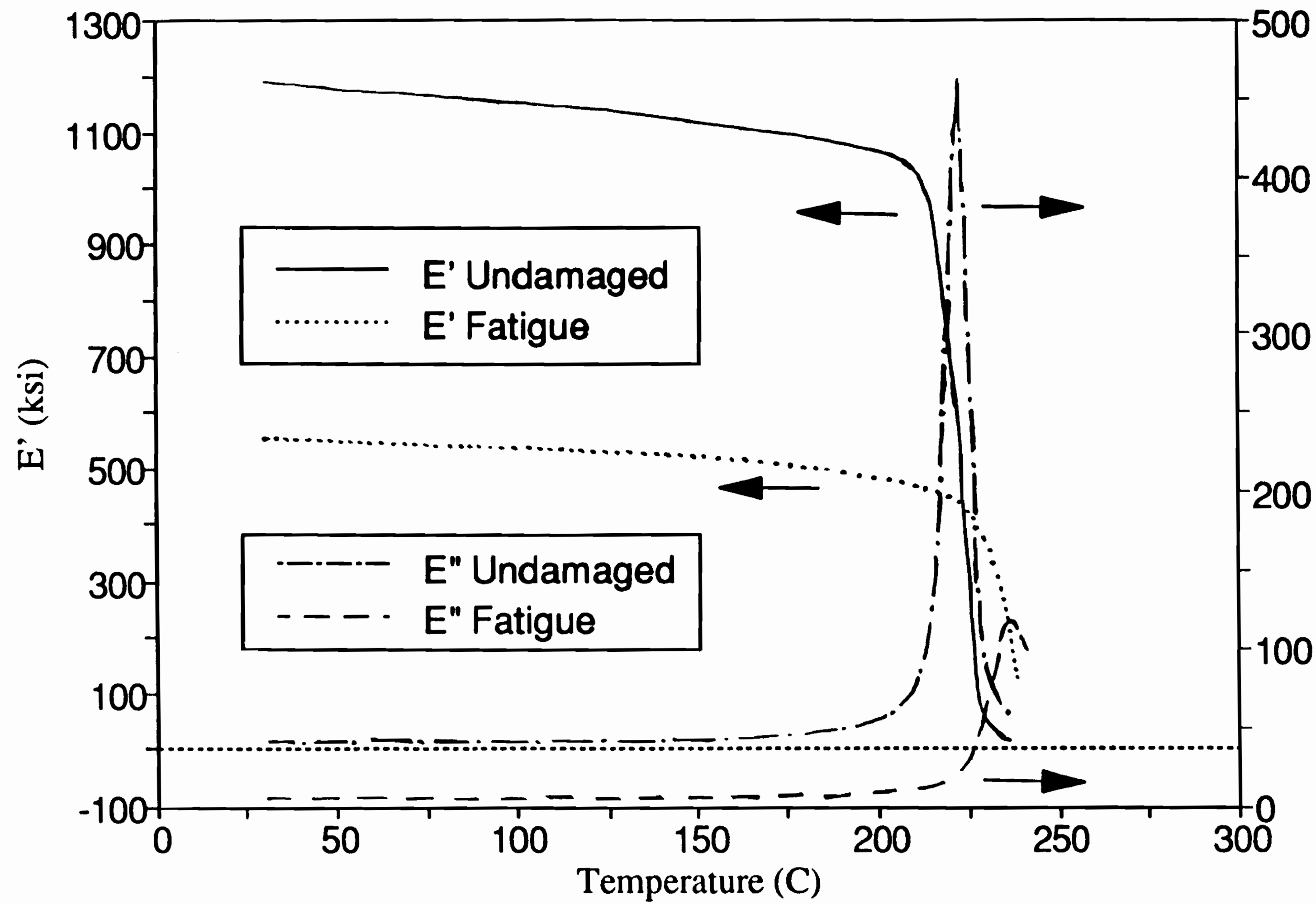

Figure 5.44 **Storage and Loss moduli for undamaged and fatigued 90° coupons**

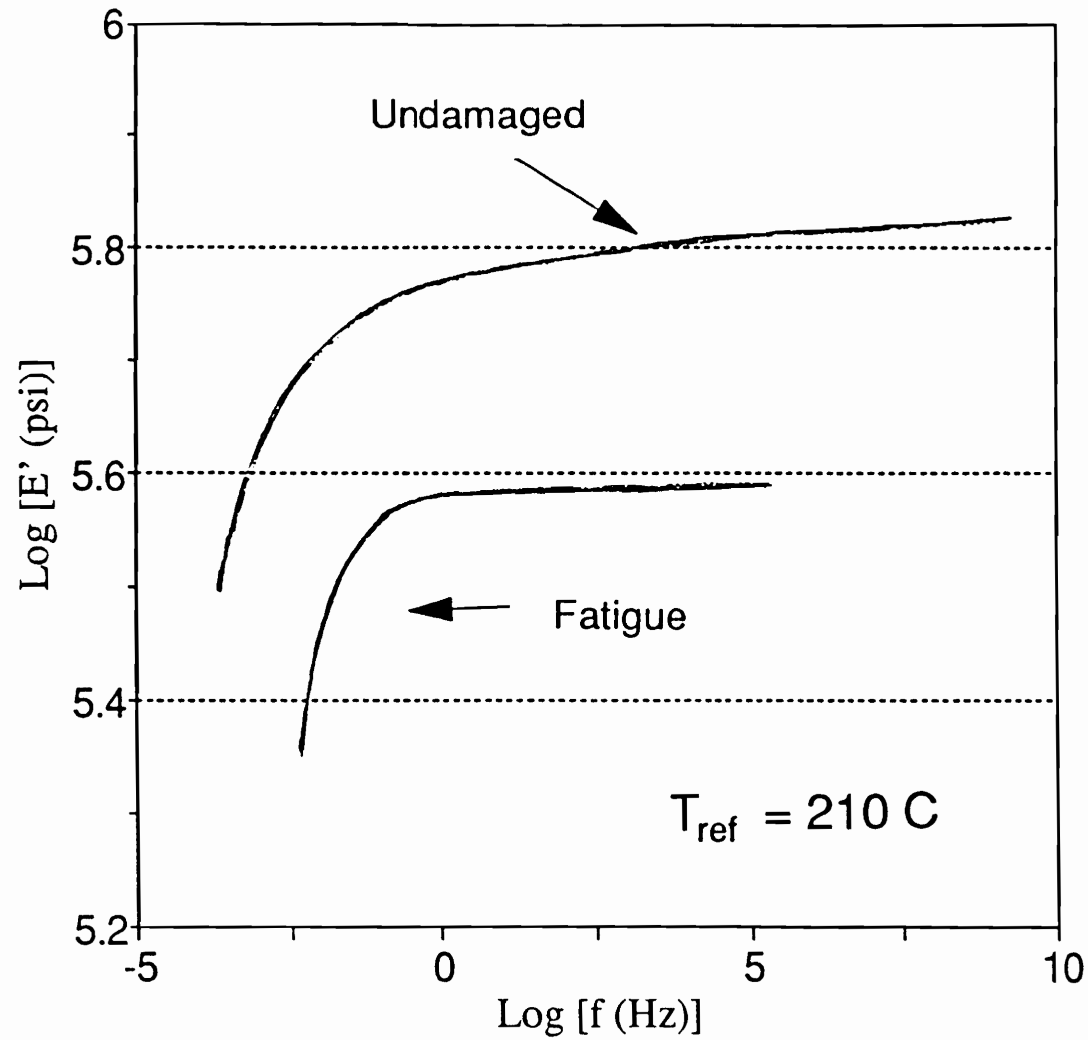

Figure 5.45.a E'(ω) master curves of virgin and cycled 90° specimens

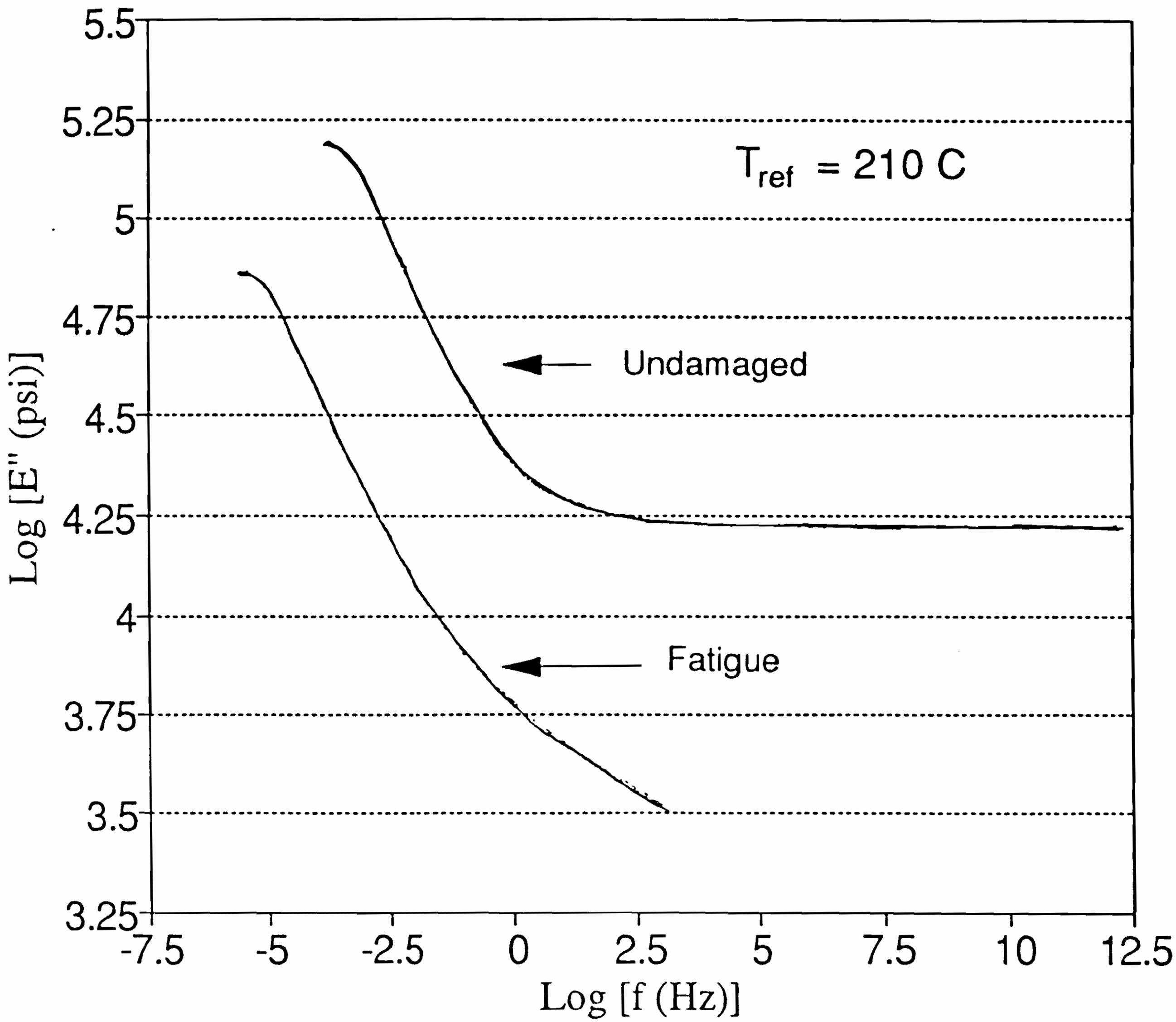

Figure 5.45.b **E"(ω) master curves of virgin and cycled 90° specimens**

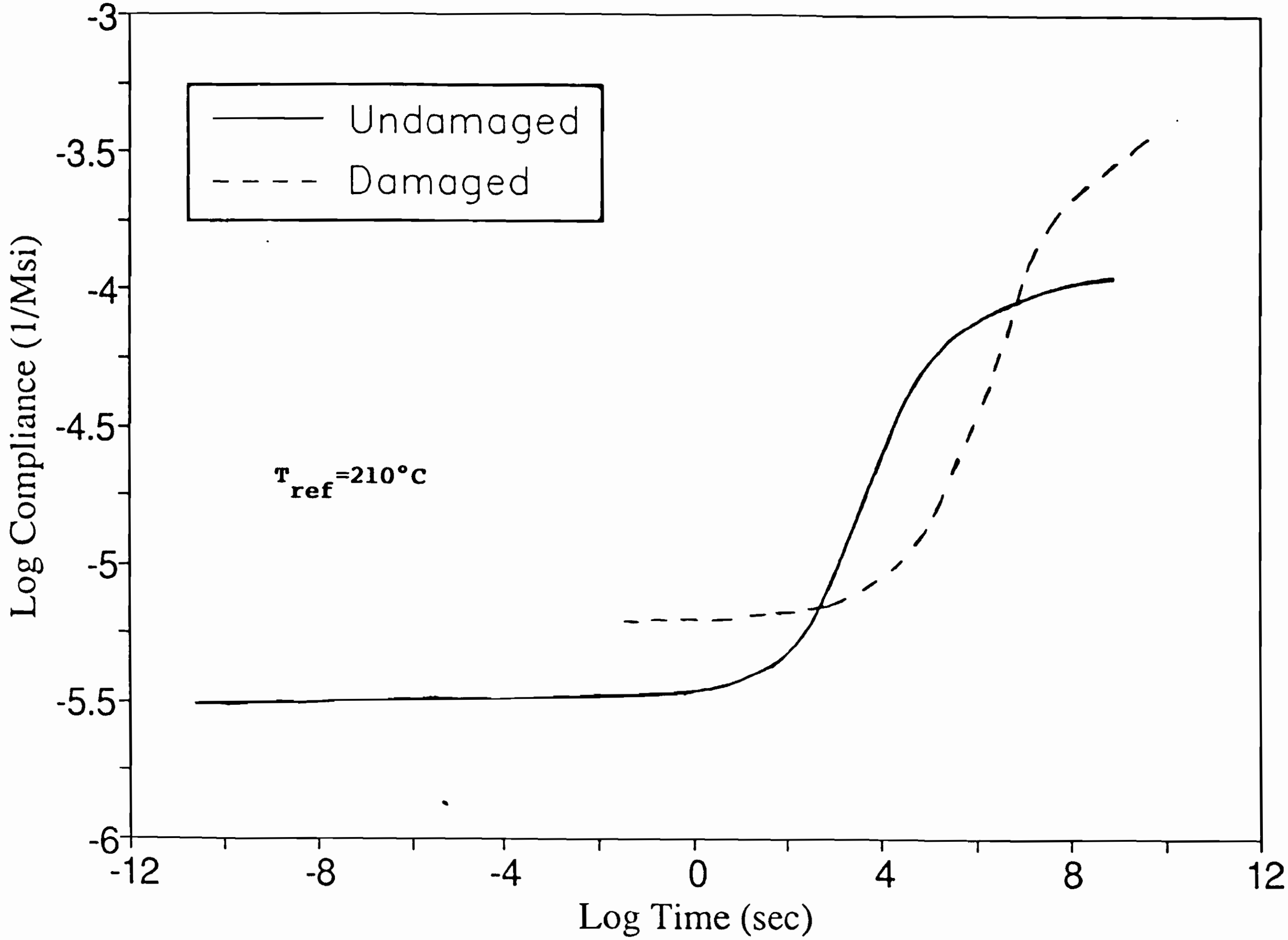

Figure 5.46 Creep compliance master curves, virgin and cycled 90° specimens

if the shift factors are taken into account, the relative horizontal position of the above mastercurves is reversed at room temperature. The overall effect of cyclic damage on the time dependent behavior of the 90° plies at room temperature is to accelerate the deformation process.

Cross Ply Laminates

The effects of cyclic damage on the thermoviscoelastic behavior of cross ply laminates were examined in some detail. In addition to undamaged laminates, specimens were cut from coupons cycled at S=0.55 for 4000, 50000 and 1 million cycles. The details of the damage state after such cyclic loading have been described in sections 5.4 and 5.5.

The fixed frequency storage and loss moduli traces are compared in Figures 5.47 and 5.48. The storage modulus vs. temperature response decreases in magnitude at 4000 and 50000 cycles keeping the characteristic shape of the undamaged laminate. The response increases slightly for 1 million cycles and it assumes the characteristic shape of the 0° unidirectional laminates (as shown in Figure 5.11). The loss modulus vs. temperature response retains its original shape with a peak centered at 225°C. The magnitude of the peak decreases at 4000 and 50000 cycles.

The storage and loss moduli master curves obtained from multiplexing experiments are shown in Figures 5.49 and 5.50 at a reference temperature of 210°C. The storage modulus vs. frequency master curve of the undamaged laminate shows a small reduction in

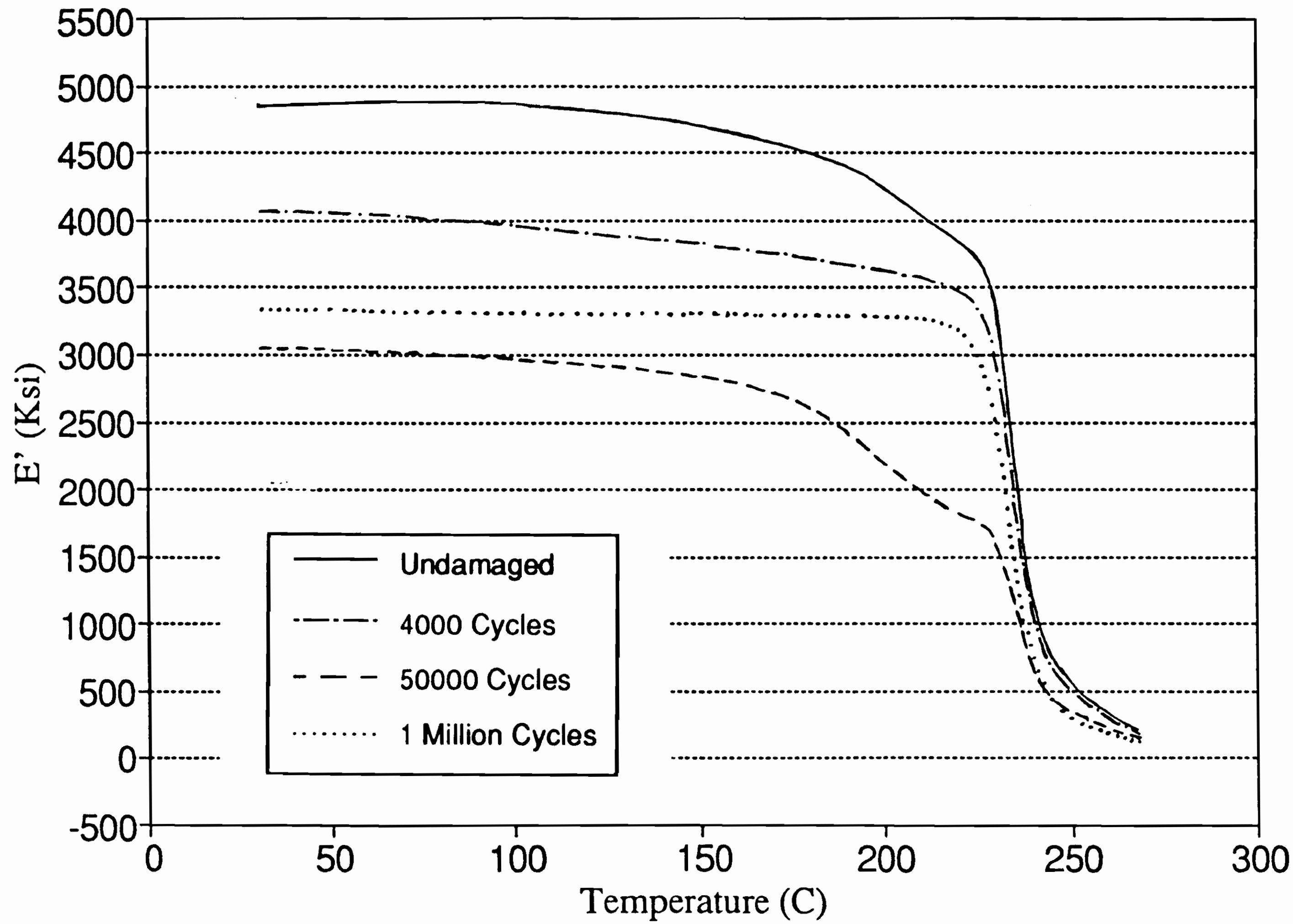

Figure 5.47 E'(T) of virgin and cycled cross ply laminates

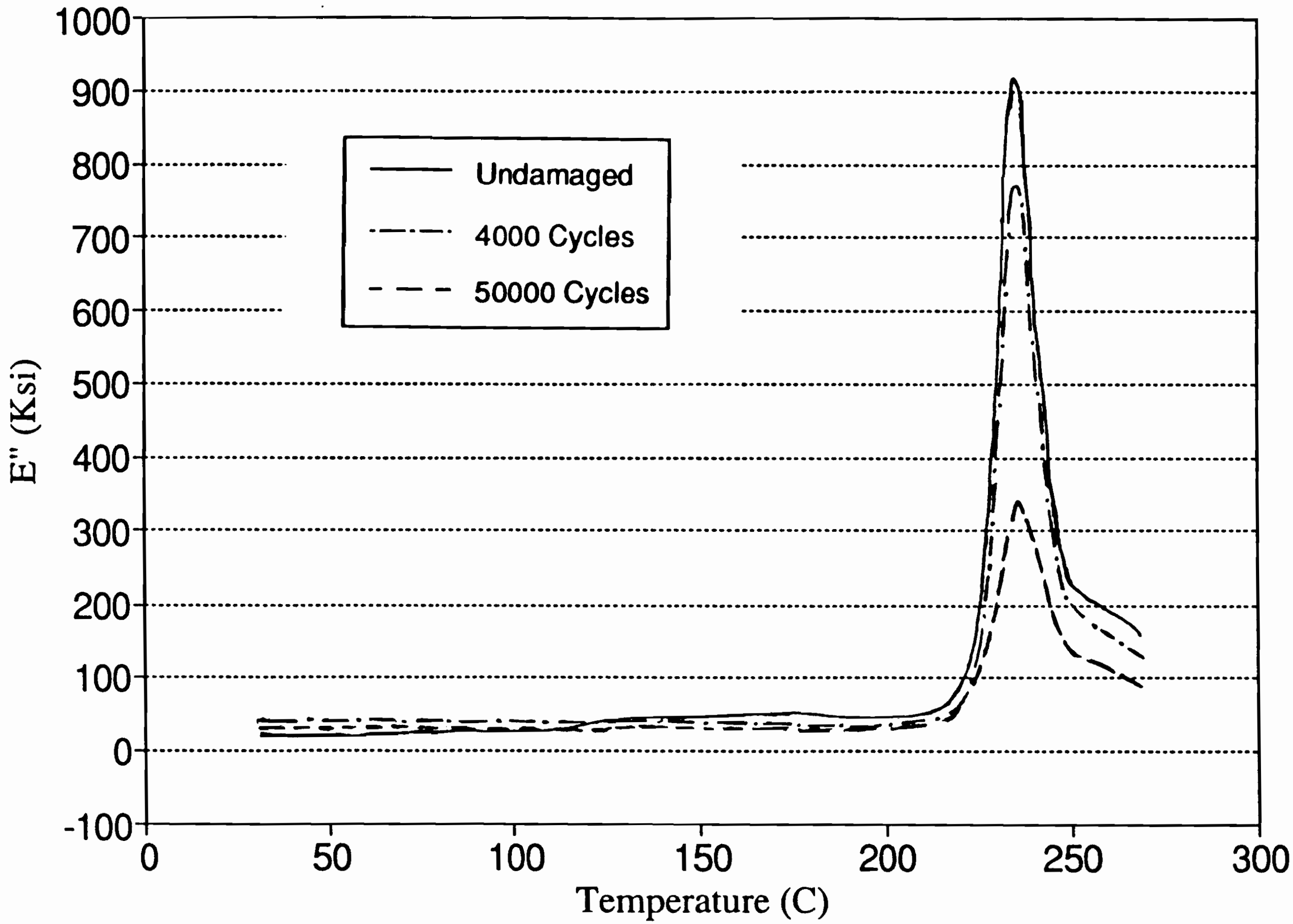

Figure 5.48 **E"(T) of virgin and cycled cross ply laminates**

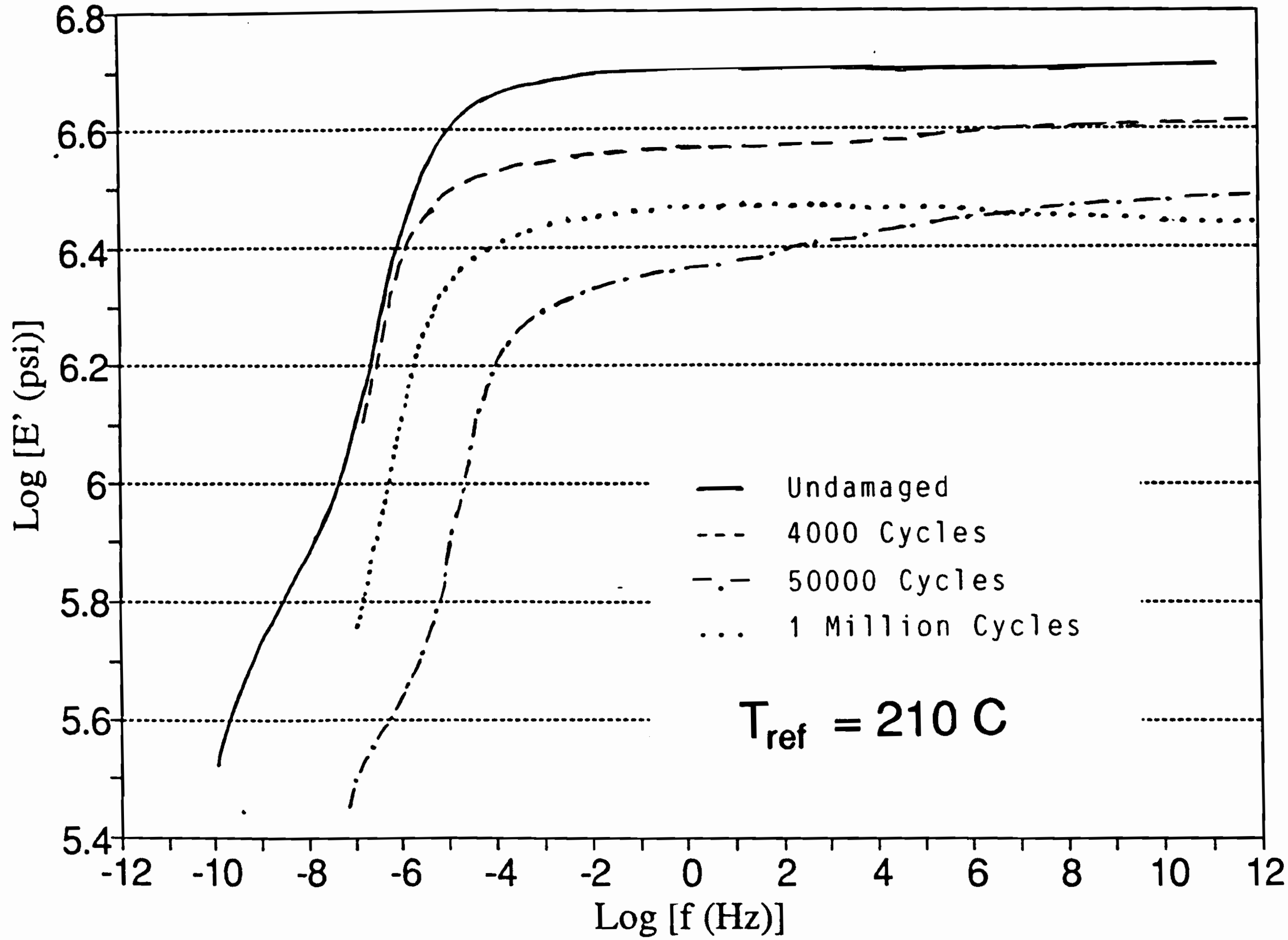

Figure 5.49 E'(ω) master curves of virgin and cycled cross ply laminates

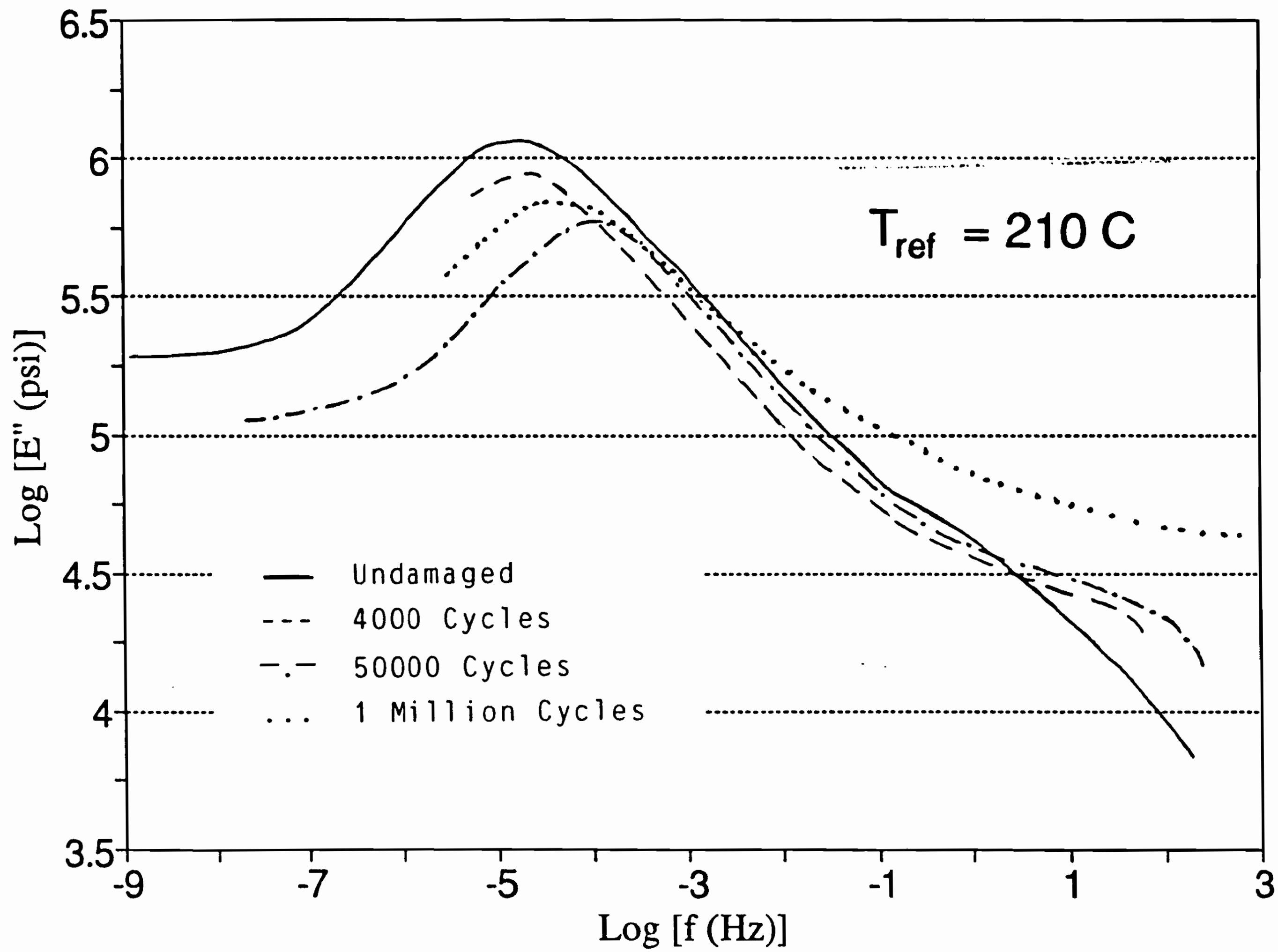

Figure 5.50 E"(ω) master curves of virgin and cycled cross ply laminates

modulus with decreasing frequency in the range of log[f(Hz)]=-4 to 11, a sharp drop between log[f(Hz)]=-4 and -6, and a secondary shoulder centered at log[f(Hz)]=-9. The master curves of the damaged coupons show a decreasing magnitude and a shift to the right as damage progresses. The traces for 4000 and 50000 cycles retain the shape of the undamaged laminate. Again, the trace for 1 million cycles shows some increase in magnitude with respect to 50000 cycles and a shallower frequency response.

The loss moduli master curve of the undamaged laminate shows one broad peak centered at log[f(Hz)]=-5 and a shoulder at -1. The loss modulus of coupons cycled for 4000 and 50000 cycles exhibits a diminishing magnitude and a shift to the right. The curves retain the shape of the curve for the undamaged laminate. The higher frequency end seems to rise as damage progresses. Once again, the trace of the 1 million cycles specimen is slightly higher than that of the 50000 cycles specimen and has no secondary shoulder.

A comparison of creep behavior at elevated temperature and creep compliance master curves is presented in Figures 5.51 and 5.52. Both figures indicate that creep of the cross ply laminates is magnified by progressive damage and that no additional changes in the creep behavior are found between 50000 and 1 million cycles (S=0.55). This would confirm the trend found in the complex moduli frequency response.

As was the case for 90° unidirectional laminates, none of the shift factors, whether creep compliance or complex moduli frequency

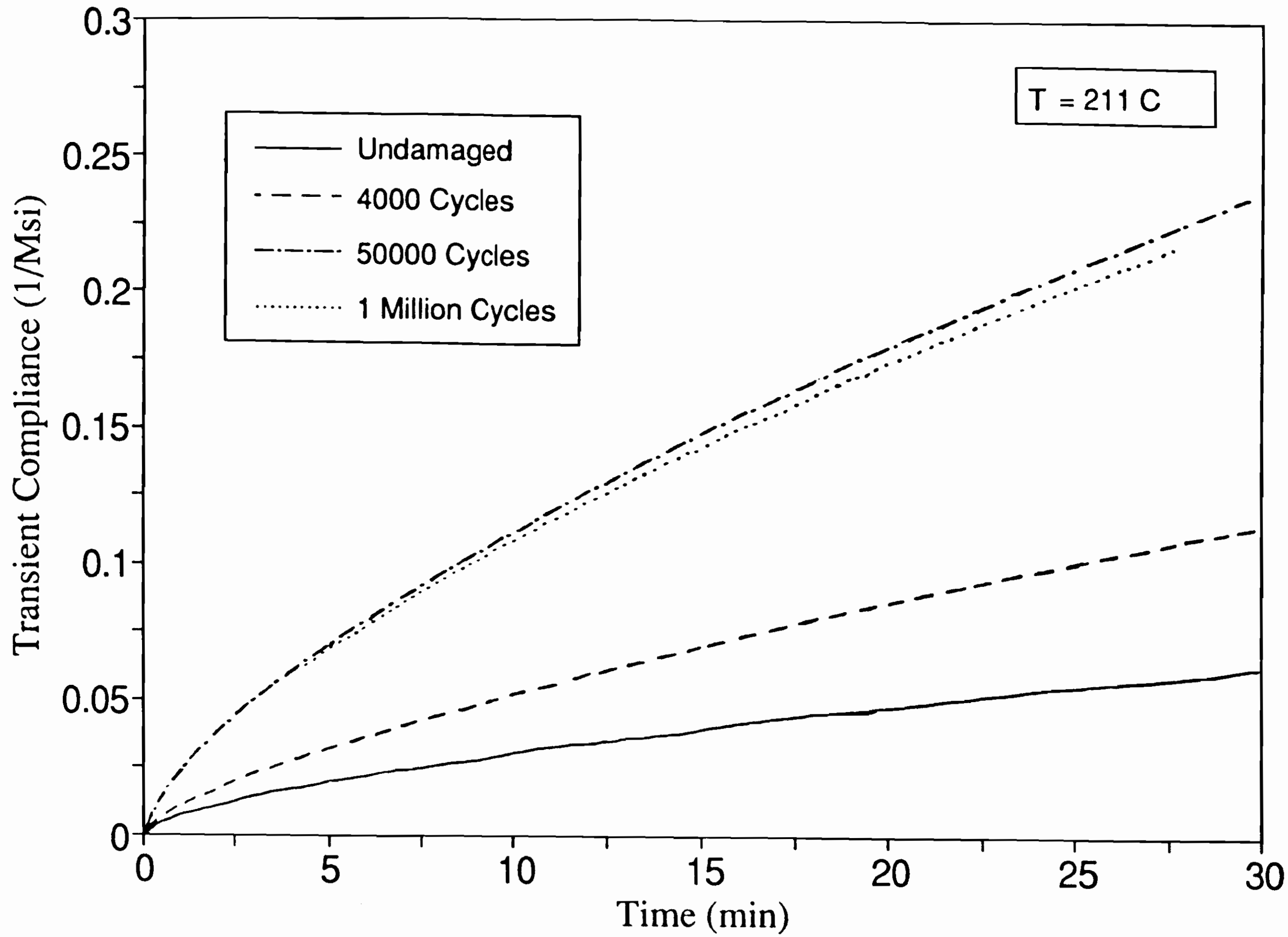

Figure 5.51 **Creep, virgin and cycled cross ply laminates @ high temperature**

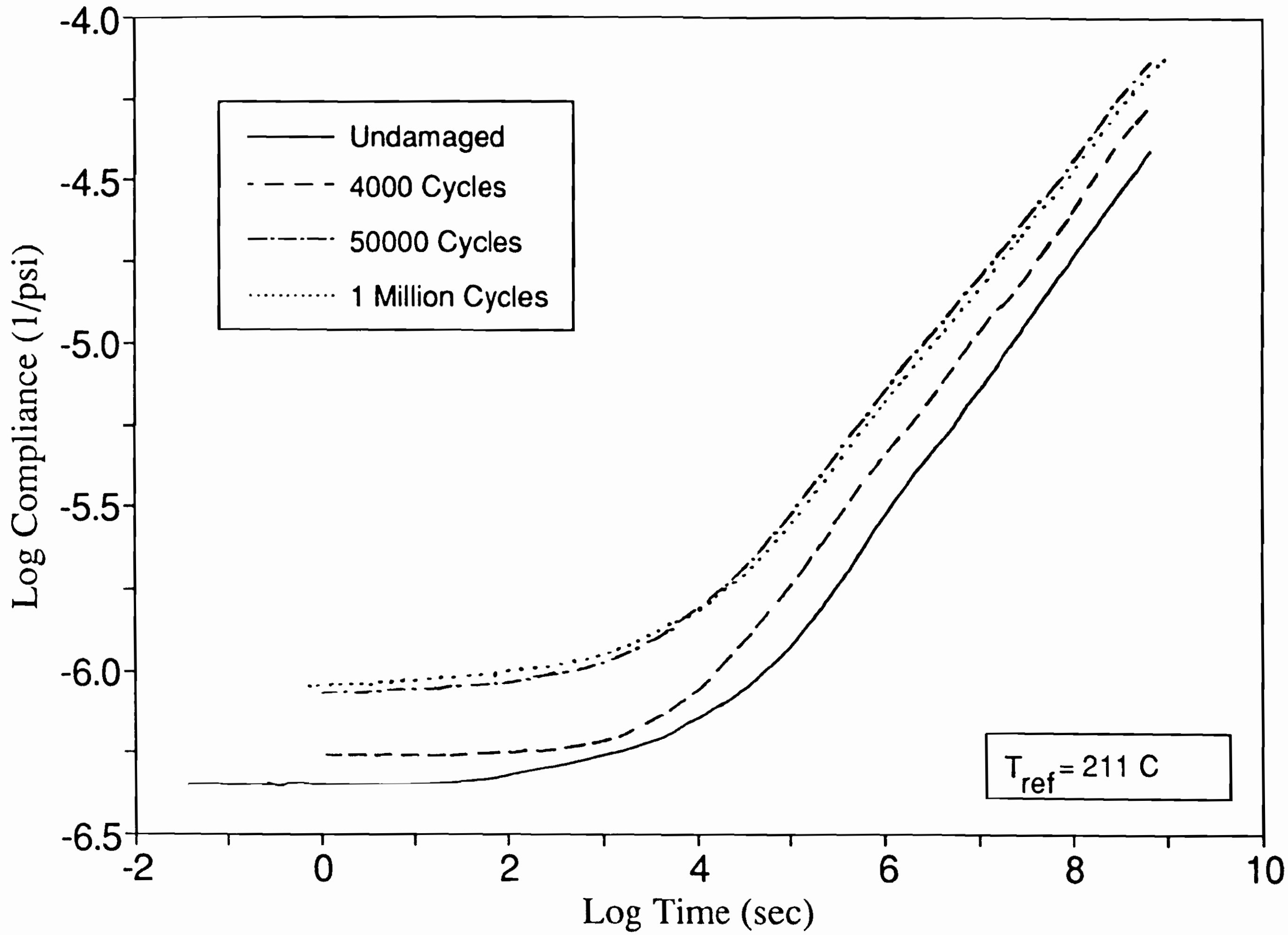

Figure 5.52 **Creep Compliance of virgin and cycled cross ply laminates**

mastercurves, obey Arrhenius or WLF relationships. The shift factors exhibit significantly different behavior below and above the glass transition temperature (215°C), and are greatly influenced by the presence of damage. Above T_g the shift factors decrease rapidly while they change very little for temperatures below the glass transition temperature. In general, damage results in higher initial compliance, smaller dissipation at peak frequency/temperature but higher dissipation at low temperatures/high frequencies, shifts of the apparent T_g, and temperature dependent acceleration or retardation of the deformation process. Some of the implications are discussed in Chapter 7.

5.6.3 The PAM Parameters

The techniques developed in Chapters 3 and 4 were used to evaluate the pseudo-analog parameters.

In the fiber orientation, the elastic response is nonlinear with marked stiffening. It also exhibits certain temperature dependence. Since no significant time dependent deformation was measured, the model for the 0° plies is reduced to one parameter, eb0. The temperature and stress dependence of the elastic response in the fiber orientation was determined from the initial deformation measured in mechanical (ISC) and thermal (DMA) creep experiments. Recalling Equations 4.4.4 and 4.4.5, the parameter eb0 is given by,

$$- \ln(eb0) = al_0 + bl_0\sigma + cl_0 \ln T^* + dl_0\sigma \ln T^* \qquad (5.6.6)$$

Using linear regression, the coefficients are

$al_0 = -16.94967$ $\quad$ $bl_0 = -2.35736\text{e-}8$ $\quad$ $cl_0 = -3.2593\text{e-}3$ $\quad$ $dl_0 = 0$

In the transverse direction the stress-strain curve is linear and the time dependent response is linear viscoelastic. Thus, the number of coefficients to be determined is reduced by half. The temperature dependence in the transverse direction is given by the following relationships derived from Equations 4.4.4 through 4.4.9,

$$-\ln(ea0) = at_0 + ct_0 \ln T^* \qquad (5.6.1)$$

$$-\ln(ea1) = at_1 + ct_1 \ln T^* \qquad (5.6.2)$$

$$-\ln(-ea2) = at_2 + ct_2 \ln T^* \qquad (5.6.3)$$

$$\ln(ma1) = (at_3 - at_1) + (ct_3 - ct_1) \ln T^* \qquad (5.6.4)$$

$$\ln(ma2) = (at_4 - at_2) + (ct_4 - ct_2) \ln T^* \qquad (5.6.5)$$

and the values of the coefficients from linear regression are,

$at_0 = -13.9403$ $ct_0 = -0.046583$

$at_1 = -18.71165$ $ct_1 = -0.046762$

$at_2 = -17.76082$ $ct_2 = -0.046867$

$at_3 = 8.2633$ $ct_3 = 1.37179$

$at_4 = 13.06797$ $ct_4 = 1.37195$

There is not enough data to analyze the comprehensive effect of damage (modes, extent, etc.) on each and every one of the PAM model parameters of the 90° plies. In Chapter 6 (the numerical code), power law relationships were used to correlate damage-induced changes in the transient compliance to the elastic response.

6 CYPERS, Cyclic Performance Simulation

6.1 Introduction

As part of the analytical effort, the cyclic performance simulation code CYPERS has been developed. It is able to predict the performance of cross ply laminates subjected to cyclic loading on the basis of elastic, fatigue and thermorheological lamina characterization. The basic premise is that for a certain interval of time (or cycles), the constitutive equations (presented in chapter 3) hold true. The length of each interval is determined by a series of criteria involving the magnitude and rate of change of the internal state of stress, temperature, and damage. At the end of each interval, the lamina properties and test conditions are updated before initiating the next step. Maximum strain, residual strength, and the critical element remaining life failure criteria are checked for laminate failure. Figure 6.1 shows a schematic of the computer program structure. The present version can be readily extended to handle arbitrary laminates subjected to any combination of static and cyclic loads. The main procedures, necessary data input, and available output are reviewed in this chapter.

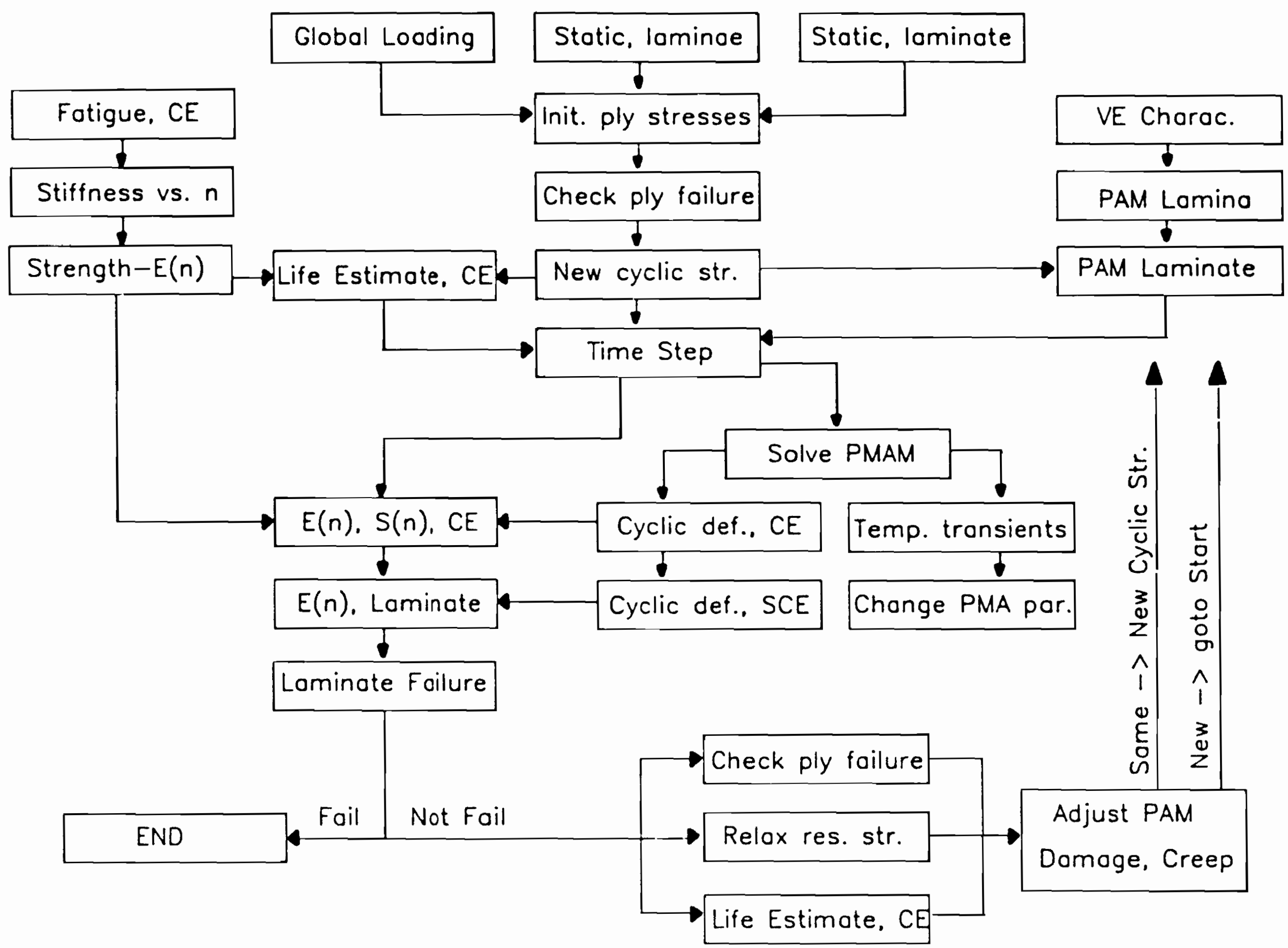

Figure 6.1 CYPERS code flowchart

6.2 Data Input

The data requirements of the CYPERS code are quite large. Inputs include quasi-static, fatigue, thermal and viscoelastic characteristics for all lamina materials and/or orientations in addition to stacking sequence, loading conditions and more.

The quasi-static mechanical characteristics at lamina level include,

- Ultimate tensile strength, longitudinal and transverse
- Compressive strength, longitudinal and transverse
- Shear strength
- Tensile, compressive and shear stiffness
- Strain to failure, longitudinal and transverse
- Major Poisson's ratio
- Damage and fracture modes

The fatigue characteristics at lamina level include,

- Life at varying stress levels (S/N curve)
- Dynamic stiffness
- Residual strength
- Temperature history
- Damage modes, sequence and fracture

The required thermal and moisture characteristics include,

- Longitudinal and transverse coefficients of thermal expansion
- Longitudinal and transverse heat conduction coefficients

- Heat transfer coefficient
- Initial ambient temperature
- Glass transition temperature
- Stress free temperature
- Longitudinal and transverse coefficients of moisture expansion
- Moisture content

In addition, some prior analysis of the laminate response is necessary to determine the relationships between transverse ply stiffness and crack spacing of the 90° plies, and the stress concentration at the crack tip and crack spacing. This analysis is described in Chapter 3 and was performed using available in-house Shear-Lag software. The resulting master curves were shown in Chapter 5.

The formulation of the generalized pseudo-analog model requires that for each lamina materials and/or orientation, up to 20 coefficients are specified.

Simple loading histories can be introduced by global definitions; e.g., load and temperature for isothermal creep; initial temperature, maximum cyclic load, stress ratio, and frequency for cyclic fatigue. In more complex cases, the loading history is introduced by defining all relevant parameters for each loading block.

In the initial phase of the program, most of the input data, as well as the preliminary stress evaluation (CLT) and other initial values are presented in table format, as shown in Figure 6.2. The

```
                    Information Screen
------------------------------------------------------------------
The normalized max. load is 0.600      Ultimate Strength    72434 psi
DELN=  118 cycles  R=  0.10            Freq= 10.00 Hz       Temp= 72.0 F
CDS(in)= 0.060     beta=-0.7539        b90=-0.0978          b0=-0.0263
EA0CDS= 658700 psi                     EB0TCDS= 820300 psi
The initial geometry and properties of the laminate
Long. properties   eb0(0)= 2.290E+07
Trans. properties  ea0(0)= 1.085E+06    ea1= 1.280E+08     ma1= 1.250E+11
                                        ea2=-0.494E+08     ma2= 6.420E+12
Initial laminate stiffness (psi)   6.574E+06
Orientation                           90                      0
Volume fraction                    0.750                   0.250
Init. residual stresses (psi)      3.001E+03              -0.900E+04
Init. applied stresses (psi)       1.015E+04               1.433E+05
Max. allowable stresses (psi)      1.056E+04               3.200E+05
Init. fraction of Ult. Str.        0.962                   0.448
Init. R ratio                      0.366                   0.043
------------------------------------------------------------------
Heat cond. coeff.(Btu/in*sec*F)    2.338E-08               2.083E-07
Eff. heat cond. & transfer coeff.  6.961E-08               3.800E-09
Max. Allow. Def.                   1.397E-02
The max. # of iterations             70
Press ENTER to continue, please.
```

Figure 6.2 Initial information screen capability to change any of these parameters is built into the code by following the prompts.

6.3 Main Procedures

Although this particular code could be readily generalized to handle any arbitrary laminate, this version is limited to cross ply laminates. Thus, the procedures are described in terms of their effect on the 0° and 90° plies.

Since a closed form solution for the static load situation exists, as stated in Eqn. 3.3.25, the numerical code is superfluous in this case. This code was developed to predict the response under cyclic loads only, but it can easily be extended to handle static loads or combinations of static and cyclic loads.

Strain and temperature are the two independent variables used by this code to evaluate the cyclic performance of the laminate. As described in paragraph 6.2 the ply stresses, the initial elastic deformation, stress concentration, and the PAM parameters are known before the first interval begins. The main steps of the iterative code are described in the next few paragraphs.

Life Fraction

The first step is to evaluate the remaining "life" and the fraction of "used up" life of each ply at the current stress levels.

In the case of the 90° plies, life is defined as the number of cycles to attain the Characteristic Damage State (CDS). For the 0° plies, "life" is the number of cycles to failure at the local level. To do so, the stresses are amplified by the current stress concentration factor, a function of the current crack spacing. To account for multiaxial stresses and the local stress concentration, the equivalent stress level in the 0° plies is redefined on the basis of the Tsai-Hill criterion,

$$\text{snbloc} = \left[\left(\frac{\sigma_1 * K}{XT} \right) - \left(\frac{\sigma_1 * K * \sigma_2}{XT^2} \right) + \left(\frac{\sigma_2}{YT} \right)^2 + \left(\frac{\tau_{12}}{S} \right)^2 \right]^{1/2} \tag{6.3.1}$$

where snbloc is the local stress level in the 0° plies, K is the magnitude of the stress concentration, and

XT, YT, S	longitudinal, transverse and shear strength, 0° plies
σ_1, σ_2, τ_{12}	in-plane stresses, 0° plies

In both cases the used up fraction of life corresponds to the successive addition of the ratios between the length of the interval and the remaining life. When the life fraction of the 90° plies reaches the value of 1, CDS is attained. From that point on, the crack spacing and stress concentration remain constant. The life of the 0° plies, the critical element, determines the life of the laminate. By virtue of stress reintroduction into the cracked plies and the time-dependent behavior of the 90° plies, life after the CDS is achieved cannot be determined by simple addition of the number of cycles to attain the CDS and the remaining life of the 0° plies at that moment. Such course leads to large over prediction of the life of the laminate. Once the used life fraction of the critical element reaches the value of 1, failure occurs and the run is ended.

Viscoelastic Response

The second step is to evaluate the viscoelastic response of the laminate. First the coefficients of the differential constitutive relationship (Eqn. 3.3.17) are determined, taking into account the current ply stresses and specimen temperature. Then, the current complex moduli and compliance of the laminate, the phase lag angle and the energy dissipated per unit volume per cycle (or time) are evaluated. Using this information and the temperature determined from the previous interval, the temperature distribution and maximum specimen temperature at the end of the current interval are derived.

The strains at mean and maximum load at the end of the interval are found by solving Eqn. 3.3.34. The local strain concentration in the 0° plies is calculated from Eqn. 3.3.9. The apparent creep rate and the residual strain (corresponding to zero load) are also evaluated.

Damage Evaluation

The third step is to evaluate the damage accumulated by the different plies at the end of the interval. Damage is represented by changes in the stiffness and strength of each ply.

The longitudinal, transverse, and shear stiffness of each ply are reduced separately. No procedure exists to alter the Poisson ratios, but the apparent laminate Poisson ratio is drastically changed by the degradation of the lamina properties.

Recalling Equation 5.4.3, the remaining longitudinal stiffness is reduced according to the experimentally measured degradation of the unidirectional 0° laminates,

$$eb0 = eb0(0)*\left[1-(1-snb) * \left(fracb + \frac{deln}{tfbint}\right)^{pb}\right] \qquad (6.3.2)$$

where,

eb0 is the current longitudinal stiffness, 0° plies

eb0(0) is the initial longitudinal stiffness, 0° plies

snb is the ratio between the maximum stress level in 0° plies to the ultimate tensile strength of the 0° plies,

fracb "used up" life fraction of 0° plies at beginning of interval,

tfbint is the remaining life at the beginning of current interval,

deln is the length of current interval, and

pb is an experimental stiffness degradation power, 0° plies.

The apparent transverse stiffness of the 90° plies is reduced using Eqn. 3.3.8, a function of crack spacing and the life relationship for this ply orientation. Once the CDS has been achieved, it remains relatively constant, changing only if the stiffness of the constraining 0° plies is degraded. The transverse stiffness of the 0° plies is degraded in a similar fashion, but its minimum crack spacing and the CDS apparent transverse stiffness are different from those of the 90° plies. It is assumed that the CDS in the 0° plies is reached at the same time as that in the 90° plies. Eqn. 3.3.8 is replaced by,

$$ea0 = \frac{eb0 * YT * (t0int + deln)^{b90}}{S *(1 + k90) - k90 * YT *(t0int + deln)^{b90}} \qquad (6.3.3)$$

where,

ea0 is the transverse stiffness of the 90° plies,

eb0 longitudinal stiffness of the 0° plies given by Eqn. 6.3.1,

YT is the transverse strength, unidirectional laminate,

t0int is the number of cycles at the beginning of the interval,

S is the maximum applied global stress,

k90 is the ratio of 90° to 0° thickness, and

b90 is the experimental life power, 90° plies (Eqn. 3.3.5).

The shear stiffness of both orientations is reduced by an amount proportional to the degradation of the transverse stiffness of the relevant ply.

The residual strength of the laminate is considered to be the sum of the stresses supported by all plies at the laminate's failure strain of 1.202%. Recalling Equation 5.4.4, the remaining strength of the 0° plies is calculated from their experimentally measured residual strength, given by,

$$restrb = XT - XT * (1\text{-}snbloc)*\left(fracb + \frac{deln}{tfbint}\right)^{qb} \qquad (6.3.4)$$

where,

snbloc is the local maximum stress in the 0° plies, Equation 6.3.1,

restrb is the residual strength of 0° plies,

XT is the initial tensile strength of 0° plies, and

qb is the experimental strength degradation power, 0°

The stress supported by the 90° plies is calculated by multiplying the strain to failure of the laminate by the current apparent stiffness of the 90° plies. The remaining strength of the laminate - RS - is the sum of both contributions multiplied by the corresponding volume fractions, taking into account the current residual stresses and stress concentration.

Failure Criteria

The computer run is ended once the used life fraction of the 0° plies reaches the value of 1. Two additional failure criteria are employed.

The residual strength failure criterion is based on the normalized residual strength at the local level. It has an initial value of 1, and it is 0 when the strength of the laminate reaches the maximum applied stress, as shown schematically in Figure 6.3. It is

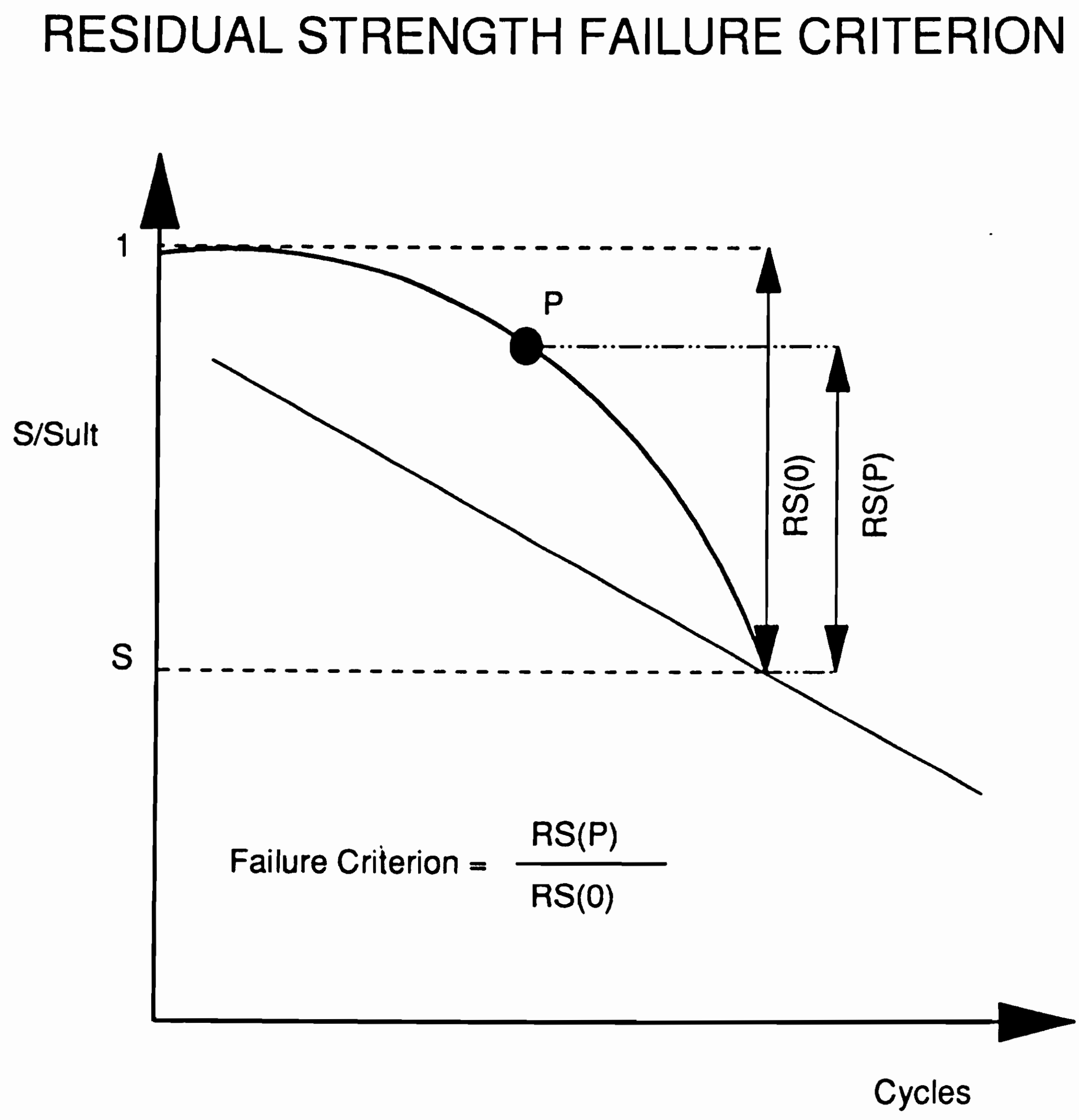

Figure 6.3 Residual strength failure criterion, schematic

defined as,

$$\text{fcrestr} = \frac{RS - S}{SF - S} \equiv \frac{RS(P)}{RS(0)} \tag{6.3.5}$$

where,

fcrestr is the residual strength failure criterion,

RS is the local residual strength, and

SF is the undamaged laminate strength, quasi-static test.

The deformation failure criterion is based on the ratio of the maximum local deformation of the 0° plies and the strain to failure of a unidirectional 0° laminate. Its initial value is 1, and reaches 0 when the laminate fails. A schematic is shown Figure 6.4. It is defined as,

$$\text{fcmaxe} = \frac{\text{maxe} - \text{toeloc}}{\text{maxe} - \text{toeloc}(0)} \equiv \frac{RE(P)}{RE(0)} \tag{6.3.6}$$

where,

fcmaxe is the maximum strain failure criterion,

maxe is the strain to failure, unidirectional 0° laminate,

toeloc is the strain at point of maximum strain concentration, and

toeloc(0) maximum strain at point of strain concentration for 1 crack

Although the main mechanism designed to end the computer run is the fatigue criterion, the program is interrupted if the values of

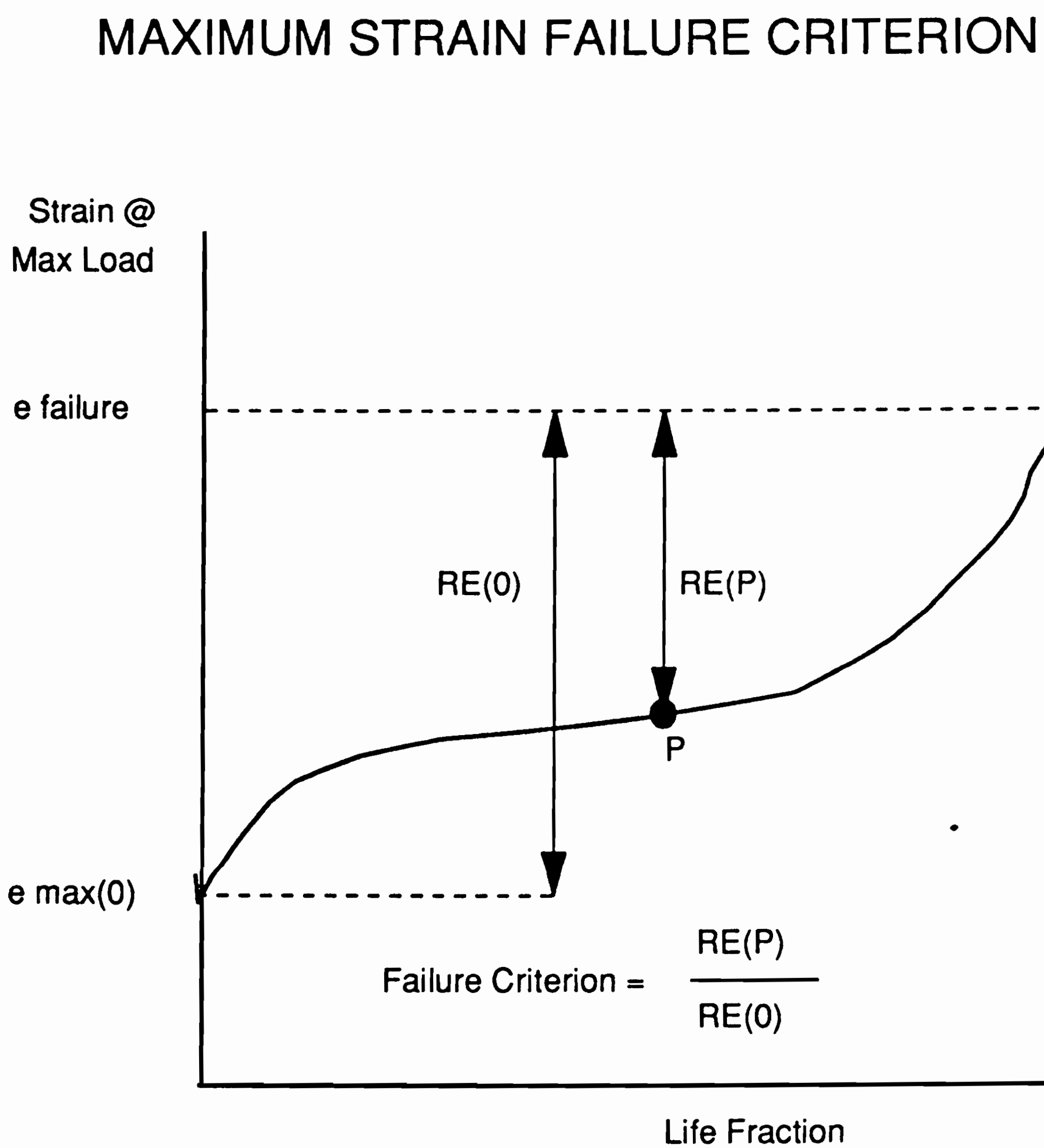

Figure 6.4 Maximum strain failure criterion, schematic

both additional criteria reach the value of 0. Since there is an implicit relationship between fatigue life, strength, and deformation, all three failure criteria are in good agreement.

Time Interval

The fourth step of the iterative portion of the code is to determine the next time interval; i.e., the number of cycles for the next iteration. This special procedure is designed to save computation time and storage memory when compared with fixed interval schemes. The time intervals are successively reduced when the rate of change in the material properties accelerates and progressively increased when stable periods occur.

Steps which are too large tend to skip over important periods of change and grossly over predict life. Steps which are too small tend to clog the available memory and may introduce significant error when small changes are assigned a zero value due to the limitations of computer accuracy. While not infallible, varying the interval length greatly reduces the number of iterations required to accurately portray the cyclic performance of the laminate. Within broad limits, variations of the cyclic intervals do not affect the predicted life, deformation, stiffness and strength.

Data Storage & Interval Initiation

The last step is to store all the performance raw data in the corresponding arrays. The values at the end of the interval are used to compute the ply stresses, stress concentration, used life fractions and PAM parameters for the next interval.

6.4 Predictive Output

The code predictions are presented in both, numeral and graphical form, at the beginning of each interval and at the end of the run.

The options for each interval are,

1. Stress-strain loop - a complete loop is drawn every time the global stiffness change exceeds a predetermined value, Figure 6.5.
2. Stress and strain vs. time, for one cycle - plotted every time the change in global stiffness exceeds a predetermined value, Figure 6.6.
3. Frequency response - the storage and loss moduli are plotted vs. frequency (logarithmic scale), Figure 6.7.
4. The temperature axial distribution in the specimen, Figure 6.8 - plotted every time the maximum temperature in the specimen changes by a predetermined value.
5. Interval statements, similar to the statement shown in Figure 6.2
6. A one line statement of up to 8 values of raw or normalized data, as shown in Figure 6.9.

For options 1 through 4, the iteration number and corresponding number of cycles appear on the top right side of the screen. The line statement in option 6 can be readily changed to list up to eight

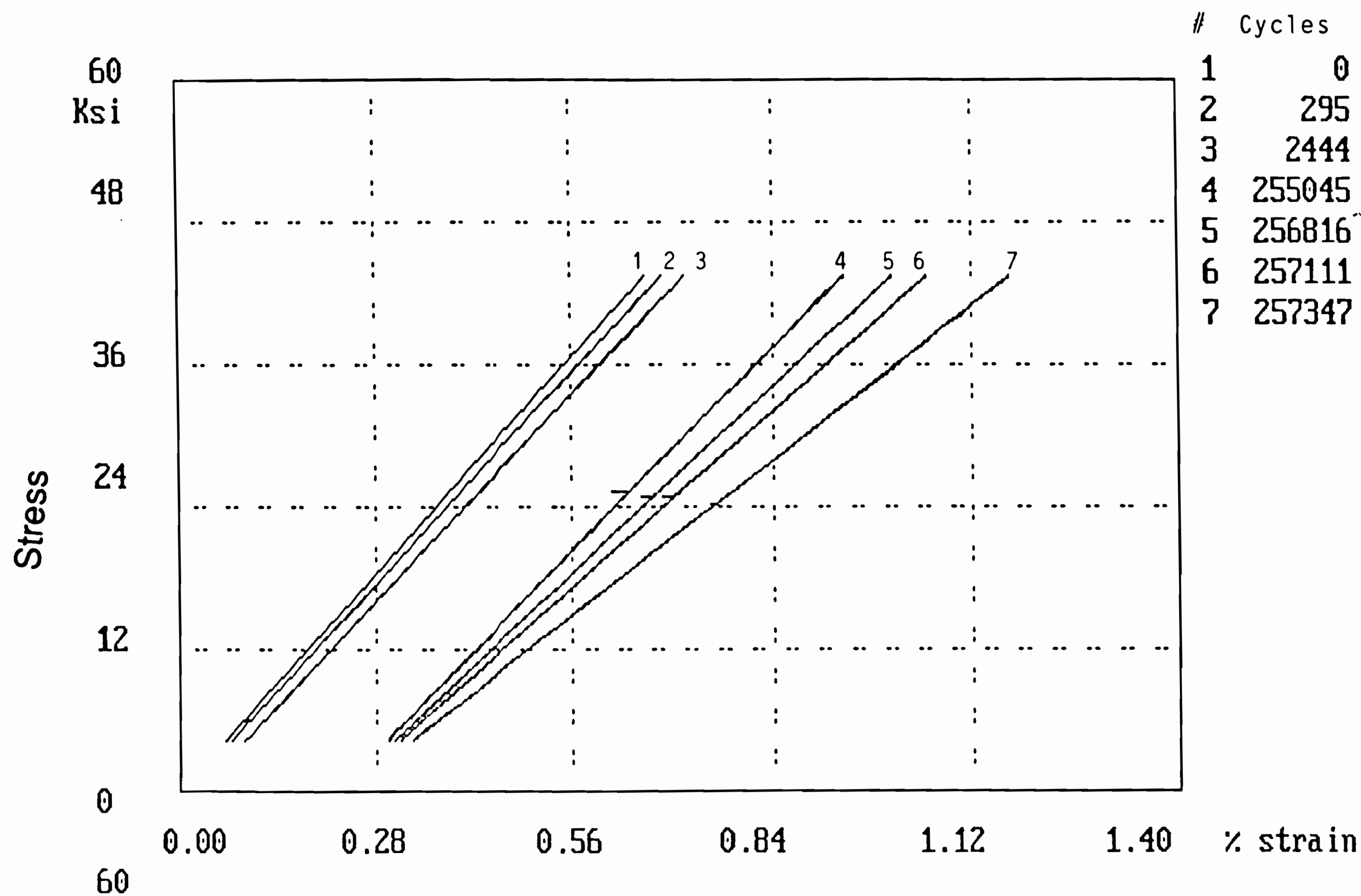

Figure 6.5 Cylic stress-strain loops

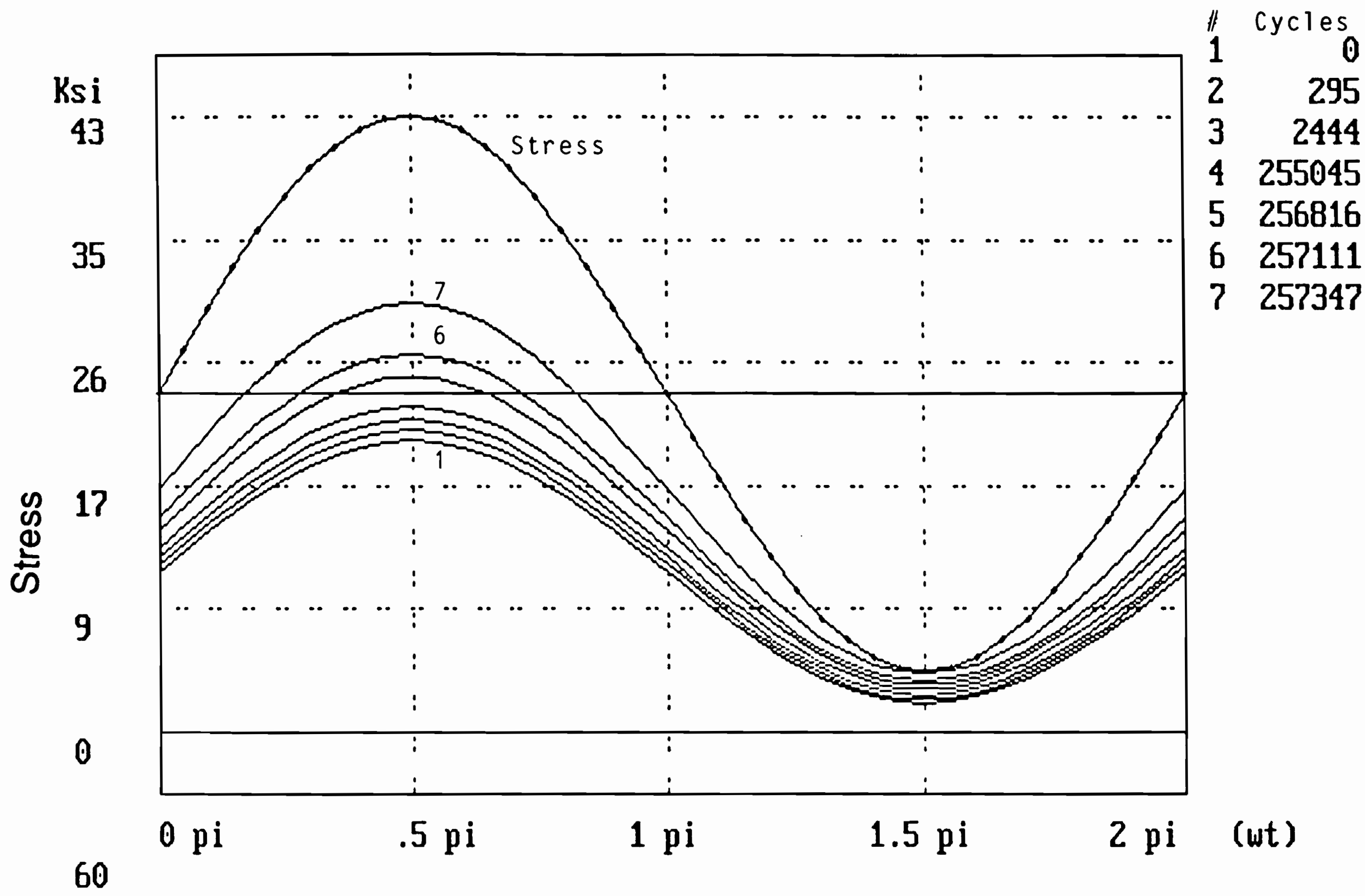

Figure 6.6 Cyclic stress and strain for one cycle

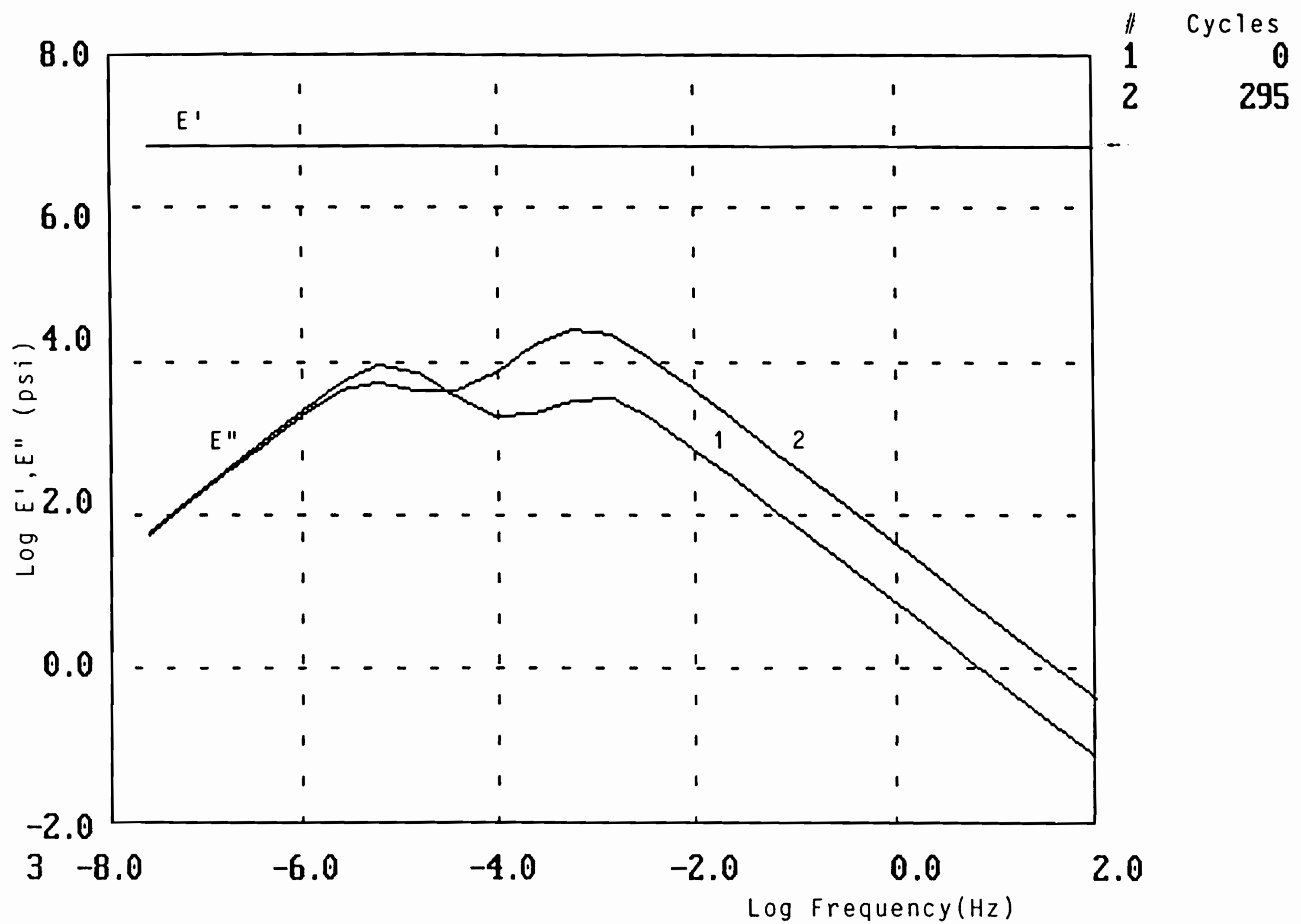

Figure 6.7 Cyclic frequency response, storage and loss moduli

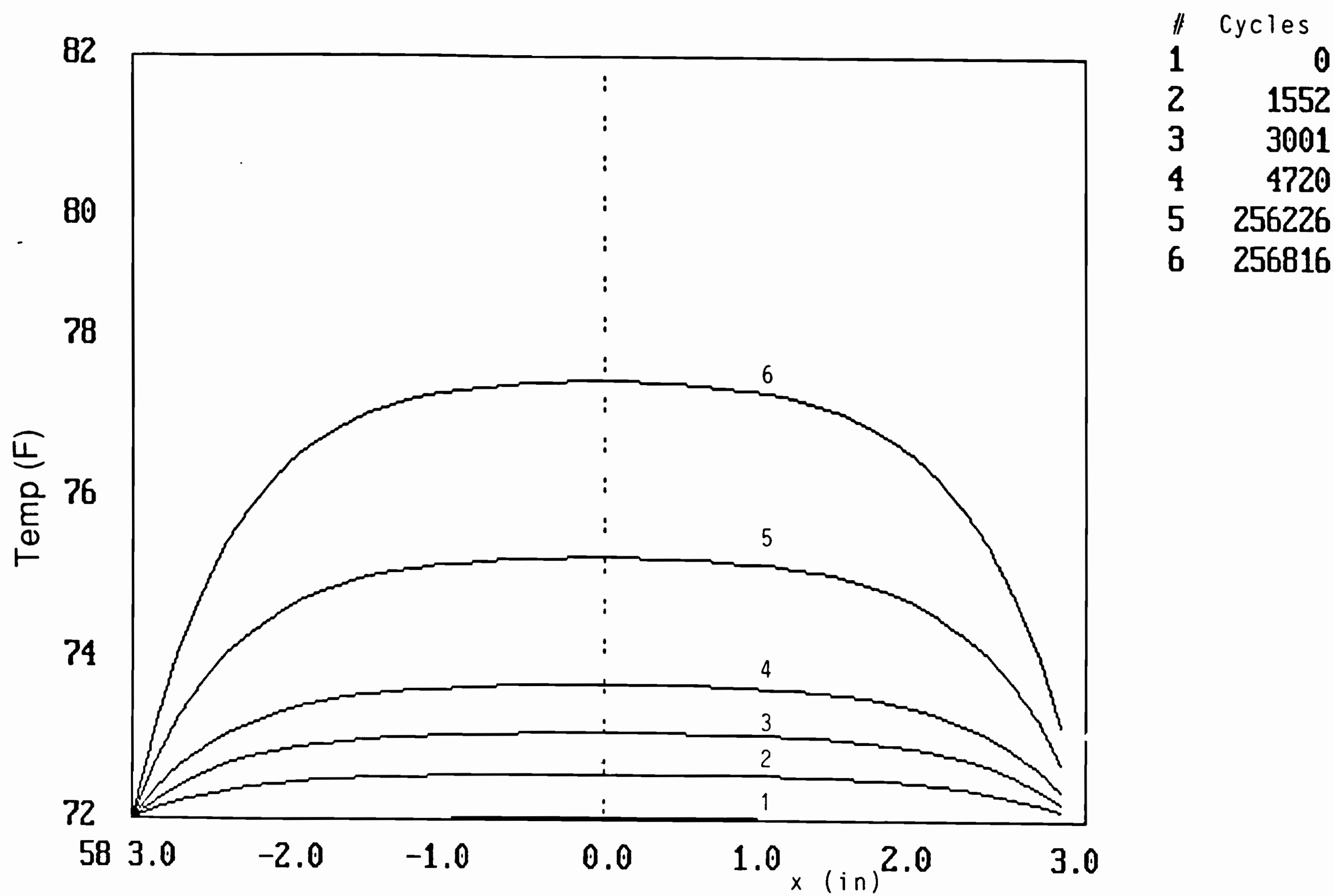

Figure 6.8 Cyclic temperature distribution in specimen (length)

Be patient, I'm working ...

#	cycles	E(0)	E(90)	Ex/Ex(0)	RS/RS(0)	1-fracb	FCrs	FCme
1	0	2.290E+07	1.085E+06	1.000E+00	1.000E+00	1.000E+00	1.000	1.000
2	118	2.290E+07	9.855E+05	9.779E-01	1.000E+00	9.984E-01	1.000	1.000
3	295	2.290E+07	8.911E+05	9.569E-01	9.754E-01	9.959E-01	0.939	0.987
4	560	2.290E+07	8.310E+05	9.435E-01	9.521E-01	9.934E-01	0.880	0.974
5	957	2.290E+07	7.842E+05	9.331E-01	9.372E-01	9.906E-01	0.843	0.964
6	1552	2.290E+07	7.444E+05	9.242E-01	9.255E-01	9.873E-01	0.814	0.953
7	2444	2.290E+07	7.091E+05	9.163E-01	9.157E-01	9.830E-01	0.789	0.938
8	2667	2.290E+07	7.024E+05	9.149E-01	9.069E-01	9.821E-01	0.767	0.914
9	3001	2.290E+07	6.936E+05	9.129E-01	9.052E-01	9.808E-01	0.763	0.906

Figure 6.9 Simple cyclic line information output

parameters of interest. A statement appears at the end of each run. In this statement the following predictions are presented:

- Whether the specimen has failed within the maximum number of cycles or intervals specified.
- The predicted number of cycles to failure according to the fatigue life of the critical element (the last ply to fail), criterion 1.
- The predicted number of cycles to failure according to the local residual strength, criterion 2.
- The predicted number of cycles to failure according to the local maximum strain, criterion 3.

If the fatigue failure of the critical element has interrupted the run (criterion 1) while the other two criteria are still nonzero, approximations of total life are presented according to the last measured rate of change in these criteria.

At the end of this statement a prompt for graphic outputs appears. Using this option, graphical displays of the cyclic behavior of the laminate are presented. Some of these options are,

1. Maximum specimen temperature vs. cycles
2. The laminate and ply (apparent) stiffness vs. cycles
3. Global ply stresses and local stress for 0° plies vs. cycles
4. Strain at mean and maximum load vs. cycles
5. Strength vs. cycles in linear and logarithmic scales, with a display of available cyclic life data and the predicted failure.
6. Laminate strength, stiffness and/or transient deformation vs.

life fraction.

Most graphic displays have a normalized y-axis. The normalizing factors, date, time and other relevant data are shown on the screen in or around the graphic plot. Samples of these and other plots are shown in Chapter 7 as part of the discussion and comparison with experimentally measured results.

7 Discussion

The thrust of this research effort has been directed at understanding the magnitude and possible interaction mechanisms of rate dependent (viscoelastic deformation and energy dissipation) and independent (cyclic damage evolution) processes during cyclic loading of composite laminates. The intention is to bring forth a complementary tool to be eventually implemented in much more detailed performance codes, such as the MRLife [178], developed by the Materials Response Group at VPI & SU.

A great deal of effort was given to the characterization of the fatigue and viscoelastic behavior of the constituents of the laminate, creating models to handle the evolutionary response in a comprehensive but mathematically tractable manner, and developing rudimentary numerical procedures to predict the long term performance of cross ply laminates subjected to tensile cyclic loading. The experimental, analytical, and numerical results are discussed individually and collectively. Possible applications to loading situations other than those encountered in this program are also discussed.

7.1 Viscoelastic Characterization

Several experiments were performed to evaluate the capabilities of the PAM model (Chapter 3) and measured coefficients (Chapter 5) to predict the time dependent deformation of 90° unidirectional and cross ply laminates subjected to various loading conditions.

The simplest case is the cyclic loading of the 90° unidirectional laminate. To avoid fatigue damage, the specimens were tested at mean cyclic loads corresponding to 60, 70 and 80% of the ultimate tensile strength with an amplitude of 10% of the UTS and at 0.1 Hz. Stiffness measurements and C-scans did not reveal any matrix cracking during this procedure. Temperature measurements show no heating due to cyclic loading. The measured strain at mean load and the model predictions, shown in Figure 7.1, are in very good agreement.

Figure 7.2 shows the analytically evaluated added strain at mean load (static load) for a 90° unidirectional laminate subjected to a static or mean stress of 60% UTS. In the cyclic case the amplitude is 30% UTS and the frequency is 0.033 Hz. It is evident that the viscoelastic response is altered by the additional dynamic loading. As predicted by Equation 3.3.45, the difference lies in the out-of-phase response and a transient cyclic term. For this laminate and at room temperature, cyclic loading results in modest creep acceleration. The cumulative difference curve (Figure 7.2) has a sigmoidal shape, suggesting that after an initial period of added strain the cyclic effect disappears. The sign (acceleration or retardation), magnitude, rate and shape of this curve depend on the combination of PAM parameters, laminate configuration, frequency, and cyclic loads.

The creep of cross ply laminates was measured and compared to

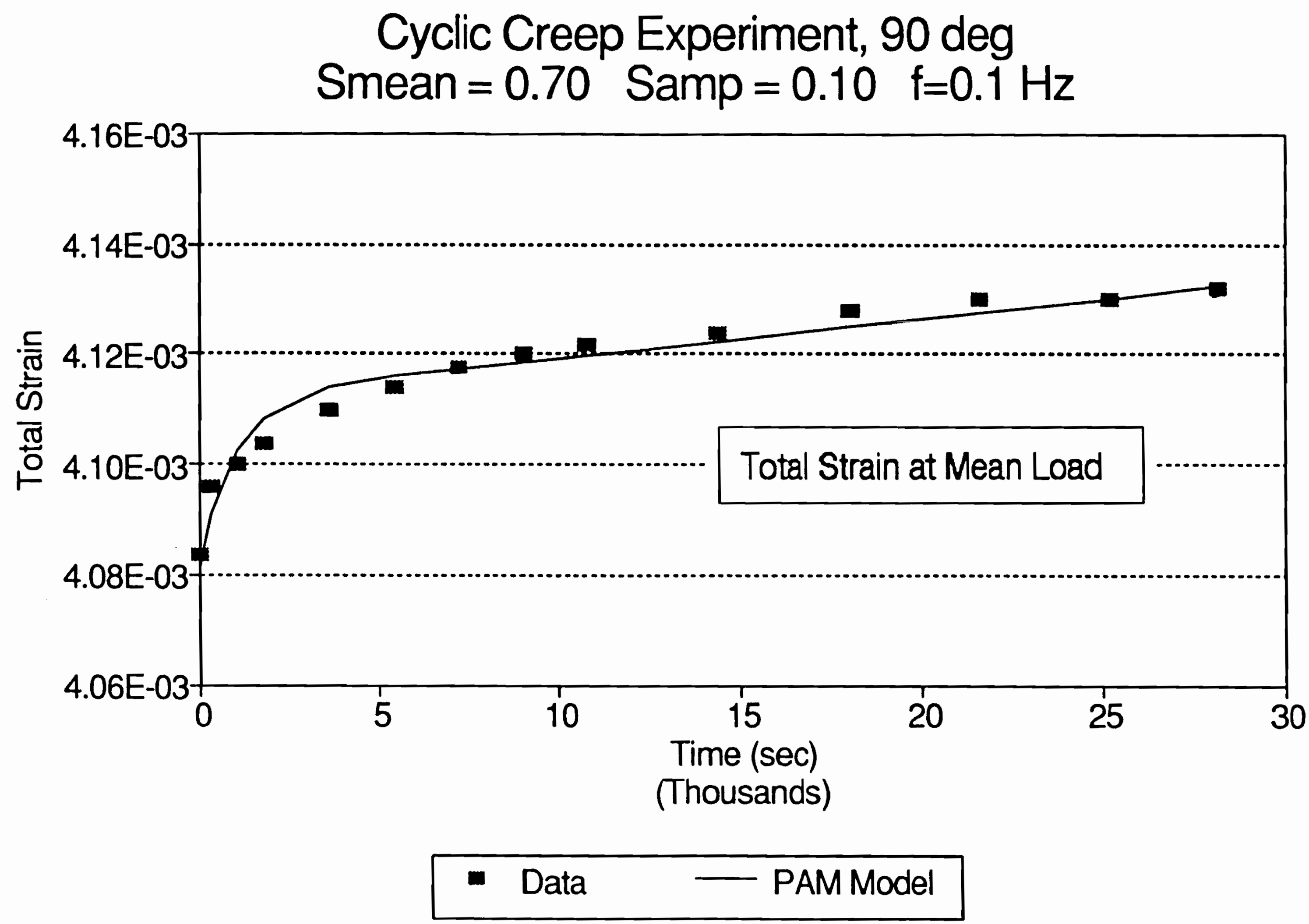

Figure 7.1 Cyclic creep, 90° orientation

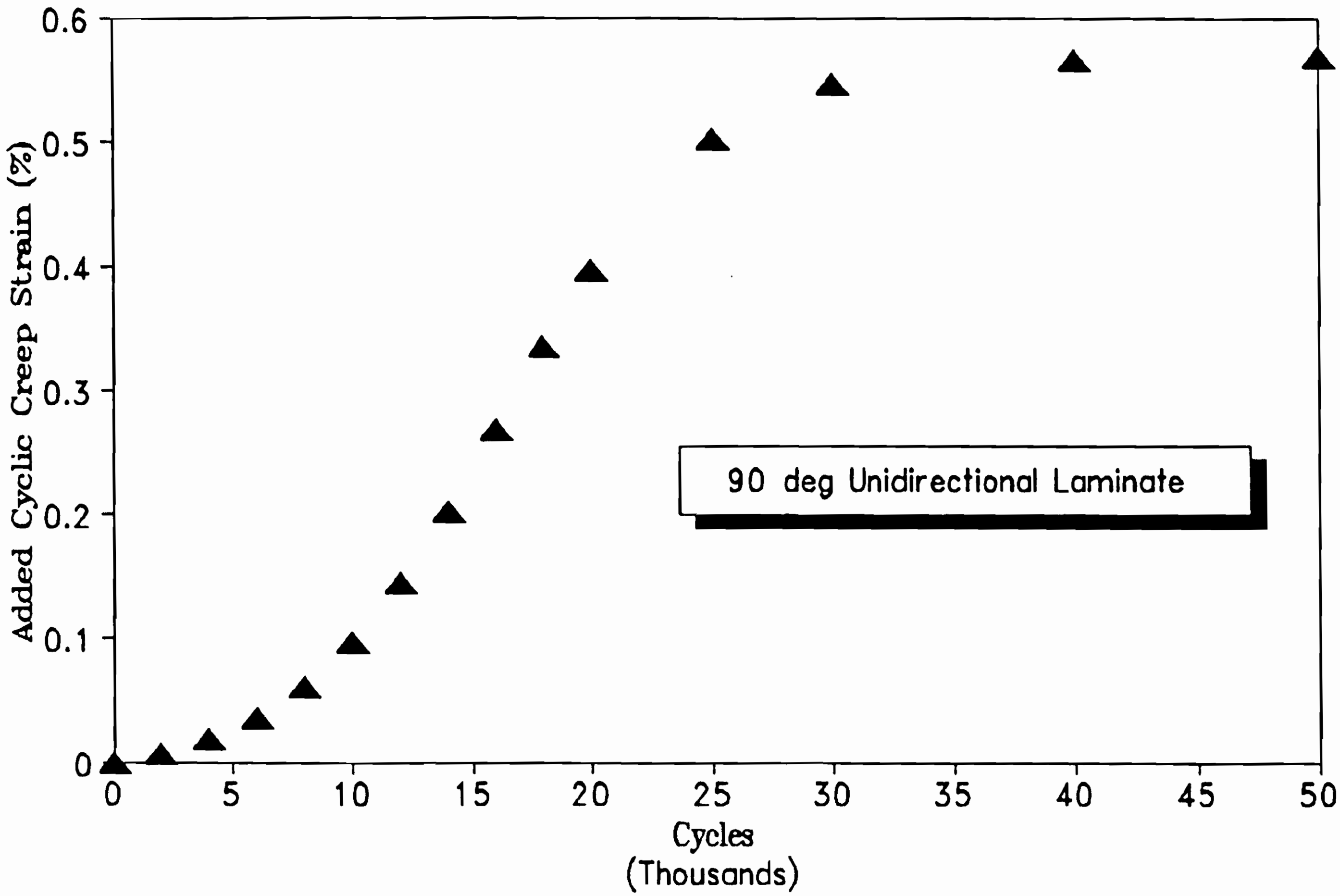

Figure 7.2 Static and cyclic creep predictions, 90° orientation

analytical predictions. All stress levels were chosen below the knee point in the stress-strain response of the laminate to preclude initial matrix cracking of the 90° plies. The results and predictions are shown in Figure 7.3 for S=0.25, 0.40 and 0.55. The magnitude of the strains is very small because the deformation is the result of the internal stress relaxation in the 90° plies which redistribute the loads towards the 0° plies. The agreement between experiment and prediction is very good.

Creep recovery of cross ply laminates can be easily represented with this model. Since no additional damage develops during periods of unloading, the solution to the creep recovery situation does not involve the second "negative" Kelvin element in the PAM model of the 90° plies. A comparison of the analytical prediction and the measured response is shown in Figure 7.4. The model predicts the general rate and magnitude of the recovery process in a satisfactory manner.

The modified Wilshire-Evans approach at the lamina level together with classical laminate stress analysis yields very encouraging results. The combination of static mechanical tests and dynamic thermo-mechanical analysis offers an efficient path to fully characterize the thermorheological behavior at the lamina or laminate level (albeit Dupont's DMA software needs to be modified to correctly compute the viscoelastic functions of orthotropic materials). Only different materials, orientations and/or basic sublaminates need be characterized. A minimum of experimentally determined coefficients is required to formulate the time dependent constitutive relationships of

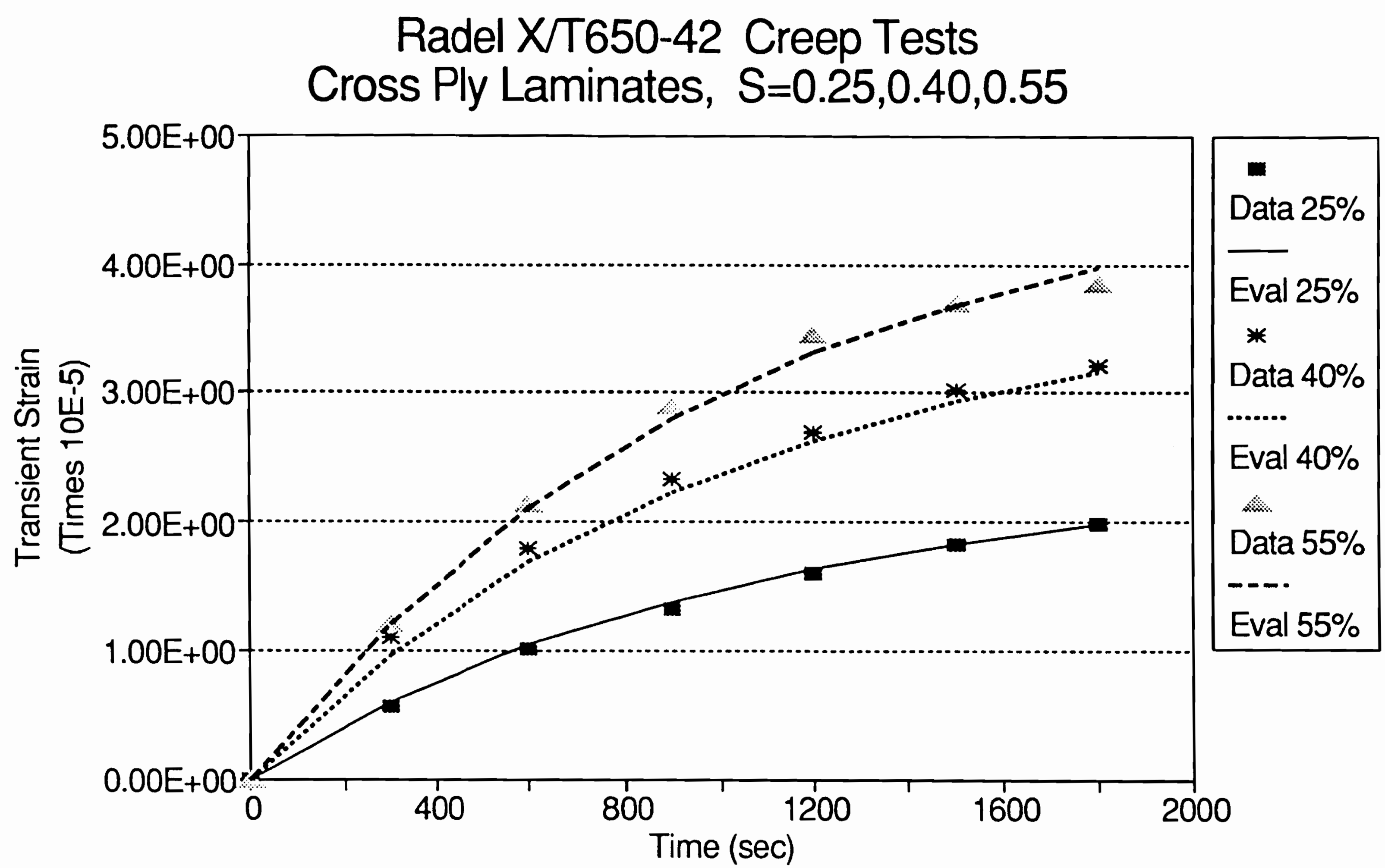

Figure 7.3 Creep of cross ply coupons

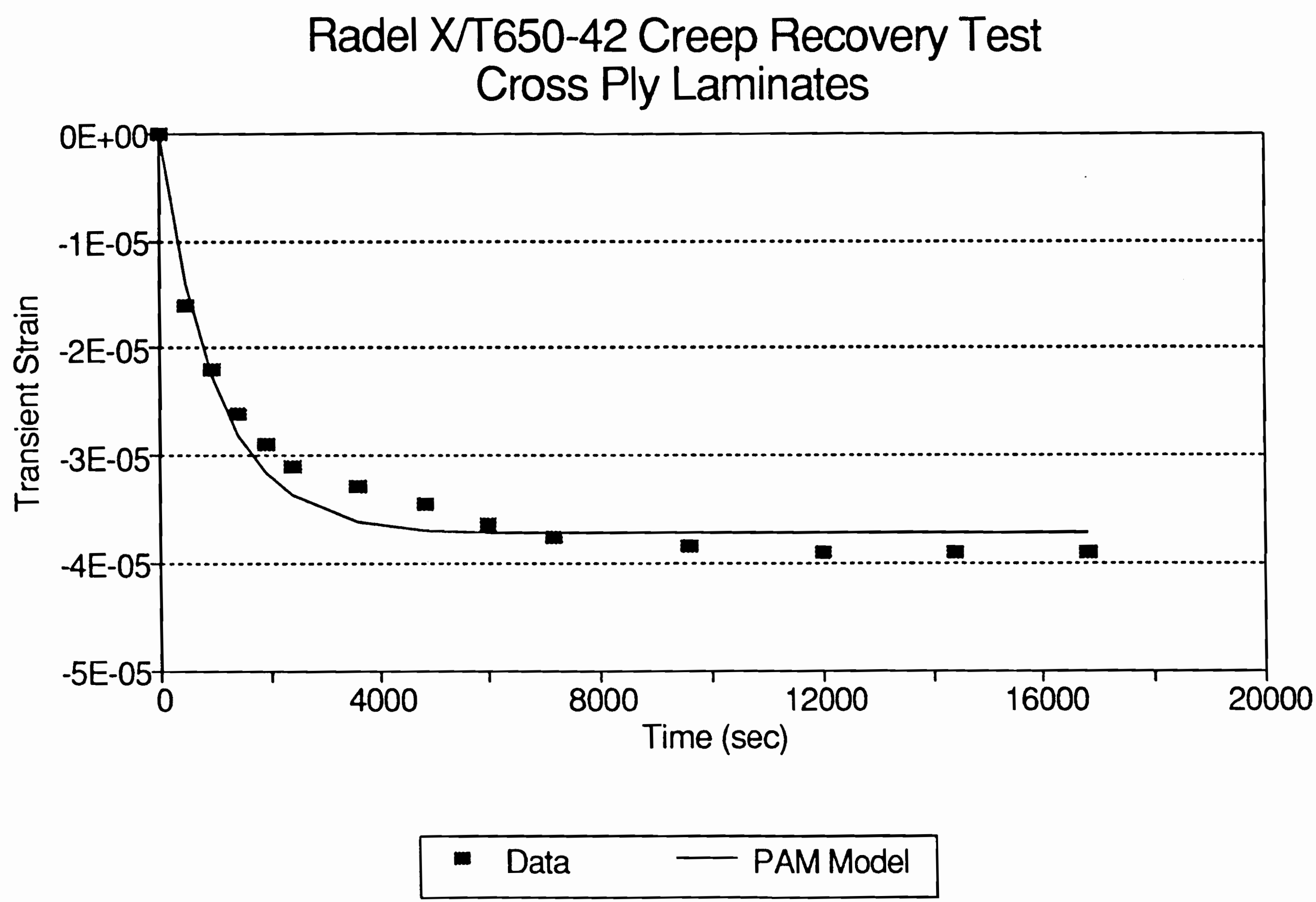

Figure 7.4 Creep recovery of cross ply coupons

the laminate with implicit temperature and stress dependence.

These relationships can be applied to any arbitrary loading history to analytically evaluate the effects of loading rate, strain rate, frequency, temperature, mean stress and amplitude, nonlinear behavior and more. Solutions maybe closed form or numerical, depending on the complexity of the loading case. Further refinement and understanding of the role of all the physical processes taking place could lead to substantial improvements in the PAM laminate representation and the prediction of long term performance of composite laminates.

It was amply demonstrated in Chapter 5 that the presence of cyclic damage alters the viscoelastic response of uni- and multidirectional laminates. It results in horizontal (rate) and vertical (magnitude) shifts in the frequency and creep response, and changes the apparent transition temperature. Different damage modes may also obliterate or overshadow some of physical processes. In addition, damage always changes the stress distribution at the local level. In the most general terms, the effects of cyclic damage on the viscoelastic behavior of Radel X/T50-42 laminates seem to fall under two main categories. First, the elastic response changes due to the initiation and growth of cracks, delaminations, matrix-fiber debonding, and all other damage modes. Second, stress redistribution in regions adjacent to damaged areas and among plies promote local damage-enhanced deformation. Damage to the fiber-matrix interphase by itself could explain the temperature shift of the loss modulus peak, as demonstrated for graphite/epoxy by Theocaris [177].

Both mechanisms are affected differently by temperature. Figures 7.5.a and b reveal contradictory behavior. At elevated temperatures (close to, but below T_g), the transient response of the damaged 90° laminate is much smaller than that of the virgin specimen. The situation is reversed at room temperature. This behavior is confirmed by the shift in loss modulus temperature peak, the creep compliance master curves shown in Figure 5.46, and the corresponding shift factors.

The combination of these mechanisms and their temperature dependence may lead to apparent nonlinear behavior, time dependent activation energy, and the creation of permanent deformation. In the next sections the implications of time dependent behavior during fatigue loading are discussed.

7.2 Fatigue Characterization

The basic fatigue characterization process begins at the lamina level. It encompasses all aspects of the cyclic performance as measured in unidirectional or basic sublaminates. In this study, the fatigue behavior of 0° and 90° unidirectional laminates was investigated. Unfortunately the information obtained during cyclic loading of unidirectional laminates is limited. The damage and fracture modes bear only partial resemblance to those present when the

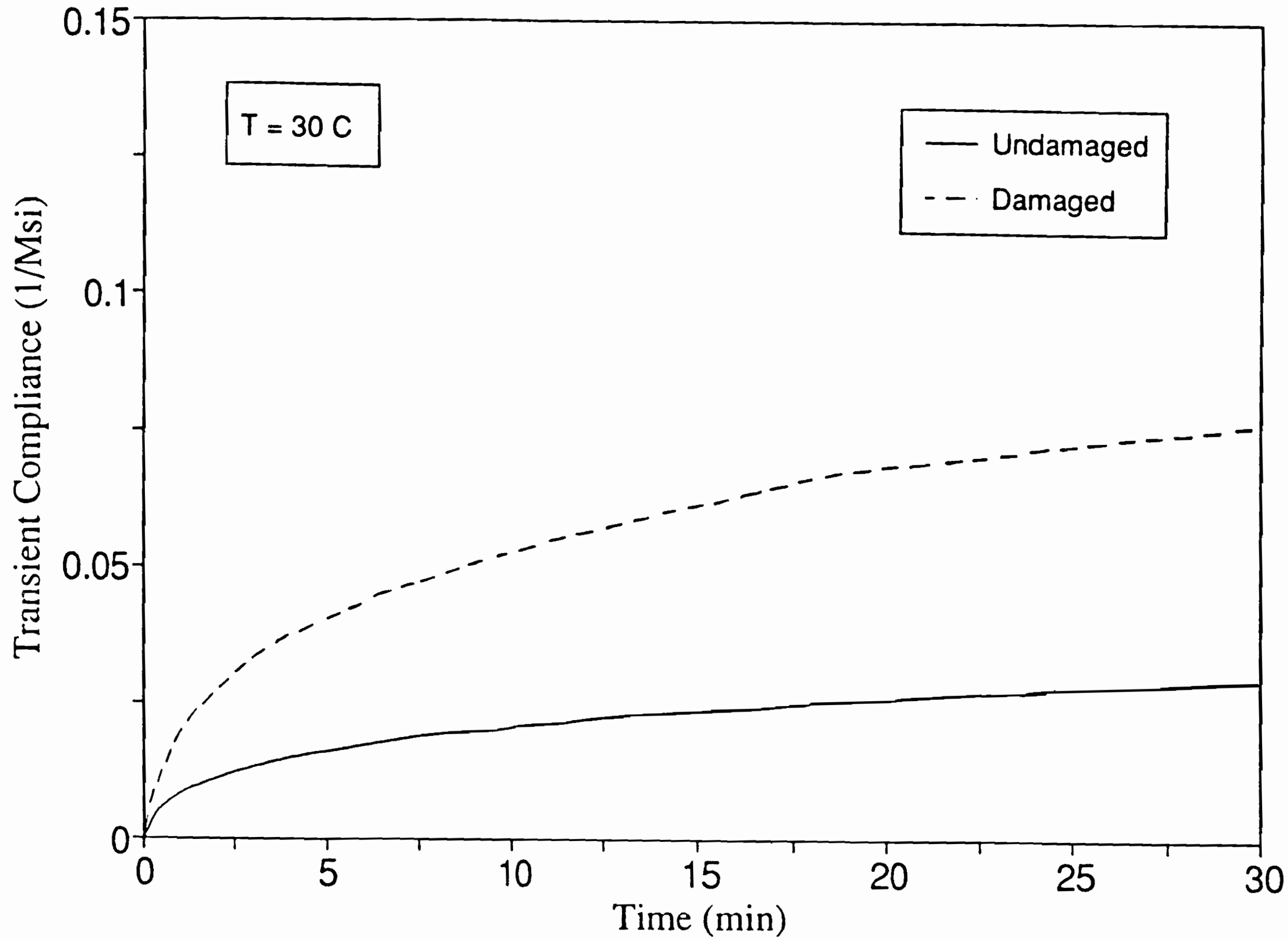

Figure 7.5.a **Creep compliance of 90° coupon at 30°C**

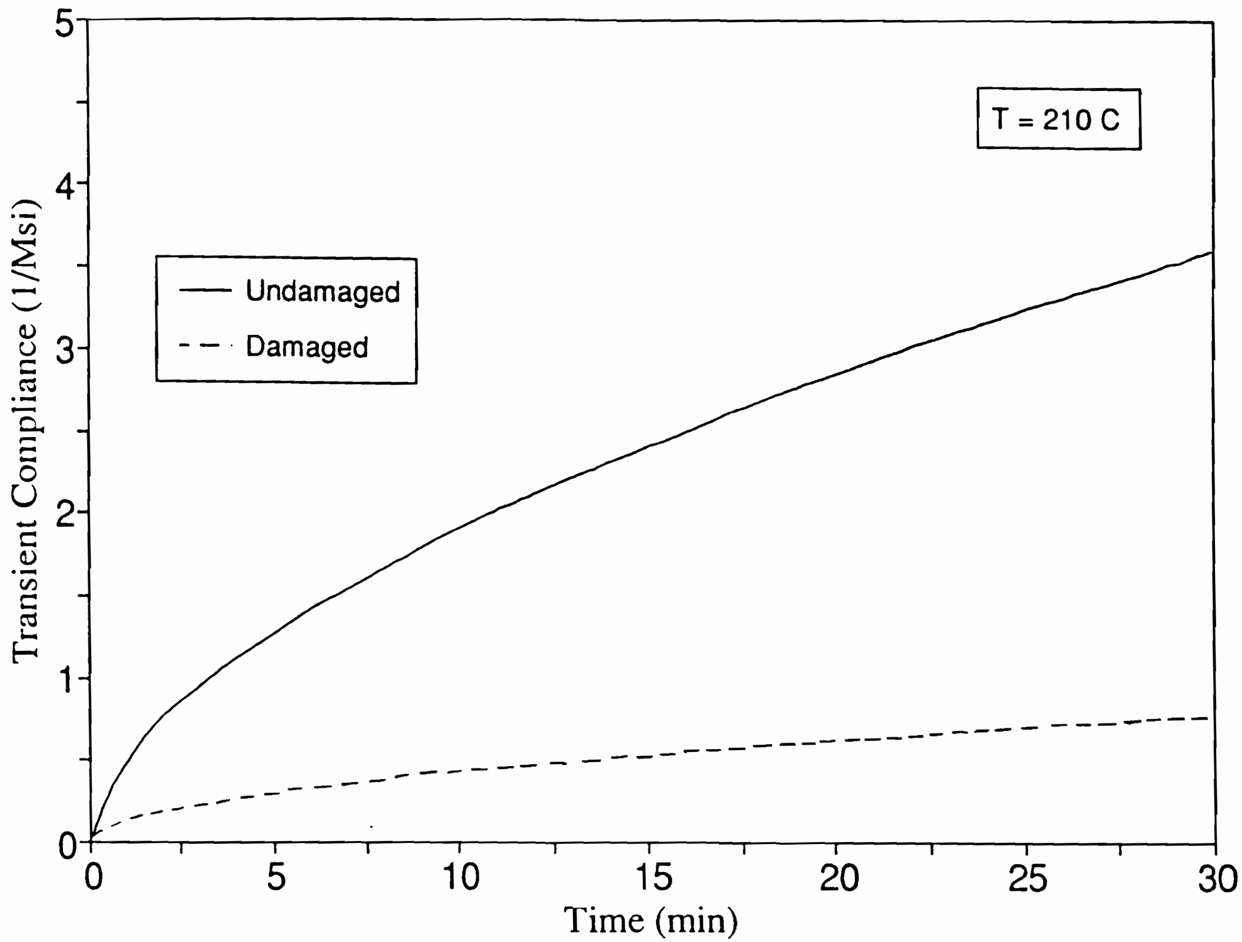

Figure 7.5.b Creep compliance of 90° coupon at 210°C

same plies are part of a multiaxial laminate. The stiffness and strength reduction, temperature profiles and other characterization data suggest very small changes during fatigue. Failure is abrupt with a relatively large scatter of fatigue life data. The usefulness of these data in a cyclic performance predictive code depends largely on the amount of details known (experimentally and/or analytically) about the damage modes that occur in the actual laminate, their impact on ply properties, and the ability to evaluate multiaxial stress situations at the **local** level.

The observed damage sequence during fatigue loading of cross ply laminates consists of the following stages. When appropriate, reference is made to differences attributable to the stress level.

7.2.1 Characteristic Damage State

Matrix cracking is the first damage mode to appear. From the acoustic scan images it is evident that a crack array develops in the 90° plies. Cracks grow from the edges of the laminate across the width of the coupons. At first the cracks appear at random locations but soon they multiply and create a regular spacing, as predicted by the Shear Lag model. The measured average spacing is 0.063", which agrees reasonably well with the analytical prediction of 0.06". When the transverse crack array reaches this saturation spacing, the laminate achieves its Characteristic Damage State (CDS).

Simultaneously, cracks develop in the 0° plies. These cracks span the length of the gripped section and do not develop into a regular array, nor is it clear whether it reaches saturation. The experimentally measured spacing varies between 0.035" and 0.065" for specimens examined shortly after the CDS is achieved in the transverse plies and at 20 times that number of cycles. The Shear Lag model predicts 0.055" saturation spacing, but again this model is not particularly designed to handle this situation and could only serve as a guideline.

Local delaminations appear in the [0/90] interfaces at the intersection of longitudinal and transverse cracks. The delaminations first grow across the width of the specimen along transverse cracks. Then, they extend in the load direction by an amount that is inversely proportional to the stress level. No delaminations were observed to grow from the longitudinal cracks in a direction transverse to the load, and none were observed to originate at the edges.

The development of matrix cracks is accompanied by changes in the laminate stiffness. The apparent stiffness of the cracked laminae, as well as the strain concentration at the crack tip, can be predicted using the same model (Equations 3.3.8 and 3.3.10). Accordingly, the stiffness should decrease and reach a stable value. The predicted decrease is 10.5% of the undamaged laminate stiffness, and it is independent of stress level. Strength is also related to the capability of the cracked plies to carry load. As presented in Chapters 3, 5 and 6, the changes in crack spacing also change the local strain concentration. The reduction in strength depends on stress level and the extent of viscoelastic deformation and delaminations.

The surface temperature of the specimens rises rapidly upon loading and then reaches a steady state directly proportional to the stress level. The temperature rise is small, and for these laminates, has little effect on their cyclic performance.

7.2.2 Critical Element Degradation

The second stage begins once the CDS is achieved and continues until significant fiber fracture in the 0° plies leads to additional degradation of stiffness and strength. The duration of this stage depends on the fatigue properties of the 0° plies and the constraint applied by the neighboring plies. It is short for high stress levels and over 1 million cycles for S=0.55.

During this stage there is very little change in temperature, stiffness or residual strength. No additional matrix cracking is encountered but the delaminations progress in the load direction. For the lower stress levels, the [0/90] interfaces debond extensively. For the higher stress levels, delaminations are more limited. Gradually, fibers in the outer plies may break loose next to the coupon edges, or a small area between longitudinal splits may debond from the inner plies.

The most significant event in this stage is the continuous redistribution of stress among the plies due to viscoelastic effects. The global deformation increases monotonically as predicted by Equation 3.3.34, and its magnitude depends on the pertinent stress level.

7.2.3 Final Fracture

The events leading to final fracture are not completely understood and have not been introduced into the analytical treatment yet. This stage is very short, with rapid degradation in strength and stiffness, increased global deformation and sometimes accompanied by a sharp temperature peak.

Under tension, the final fracture is controlled by the critical element - the 0° plies. The failure mode is characteristic of the stress level (Figure 5.22). At high stress levels (S>0.60) the failure resembles the quasi static fracture mode. The coupons break in two sections with a distinct crack across the width of the specimens, little delamination is noticeable and the fibers break in a straight fashion. A different fatigue failure mode is present at lower stress stress levels (S≤0.60). The 0° plies appear to be significantly delaminated from the 6-ply core of 90° layers and this core disintegrates into several small pieces along the gripped section. The 0° plies fail in a broom fashion, similar to the fatigue failure of 0° unidirectional specimens.

Residual strength tests performed after cycling at the lower stress levels (S≤0.60) indicate that there is a transition in failure mode not only dependent on stress level but also on life fraction. At small life fractions, failure resembles the quasi static fracture mode of undamaged specimens, with very little strength degradation. After the CDS is achieved and at high life fractions, fatigue-type fracture is predominant, and significant strength reduction was measured.

The sequence of events described above summarizes the damage development observations made during this investigation. Though the actual life fraction spent at each stage varies with stress level, the order is maintained for all the tested stress levels.

7.3 Fatigue, Analytical - Experimental Comparison

The fatigue performance of cross ply laminates has been measured and modeled in terms of global deformation, remaining stiffness, residual strength, temperature profiles and life.

Figures 7.6 through 7.8 show a comparison of the measured and predicted global transient deformation as a function of cycles for S=0.65, 0.60 and 0.55. The transient deformation is the amount of additional strain measured at maximum cyclic load in excess of the initial response. By itself it could be considered a failure criterion since many components will not perform their functions once the total deformation exceeds some predetermined limit. The prediction of cyclic global deformation is a unique feature of this model. Excellent agreement has been found between the CYPERS predictions and the measured values.

Figures 7.9 through 7.11 present the normalized stiffness vs. cycles for the same stress levels. It has already been shown in

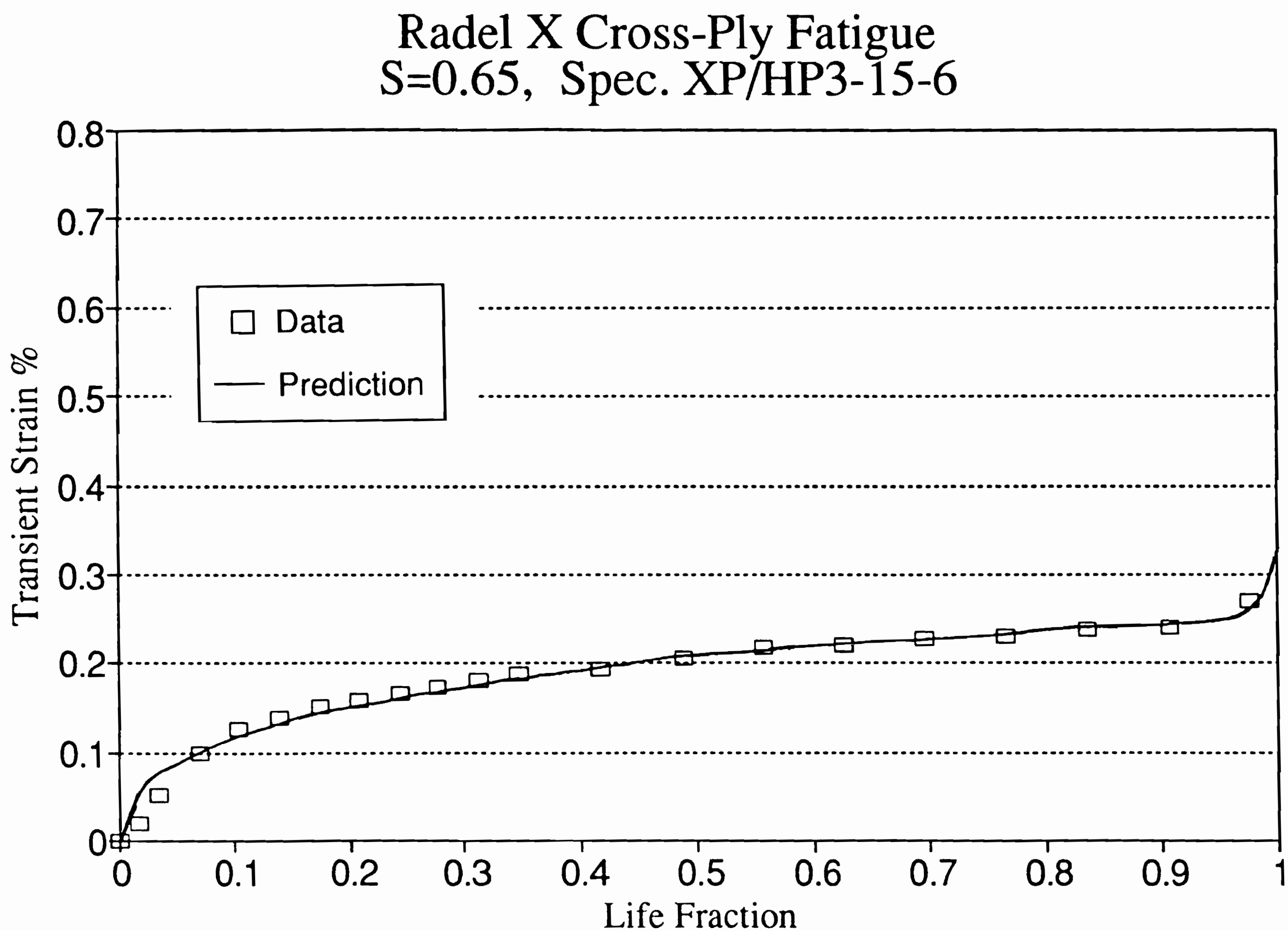

Figure 7.6 Global deformation vs. cycles, S=0.65, cross ply laminate

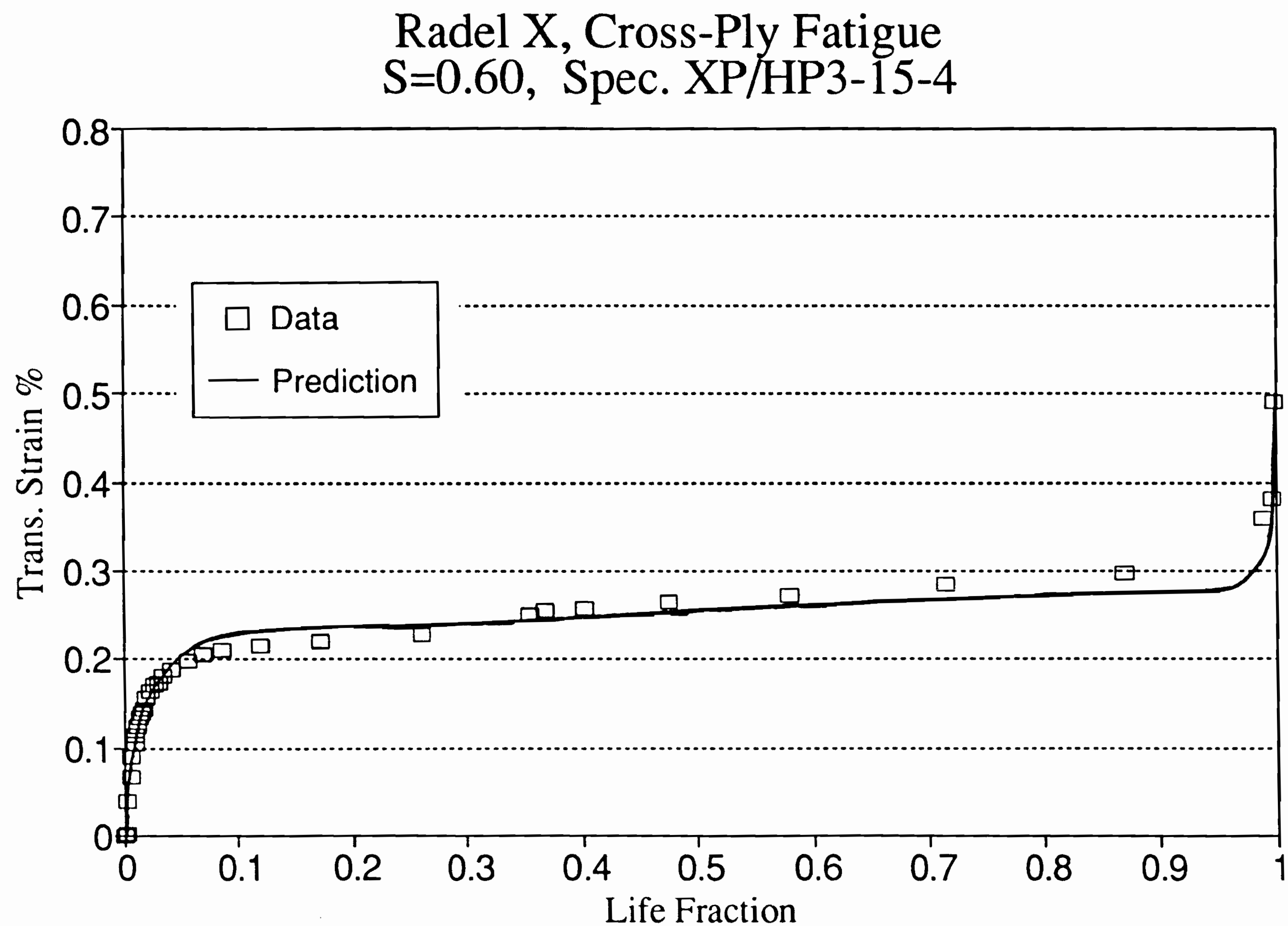

Figure 7.7 Global deformation vs. cycles, S=0.60, cross ply laminate

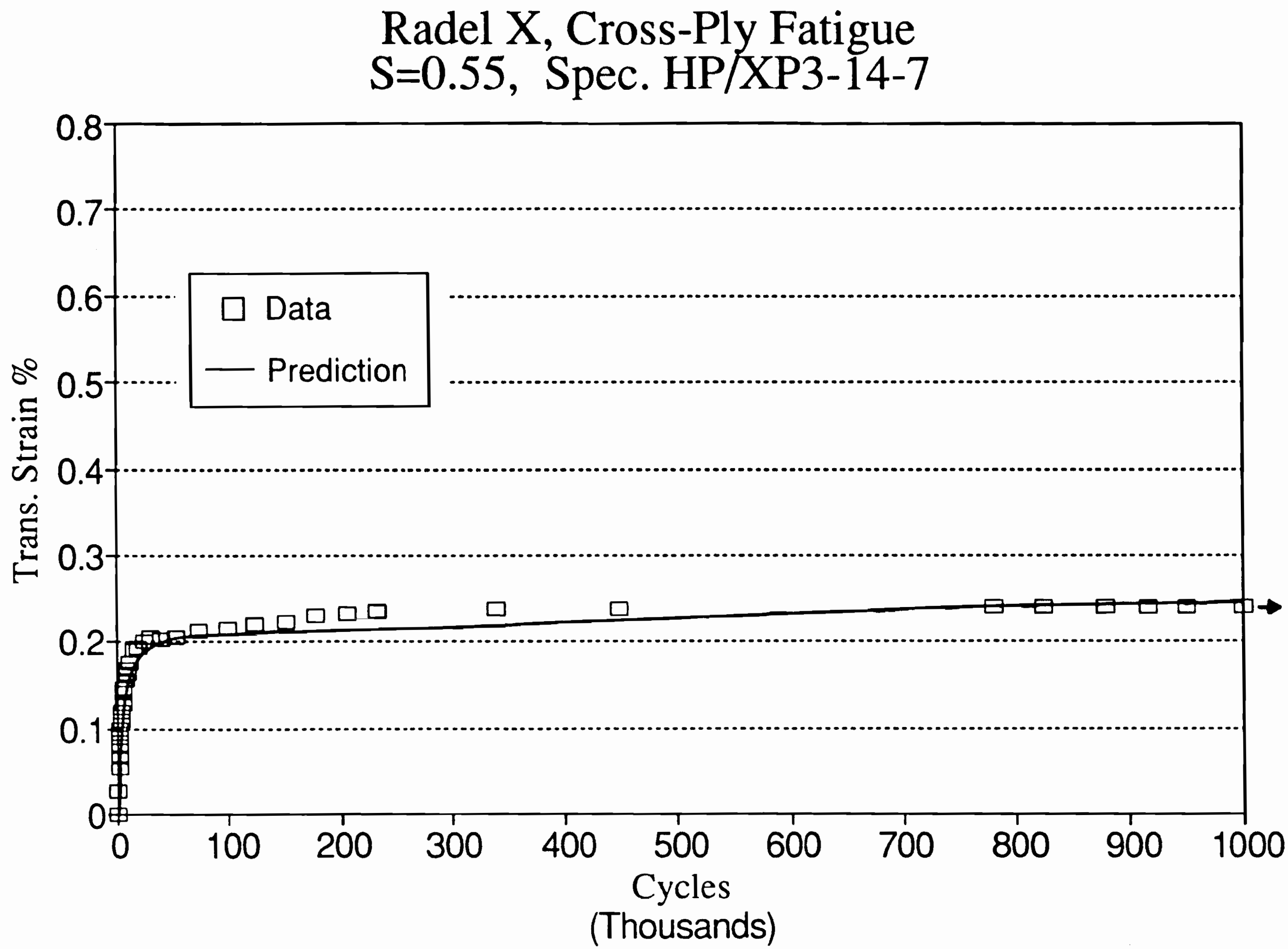

Figure 7.8 Global deformation vs. cycles, S=0.55, cross ply laminate

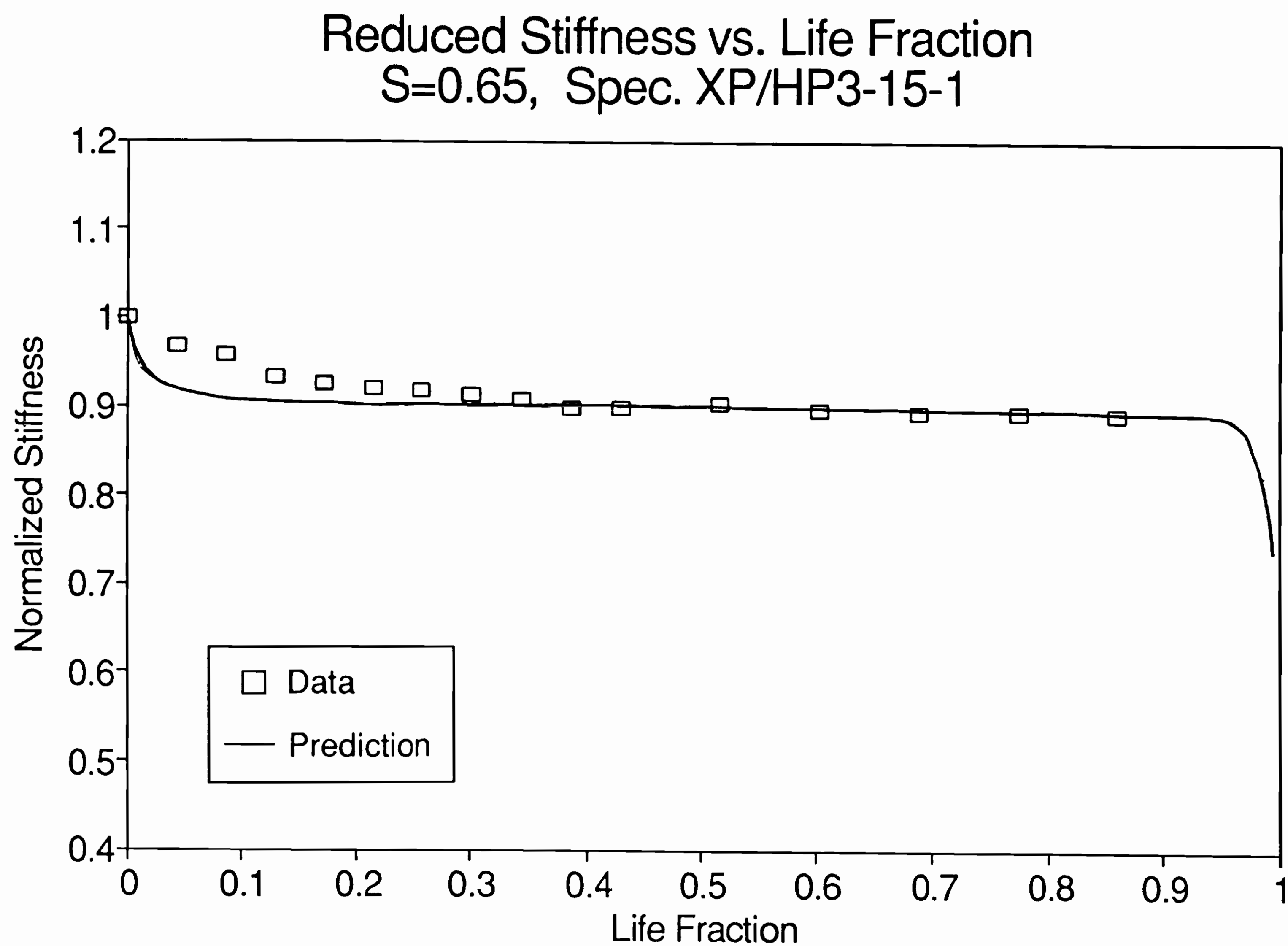

Figure 7.9 Normalized stiffness vs. cycles, S=0.65, cross ply laminate

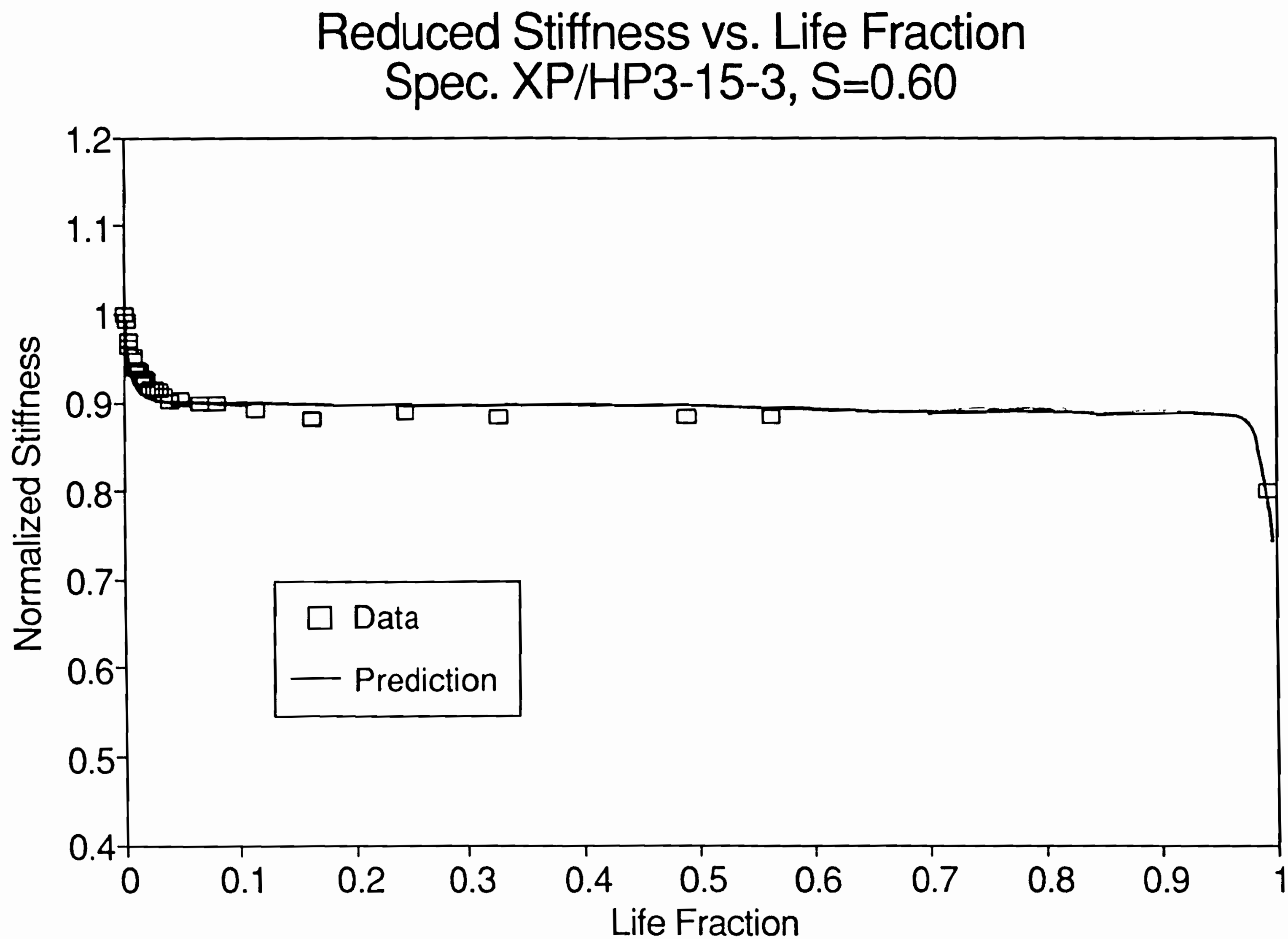

Figure 7.10 Normalized stiffness vs. cycles, S=0.60, cross ply laminate

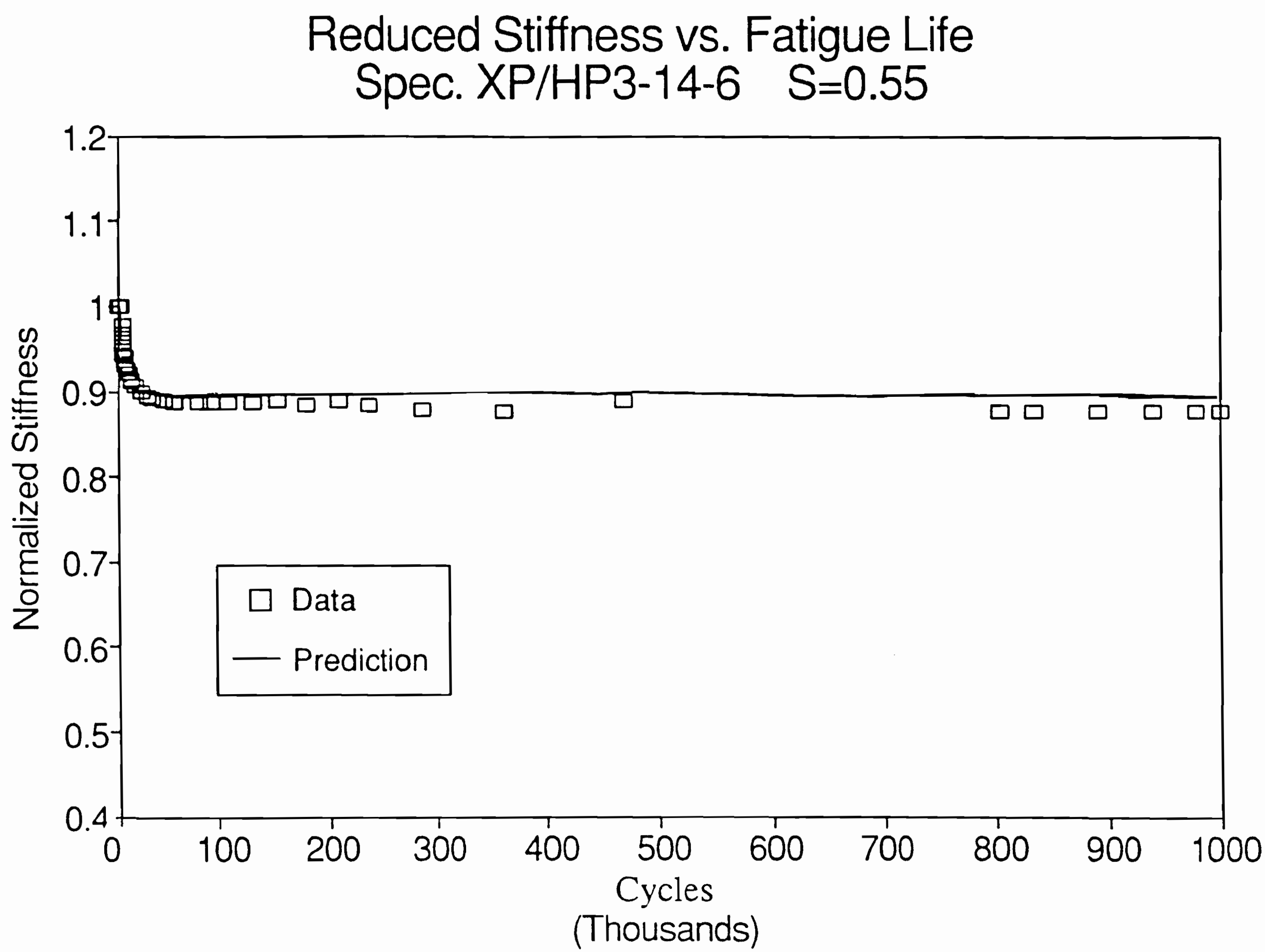

Figure 7.11 Normalized stiffness vs. cycles, S=0.55, cross ply laminate

Figures 5.23.a to c that stiffness reduction due to matrix cracking by itself accounts for only 40% of the transient deformation. In this respect, it is encouraging that very good agreement has been found with the measured data. It is significant that the model seems to be able to discern between damage-induced (related to stiffness degradation), viscoelastic and anelastic deformation.

The global deformation and remaining stiffness curves exhibit similar (albeit inverse in nature) behavior. Three distinct regimes could be defined, matching the three stages in the damage evolution described in the previous section. A rapid decrease in stiffness at first, then a period of little or no change and last, a rapid reduction (which can seldom be extensively measured) leading to final failure.

The first stage involves matrix cracking until the CDS is reached. Using a simplistic approach, the duration of this process could be evaluated by solving Equation 3.3.7 for the CDS crack spacing,

$$N_{cds} = \left\{ \left[\frac{E_2(0)*(1+k90)*(1+\ \beta(90)\lambda_{cds}h90)}{E_1 + E_2(0)*k90*(1+\beta(90)\lambda_{cds}h90)} \right] \frac{\sigma_{max}}{YT} \right\}^{1/b90} \qquad (7.3.1)$$

where N_{cds} is the number of cycles to achieve the CDS and all other parameters have been defined in Chapters 3 and 5. The number of cycles to achieve the CDS can also be determined from the numerical procedure with ease, by choosing the point where the 90° ply cracking reaches the saturation spacing. In this case, the viscoelastic redistribution of stresses is taken into account. Examining Figures 7.9 through 7.11 it is hard to determine the exact point where the CDS is achieved, only an estimate can be made. Table 7.1 shows the number of cycles to achieve CDS according to Equation 7.3.1, the CYPERS code and the estimated experimental values.

In general, Equation 7.3.1 seems to predict shorter times than the CYPERS code. In turn, the predictions of Equation 7.3.1 underestimate the experimental values, while the CYPERS code is in better agreement. Both analytical solutions are derived using the same Shear Lag analysis results and the same set of data regarding the fatigue behavior of unidirectional laminae. The inference is that viscoelastic stress redistribution slows down the process of matrix cracking in the 90° plies by shedding load to the 0° plies.

In essence, the second stage comprises the fatigue cycling of the 0° plies. Theoretically, the remaining fatigue life of the laminate could be determined from the 0° ply stresses at the moment the CDS is achieved. But the delaminations that grow at the [0/90] interfaces and the viscoelastic stress redistribution change the state of stress continuously. The viscoelastic stress relaxation in the off-axis plies tends to shed load to the critical element and shorten the remaining life of the laminate.

The residual strengths predicted by the CYPERS code for S=0.55, 0.60, 0.65 and 0.70 are presented in Figures 7.12 through 7.15

Table 7.1 Number of cycles to achieve the CDS

Stress Level	Equation 7.3.1	CYPERS code	Experimental range
0.70	845	874	N/A
0.65	1760	1871	2500 - 3500
0.60	3885	4956	4500 - 6000
0.55	9192	10845	9000 - 12000

respectively. In these figures the predicted fatigue life is the coincidence of the residual strength value and the maximum applied load. The experimentally measured fatigue life range is indicated by a horizontal bar. Residual strength measurements (empty squares) for S=0.55 and 0.60 appear in Figures 7.12 and 7.13. Life predictions and the available data are also presented in Table 7.2.

The predictions of fatigue life are in good agreement with the measured values, which vary over three and a half decades for a range of only 20% of the UTS in the maximum cyclic load. Neglecting additional damage modes, such as delaminations and fiber fracture can partially contribute to the deviations. These damage modes are more extensive at the lower stress levels. The agreement with the residual strength data is satisfactory for S=0.60 but less so for S=0.55 which has a much larger degradation than anticipated at 1 million cycles. The uncertainty of the actual fatigue life of these specimens adds to the inaccuracy. These specimens are extensively delaminated, a damage mode not accounted for in this model but that significantly affects strength.

All residual strength curves exhibit similar behavior. In the first stage, matrix cracking and stiffness degradation are accompanied by a matching reduction in strength. Once the CDS is achieved, strength is relatively constant with only a small reduction attributable to the strength degradation of the 0° plies. The last stage precedes failure. Strength reduction is rapid and occurs over a small number of cycles. The length of each stage is dependent on

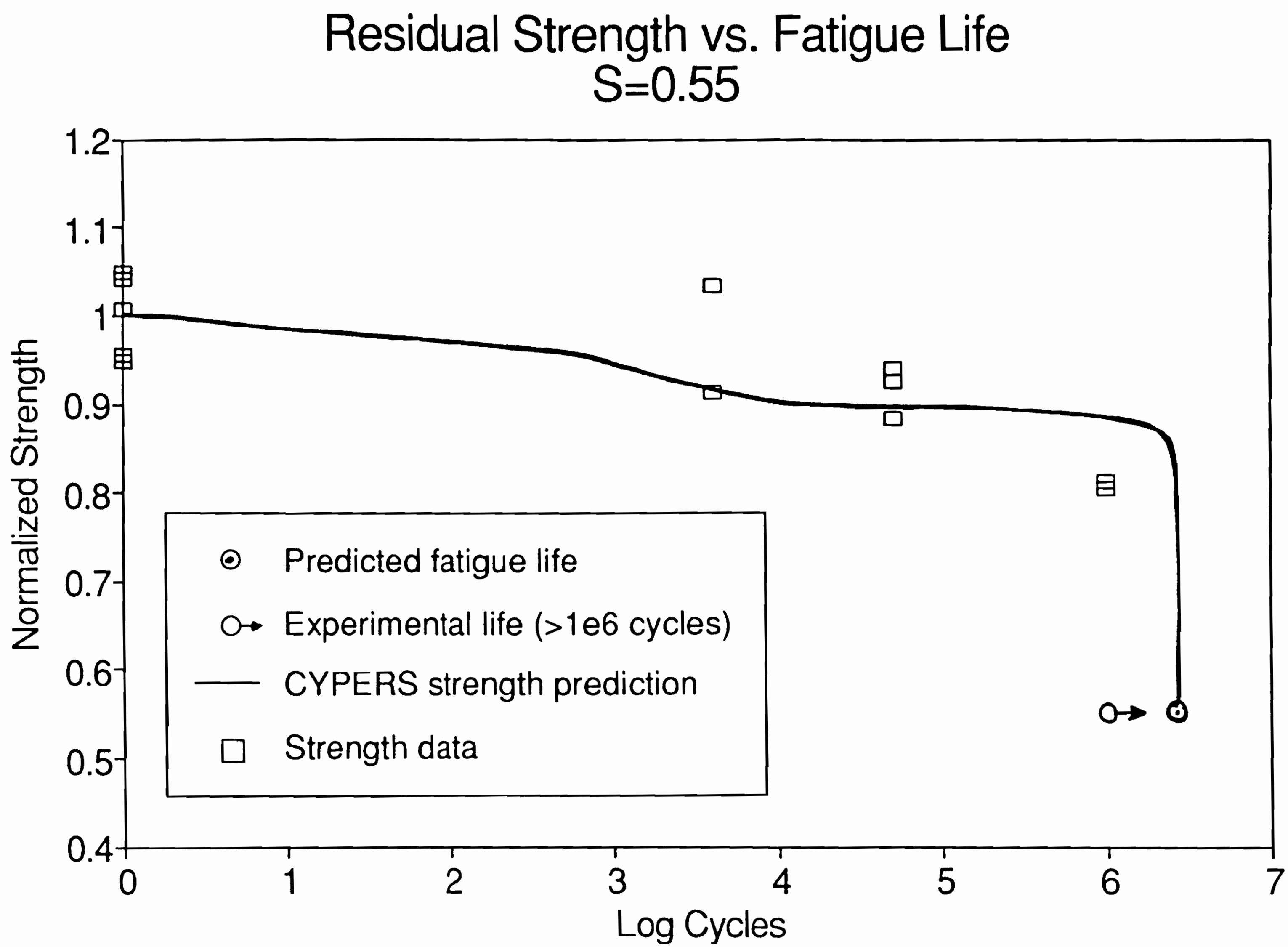

Figure 7.12 Residual strength vs cycles, S=0.55, cross ply laminate

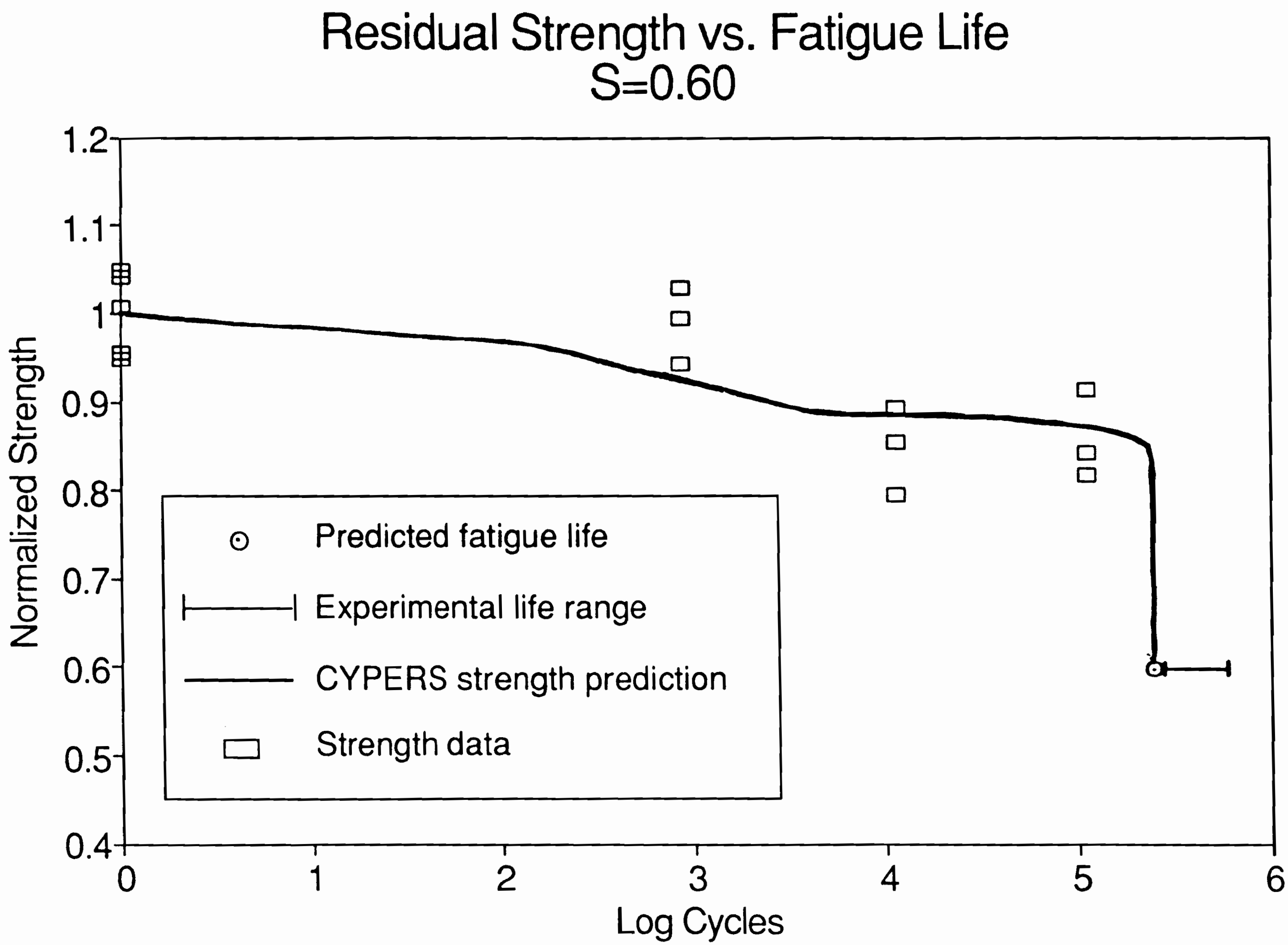

Figure 7.13 Residual strength vs cycles, S=0.60, cross ply laminate

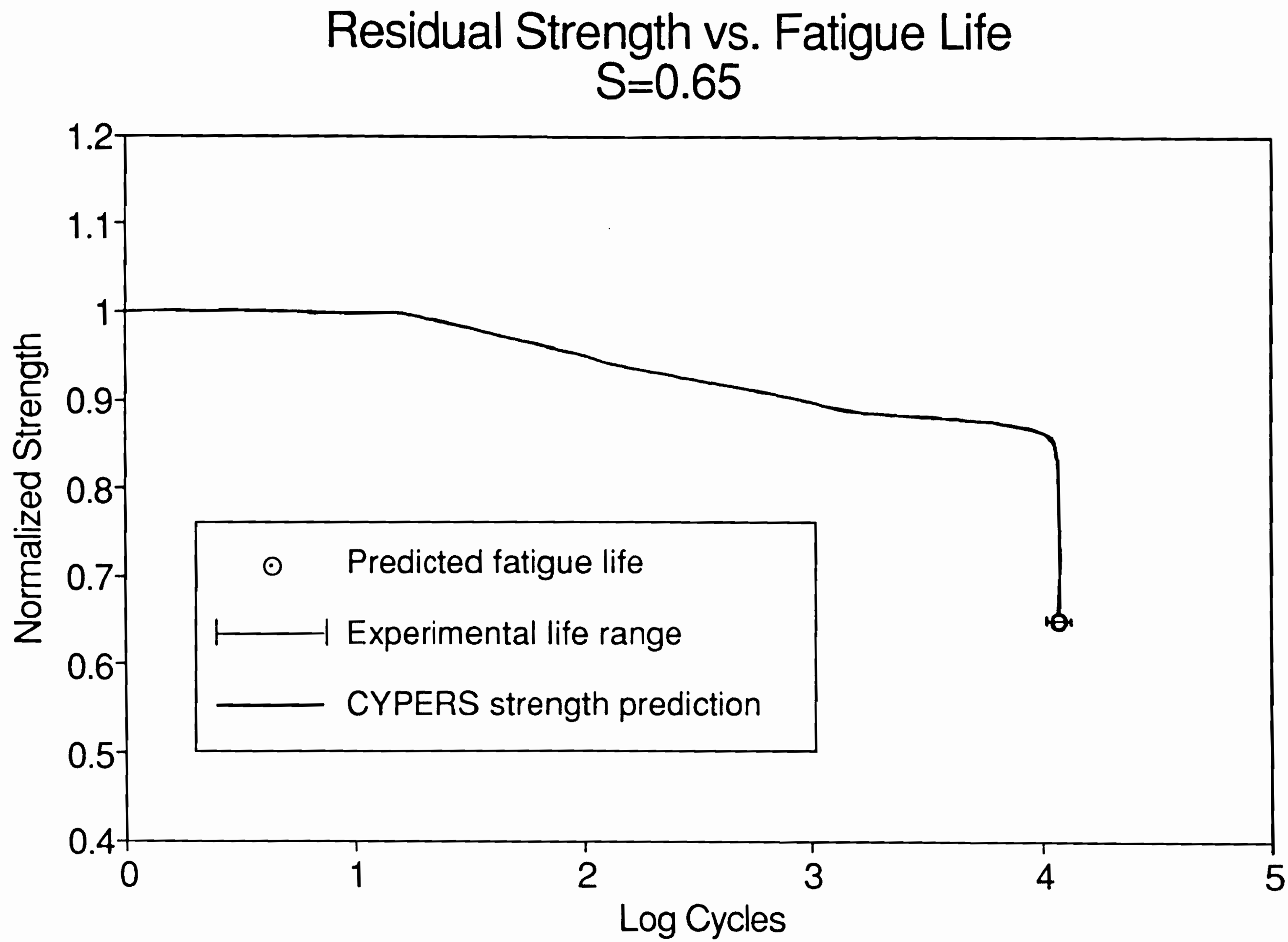

Figure 7.14 Residual strength vs cycles, S=0.65, cross ply laminate

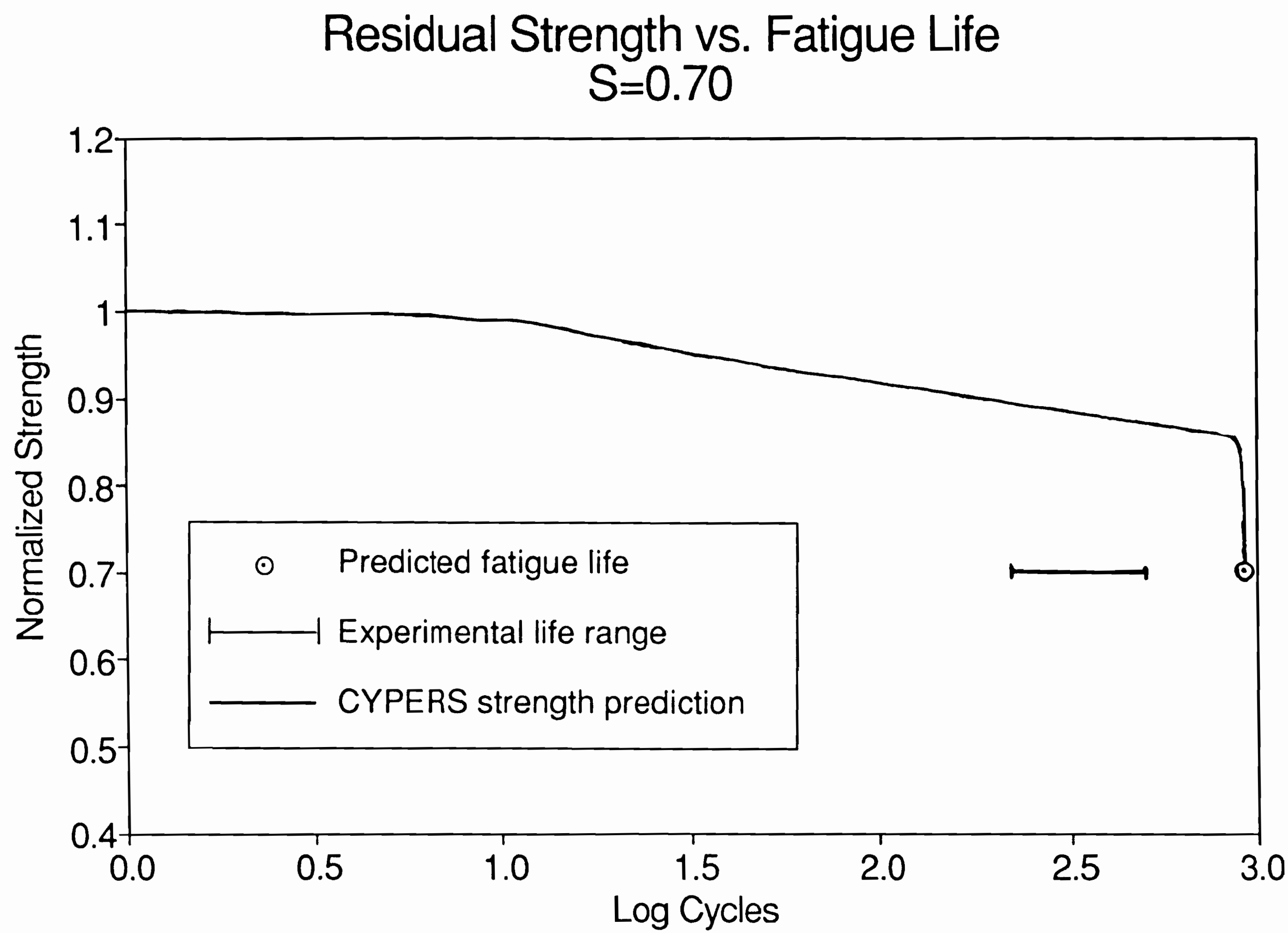

Figure 7.15 Residual strength vs cycles, S=0.70, cross ply laminate

Table 7.2 Fatigue life (cycles) of cross ply laminates

Stress Level	Fatigue Life Data Range	CYPERS code prediction
0.55	$> 10^6$	4.06×10^6
0.60	287,520 - 618,470	257,280
0.65	10800 - 14340	12960
0.70	230 - 520	960

stress level. For the higher stress level (S=0.7), the transfer of load due to matrix cracking in the 90° plies is enough to reduce life to a few cycles after the CDS is achieved. For the lower stress levels (S≤0.60), most of the fatigue life is spent on the second stage.

7.4 Damorheology

The large amount of evidence collected during this experimental program indicates that indeed there are damage induced changes in the global viscoelastic behavior of uni- and multiaxial laminates and that time dependent effects alter the process of fatigue damage evolution (only matrix cracking was modeled). Damorheological effects are evident in the temperature, frequency, and long term response of fiber reinforced composite laminates. The physical phenomenon named damorheology provides a basis for some of the intriguing behavior observed in composite materials by many investigators.

The damage mechanisms that affect global viscoelastic behavior of polymeric based composites are threefold: damage to the organic matrix, damage to the fiber/matrix interface/interphase, and macroscopic structural damage in the from of matrix cracking, crazing, delaminations, etc. The physical scale of each mechanism varies from the molecular level to the laminate level, affecting a different range of molecular motions and their effect on the deformation process is characteristic of the material system.

Damage continuously changes load redistribution paths among plies and the constraint imposed by the fibers on the matrix. On the other hand, the viscoelastic nature of the matrix (in other cases the fibers may be viscoelastic as well) introduces a new factor to stress redistribution within the laminate. In the case of cross ply laminates, such as the ones tested in this program, the evidence suggests that viscoelastic stress redistribution affects cyclic performance in two major ways. Specifically, relief of local stress concentrations and stress redistribution among plies. At an early stage, time dependent behavior seems to slow the process of matrix cracking by relieving the stress concentration at the tip of the cracked plies. After the CDS is attained, load is redistributed to the critical element from the off-axis plies. This has the effect of reducing the remaining life of the laminate.

Although the small temperature rise measured in cross ply laminates does not affect ply properties significantly, it is possible that other laminate configurations or material systems could dissipate large amounts of heat. The resulting change in temperature may alter the fatigue behavior radically. This is especially true in the vicinity of stress raisors such as holes and notches, where local damorheological effects (for example, shifts in the frequency response of the loss compliance) could explain otherwise puzzling behavior.

The higher toughness of fiber reinforced thermoplastic polymers as measured in quasi static tests does not always translate into better long term performance [54,55,56,57]. In general, thermoplastic composites subjected to fatigue loading have fewer matrix cracks and less delaminations adjacent to notches and/or cracks than thermoset composites. The higher stress concentrations usually result in shorter fatigue lives and different damage modes.

Damorheological effects may alter the fatigue performance of composite laminates in a variety of ways,

- changing the elastic properties of the constituents
- reducing the strength of the constituents
- accelerating time dependent, thermally activated processes
- changing the extent of different fatigue damage modes
- promoting additional damage mechanisms characteristic of creep loading

In light of this discussion is it is worthwhile considering the possible consequences of other types of loading. The investigation of creep-fatigue interaction in composite materials (Chapter 2) has revealed interesting facts. In many cases investigators have attributed unexpected fatigue behavior to the viscoelastic matrix. Some of this phenomena could be analytically derived in terms of the proposed model.

Consider the effect of intermittent periods of unloading. These intervals result in the relaxation of the stresses adjacent to stress concentration loci (notches or cyclic damage) and cooling of the specimen to ambient temperature. Both mechanisms tend to increase fatigue life. If, during the interval, the specimen sustains a constant load, then creep deformation would also reduce the stress concentration in the vicinity of notches (supported by the experiments of Sun and Chim [163]).

It is useful to examine the ply stresses and temperature profiles derived from the solution of the PAM model for these situations. For the cross ply laminate investigated, the global strain response to constant load is given by Equation 3.3.25 where the constants are defined in Equations 3.3.29 through 3.3.31. Using this strain as the input, the constitutive relationship for the 5 parameter PAM model (Equation 3.2.14) of the 90° plies is now,

$$\sigma + pa1\ \dot{\sigma} + pa2\ \ddot{\sigma} = \sigma_0{*}qa0/ql0 + qa2{*}\left(C1{*}r^2{*}\exp(rt)+C2{*}s^2{*}\exp(st)\right) +$$

$$qa1{*}\left(C1{*}r{*}\exp(rt)+C2{*}s{*}\exp(st)\right)+qa0{*}\left(C1{*}\exp(rt)+C2{*}\exp(st)\right) \quad (7.4.1)$$

where σ_0 is the applied load and σ represents the stress in the 90° plies in the direction of the applied load. The other coefficients have been defined in Chapter 3. Solving for the time dependent stresses and after some tedious algebra,

$$\sigma = M1\ \exp((m1{*}t) + M2\ \exp(m2{*}t)$$

$$+ M3\ \exp(r{*}t) + M4\ \exp(s{*}t) + \sigma_0 qa0/ql0 \qquad (7.4.2)$$

where the C1, C2 and r,s are the coefficients and roots of the laminate's creep response and,

$$m1,\ m2 = \frac{-pa1 \pm \sqrt{pa1^2 - 4*pa2}}{2 * pa2} \tag{7.4.3}$$

$$M3 = \frac{C1*(\ qa0 + r*qa1 + r^2*qa2\ )}{1 + r*pa1 + r^2*pa2} \tag{7.4.4}$$

and $$M4 = \frac{C2*(\ qa0 + s*qa1 + s^2*qa2\ )}{1 + s*pa1 + s^2*pa2} \tag{7.4.5}$$

To find M1 and M2 apply the boundary conditions,

$\sigma(t=0) = \sigma(0)$ as evaluated by CLT analysis

and the initial stress relaxation rate - φ - may be approximated by,

$$\dot{\sigma}(t=0) = \varphi = \frac{(\ C1 + C2 + \sigma_0/ql0\ )\ E_1^{\ 2}}{E_0 * E_1 + E_0 * E_2 + E_1 * E_2} \times$$

$$\times \left[\frac{-E_2 * \mu_2 *(\ E_0 + E_1) - E_1 * \mu_1 *(\ E_0 + E_2)}{\mu_1 * \mu_2} \right] \tag{7.4.6}$$

where E_i and μ_i are the coefficients of the 90° plies as defined in

Chapter 3. Then,

$$M2 = \frac{1}{m2\text{-}m1}\left(\varphi - \sigma(0)\ m1 + \sigma_0(qa0/ql0)\ m1 + M3(m1\text{-}r) + M4(m1\text{-}s)\right) \quad (7.4.7)$$

and $$M1 = \sigma(0) - \sigma_0(qa0/ql0) - M3 - M4 - M2 \quad (7.4.8)$$

Making use of the properties measured in Chapter 5, the time dependent stress relaxation in the off-axis is plotted in Figure 7.16 for the case of the cross ply laminate. Figure 7.16 represents the situation where, under constant load, no additional damage occurs. In reality the crack array may continue to develop. The stresses in the cracked plies are reduced by the viscoelastic stress redistribution. Accordingly, the stress concentration at the crack tips is reduced during intervals of constant loading, increasing fatigue life. Periods of unloading are a particular case, $\sigma_0 = 0$. The strain input is given by the solution to the creep recovery of the cross ply laminate as shown in Figure 7.4. In this case only the residual stresses relax.

The second mechanism by which intervals of constant loading or unloading affect fatigue life is by cooling the specimen. For some cases the cooling effect could have a much larger influence than viscoelastic stress redistribution. Taking advantage of the capabilities of the PAM model it is possible to predict the magnitude and rate of this effect. Defining $T_d(x,t\text{-}t^*)$ as the temperature

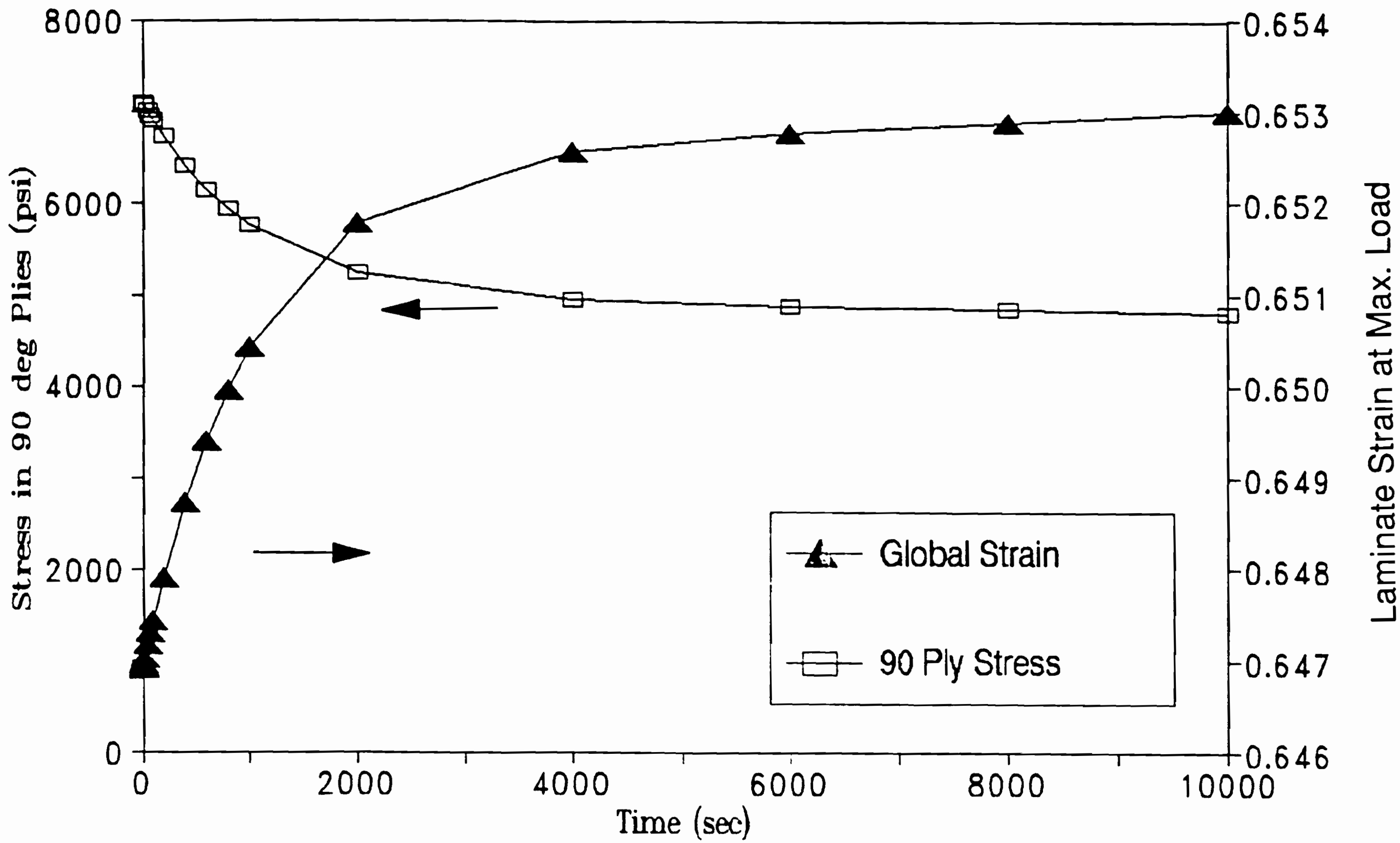

Figure 7.16 Stress relaxation in the 90° plies and global strain during unloading intervals

differential above ambient conditions after cyclic loading for a time t^*, the time dependent temperature distribution during these intervals is found by solving the transient heat transfer equation,

$$\frac{\partial^2 T_d}{\partial x^2} - \frac{h\,R}{k''} T_d = \frac{\partial\, T_d}{\partial\, t} \qquad (7.4.9)$$

where the coefficients have been defined in Chapter 3 and the boundary conditions are,

$T_d(x,\infty) = 0$ the temperature returns to ambient conditions as $t \to \infty$

$T_d(b,t) = 0$ at the grips the temperature is constant

$T_{d,x}(0,t) = 0$ the temperature gradient is 0 at x=0.

$T_d(x,0) = T_d(x,t^*)$ which is the steady state temperature distribution at the time that the cyclic loading was interrupted, given by Equation 3.5.18 for $t \to \infty$.

The solution to the transient temperature distribution is,

$$T_d\,(x,t>t^*) = T_d(x,t^*) \exp\left(- \frac{\check{W}}{k''\; T_d(x,t^*)} (t-t^*)\right) \qquad (7.4.10)$$

Figure 7.17 shows the temperature profiles of three different points along a specimen during unloading or constant loading intervals. It is evident that the loci that heat up the most (due to local stress concentration or any other reason) cool down faster. Cooling during unloading or constant load intervals retards fatigue

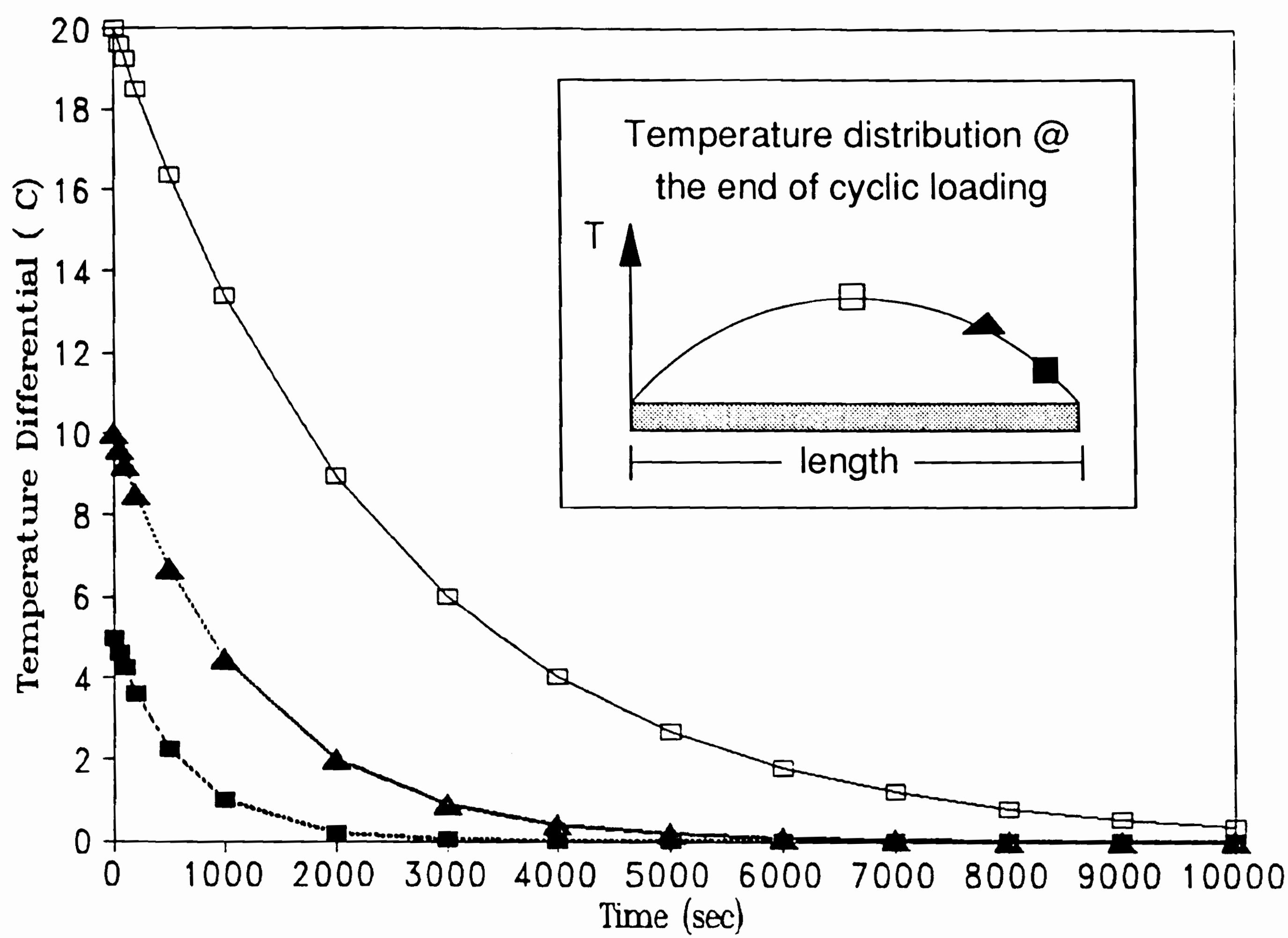

Figure 7.17 Temperature profiles during unloading intervals

damage [89, 163] and increase fatigue life.

A somewhat similar effect is accomplished when low frequency cyclic loading precedes high frequency cycling in notched laminates. At low frequencies, the viscoelastic nature of the material is dominant allowing for stress relaxation and creep deformation that reduces the local stress concentration, thus increasing the fatigue life at the higher frequency. In turn it can be argued that at low frequencies, creep phenomena dominates the damage evolution whereas at high frequencies, life is determined by the development of cyclic damage [161]. Thus, it is expected that at low frequencies, fatigue life is inversely proportional to frequency and at high frequency life is directly proportional to frequency. This would lead to a frequency range with maximum fatigue life (for the same stress level) and the locus of this frequency maxima should be inversely proportional to the maximum applied cyclic stress.

Preliminary analytical results for dual frequency fatigue of cross ply laminates with an initial period of low frequency cycling indicate that these periods do increase the total number of cycles to failure. Consider the case of the cross ply laminate investigated in this program, which has a predicted fatigue life of approximately 257000 cycles at S=0.6 and 10 Hz. An initial period of 50000 cycles at 0.1 Hz would only increase the predicted fatigue life by 11000 cycles (4%), but 100000 low-frequency cycles would increase life by a total of 102000 cycles (40%). If the initial low frequency is 0.01 Hz, 10000 initial cycles would be enough to increase the total life by 8000 cycles. Initial loading at frequencies higher than 10 Hz reduce the total life by a small fraction only, indicating that the magnitude of this effect is "saturated" at frequencies over 10 Hz (for this set of PAM parameters). Although there is no data available from this experimental program to confirm many of the computer generated predictions, there is supporting data presented by Sun and Chim [163].

These and other damorheological effects are within the capabilities of the PAM model and the present CYPERS code. Further refinement and understanding of the role of all the physical processes taking place during fatigue loading could lead to substantial improvements in the modeling of time dependent laminate behavior. This code was developed as a subset of the MRLife family of codes [178]. Together with the detailed fatigue damage representation and sophisticated stress analysis already available in the MRLife codes developed at VPI&SU, this model could improve the prediction of the long term engineering performance of composite laminates.

8 Summary and Conclusions

The present investigation addressed the interaction mechanisms between time dependent material behavior and cyclic damage during fatigue loading of fiber reinforced composite laminates. Damorheology is a new term that has been coined to describe such physical behavior. Classical representations that isolate cyclic mechanical behavior (fatigue) and time dependent behavior (creep rupture) ignore the fundamental coupling of these effects, and many experimental observations escape the grasp of such theories.

The body of knowledge and understanding of fatigue of composites has been extended to include creep-fatigue interactions. This is particularly significant for thermoplastic matrix composites because of their inherent viscoelastic behavior. In this study the extent of the damorheological effect has been quantified, a model sensitive to all the relevant parameters has been formulated, and the concept of damorheology has been extended to other loading conditions.

The lamina has been chosen as the building block and a cross ply laminate configuration was the selected test case. The chosen material system is the Radel X/T65-42 thermoplastic composite by Amoco. The fatigue performance at the lamina level is represented by the dynamic stiffness, residual strength and fatigue life of unidirectional laminates. The time dependent behavior has been represented at the lamina level by modifying the Wilshire-Evans "θ Projection" model, developed for polycrystalline isotropic materials. The procedure combines mechanical (creep) and thermal (dynamic mechanical analysis) characterization techniques. The proposed Pseudo-Analog Mechanical (PAM) model provides a complete representation of the effects of temperature and stress on the viscoelastic response. It is only a tool that can be further refined and adapted to different material categories. Eventually, it should be replaced by a model based on micromechanics.

The experimental investigation of unidirectional (90°) and cross ply laminates revealed that indeed there are significant changes in the time dependent response of a laminate due to fatigue loading. In turn, the viscoelastic stress redistribution (at all physical scales) is responsible for the changes in the rate of damage evolution and varying extent of damage modes. Due to time and other constraints, the amount of experimental data collected in this respect is limited. There are no deterministic theories that correlate each damage mode with a specific variation in the viscoelastic response. In general, damorheological effects have been found to have significant impact on the failure mode and the long term performance of these laminates.

Employing the PAM model, time dependent constitutive relationships were derived for the laminate in the from of differential equations that may be solved for a variety of loading conditions. Applying classical lamination stress analysis together with the Shear Lag model, the damage evolution of cross ply laminates was evaluated. Master curves which correlate the apparent lamina stiffness and local stress concentration to the normalized crack spacing were presented.

Based on the laminae viscoelastic and fatigue characteristics, a cyclic performance simulation code - CYPERS - was developed. The code was designed to predict the long term performance of cross ply laminates subjected to cyclic loads. The numerical procedure assumes that for a certain interval (cycles or time) the state of stress and state of the material are constant and the constitutive equations derived from the PAM model hold true. At the end of each interval the effects of damage and temperature are taken into account and the material parameters are adjusted. The redistributed stresses are evaluated and the process continues until the residual strength of the laminate is degraded to the the level of the maximum applied load, at which point the laminate fails. The code could be easily extended to handle a variety of loading conditions and arbitrary laminates.

The analysis and/or accompanying code have produced satisfactory predictions of the response for a variety of situations,

1. Unidirectional 90° laminates:
   - Long term creep
   - Cyclic creep at low amplitude and low frequency
2. Cross ply laminates:
   - Short term creep
   - Creep recovery
   - Tension-tension fatigue (residual strength and life)

The model provides a complete laminate performance description. It includes dynamic stiffness, global deformation, complex moduli and compliance, temperature history, frequency response of the complex moduli, damage state, time dependent stress redistribution, residual strength and fatigue life.

The present analysis was also able to predict, in a qualitative way, the experimental findings of other investigators. The effects of periods of unloading, constant loading and initial low-frequency loading were considered. The measured behavior supports the predicted variations of ply stresses and temperature profiles.

These and other damorheological effects are within the capabilities of the PAM model and the present CYPERS code. Further refinement and understanding of the role of all the physical processes (particular to the material system constituents) taking place during fatigue loading could lead to substantial improvements in the modeling of time dependent laminate behavior. This code was put together as a subset of the MRLife family of codes developed at VPI&SU. Together with the detailed fatigue damage representation and sophisticated stress analysis already available in these codes, this model could add a new dimension to the long term engineering performance prediction of composite laminates.

9 References

1. Sobotka, Z., Rheology of Materials and Engineering Structures, Elsevier, 1984.

2. Reiner, M., Deformation, Strain and Flow", H.K. Lewis Co., Ltd., London, 1960.

3. Flugge, W., Viscoelasticity, Springer-Verlag, 1975.

4. Findley, W.N., Lai, J.S., Onaran, K., Creep and Creep Relaxation of Nonlinear Viscoelastic Materials, North Holland Pub. Co., 1972.

5. Huang, F.H., Yamada, H., Li, C.W., "Constitutive relation based on state variables for nonelastic deformation in type 304 and 316 stainless steels", Characterization of Materials for Service at Elevated Temperatures, ASME/CSME Montreal PVP Conference, G.V. Smith, ed., ASME, June 1978.

6. Hayman, B., "Creep buckling, a general view of the phenomena", Creep in Structures, A.R.S. Ponter, D.R. Hayhurst, eds., 1980.

7. Amijima, S., Fujii, T., Hashimoto, H., "Effect of time and temperature on compressive failure of FRP in Edge-wise direction", Proc. Int. Symp. on Composite Materials and Structures, C.T. Sun and T.T Loo, eds., June 1986, Beijing, China, Technomic, 1986.

8. Szyszkowski, W., Glockner, P.G., "A hereditary constitutive law for nonlinear time dependent materials", Constitutive Laws for Engineering Materials, Theory and Applications, v. 1, C.S. Desai, ed., Elsevier, 1987.

9. Inoue, T., Imatani, S., "Inelastic constitutive relationship of high temperature materials under creep-plasticity interaction conditions", High Temperature Creep-Fatigue, R. Ohtani, M. Ohnami, T. Inoue, eds., Elsevier Applied Science, 1988.

10. Leaderman, H., "Elastic and creep properties of filamentous materials and other high polymers", The Textile Foundation, Washington, 1943.

11. Barenblatt, G., Kozyrev, Y.I., Malinin, N.I., Pavlov D.Y., Shesterikov, S.A., "On the thermal vibrocreep of polymers", Recent Progress in Applied Mechanics, Folke Odqvist Volume, B. Broberg, J. Hult, F. Niordson, Eds., 1967.

12. Ponter, A.R.S., "On the creep modified shakedown limit", Creep in Structures, A.R.S. Ponter, D.R. Hayhurst, eds., 1980.

13. Parkus, H., "On the lifetime of viscoelastic structures in a random temperature field", Recent Progress in Applied Mechanics, The Folke Odqvist Volume, B. Broberg, J. Hult, F. Niordson, Eds., 1967.

14. Ohno, N., Murakami, S., Kawabata, M., "Modification of creep-hardening surface model by incorporating aging effects", Constitutive Laws for Engineering Materials, Theory and Applications, vol. 2, C.S. Desai et al., eds., Elsevier, 1987.

15. Green, A.E., Rivlin, R.S., "The Mechanics of Nonlinear Materials with Memory", *Arch. Rational Mech Anal*, Vol 1, No.1, 1957, pp. 1-21.

16. Schapery, R.A., "Further development of a thermodynamic constituitive theory: stress formulation", Perdue Research Foundation, Project 4958, 1969.

17. Tuttle, M.E., Brinson, H.F., "Accelerated Viscoelastic Characterization of T300/5208 Graphite - Epoxy Laminates", VPI & SU, VPI-E-84-9, March 1984.

18. Torvik, P.J., Bagley, R.L., "On the appearance of the fractional derivative in the behavior of real materials", *J. of Applied Mechanics*, no. 23, 1984, pp. 1-5.

19. Koeller, R.C., "Applications of fractional calculus on the theory of viscoelasticity", *J. of Applied Mechanics*, no. 20, 1984, pp. 1-9.

20. Daugste, C.L., "Joint application of time-temperature and time-stress analogies to constructing unified curves", *Polymer Mechanics*, no. 3, 1974.

21. Griffith, W.I., Morris, D.H., Brinson, H.F., "Accelerated characterization of graphite/ epoxy composites", Advances in Composite Materials, ICCM 3, A.R. Bunsell, ed., Paris, France, Pergamon Press, 1980.

22. Evans, R.W., Wilshire, B., "Power law creep of polycrystalline copper", Creep and Fracture of Engineering Materials and Structures, Proceedings of the Third Int. Conf., Swansea, April 1987, B. Wilshire and R.W. Evans, eds., The Institute of Metals, London, 1987.

23. Betten, J., "Representation of constitutive equations in creep mechanics of isotropic and anisotropic materials", Creep in Structures, A.R.S. Ponter, D.R. Hayhurst, eds., 1980

24. Onat, E.T., "Representation of inelastic behavior in the presence of anisotropy and of finite deformations", Recent Advances in Creep and Fracture of Engineering Materials and Structures, B. Wilshire, D.R.J. Owen, eds., 1982.

25. Schapery, R.A., "Deformation and fracture characterization of inelastic composite materials using potentials", *Polymer Engineering and Science*, Vol. 27, No. 1, 1987.

26. R.D. Tonda, R.D., Schapery, R.A., "A method for studying composites with changing damage by correcting for the effects of matrix viscoelasticity", Damage Mechanics in Composites, A.S.D. Wang, G.K. Haritos, eds., ASME WAM, Boston, Massachussets, December 1987.

27. Brouwer, H.R., "Mechanical behavior of polymeric matrix composites in biaxial stress fields", ICCM & ECCM, July 1987, London, UK,. vol. 4, F.L. Matthews, N.C.R. Buskell, J.M. Hodgkinson, J. Morton, eds., Elsevier, 1987.

28. Cardon, A.H., Hiel, C.C., Brouwer, H.R., "Nonlinear viscoelastic behavior of epoxy matrix composites under combined mechanical and environmental loadings", Proc. Int. Symp. on Composite Materials and Structures, C.T. Sun and T.T Loo, eds., June 1986, Beijing, China, Technomic, 1986.

29. Oytana, C., Varchon, D., Dody, H., Pierre, M., "Viscoplastic strains of a glass woven fabric based laminate", Composites Structures 3, 3rd International Conference on Composite Structures, I.H. Marshall, ed., 1985.

30. Sun, C.T., Chen, J.L., "A simple flow rule for characterizing nonlinear behavior of fiber composites", ICCM & ECCM, July 1987, London, UK,. v. 1, F.L. Matthews, N.C.R. Buskell, J.M. Hodgkinson, J. Morton, eds., Elsevier, 1987.

31. Amijima, S., Adachi, T., "Effect of time on the mechanical behavior of laminated composites", Progress in Science and Engineering of Composites, T. Hayashi, K. Kawata, S. Umewaka, eds., ICCM-IV, Tokyo, 1982.

32. Beckwith, S.W., "Creep evaluation of a glass/epoxy composite", *SAMPE Quaterly*, January 1980, pp. 8-15.

33. Yancey, R.N., Pindera, M-J, "Radiation and temperature effects on the time- dependent response of T300/934 Graphite/ Epoxy", VPI-E-88-5, College of Engineering, VPI & SU, March 1988.

34. Hashin, Z., "Theory of fiber reinforced materials", NASA Contractor Report 1974, March 1972.

35. Aboudi, J., "A continuum theory for fiber reinforced elastic-viscoplastic composites", *International Journal of Engineering Science*, vol. 20, no. 5, pp. 605-621, 1982.

36. Pyrz, R., "Strength reduction of woven glass fabric composite after creep deformation", ICCM & ECCM, July 1987, London, UK,. vol. 4, F.L. Matthews, N.C.R. Buskell, J.M. Hodgkinson, J. Morton, eds., Elsevier, 1987.

37. Xiao, X., "Studies of the viscoelastic behavior of a thermoplastic resin composite", *Composite Sci. and Tech.*, vol. 34, 1989, pp. 163-182.

38. Brinson, H.F., Morris, D.H., Yeow, Y.T., "The viscoelastic behavior of the principle compliance matrix of a unidirectional graphite/epoxy composite", VPI&SU, VPI-E-79-9, Blacksburg, VA, 1979.

39. Griffith, W.I., Morris, D.H., Brinson, H.F., "The accelerated characterization of viscoelastic composite materials", VPI&SU, VPI-E-80-15, Blacksburg, VA, 1980.

40. Dillard, D.A., Morris, D.H., Brinson, H.F., "Creep and creep rupture of laminated graphite/epoxy composites", Virginia Polytechnic Institute and State University, VPI-E-81-3, Blacksburg, VA, 1981.

41. Hiel, C., Cardon, A.H., Brinson, H.F., "The nonlinear viscoelastic response of resin matrix composite laminates", Virginia Polytechnic Institute and State University, VPI-E-83-6, Blacksburg, VA, 1983.

42. Gramoll K.C., Dillard, D.A., Brinson, H.F., "Thermoviscoelastic Characterization and Prediction of Kevlar/Epoxy Composite Laminates", VPI & SU, VPI-E-88-12; CAS/ESM-88-5, May 1988.

43. Reifsnider, K.L., Henneke, E.G., Stinchcomb, W.W., Duke, J.C., "Damage mechanics and NDE of composite laminates", IUTAM Symposium on Mechanics of Composite Materials, VPI & SU, Pergamon Press, 1982.

44. Stinchcomb, W.W., Reifsnider, K.L., "Fatigue damage mechanisms in composite materials: a review", Fatigue Mechanisms, ASTM STP 675, J.F. Fong, Ed., ASTM, 1979, pp.762-787.

45. Schapery, R.A., "Models for damage growth and fracture in nonlinear viscoelastic particulate composites", MM3168-82-5, Mechanics and Materials Center, Texas A&M University, 1982.

46. Christensen, R.M., Theory of Viscoelasticity - An Introduction, Second Edition, Academic Press, New York, 1982.

47. Jamison, R.D., Reifsnider, K.L., "Advance fatigue damage development in graphite epoxy laminates", AFWAL TR-82-3103, 1982.

48. Quinn, K.R., O'Brien, G., "Designing with the new high temperature thermoplastic composites", 43rd Annual Conference, Composite Institute, The Society of the Plastics Industry, February 1988.

49. O'Connor, J.E., Murtha, T.P., Lindstrom, M.R., Lou, A.Y., "Polyarylene sulfide high performance thermoplastic composites", ICCM & ECCM, July 1987, London, UK,. vol. 1, F.L. Matthews, N.C.R. Buskell, J.M. Hodgkinson, J. Morton, eds., Elsevier, 1987.

50. Kim, K.S., Hahn, T., Croman, R.B., "The effect of cooling rate on residual stress in a thermoplastic composite", *J. of Composite Technology and Research*, vol. 11, no. 2, 1989, pp. 47-52.

51. Jeronimidis, G., Parkyn, A.T., "Residual stresses in carbon fiber-thermoplastic matrix laminates", *J. of Composite Materials*, vol. 22, May 1988, pp. 401-415.

52. Davies, P., Benzeggagh, M.L., de Charentenay, F.X., "Delamination of continuous carbon fiber reinforced thermoplastic composites", Proc. Int. Symp. on Composite Materials and Structures, C.T. Sun and T.T Loo, eds., June 1986, Beijing, China, Technomic, 1986.

53. Newaz, G.M., Mall, S., "Relaxation-controlled cyclic delamination growth in advanced thermoset and thermoplastic composites at elevated temperature", *J. of Composite Materials*, vol. 23, February 1989, pp. 133-145.

54. Curtis, P.T., "In investigation of the tensile fatigue behavior of improved carbon fiber composite materials", ICCM & ECCM, July 1987, London, UK,. vol. 4, F.L. Matthews, N.C.R. Buskell, J.M. Hodgkinson, J. Morton, eds., Elsevier, 1987.

55. Croman, R.B., "Flex fatigue of AS-4 graphite reinforced thermoplastics", ICCM & ECCM, July 1987, London, UK,. vol. 4, F.L. Matthews, N.C.R. Buskell, J.M. Hodgkinson, J. Morton, eds., Elsevier, 1987.

56. Simmonds, R.A., Bakis, C.E., Stinchcomb, W.W., "Effects of matrix toughness on fatigue response of graphite fiber composite laminates", Composite Materials: Fatigue and Fracture, Second Volume, ASTM STP 1012, P.A. Lagace, ed., ASTM, 1989.

57. Baron, Ch., Schulte, K., "Fatigue damage response of CFRP with toughened matrices and improved fibers", ICCM & ECCM, July 1987, London, UK,. v. 4, F.L. Matthews, N.C.R. Buskell, J.M. Hodgkinson, J. Morton, eds., Elsevier, 1987.

58. Henneke, E.G., "Nondestructive evaluation of fiber reinforced composite laminates", 11th World Conference on Nondestructive Testing, vol. 2, 1985, pp. 1332-1343.

59. O'Brien, T.K., "Stiffness change as a nondestructive damage measurement", Mechanics of Nondestructive Testing, W.W. Stinchcomb, Ed.,Plenum Press, New York, 1980, pp. 101-122.

60. Daniel, I.M., Lee, J.W., Yaniv, G., "Damage mechanisms and stiffness degradation in graphite/epoxy composites", ICCM & ECCM, July 1987, London, UK,. vol. 4, F.L. Matthews, N.C.R. Buskell, J.M. Hodgkinson, J. Morton, eds., Elsevier, 1987.

61. Reifsnider, K.L., Stinchcomb, W.W., "Stiffness change as a fatigue damage parameter for composite laminates", Advances in Aerospace Structures, Materials and Dynamics, Yuceoglu, U., Sierakowski, R.L., Glasgow, D.A., Editors, ASME, New York, 1983.

62. Laws, N., Dvorak, G.J., Hejazi, M., "Stiffness changes in unidirectional composites caused by crack systems", Mechanics of Materials 2, 1983.

63. Gottesman, T., Hashin, Z., Brull, M.A., "Effective elastic moduli of cracked fiber composites", Advances in Composites Materials, Proceedings of the 3rd Int. Conf. on Composite Materials, A.R. Bunsell, ed., Paris, 1980.

64. Camponeschi, E.T., Stinchcomb, W.W., "Stiffness reduction as an indicator of damage in graphite/epoxy laminates", Composite Materials: Testing and Design (Sixth Conference), ASTM STP 787, I.M. Daniel, Ed., ASTM, 1982, pp. 225-246.

65. Rotem, A., "Stiffness change of a graphite epoxy laminate under reverse fatigue loading", *J of Composites Technology and Research*, vol. 11, no. 2, 1989, pp. 59-64.

66. Daniel, I.M., Lee, J.W., Yaniv, G., "Damage development and property degradation in composite materials", Mechanics of composites materials - 1988, G.J. Dvorak, N. Laws, eds., Joint ASME/SES Applied Mechanics and Engineering Sciences Conference, Berkeley, California, ASME, June 1988.

67. Talreja, R., "Stiffness based fatigue damage characterization", Fatigue of composite materials, Ch. 5, Technomic, 1987.

68. Tsai, G.C., "Frequency effects on stiffness reduction of graphite/ epoxy composite laminates", 34th International SAMPE Symposium, May 1989.

69. Davidson, R., Saddler, C.J., "The torsional fatigue characteristics of unidirectional glass reinforced materials", ICCM & ECCM, July 1987, London, UK, vol. 4, F.L. Matthews, N.C.R. Buskell, J.M. Hodgkinson, J. Morton, eds., Elsevier, 1987.

70. Neubert, H., Harig, H., Schulte, K., "Monitoring of fatigue induced damage processes in CFRP by means of thermometric methods", ICCM & ECCM, July 1987, London, UK, vol. 4, F.L. Matthews, N.C.R. Buskell, J.M. Hodgkinson, J. Morton, eds., Elsevier, 1987.

71. Wevers, M., Verpoest, I., Aernoudt, E., de Meester, P., "Fatigue damage development in carbon fiber reinforced epoxy composites: correlation between the stiffness degradation and the growth of different damage types", ICCM & ECCM, July 1987, London, UK, vol. 4, F.L. Matthews, N.C.R. Buskell, J.M. Hodgkinson, J. Morton, eds., Elsevier, 1987.

72. Withworth, H.A., "Modelling stiffness reduction of graphite/ epoxy composite laminates", *J. of Composite Materials*, vol. 21, April 1987.

73. Ting, T.C.T., "Dynamic response of composites", Applied Mechanics Update, C.R. Steele,G.S. Springer, eds., ASME, 1986.

74. Schultz, A.B., Tsai, S.W., "Measurements of complex dynamic moduli for laminated fiber reinforced composites", *J. of Composite Materials*, vol. 3, July 1969, pp. 434-444.

75. Heller, R.A., Thakker, A.B., Arthur, C.E., "Temperature dependence of the complex modulus for fiber reinforced materials", ASTM STP 580, Composite Reliability, ASTM, 1975.

76. Sichina, W., Gill, P.S., "Characterization of composites using dynamic mechanical analysis", Materials - Pathway to the Future, 33rd International SAMPE Symposium, G. Carrillo, E.D. Newell, W.D. Brown, P. Phelan, eds., Anaheim, California, March 7-10, 1988.

77. Zhang, J., Xu, Y., Yu, D., "Measurement of dynamic moduli and damping of carbon/epoxy", Proc. Int. Symp. on Composite Materials and Structures, C.T. Sun and T.T Loo, eds., June 1986, Beijing, China, Technomic, 1986.

78. Camponeschi, E.T., Stinchcomb, W.W., Kraige, L.G., "Effects of moisture on the dynamic response of graphite epoxy laminates", Proc. of the 2nd Int. Conf. on Environmental Degradation of Eng. Materials, VPI&SU, September 1981.

79. Curtis, P.T., Davies, P., Partridge, I.K., Sainty, J.P., "Cooling rate effects in PEEK and carbon fibre-peek composites", ICCM & ECCM, July 1987, London, UK, vol. 4, F.L. Matthews, N.C.R. Buskell, J.M. Hodgkinson, J. Morton, eds., Elsevier, 1987.

80. Ha, S.K., Springer, G.S., "Mechanical properties of graphite epoxy composites at elevated temperatures", ICCM & ECCM, July 1987, London, v. 4, F.L. Matthews, N.C.R. Buskell, J.M. Hodgkinson, J. Morton, eds., Elsevier, 1987.

81. Travis, A.R., Wang, S.F., Ogale, A.A., "Influence of aging on dynamic and fracture properties of polymer composites", Materials - Pathway to the Future, 33rd International SAMPE Symposium, G. Carrillo, E.D. Newell, W.D. Brown, P. Phelan, eds., Anaheim, California, March 7-10, 1988.

82. Suzuki, Y., Saitoh, J., "Characterization of cowoven fabrics using dynamic mechanical spectroscopy", 34th International SAMPE Symposium, May 8-11, 1989

83. Banerjee, A., Ogale, A.A., Edie, D.D., "Interfacial characterization of composites by dynamic mechanical analysis", 34th International SAMPE Symposium, May 1989.

84. Chua, P.S., "Dynamic mechanical analysis studies of the interphase", *Polymer Composites*, October 1987, vol. 8, no. 5, pp. 308-313.

85. Silverman, E.M., Jones, R.J., "Graphite thermoplastic composites for spacecraft applications", Materials - Pathway to the Future, 33rd International SAMPE Symposium, G. Carrillo, E.D. Newell, W.D. Brown, P. Phelan, eds., Anaheim, California, March 7-10, 1988.

86. Reifsnider, K.L., Williams, R.S., "Determination of fatigue related heat emission in composite materials", *Experimental Mechanics*, vol. 14, no. 12, December 1974, pp. 479-485.

87. Reifsnider, K.L., Stinchcomb, W.W., Marcus, L.A., Williams, R.S., "Frequency effects on flawed composite fatigue reliability", ASTM STP 580, Composite Reliability, E.M. Wu, ed., ASTM, 1975.

88. Stinchcomb, W.W., Reifsnider, K.L., Marcus, L.A., Williams, R.S., "Effect of cyclic frequency on the mechanical properties of composite materials", TR 73-1907, VPI&SU, AFOSR-72-2358, 1973.

89. Reifsnider, K.L., Henneke, E.G., Stinchcomb, W.W., "The mechanics of vibrothermography", Mechanics of Nondestructive Testing, W.W. Stinchcomb, ed., Plenum, 1980, pp. 249-276.

90. Dally, J.W., Broutman, L.J., "Frequency effects on the fatigue of glass reinforced plastics", *J. of Composite Materials*, vol. 1, no. 4, 1967, pp. 424-443.

91. Broutman, L.J., Gaggar, S.K., "Fatigue behavior of epoxy and polyester resins", *Int. J. Polymeric Materials*, vol. 1, 1972, pp. 295-316.

92. Davies, M., Leach, D.C., Moore, D.R., Turner, R.M., "Mechanical performance of semi-crystalline thermoplastic matrix composites for elevated temperature service", ICCM & ECCM, July 1987, London, UK, vol. 1, F.L. Matthews, N.C.R. Buskell, J.M. Hodgkinson, J. Morton, eds., Elsevier, 1987.

93. Putter, S., Buchanan, D.L., Rehfield, L.W., "Influence of frequency and environmental conditions on dynamic behavior of graphite/epoxy composites", Composite Materials: Testing and Design (6th Conference), I.M. Daniel, Ed., ASTM STP 787, ASTM, 1982.

94. Adams, R.D., Walton, D., Flitcroft, J.E., Short, D., "Vibration testing as a nondestructive test tool for composite materials", ASTM STP 580, Composite Reliability, ASTM, 1975.

95. Drew, R.C., White, R.G., "An experimental investigation into damage propagation and its effects upon dynamic properties in CFRP composite material", Composite Structures 4, vol. 2, I.H. Marshall, ed., Elsevier, 1987.

96. Sims, G.D., Bascombe, D., "Continuous monitoring of fatigue degradation in composites by dynamic mechanical analysis", ICCM & ECCM, July 1987, London, UK, vol. 4, F.L. Matthews, N.C.R. Buskell, J.M. Hodgkinson, J. Morton, eds., Elsevier, 1987.

97. Hahn, H.T., Kim, R.Y., "Fatigue behavior of composite laminates", *J. Composite Materials*, Vol. 10, 1976, pp. 156-179.

98. Rotem, A., *Mechanics of Composite Materials, Recent Advances*, Z. Hashin, C.T. Herakovich, Eds., Pergamon Press, 1983, pp. 421-436.

99. Wilkins, D.J., Eisenman, J.R., Camin, R.A., Margolis, W.S., Bensom, R.A., *Damage in Composite Materials, ASTM STP 775*, ASTM, 1982, pp. 168-183.

100. Chou, P.C., Wang, A.S.D., Miller, H., "Cumulative damage model for advanced composite materials", *TR-82-4083*, Air Force Wright Aeronautical Laboratories, Dayton, OH, 1982.

101. Wang, A.S.D., Slomiana, M., "Fracture mechanics of delamination initiation and growth", *NADC-TR-79056-60*, Naval Air Development Center, 1982.

102. Hashin, Z., Rotem, A., *Materials Science and Engineering*, Elsevier-Sequoia, Lausanne, Switzerland, 1978, pp. 147-160.

103. Poursartip, A., Ashby, M.F., Beaumont, P.R., *Fatigue and Creep of Composite Materials*, H. Lilholt, R. Talreja, Eds., Denmark, 1982, pp. 279-284.

104. Charewicz, A., Daniel, I.M.,"Damage mechanisms and accumulation in graphite epoxy laminates", *Composite Materials: Fatigue and Fracture, ASTM STP 907*, H.T. Hahn, Ed., ASTM, 1986, pp. 274-297.

105. Reifsnider, K.L., Miller, H.R., Stinchcomb, W.W., Ulman, D.A., Bruner, R.D., Liechti, K.M.,"Cumulative damage model for advanced composite materials", AFWAL-TR-84-4007, 1984.

106. Reifsnider, K.L., Stinchcomb, W.W., "A critical element model of the residual strength and life of fatigue loaded composite coupons", Composite Materials: Fatigue and Fracture, ASTM STP 907, H.T. Hahn, ed., ASTM, 1986.

107. Reifsnider, K.L., "A Hybrid approach to composite component life prediction", Proc. Int. Symp. on Composite Materials and Structures, C.T. Sun and T.T Loo, eds., Beijing, China, Technomic, June 1986.

108. Wareing, J., Tomkins, B., "Creep-fatigue failure in high temperature alloys", Creep in structures, 3rd IUTAM Symposium, Leicester, UK, A.R.S. Ponter, D.R. Hayhurst, eds., Springer-Verlag, 1980, pp. 477-503.

109. Manson, S.S., Halford, G.R., Spera, D.A., Advances in Creep Design, Chapter 12, Smith, A.I., Nicolson, A.M., eds., 1971.

110. Manson S.S., "Some useful concepts for the designer in treating cumulative fatigue damage at elevated temperatures", Mechanical Behavior of Materials, K.J. Miller and R.F. Smith, eds., Pergamon Press, 1980.

111. Batte, A.D., "Creep-fatigue life predictions", Fatigue at High Temperature, R.P. Skelton, ed., Applied Science, 1983.

112. Del Puglia, A., Manfredi, E., "High temperature low cycle fatigue", Creep of Engineering Materials and Structures, G. Bernasconi, G. Piatti, Eds., 1978.

113. Plumtree, A., "Fracture mechanisms during creep fatigue interaction in stainless steel", Creep and Fracture of Engineering Materials and Structures, Proceedings of the 3rd Int. Conf., Swansea, April 1987, B. Wilshire and R.W. Evans, eds., The Institute of Metals, London, 1987.

114. Piechnik, S., Pachla, H., "The continuous field of damage and its influence on the creep process in concrete under tensile loading", Creep in Structures, A.R.S. Ponter, D.R. Hayhurst, eds., 1980.

115. Lloyd, G.J., "High temperature fatigue and creep fatigue crack propagation: mechanics, mechanisms and observed behavior in structural materials", Fatigue at High Temperature, R.P. Skelton, ed., Applied Science, 1983.

116. Pineau, A., "High temperature fatigue behavior of engineering materials in relation to microstructure", Fatigue at High Temperature, R.P. Skelton, ed., Applied Science, 1983.

117. Evans, W.J., "Creep-fatigue interactions in Ti-6Al-4V at ambient temperatures", Creep and Fracture of Engineering Materials and Structures, Proceedings of the 3rd Int. Conf., Swansea, April 1987, B. Wilshire and R.W. Evans, eds., The Institute of Metals, London, 1987.

118. Harrison, G.F., Tranter, P.H., Winstone, M.R., Evans, W.J., "The influence of low temperature cyclic creep on the fatigue resistance of a near alpha titanium alloy", Creep and Fracture of Engineering Materials and Structures, Proceedings of the 3rd Int. Conf., Swansea, April 1987, B. Wilshire and R.W. Evans, eds., The Institute of Metals, London, 1987.

119. Wang, Z.G., Rahka, K., Laird, C., "Cyclic creep acceleration and retardation in Cr-Mo-V rotor steel at ambient and elevated temperature respectively", *Fatigue and Fracture of Engineering Materials and Structures*, vol. 9, no. 3,1986, pp. 219-230.

120. Freed, A.D., Sandor, B.I., "Localised time-dependent and cycle-dependent creep in notched plates", Cavities and Cracks in Creep and Fatigue, J. Gittus, ed., 1981.

121. Wareing, J., "Mechanisms of high temperature fatigue in creep-fatigue failure in engineering materials" Fatigue at High Temperature, R.P. Skelton, ed., Applied Science, 1983.

122. Sadananda, K., Shahinian, P., "Creep-fatigue crack growth", Cavities and Cracks in Creep and Fatigue, J. Gittus, ed., 1981.

123. Ohji, K., Kubo, S., "Fracture mechanics evaluation of crack growth behavior under creep and creep-fatigue interaction", High Temperature Creep-Fatigue, R. Ohtani, M. Ohnami, T. Inoue, eds., Elsevier Applied Science, 1988.

124. Kachanov, L.M., "Introduction to continuum damage mechanics", Martinus Nijhoff, 1986.

125. Tobolsky, A.V., "Properties and structure of polymers", Wiley, 1960.

126. Murakami, K., Ono, K., "Chemorheology of polymers", Elsevier, 1979.

127. Rabotonov, Y.N., Creep problems in structural members, North Holland, (in USA by Elsevier), 1969.

128. Lemaitre, J., Chaboche, J., "A nonlinear model of creep-fatigue damage cumulation and interaction", J. Hult, Ed., Mechanics of Viscoelastic Media and Bodies, Springer-Verlag, 1975, 291-300.

129. Chaboche, J.L., "Constitutive equations in creep-fracture damage", Engineering Approaches to High Temperature Design, B. Wilshire, D.R.J. Owen, eds., 1983.

130. Krajcinovic, D., "Constitutive theories for solids with defective microstructure", Damage Mechanics and Continuum Modeling, N. Stubbs, D. Krajcinovic, eds., ASCE Convention, Detroit, MIchigan, October 1985.

131. Krajcinovic, D., "Continuum damage mechanics", Applied Mechanics Update, C.R. Steele, G.S. Springer, eds., ASME, 1986.

132. Belloni, G., Bernasconi, G., Piatti, G., "Creep damage models", Creep of Engineering Materials and Structures, G. Bernasconi and G. Piatti, Eds., 1978.

133. Leckie, F.A., "Constitutive equations of creep deformation and rupture and their application", Creep of Engineering Materials and Structures, G. Bernasconi and G. Piatti, Eds., 1978.

134. Hult, J., "Effects of voids on creep rate and strength", Damage Mechanics and Continuum Modeling, N. Stubbs, D. Krajcinovic, eds., ASCE Convention, Detroit, Michigan, October 1985.

135. Betten, J., "Tensorial generalization of Norton's creep law", Creep and Fracture of Engineering Materials and Structures, Proceedings of the 3rd Int. Conf., Swansea, April 1987, B. Wilshire and R.W. Evans, eds., The Institute of Metals, London, 1987.

136. Murakami, S., Ohno, N., "A continuum theory of creep and creep damage", Creep in Structures, A.R.S. Ponter, D.R. Hayhurst, eds., 1980.

137. Murakami, S., Ohno, N., "Continuum theory of material damage at high temperature", High Temperature Creep-Fatigue, R. Ohtani, M. Ohnami, T. Inoue, eds., Elsevier Applied Science, 1988.

138. Sidoroff, F., "Fatigue damage modelling of composite materials from bending tests", ICCM & ECCM, July 1987, London, UK, vol. 4, F.L. Matthews, N.C.R. Buskell, J.M. Hodgkinson, J. Morton, eds., Elsevier, 1987.

139. Beaumont, P.W.R., "The fatigue damage mechanics of composite laminates", Damage Mechanics in Composites, A.S.D. Wang, G.K. Haritos, eds., ASME WAM, Boston, Massachussets, December 1987.

140. Withworth, H.A., "Cumulative damage in composites", Recent Advances in the Macro and Micro-mechanics of Composite Materials Structures, ASME WAM, D. Hui, J.R. Vinson, eds., Chicago, Illinois, November 1988.

141. Wnuk, M.P., Kriz, R.D., "CDM model of damage accumulation in laminated composites", *Int. Journal of Fracture*, vol. 28, 1985.

142. Shen, W., Rao, B., Lee, H., "A crack-damage mechanics model for composite laminate", *Engineering Fracture Mechanics*, vol. 21, no. 5, pp. 1019-1029, 1985.

143. Peng, L., Yang, F., Xiao, Z., Zhu, H., "Anisotropic damage in orthotropic fiber reinforced composite plate", Proc. Int. Symp. on Composite Materials and Structures, C.T. Sun and T.T Loo, eds., June 1986, Beijing, China, Technomic, 1986.

144. Talreja, R., "Modeling of damage development in composites using internal variables concepts", Damage mechanics in composites, A.S.D. Wang, G.K. Haritos, eds., ASME WAM, Boston, Massachussets, December 1987.

145. Talreja, R., Fatigue of Composite Materials, Ch. 6, Technomic, 1987.

146. Allen, D.H., Harris, C., Nottorf, E., "A thermomechanical constitutive theory for elastic composites with distributed damage", Part 1 and 2, Texas A&M report MM-5023-85-15, 1985.

147. Harris, C.E., Allen, D.H., Nottorf, E.W., "Damage induced changes in the Poisson ratio of crossply laminates: an application of a continuum damage mechanics model for laminated composites", Damage Mechanics in Composites, A.S.D. Wang, G.K. Haritos, eds., ASME WAM, Boston, December 1987.

148. Allen, D.H., Groves, S.C., Harris, C.E., "A cumulative damage model for continuous fiber composite laminates with matrix cracking and interply delaminations", Composite Materials: Testing and Design, Eigth Conference, J.D. Whitcomb, ed., ASTM STP 972, ASTM, 1988.

149. Allen, D.H., Nottorf, E.W., Harris, C.E., "Effect of microstructural damage on ply stresses in laminated composites", Recent Advances in the macro and micro-mechanics of composite materials structures, ASME WAM, D. Hui, J.R. Vinson, eds., Chicago, Illinois, November 1988.

150. Shen, Z., Tang, X., Shen, W., "Experimental study on damage mechanics of composite laminates - damage strain energy release rate failure criterion", Proc. Int. Symp. on Composite Materials and Structures, C.T. Sun and T.T Loo, eds., June 1986, Beijing, China, Technomic, 1986.

151. Engblom, J.J., "Modelling the effects of intraply cracking in composite laminates at the sublaminate level", Design and Analysis of Composite Material Vessels, ASME PVP Conference, June 28-July 2, 1987, D. Hui and T.J. Kozik eds., ASME, pp. 105-115.

152. Weitsman, Y., "Coupled damage and moisture transport in fiber reinforced polymeric composites", *Int. J. Solids and Structures*, vol. 23, no. 7, pp. 1003-1025, 1987.

153. Weitsman, Y., "Damage coupled with heat conduction in uniaxially reinforced composites", *Journal of Apllied Mechanics*, vol. 55, 1988.

154. Weitsman, Y., "A continuum damage model for viscoelastic materials", *Journal of Applied Mechanics*, December 1988, vol. 55, pp. 773-780.

155. Rotem, A., "Fatigue mechanism of multidirectional laminate under ambient and elevated temperature", 3rd International Conference on Composite Materials: Advances in Composite Materials, A.R. Bunsell, ed., Paris, 1980, pp.146-161.

156. Rotem, A., Nelson, H.G., "Fatigue behavior of graphite-epoxy laminates at elevated temperatures", *Fatigue of Fibrous Composite Materials, ASTM STP 723*, ASTM, 1981, pp.152-173.

157. Menges, G., Thebing, U., "On dimensioning composites under alternating loads", ICCM 3, A.R. Bunsell, ed., Paris, France, Pergamon Press, 1980.

158. Jinen, E., "Accumulated strain in low cycle fatigue of short carbon-fiber reinforced nylon 6", *Journal of Material Science,* Vol. 21, 1986, pp. 435-443.

159. Lifshitz, J.M., "Deformational behavior of a unidirectional graphite/ epoxy composite under compressive fatigue", *J. of Composites Technology & Research,* Vol. 11, No. 3, Fall 1989, pp. 99-105.

160. Sturgeon, J.B., "Creep, repeated loading, fatigue and crack growth in ±45° oriented carbon fiber reinforced plastics", *J. of Materials Science*, vol. 13, 1978, pp. 1490-1498.

161. Sun, C.T., Chan, W.S., "Frequency effect on the fatigue life of a laminated composite", Composite Materials: Testing and Design (Fifth Conference), ASTM STP 674, S.W. Tsai, ed., ASTM, 1979, pp. 418-430.

162. Saff, C.R., "Effect of load frequency and lay-up on fatigue life of composites", *Long Term Behavior of Composites, ASTM STP 813*, T.K. O'Brien, ed., ASTM, 1983, pp.78-91.

163. Sun, C.T., Chim, E.S., "Fatigue retardation due to creep in a fibrous composite", Fatigue of Fibrous Composite Materials, ASTM STP 723, ASTM, 1981.

164. Mandell, J.F., Meier, U., "Effects of stress ratio, frequency and loading time on the tensile fatigue of glass reinforced epoxy", *Long Term Behavior of Composites, ASTM 813,* T.K. O'Brien, ed., ASTM, 1983, pp. 55-77.

165. Dan-Jumbo, E., Zhou, S.G., Sun, C.T., "Load-frequency effect on fatigue life of IMP6/APC-2 thermoplastic composite laminates", *Advances in Thermoplastic Matrix Composite Materials,* ASTM STP 1044, ASTM 1989, pp.113-132.

166. Lang, R.W., Manson, J.A., Hertzberg, R.W., "Fatigue crack propagation in short glass fiber reinforced nylon 66: effect of frequency", Joint U.S.-Italy Symposium on Composite Materials, J.C. Seferis and L. Nicolais, eds., 1981, pp. 377-396.

167. Ke, Y., Wang, S., Meng, X., Su, B., Tian, X., "Effect of cyclic loading on the dynamic viscoelastic properties of epoxy composites", Proc. Int. Symp. on Composite Materials and Structures, C.T. Sun and T.T Loo, eds., June 1986, Beijing, China, Technomic, 1986.

168. Vogelesang, L.B., Marissen, R., Schijve J., "A new fatigue resistant material: aramid reinforced aluminum laminate (Arall)", 11th Symposium, International Committee on Aeronautical Fatigue", 1981.

169. Osiroff, R., Stinchcomb, W.W., "Long term characterization of ARALL laminates", CCMS-89-06 Report, VPI & SU, 1989.

170. Jones, R.M., "Mechanics of composites materials", Hemisphere Publishing Corp., 1975.

171. Highsmith, A.L., Stinchcomb, W.W., Reifsnider, K.L., "Stiffness reduction resulting from transverse cracking in fiber-reinforced composite laminates", ESM, VPI & SU, VPI-E-81.33, November 1981.

172. Reifsnider, K.L., "Some fundamental aspects of the fatigue and fracture response of composite materials", Proceedings, 14th Annual Conference, Lehigh University, Bethlehem, PA, 1977, pp.373-384.

173. Highsmith, A.L., Reifsnider, K.L., "Stiffness-reduction mechanisms in composite laminates", *Damage in Composite Materials*, ASTM STP 775, K.L. Reifsnider, ed., ASTM, 1982, pp.103-117.

174. Moore, R.H., Dillard, D.A., "Elastic and time dependent matrix cracking in cross-ply composite laminates", CCMS-88-19 Report, VPI&SU, April 1988.

175. Lee, J.W., Daniel, I.M., Yaniv, G., "Fatigue life prediction of cross-ply composite laminates", *Composite Materials: Fatigue and Fracture, 2nd Volume,* ASTM STP 1012, P.A. Lagace, ed., 1989, pp. 19-28.

176. Ryder, J.T., Crossman, F.W., "A study of stiffness, residual strength and fatigue life relationships for composite laminates", NASA CR-172211, October 1983.

177. Theocaris, P.S., The Mesophase Concept in Composites, Chapter 7, pp.125-131, Springer-Verlag, 1987.

178. Reifsnider, K.L., "Life prediction methodology for composite material systems", Indo-U.S. Workshop on Composite Materials for Aerospace Applications, Bangalore, India, July 23-27, 1990,

179. Du Pont Instruments Dynamic Mechanical Analyzer 983, Operator's Manual, Du Pont, November 1986.

Vita

Ricardo Osiroff was born on December 6, 1955 in Montevideo, Uruguay. In 1970 he and his family emigrated to Israel. In 1974, following his graduation from high school, he enrolled in the Academic Army Reserve. After serving one year in the Armored Corps, he began his studies in the Chemical Engineering Department at the Technion, Israel Polytechnic Institute. Upon graduating cum laude in 1979, and successfully completing army training as an officer in 1980, he returned to the service within the Ministry of Defense in the capacity of research engineer in the field of composite materials. In 1982 he was appointed head of a research team, and in such capacity he received several national awards.

Mr. Osiroff has been on leave of absence from the Israel Ministry of Defense since September 1986, at which time he enrolled in the Engineering Science and Mechanics Department at the Virginia Polytechnic Institute and State University. In 1988 he completed his M.Sc. degree and is presently a Ph.D. candidate in the Materials Engineering Science program at the same university.

Mr. Osiroff married Talia in 1980 and has two sons, Nir born in 1984, and Gal born in 1987.

Ricardo Osiroff